Imperial College of Science, Technology and Medicine
University of London

Model Updating of Large Structural Dynamics Models Using Measured Response Functions

by
Henning Grafe

A thesis submitted to the University of London
for the degree of Doctor of Philosophy

Department of Mechanical Engineering
Dynamics Section
London, South Kensington

October 1998

Abstract

In the field of structural dynamics, reliable finite element (FE) response predictions are becoming increasingly important to industry and there is a genuine interest to improve these in the light of measured frequency response functions (FRFs). Unlike modal-based model updating formulations, response-based methods have only been applied with limited success due to incomplete measurements and numerical ill-conditioning problems. This thesis investigates the fundamental concepts of FRF model updating methods and identifies the underlying principles of these limitations.

After proposing the use of component mode synthesis methods for FE model reduction, two new FRF correlation functions are introduced, the shape- and amplitude-correlation coefficients. Both correlation measures may be used across the full measured frequency range and uniquely map any complex response to a real scalar between zero and unity. An analytical closed-form solution of the derivatives of the correlation functions is then used advantageously to formulate the predictor-corrector model updating formulation. This correlation-based technique resolves problems associated with incomplete measurements and updating frequency point selection and is also robust against measurement noise. As a result of this new philosophy of FRF model updating, modal damping coefficients may also be identified. The underlying algorithm is based on analytically-defined sensitivities and is not subject to numerical approximations. Similarly, an error localisation method is proposed which takes advantage of the information provided by the sensitivities of the correlation functions.

The thesis concludes with three case studies of increasing size. The first structure is an assembly of three beams whose ends are clamped and in need of validation. The second case study is concerned with a 3-plate, 2-beam assembly and the final test case updates an automotive muffler, the largest of all the structures (13 176 DOFs). Throughout the case studies, the predictor-corrector method exhibits good convergence properties and allows for large design parameter modifications. However, it is concluded that the subject of error-localisation must be addressed further and that the non-uniqueness of design parameter estimates in model updating seems inevitable.

Acknowledgements

I wish to express my gratitude to my supervisors, Dr. M. Imregun and Prof. D.J. Ewins, for their sustained encouragement and guidance throughout the duration of the BRITE-EURAM project. It was their experience and inspiration that kept the research going.

I would also like to thank the European Union who provided the financial funding for running the URANUS project.

Thanks are also due to past and present colleagues who never hesitated to give a helping hand.

Finally, I would like to mention Dr. M. Vahdati who shared his insight into many related fields of interest.

Contents

Notation

Basic Terms, Dimensions and Subscripts

$x(t)$	time varying displacement vector in Cartesian co-ordinates
$\dot{x}(t)$, $\ddot{x}(t)$	1_{st} and 2_{nd} time derivatives of $x(t)$
$X(\omega)$	Fourier transform of $x(t)$
$f(t)$	time varying excitation force
$F(\omega)$	Fourier transform of $f(t)$
$q(t)$	time varying displacement vector in modal co-ordinates
$\dot{q}(t)$, $\ddot{q}(t)$	1_{st} and 2_{nd} time derivatives of $q(t)$
q	Fourier transform of $q(t)$
t	time variable
i, j, k, l	running indices, pointer to data
r	current mode number or matrix rank
ω	frequency of vibration [rad/s]
i	imaginary i, i.e. $\mathrm{i} = \sqrt{-1}$
n	number of measured DOFs
m	number of modes
N	number of DOFs in FE model
N_f	number of frequency points
N_{f_u}	number of updating frequencies
N_s	number of substructures
N^k	number of DOFs in substructure k
N_b	number of boundaries in sub-structured FE model
N_φ	number of design parameters (N_p =number of p-values)
$N_m, N_k, ...$	number of mass-, stiffness-... matrices
n^k	number of sub-structures attached to boundary l

Matrices, Vectors, Scalars

$[\,], \{\,\}, (\,)$	matrix, column vector, single element
$\begin{bmatrix} \searrow & \\ & \searrow \end{bmatrix}$	diagonal matrix
$[\,]^T, \{\,\}^T$	transpose of a matrix, column vector
$[\,]^H, \{\,\}^H$	complex conjugate (Hermitian) transpose of a matrix, column vector
$[]^*, \{\}^*, ()^*$	complex conjugate of matrix; vector; single element
$[\,]^{-1}$	inverse of a square matrix
$[\,]^+$	generalised / pseudo inverse of a matrix
$[\quad^R], [\quad^E]$	reduced, expanded matrix
$\|\quad\|_p$	p-norm of a matrix / vector if vector x, $\| x \|_p = (\|x_1\|^p + \|x_2\|^p + \|x_3\|^p \cdots)^{1/p}$

$\left[\diagdown I \diagdown\right]$	identity matrix
$[0]$	null matrix
$[U], [V]$	matrices of left and right singular vectors
$[\Sigma] = \left[\diagdown \sigma_j \diagdown\right]$	rectangular matrix of singular values (σ_j is the j-th singular value)
$\left[\diagdown W_f \diagdown\right]$	frequency point weighting matrix
$\left[\diagdown W_\varphi \diagdown\right]$	design parameter weighting matrix
$[S]$	sensitivity matrix with N_φ columns
$[T]$	transformation matrix
J	cost function of optimisation problem
L_i	leverage of design parameter i
ϵ	machine precision of machine
κ,β,γ	mathematical constants, proportionality factors
κ_∞	maximum allowable condition of square matrix

Spatial Model Properties

$\{\varphi\}$	design parameters of FE model
$\{\Delta\varphi\}$	change in design parameters of FE model
$[M], [K]$	mass, stiffness matrices
$[C], [D]$	viscous, structural (hysteretic) damping matrices
$[Z(\omega)]$	general impedance matrix (either dynamic stiffness, mechanical impedance or apparent mass)
$[M_A], \ldots$	analytical / theoretical / predicted mass matrix
$[M_X], \ldots$	experimentally derived / test mass matrix
$[\Delta M] = [M_X] - [M_A], \ldots$	mass, ... error / modification matrix
$\begin{bmatrix} [M_{11}] & [M_{12}] \\ [M_{21}] & [M_{12}] \end{bmatrix}$	partitioned mass, ... matrix

Modal Properties

ω_r	natural frequency of r-th mode [rad/s]
λ_r	eigenvalue of r-th mode, $\lambda_r = \alpha + \mathrm{i}\,\beta$
ζ_r	viscous damping ratio of r-th mode
η_r	structural damping loss factor of r-th mode
m_r	modal / effective mass of r-th mode
k_r	modal / effective stiffness of r-th mode
c_r	modal / effective viscous damping of r-th mode
$\left[\diagdown \lambda_r \diagdown\right]$	eigenvalue matrix
$[\Psi]$	mode shape / eigenvector matrix
$[\Phi]$	mass-normalised mode / eigenvector matrix
$\{\psi\}_r$, $\{\phi\}_r$	r-th mode shape / eigenvector
ψ_{jr}, ϕ_{jr}	j-th element of r-th mode shape / eigenvector
${}_rA_{ij} = \phi_{ir}\,\phi_{jr}$	modal constant / residue
$[\Theta]_{2N\times 2N} = \begin{bmatrix} [\Psi] & [\Psi]^* \\ [\Psi]\left[\diagdown \lambda_r \diagdown\right] & [\Psi]^*\left[\diagdown \lambda_r \diagdown\right]^* \end{bmatrix}$	eigenvector matrix for viscously (and structurally) damped system (see eqn. 6.2, p. 103)

$\{\Theta\}_{r(2N\times 1)} = \left\{ \begin{array}{c} \{\Psi\}_r \\ \lambda_r \{\Psi\}_r \end{array} \right\}$	r-th mode shape of above eigenvector matrix

Response Properties

$[H(\omega)]$	general frequency response function matrix (either receptance, mobility or inertance)
$[\alpha(\omega)]$, $[Y(\omega)]$, $[A(\omega)]$	receptance, mobility, accelerance matrix
$\{H_j(\omega_k)\}$	general frequency response vector, all responses, excitation DOF j, frequency point k
$\{H_{ij}(\omega)\}$	general frequency response vector, response DOF i, excitation DOF j, all N_f frequency points
$H_{ij}(\omega_k)$	general frequency response element, response DOF i, excitation DOF j, frequency point k
$\{H(\omega_k)\}$	general frequency response vector at frequency point k and arbitrary excitation and response coordinates
$\{\varepsilon\}$	vector of response residuals
$\chi_s(\omega_k)$	shape correlation coefficient at frequency point k
$\chi_a(\omega_k)$	amplitude correlation coefficient at frequency point k

1

[1] The notation of this thesis largely complies with the "Notation for Modal Testing & Analysis" – Version A1.01, 1993

Standard Abbreviations

AIAA	American institute of aeronautics and astronautics
CMS	component mode synthesis
COMAC	co-ordinate modal assurance criterion
dB	decibel, i.e. $20\log\|x\|$
DOF(s)	degree(s) of freedom
EOM	equation of motion
FE	finite element
FEM	finite element method
FRF(s)	frequency response function(s)
IDOF(s)	internal degree(s) of freedom
JDOF(s)	junction degree(s) of freedom
LHS	left hand side (of an equation)
MAC	modal assurance criterion
MDOF(s)	master degree(s) of freedom
P-C	predictor-corrector
PRF(s)	principal response function(s)
RFM	response function method
SDOF(s)	slave degree(s) of freedom
SVD	singular value decomposition
RHS	right hand side (of an equation)
3D	3-dimensional
2D	2-dimensional

List of Figures

List of Tables

Chapter 1

Introduction

1.1 Motivation of Research

Engineers are constantly challenged to reduce the levels of vibration and noise, increase the life expectancy of components and improve the efficiency of machines. Such design requirements usually arise from economic and environmental aspects but may also be imposed by governing bodies to ensure safety standards and performance-related issues of operating machinery. Companies operating in the engineering industry must be flexible enough to adopt, incorporate and build on new technologies more than ever and need to be innovative to stay competitive. At the same time, as the list of design constraints gets longer, the product design cycle time must be reduced. A common interest of design offices in engineering science is to advance modern design technologies. Model updating using **F**requency **R**esponse **F**unctions (FRFs) is one of those technologies and improves the predictive capabilities of computer-based models of structural dynamics problems.

With the advent of computer technology, pioneering work in the aerospace industry developed and exploited numerical analysis techniques in the 1950s and 1960s. The **F**inite **E**lement **M**ethod (**FEM**) (Zienkiewicz 1967) found its application for the first time in industrial problems and has proven itself as a very flexible numerical analysis technique to obtain approximate solutions for otherwise intractable problems. Computer-based analysis techniques have changed the design and product development ever since in many other industries.

In the field of structural dynamics, the analysis of structures was traditionally confined to the modal properties of the system and the theoretical predictions were frequently compared with the measured mode shapes and eigenvalues (Ewins 1984). A variety of numerical correlation tools were developed to validate the predicted and measured quantities and subsequently algorithms for the systematic improvement of FE models using the measured dynamic properties – model updating – were employed with some success.

Despite having proved their value, the success of modal-based model updating techniques is directly dependent on the quality of the modal parameter extraction. In fact, the analysis of measured FRFs to identify the system's modal parameters is a process which inevitably introduces inaccuracies and errors over and above those already present in the measurements.

As a result of the increasing difficulty of extracting modal parameters in frequency regions of high modal density, and the intrinsic limitations of modal-based FE model updating

techniques, a growing number of researchers focused on model updating algorithms using the measurements directly. Initial attempts to formulate such algorithms, however, hardly went past their prototype stage and it was found that FRF updating algorithms have their own limitations (Natke 1983).

In 1995, the state-of-the-art in model updating technology was still concentrated on the use of modal-based updating algorithms for practical applications, as they were generally more robust and better understood than methods using measured responses directly (Friswell and Mottershead 1995). Stringent design requirements and the limits associated with modal-based model updating procedures, however, were the motivating factors to initiate further research in the subject of FRF model updating (URANUS 1994). The mechanics of FRF model updating techniques needed to be understood in order to advance this technology and make it accessible to problems of industrial size.

1.2 Mechanical Vibration Analysis

Essential to the analysis of vibrating structures is the ability to describe the response of a structure as a function of position, $\{x\}$, and time, t, given an exciting input force, $\{f(t)\}$. The phenomenon of "vibration" is the result of the interaction between mass and elasticity properties of the materials involved. In structural dynamics, the mass and stiffness properties of the system are the key ingredients to formulate mathematical relations between the input and output of the system under study. Such descriptive model relations can be derived from force balance considerations using Newton's second law (Sir Isaac Newton, 1642–1727) or the fact that the energy content of a conservative system is constant. The method of Lagrange (Joseph Louis Lagrange, 1736–1813) is such a tool and lends itself to scalar energy expressions, as opposed to vectors for the force balance method. The mathematical description (or "model") of the structure is the centre piece in mechanical vibration analysis and allows one to gain insight into the dynamic behaviour of the structure under study.

Models are formally distinguished by the number of **D**egree**s** **O**f **F**reedom (DOFs) of the system, N. Structures of practical interest are usually *continuous* (so that $N \rightarrow \infty$) and complex in geometry. An exact analysis of continuous systems leads to partial differential equations as functions of time and space, but for structures other than the very simplest, obtaining a closed-form solution of more complex geometries soon becomes an intractable task. In cases where no closed-form solution is feasible, approximate analysis techniques are employed. These constitute a compromise to the analytically exact solution and represent the structure as a finite collection of *discrete* coordinates with corresponding mass and stiffness properties ($N \ll \infty$).

The modelling of a discrete representation along with its simplifying assumptions determines the success of mechanical vibration analysis. The difficulties associated with solving partial differential equations is traded for the problem of assessing the quality of the solution obtained from an approximate discretised model representation. Actually, the necessity of validating and improving the quality of discrete models gave rise to the development of technologies like model updating.

Good introductions to the theory of vibration are provided by Thomson (1950) and Bishop and Johnson (1960). More advanced treatments, including numerical analysis techniques, can be found in the books by Newland (1989) and Gasch and Knothe (1987).

1.2.1 Equations of Motion

The mass and stiffness distribution of a given, often idealised, dynamic system can be used to express the balance between interacting forces at N DOFs. Unlike the force balance for continuous system models, the corresponding **E**quation **O**f **M**otion (EOM) for discrete, time-invariant and conservative (undamped) systems is conveniently expressed in a matrix/vector notation as:

$$[M]\{\ddot{x}(t)\} + [K]\{x(t)\} = \{f(t)\} \tag{1.1}$$

where Ewins (1984) classifies the mass and stiffness matrices, $[M]$ and $[K]$, as the "Spatial Model" of the system.

Equation (1.1) comprises N linear ordinary differential equations with constant coefficients and states that the internal stiffness- and inertia-related forces are in equilibrium with the externally applied force, $\{f(t)\}$. It is customary to include translational as well as rotational DOFs, $\{x(t)\}$, and it should be noted that these are the displacements relative to the structure at rest, $\{x_0(t)\}$. The system as described by equation (1.1) can be analysed for its steady-state harmonic response properties by assuming that $\{x(t)\} = \{X\}\, e^{\mathrm{i}\,\omega t}$ when $\{f(t)\} = \{F\}\, e^{\mathrm{i}\,\omega t}$. In this case, equation (1.1) becomes:

$$\left(-\omega^2\,[M] + [K]\right)\{X\} = \{F\} \tag{1.2}$$

where $[H] = [H(\omega)]$, the FRF matrix, is

$$\{X\} = [H]\{F\} \tag{1.3}$$

and represents another way to describe the system completely. Ewins (1984) refers to $[H]$ at the "Response Model". Strictly speaking, equation (1.2) identifies the receptance matrix, $[\alpha] = [H]$, as the ratio of displacement to force. Other forms of FRF matrices are:

$$[Y] = \mathrm{i}\,\omega[\alpha] \quad \text{and} \quad [A] = -\omega^2[\alpha] \tag{1.4}$$

known as mobility matrix, $[Y]$, and accelerance (or inertance) matrix, $[A]$, respectively. These relate velocity and acceleration to the input force.

1.2.2 Linear System Analysis

If the physical properties of the system are referred to as "design parameters" and denoted by the elements of the vector, $\{\varphi\}$, then one can deduce from the above discussion that generally, $[H] = [H(\omega, \{\varphi\})]$.

An assumption made throughout this thesis is the linearity of the system described $[H]$. From the definition of linearity, in a strict mathematical sense, the following identity must hold:

$$[H]\{\kappa_1\{F_1\} + \kappa_2\{F_2\}\} = \kappa_1[H]\{F_1\} + \kappa_2[H]\{F_2\} \tag{1.5}$$

which states that the scaled sum of responses induced by individual forces, $\{F_1\}$ and $\{F_2\}$, equals the response of the system generated by the sum of the forces, $\{F_1\}$ and $\{F_2\}$, scaled by arbitrary constants, κ_1 and κ_2. In other words, any linear combination of forces results in a corresponding linear combination of individual responses. For non-linear systems, this statement cannot be made and, in general, response matrix changes are not independent of $\{X\}$ and $\{F\}$, i.e. $[H(\omega, \{\varphi\})] \rightarrow [H(\omega, \{\varphi\}, \{X\}, \{F\})]$.

The condition of linearity (1.5) is also known as the principle of superposition (Magnus and Popp 1997). This additive property simplifies the analysis of vibrating structures immensely and it is because of this that even non-linear structures are often temporarily linearised at $\{F_0\}$ and a system solution is obtained by successively solving linear systems. A characteristic shared by both linear and non-linear systems, however, is that the dynamic properties generally do not change linearly with changes in $\{\varphi\}$. This non-linear relationship between the spatial parameters and the dynamic properties of the system is the major problem in model updating.

1.2.3 The Finite Element Method

Many practical problems in engineering are either extremely difficult or impossible to solve by conventional analytical methods. System idealisations such as the use of lumped parameter representations for structural dynamic analysis can, in some circumstances, give valuable insight into the dynamics of structures (e.g. civil engineering structures which are often represented by simple spring, mass, and damper systems to model the first (two) mode(s) of vibration). For the majority of problems found in industry, however, such an idealisation is often inappropriate or difficult to derive. These structural problems can alternatively be solved by using approximate numerical solution techniques of which the finite element method forms one of the most versatile classes.

All finite element modelling methods involve dividing the physical domain, the geometry of the structure, into a small subregions or "elements". Each element forms essentially a simple unit, the behaviour of which can be readily analysed. The set of points in space interconnecting each element is commonly known as the "mesh" and the individual points are known as "nodes". The discretisation of the structure is generally detrimental to the accuracy of the representation, and if model updating procedures are to follow, the mesh density often needs to be finer than usual (Imregun and Ewins 1994; Mottershead et al. 1995; Mottershead 1996; Link and Mardorf 1996).

Complexities in geometry are frequently accommodated by using a larger number of finite elements and a dynamic analysis of the structure can still be performed by assembling all the elements into one system representation, i.e. $[M]$ and $[K]$ in equation (1.1). The choice of elements, the solution algorithms used and, of course, the level of discretisation all influence the result significantly. Indeed, surveys have shown that dynamic FE analysis is not always as reliable as one assumes and it was found that if an analysis is performed by different sites independently of each other, the computed solutions can differ considerably (Ewins and Imregun 1986; Ewins and Imregun 1988; Maguire 1996).

The price that must be paid for flexibility and simplicity of individual elements is the amount of numerical computation required. Very large sets of simultaneous algebraic equations have to be solved. The storage needed for such calculations can be well in excess of the local memory available on the computer.

There is a wealth of literature available on the subject of finite elements and among those, Zienkiewicz (1967), Bathe (1982) and Hughes (1987) provide a comprehensive introduction to the subject. Less comprehensive are the books by Fenner (1986)(1996).

1.2.4 Modal Analysis

A forced response analysis, however, can turn into a computationally very expensive exercise if performed directly from equation (1.1) since the dynamic stiffness matrix, $[Z]$, of the system must be inverted ($[H] = [Z]^{-1} = [-\omega_k^2[M] + [K]]^{-1}$) at each frequency point ω_k. Modal analysis is a tool to considerably reduce these costs.

The modal parameters of an undamped system are a set of eigenvalues (natural frequencies) and corresponding eigenvectors (mode shapes) and may be envisaged as the frequencies and corresponding deflections with which the structures "wants" to vibrate naturally. Accordingly, if there is no external excitation (disturbance), i.e. $\{f(t)\} = \{0\}$, the structure is capable of vibrating naturally, and therefore, the eigenvalues and eigenvectors are called the "natural" or "normal" modes of the structure (Ewins 1984).

For the undamped structure, as described by equation (1.1), the vibration will not decay with time and a trial solution in the form of $\{x(t)\} = \{X\}\, e^{\mathrm{i}\,\omega t}$ can be anticipated. Since $\{f(t)\} = \{0\}$, the problem of identifying the normal modes of the structure reduces to solving:

$$\left(-\omega^2\,[M] + [K]\right)\{X\} = \{0\} \tag{1.6}$$

which is satisfied by exactly N modes for a system of N DOFs. If the mode shapes are designated by $\{\psi\}_r$ and the corresponding natural frequencies by ω_r, then

$$\left(-\omega_r^2\,[M] + [K]\right)\{\psi\}_r = \{0\} \quad \text{for} \quad r = 1, 2, 3 \cdots N \tag{1.7}$$

It is also customary to designate $\lambda_r = \omega_r^2$, the eigenvalue of mode r. Collecting all N modes, the so-called "Modal Model" (Ewins 1984) is conveniently expressed as,

$$\left[\begin{array}{cc} \lambda_r & \\ & \searrow \end{array}\right]_{N\times N} \qquad \left[\;\Psi\;\right]_{N\times N} \tag{1.8}$$

which represents the diagonal eigenvalue matrix (spectral matrix) and the eigenvector matrix. Both matrices are fully equivalent to the Response and Spatial models of the structure under study.

There are a number of numerical procedures available to compute the eigensolution. For systems with relatively small numbers of DOFs, say $N < 1000$, full system matrices are contemplated and all N modes are solved (Szabó 1956). In practical circumstances, the number of DOFs is often much larger and in these cases, only partial solutions are computed, say m out of N modes, and sub-space solvers are employed (Saad 1996).

Although the computational effort to calculate an eigensolution may prove costly, the modal model possesses the well-known property of orthogonality and allows one to simplify the analysis of the system to a great extent. The orthogonality of the mode shapes can be concisely stated as,

$$\left[\;\Psi\;\right]^T\left[M\right]\left[\;\Psi\;\right] = \left[\begin{array}{cc} m_r & \\ & \searrow \end{array}\right] \qquad \left[\;\Psi\;\right]^T\left[K\right]\left[\;\Psi\;\right] = \left[\begin{array}{cc} k_r & \\ & \searrow \end{array}\right] \tag{1.9}$$

where the eigenvector matrix diagonalises the mass and stiffness matrices to the modal masses and stiffnesses, m_r and k_r. These are not unique since the eigenvectors may be

arbitrarily scaled and still satisfy equation (1.7). However, the diagonal modal mass and stiffness matrices always relate to the eigenvalues by,

$$\left[\lambda_r\right] = \left[m_r\right]^{-1}\left[k_r\right] \tag{1.10}$$

which, at this stage, shows that the eigenvalues are unique while the eigenvector matrix is not. Each eigenvector constitutes a relative set of displacements corresponding to its natural frequency. In fact, any scaled mode shape will satisfies orthogonality (1.9).

In order to obtain a consistent scaling of mode-shapes, and unique modal masses and stiffnesses, the eigenvectors are often mass-normalised. That is if,

$$\{\phi\}_r = \frac{1}{\sqrt{m_r}}\{\psi\}_r \qquad \text{or} \qquad \left[\ \Phi\ \right] = \left[m_r\right]^{1/2}\left[\ \Psi\ \right] \tag{1.11}$$

then the modal masses are normalised to unity and,

$$\left[\ \Phi\ \right]^T\left[M\right]\left[\ \Phi\ \right] = \left[I\right] \qquad \left[\ \Phi\ \right]^T\left[K\right]\left[\ \Phi\ \right] = \left[\lambda_r\right] \tag{1.12}$$

Mass-normalisation of mode shapes is widely used and, as a matter of convenience, is used throughout the computations presented in this thesis.

Uncoupling the Equations of Motion

From the above properties of the modal model, it is readily seen that the eigenvectors effectively decouple the equation of motion and that this transformation into the modal domain leads to a new set of coordinates which are completely independent of each other. That is to say, the system is represented by as many single DOF systems as there are modal coordinates, $\{q(t)\}$. If the mode-shapes are mass-normalised, the equation of motion (1.1) becomes:

$$\left\{\ddot{q}(t)\right\} + \left[\lambda_r\right]\left\{q(t)\right\} = \left[\ \Phi\ \right]^T\left\{f(t)\right\} \tag{1.13}$$

where the physical displacement is expressed as $\{x(t)\} = [\Phi]\{q(t)\}$.

Experience shows that some measurements do exhibit some modes stronger than others and that again other FRFs do not disclose them at all. The presence of modes in a measurement is found to be dependent on the location and distribution of the exciting forces. The fact that a structure is excited at one point or another does not mean that every mode will be visible in the measurement. This observation is unmistakably evident in the physical force vector transformed to modal coordinates, namely $\{f_q(t)\} = [\Phi]^T\{f(t)\}$.

It has been shown that the modal coordinates are independent of each other and that each coordinate can be contemplated as a single DOF system. Correspondingly, if the modal force vector, $\{f_q(t)\}$, indicates small values at some DOFs in relation to other coordinates, then the corresponding modes are less excited than others. In the extreme, but not unusual, case where a modal force is zero (or numerically close to zero), then the corresponding mode is not (hardly) excited at all. Assuming the analytical model predictions are sufficiently close to the measurements, then $\{f_q(t)\}$ can be successfully employed to identify force vectors that excite the modes of concern.

Forced Response Analysis

Assuming a linear structure is excited by an harmonic force, as shown equation (1.2), then the receptance FRF matrix $[\alpha(\omega)]$ (i.e. $[H(\omega)] \rightarrow [\alpha(\omega)]$) is defined such that,

$$\left[-\omega^2 [M] + [K]\right]^{-1} = [\alpha(\omega)] \tag{1.14}$$

where $\alpha_{ij}(\omega_k) = X_i(\omega_k)/F_j(\omega_k)$ and expresses the displacement at DOF i due to unit excitation at DOF j. The receptance matrix is symmetric, as are $[K]$ and $[M]$, and it is this symmetry which reflects the "principle of reciprocity", i.e. $\alpha_{ij}(\omega_k) = \alpha_{ji}(\omega_k)$. The direct solution of equation (1.14) for individual receptances (FRFs) for a number of frequency points ω_k, however, is expensive and inefficient as usually only a limited number of responses are required and each individual frequency point requires the inversion of the full system.

As before, the modal properties of the structure can be employed advantageously. After some algebraic manipulation (Ewins 1984), equation (1.14) can be expressed in terms of the mode-shapes and eigenvalues by,

$$\Big[\alpha(\omega)\Big] = \Big[\ \Phi\ \Big] \Big[\ (\omega_r^2 - \omega_k^2)\ \Big]^{-1} \Big[\ \Phi\ \Big]^T \tag{1.15}$$

Equation (1.15) reduces the cost of computing the response matrix to a simple inversion of a diagonal matrix. In cases where only individual FRFs are required, and not the full FRF matrix, the above equation can be further reduced to a summation:

$$\alpha_{ij}(\omega_k) = \sum_{r=1}^{N} \frac{\phi_{ir}\,\phi_{jr}}{\omega_r^2 - \omega_k^2} \tag{1.16}$$

where all N modes are included, and i and j address the response and excitation coordinates, respectively, in the eigenvector of mode r.

It has been stressed that modal analysis of large structures is often confined to a few modes and that the number of identified modes, m, is commonly small, $m \ll N$. The number of modes computed depends on the objectives of the analysis and m may be as small as 3 or 4 if only the first few modes are critical to the design. But even for the response analysis over a much wider frequency range, the FRFs can be computed from a limited number of modes with sufficient accuracy (Gasch and Knothe 1989) and equation (1.16) becomes,

$$\alpha_{ij}(\omega_k) \approx \sum_{r=1}^{m} \frac{\phi_{ir}\,\phi_{jr}}{\omega_r^2 - \omega_k^2} \tag{1.17}$$

Usually, m covers all the modes within the frequency range of interest and a few out-of-band modes. The validity of the approximation stems from the fact that higher modes participate very weakly in lower frequency regions.

1.3 Mechanical Vibration Measurements

As a direct consequence of the approximations made during the mathematical design of engineering components, the experimental validation of the predictions plays a major role in an increasing number of industrial designs.

There are principally two types of vibration measurement: the measurement of vibration responses experienced by a structure in its operating environment and the experimental investigation of the vibration properties due to a defined source of excitation and the measured response. In particular, the measurement of the input and the resulting response is of particular interest as the FRFs:

- can be used to identify the natural frequencies and mode shapes of the test specimen;
- provide an invaluable means to validate the analytical model

An illustrative booklet was presented by Ewins (1980) and provides a good primer about the subject of vibration testing.

There are two principal types of excitation in a dynamic test. The structure can either be excited by impact testing using an instrumented hammer or by a shaker attached to the structure through a push rod. Piezoelectric transducers are used to measure excitation forces and responses separately and, after some signal processing (Randall 1987; Newland 1975), these determine the FRFs. In some instances, more than one excitation source is attached to the specimen to ensure all modes of interest are excited (eqn. (1.13)).

Depending on the objectives of the experiments, a modal analysis or modal identification is routinely carried out to find the modal properties of the system. Algorithms for extracting the modal parameters from measurements have been extensively developed for quite some time. These aspects and some practical considerations are thoroughly discussed by Ewins (1984).

Although considerable advances in instrumentation and data acquisition technology have been made, the number of measurable DOFs is usually limited. This is particularly true for rotational DOFs and FE coordinates which cannot be accessed. Coordinates other than these could possibly be measured but would lead to excessive testing costs.

1.4 Model Validation and Correlation

Finite element analysis has become a widely established numerical analysis tool and often plays an integral part in the design circle. This design technology has become an affordable design tool throughout engineering industry and will continue to do so in the future with continuing advances in computer technology and the availability of more comprehensive FE packages.

The finite element method allows the analysis of complex structural dynamics problems and it is good practice to verify the validity of the FE model. However, the extend to which the model is in error is very difficult to estimate. To date, the only realistic means to validate the FE model is to compare a limited number of predicted dynamic properties with their corresponding measurements and to draw conclusions about the correctness of the model subsequently.

Probably the single most popular application of experimentally determined modal parameters is to correlate these with those computed from the FE model. In spite of the required modal analysis of the measured FRFs, modal-based correlation techniques are the most developed and commonly used correlation measures. A brief introduction to the subject can be found in the book by Ewins (1984), more extensive presentations are given in the papers presented by Heylen and Avitabile (1998) and O'Callahan (1998), including FRF-based correlation methods. In general, the presented correlation techniques are a mixture

of visual and numerical means to identify the differences between measurements and predictions. Whereas numerical correlation techniques return a numerical value, visual means of correlation are subjective and of qualitative nature.

Some of the basic correlation tools include simple tabulation or plotting of measured and predicted eigenvalues. Matching eigenvalues should lie on a 45° line and if points scatter about the straight line no correlation is found. A more strict correlation technique is the use of the so-called "**M**odal **A**ssurance **C**riterion" (MAC). The MAC has established itself as a key correlation measure ever since it was first proposed by Allemang and Brown (1982). It uniquely identifies a real scalar between zero and unity an is defined between mode i and mode j by,

$$MAC = \frac{\left|\{\psi_X\}_i^H \{\psi_A\}_j\right|^2}{\left(\{\psi_A\}_j^H \{\psi_A\}_j\right)\left(\{\psi_X\}_i^H \{\psi_X\}_i\right)} \tag{1.18}$$

Values close to unity indicate good correlation between the experimental mode shape, $\{\psi_X\}$, and the predicted eigenvector, $\{\psi_A\}$. However popular the MAC is, the correlation coefficient is incapable of distinguishing between systematic errors and local discrepancies. It may disguise the fact that only some coordinates are responsible for a low MAC value and it is also invariant to scaling.

Since the MAC does not present the whole picture, it is preferably used in conjunction with the so-called "**Co**ordinate **M**odal **A**ssurance **C**riterion" (COMAC), proposed by Lieven and Ewins (1988). This also varies between zero (no correlation) and unity (perfect correlation) but unlike the MAC, the COMAC correlates a selected DOF across a range of modes. Both the MAC and the COMAC effectively compute a least-square deviation of the shape points from a straight line correlation.

Other correlation techniques using the identified modal parameters are based on the orthogonality conditions, as stated by equations (1.9). Off-diagonal terms close to zero suggest good correlation. A representative example was proposed by Targoff (1976).

The direct correlation of measured and predicted FRFs is less well developed as for many years the validation of analytical models was confined to correlation measures in the modal domain. With the first algorithms to update FRFs directly, it became customary to overlay individual measurements with their analytical counterparts and to assess visually the level of correlation. Only more recently has attention been paid to numerical measures to quantify the level of correlation. Balmes (1993a) employed the Eucledian norm of the difference between a measurement and its corresponding prediction. In a similar fashion, Heylen and Lammens (1996) proposed the **F**requency **R**esponse **A**ssurance **C**riterion and defined it in line with the COMAC as,

$$FRAC = \frac{\left|\{H_{Xij}(\omega)\}^H \{H_{Aij}(\omega)\}\right|^2}{\left(\{H_{Xij}(\omega)\}^H \{H_{Xij}(\omega)\}\right)\left(\{H_{Aij}(\omega)\}^H \{H_{Aij}(\omega)\}\right)} \tag{1.19}$$

where $\{H_{ij}(\omega)\}$ is the FRF of response coordinate i and excitation coordinate j across the frequency spectrum ω. For identical FRFs, the FRAC value is unity and zero if the responses are uncorrelated. The authors, however, point out that a global shift in frequency between the experimental (X) and analytical (A) FRFs leads to a biased correlation value even if the FRFs are otherwise identical.

Grafe (1995) proposed a global correlation function which was derived from the MAC correlation coefficient (and will be formally introduced as $\chi_s(\omega)$ in Chapter 4). Unlike the FRAC, which is a coordinate correlation measure, the proposed correlation function examines the level of correlation at each frequency point across the spatial domain (note that the MAC is only evaluated at eigenvalues). Later, Nefske and Sung (1996) and Lenoir et al. (1998) have proposed identical correlation measures. Pascual et al. (1997) published in their paper the so-called **F**requency **D**omain **A**ssurance **C**riterion (FDAC). As the MAC table cross-examines the correlation between different modes, the FDAC cross-correlates each frequency point (across the full spatial domain) with every other measured frequency point. Therefore, the diagonal elements of the FDAC correlation table are identical to $\chi_s(\omega)$. Grafe (1997b) presented a similar frequency point correlation matrix and proposed to use this for identifying spatially-independent frequency points for the use in model updating.

1.5 Structural Damage Detection

The preceding sections were concerned with the theoretical aspects of structural dynamics, the measurements of vibrations and the combination of both disciplines to validate the predictions using visual and numerical correlation measures. All three subjects are constantly progressing technologies and research fields in their own right.

The quality of each type of analysis largely depends on the engineering knowledge and experience available and the ability to interpret the results obtained. This is particularly true if clear discrepancies between test and analysis results are apparent and the main objective is to align the analytical model. This so-called inverse problem, where the physical design parameters are sought that produce a given dynamic property, can be handled by the disciplines known as "Damage Detection", "Health Monitoring" or "Model Updating".

The underlying principle of damage detection algorithms is that any changes in the spatial model (defects) will cause detectable changes in the dynamic response. It is not difficult to see that the philosophy behind damage detection procedures is closely in line with one's intuitive inclination to conclude the presence of damage if a machine, or a simple tool, changes its operating sound from one moment to the next. In mathematical terms, the concept of damage is therefore not meaningful without the comparison between two different states of a system, one of which is assumed to represent the initial, or undamaged state.

Doebling et al. (1998) presented an extensive survey of current developments and discussed the practical aspects of damage detection algorithms. A classification of damage and the ability to identify damage was used to classify damage detection algorithms in levels of increasing complexity. There are formulations which determine the presence of damage in the structure (*level 1*), methods that identify damage and its location (*level 2*), and methods which aim to locate and quantify the damage in the structure (*level 3*). Vibration-based damage detection methods that do not make use of a corresponding theoretical model of the structure fall into the category of level 1 and level 2. If the identification of damage is performed in conjunction with a mathematical model, the method is classified as level 3 and level 3 procedures are very closely related to finite element model updating techniques.

Pioneering work in the offshore oil industry in the 1970s and 1980s led to the develop-

ment of damage location procedures. It was the objective to detect near-failing drilling equipment and to prevent expensive oil pumps from being stuck in the soil. The methods relied on detectable changes in natural frequencies and the use of these to locate defects. Because the environmental operating conditions of platforms caused varying mass-loading effects on the drilling pipe, the inconsistency of test data prohibited satisfactory results.

Further developments of damage detection techniques for applications other than offshore platforms have advanced considerably. These often make some assumptions about likely error sources in an equivalent analytical model and identify damage if anticipated changes in measured responses occur. Representative examples of damage identification procedures using a known catalogue of likely damage scenarios were presented by Friswell et al. (1994).

The majority of publications still seem to focus on algorithms using modal properties. Since the differences in modal properties between the damaged and undamaged structure are usually very small, some authors propose enriching the algorithms by using the measured FRFs directly (Mai et al. 1997). However, it seems that the required accuracy of response measurements for such approaches is practically impossible to achieve.

1.6 Finite Element Model Updating

In contrast to health monitoring or damage detection algorithms, the motivation for finite element model updating is to improve the accuracy of an initial FE model so that the predicted dynamic behaviour matches as closely as possible that observed during an experiment. With increasing reliability and confidence in measurement technology, the need to improve the numerical model representations initiated the development of model updating algorithms in the 1970s. Ever since, the interest in systematically adjusting FE models has produced a wealth of publications on the subject and a good introduction was presented by Imregun (1992), including a discussion of practical bounds of the algorithms in general terms. More mathematical and comprehensive surveys, were presented by Natke (1988), Imregun and Visser (1991), Mottershead and Friswell (1993), Natke et al. (1995) and Friswell and Mottershead (1995).

1.6.1 Direct FE Model Updating Methods

It is customary to classify model updating techniques into two broad categories. The earliest generation of algorithms produced the methods often referred to as "direct methods" which directly solved for updated global system mass and stiffness matrices by contemplating single matrix equations. The equations defining the differences in spatial parameters between the FE model and the measured structure usually make use of the measured eigenvectors and eigenvalues.

Methods using Lagrange multipliers were derived from a strict optimisation point of view and seek to minimise a predefined objective function along with additional constraints such as the system symmetry and the orthogonality conditions. Baruch (1978), for instance, corrects the system stiffness matrix whereas Berman and Nagy (1983) proposed an equation to identify the differences in the system mass matrix. Both techniques are representative of this family of methods. The applicability of these methods, however, is limited since the connectivity pattern is usually destroyed, a limited number of measured eigenvectors is employed and the measurements are assumed to be complete.

Similarly, matrix mixing methods assume that all modes are measured at all DOFs and use these to construct the inverses of the global mass and stiffness matrix. Although these data requirements are difficult to meet in practical applications and other approximations have to be introduced, Link (1986) and Caesar (1987) used the identified flexibility matrices to update an initial FE model using the computed and measured eigenvectors.

Other representative examples are the families of error matrix methods. Here the difference between the initial analytical stiffness matrix and the unknown experimental stiffness matrix is postulated and the error between both is assumed to be small. After computing pseudo-flexibility matrices using the measured eigenvectors, the error in the global mass and stiffness matrices can be computed (Sidhu and Ewins 1984).

None of the direct methods, however, gives particularly satisfactory results as they place almost impossibly high demands on the quantity and quality of experimental data required.

1.6.2 Iterative FE Model Updating Methods

The principles of model updating techniques generally described as "iterative methods" are very different to direct updating formulations. Unlike direct methods, which focus on the global system matrices, iterative model updating procedures are formulated in line with the discretised nature of the FE model. FE models are an assembly of individual finite elements and each finite element is defined by its design parameters, $\{\varphi\}$, such as its geometry or material properties.

Iterative methods work together with a parameterised FE model, the "error model", and introduce changes to a pre-defined number of design parameters on an elemental basis. The flexibility provided by the parameterisation allows an updating which is physically more meaningful than that offered by the direct methods.

Typically, the error model is advantageously used to calculate first-order derivatives of a chosen dynamic property of the system. This linearisation allows the formulations of an often over-determined linear set of algebraic equations in the form of:

$$[S]\{\Delta\varphi\} = \{\varepsilon\} \tag{1.20}$$

where $[S]$ is the sensitivity matrix, $\{\Delta\varphi\}$ the changes in updating parameters and $\{\varepsilon\}$ the residual, the difference between the measured and predicted dynamic properties. Such a system of equations is solved for the design parameter changes and the FE model is updated. The sequence of solving and updating the system has led to the description of these techniques as "iterative methods".

The system matrices of FE models updated by iterative methods can be uniquely reconstructed and, unlike direct methods, the connectivity patterns of the modified mass and stiffness matrices remain intact.

1.6.3 Minimisation of Modal Residuals

A well-established method among iterative model updating tools is the systematic minimisation of identified modes. Here, existing differences in the eigenvalues and possibly eigenvectors assume the role of residual vector $\{\varepsilon\}$, and the sensitivity matrix $[S]$ embodies the first-order sensitivities of these with respect to the selected updating parameters (Fox and Kapoor 1968). As a preliminary step, however, a number of corresponding modes

must be identified. The pairing of predicted and measured modes can be performed by visual means (animation) but is also often supported by quantitative measures such as the MAC correlation coefficient (eqn. (1.18)). Having identified pairs of correlated modes (irrespective of possible differences in natural frequencies), equation (1.20) is then solved for the design parameter changes, $\{\Delta\varphi\}$, and the FE model is updated. Following an eigensolution of the updated FE model, a new mode pairing exercise is performed and the updating calculations are repeated until convergence is reached.

Although good experience has been made with modal-based model updating methods, the number of design parameters which can be updated is usually limited as such formulations are often confined to updating eigenvalues only. Unlike the eigenvalue sensitivities, eigenvector sensitivities cannot be solved in closed form and must therefore be approximated (Appendix A.3). Furthermore, eigenvector sensitivities are generally orders of magnitude smaller than the eigenvalue sensitivities, which leads to ill-defined sensitivity matrices $[S]$.

One of the earliest papers on this subject was by Chen and Garba (1980). They addressed the case in which there are more design parameters than measurements and they introduced extra constraints to turn the parameter estimation problem into an over-determined set of equations. Zhang et al. (1987), Natke (1983) and the PhD thesis by Chen (1986) also discuss this classical updating approach extensively. Dascotte and Vanhonacker (1989) consider the eigensensitivity approach using weighted least-square solutions where the weights can accommodate engineering intuition. The relative merits of the formulation when applied to practical examples was discussed by Dascotte (1990), Link (1990) and Jung (1991).

In an excellent paper presented by Bucher and Braun (1993), the relevance of the band-limited nature of measurements was highlighted. An analytical closed form solution was presented which is able to relocate eigenvalues and adjust eigenvectors using identified left eigenvectors (Appendix A.2). The applied modifications were constrained to lie in a known subspace of the original model. The method's ability remains to be verified on larger updating problems.

1.6.4 Minimisation of Response Residuals

The next leap forward in FE model updating was the use of the measured FRFs directly. FRF model updating techniques circumvent the need to identify the modal parameters from the measurements and the necessity to perform mode pairing exercises. Another distinct difference is that, unlike the updating of eigenvalues and eigenvectors, the updating computations can be performed at many more frequency points and equation (1.20) can easily be turned into an over-determined set of equations. The residual vector, $\{\varepsilon\}$, presents the difference between the measured and predicted FRFs, and the columns of sensitivity matrix, $[S]$, hold the response sensitivities for a number of updating parameters, $\{\varphi\}$.

The idea of using the measurements directly goes as far back as 1977 where Natke employed a weighted least-square approach on an undamped model. A comprehensive survey and detailed discussions on the developments are presented by the author's book (Natke 1983) and also in the PhD thesis by Cottin (1983). Both present different forms of residuals and solution techniques.

The potential benefits of this model updating philosophy ignited an increasing interest to further develop these methods. Among various other publications, Mottershead

(1990) should be mentioned along with Foster and Mottershead (1990) who improved the spatial properties of a reduced FE model using a least-square estimation technique. Ill-conditioning issues of equation (1.20) and possible regularisation techniques were addressed by the same authors (Mottershead and Foster 1991).

Lin and Ewins (1990) derived a formulation based on a mathematical identity and proposed neither to condense nor to use any explicit numerical expansion scheme. Instead, they proposed to replace all unmeasured DOFs with their analytical counterparts in the measurement vector and, once the system described by equation (1.20) is assembled, to delete the equations of corresponding unmeasured coordinates. Case studies of practical relevance were reported by Imregun (1994) and it was shown that noise-contaminated measurements led to biased parameter estimates and that the method is more difficult to handle than inverse eigensensitivity approaches.

Other notable developments in FRF model updating include the method proposed by Larsson and Sas (1992). These authors use an exact dynamic condensation and an objective function which does not require the computation of the FRF matrix, $[H(\omega)]$. They emphasise, however, that the condensation procedure inherently puts limits on the frequency range which can be updated. As before, incomplete measurements and their implication on the FRF model updating formulation seem to restrict severely the method's ability to update larger FE model.

The FRF updating approach proposed by Arruda and Duarte (1990) is distinctly different to many other methods and defines a cost function, $J(\{\varphi\})$, based on a correlation coefficient identical to the FRAC (eqn. (1.19)). The proposed procedure to minimise $J(\{\varphi\})$ includes an external adjustment of the line search, being also an iterative scheme. In spite of the fact that only a limited number of known error sources were updated, the algorithm did not always converge. Conceptually very similar is the method presented by Balmes (1993a). He also concentrates on the error norms between the measured and predicted FRFs and stresses that the resulting objective function is convex in much larger regions if the FRFs are in logarithmic scale (Balmes 1993b). Indeed, Arruda and Duarte (1990) had made the same observation when using logarithmic FRFs.

Common to many FRF updating algorithms is the inherent coordinate incompatibility between the number of measurement DOFs and number in the FE model. Some authors propose to condense the analytical model to the number of measured DOFs, others formulate the updating algorithm along with an expansion scheme. Although such approximating tools are needed for most of the formulations proposed, the accuracy of the schemes deteriorate as the level of expansion/condensation (i.e. N/n) increases. As larger applications tend to have many more analytical DOFs than measurements, the applicability of FRF-based updating formulations is limited to smaller FE models. Other difficulties in the subject of FRF model updating include the selection of frequency points and the often encountered ill-conditioning of sensitivity matrix $[S]$.

More recent research in the field of model updating has primarily focused on these problem areas and not on developing new algorithms as there seems to be little room for further improvements of current methods. A recently published special issue of *Mechanical Systems and Signal Processing* edited by Motterhead and Friswell (1998) presents a good cross-section of later developments and the editorial provides a good summary of the recent trends in model updating research.

One of the highlighted advancements in model updating was the use of selective sensitiv-

ities originally introduced by Ben-Haim (1992) and Ben-Haim and Prells (1993). With the aim of improving the conditioning of $[S]$, the authors propose to tune the excitation so that a subset of design parameters produce large sensitivities while the sensitivities of remaining updating parameters remain comparatively small. However, the resulting, and sometimes complex, distribution of forces is often physically impractical or impossible to apply in realistic test conditions and further research is needed.

From a strict optimisation point of view, model updating is the minimisation of an objective function and the objective function is generally non-linear in the (selected) design parameters. Very different search engines for the global minimum have been proposed recently as a result of the observed convergence problems. Genetic Algorithms are one form of directed random search based on an analogy with natural evolution (Levin and Lieven 1998). Neural Networks also have been developed from a biological background and have created models with the ability to learn. This underlying theoretical model, therefore, needs always to be taught. The concept of using a trained model can be applied for model updating purposes (Atalla and Inman 1996) but the computational effort of the training phase seems to be excessive and only applicable for small problems.

1.6.5 Updating of Large FE Models

Link (1998) addressed the problem of updating large FE models and proposed to condense part of the structure using the Craig-Bampton modal synthesis method (Craig Jr. and Bampton 1968). Local updating parameters were then defined in the uncondensed partition of the structure and global parameters in the condensed component (E, ρ). Together with a modal-based sensitivity approach, these were then updated successfully. However, the presented case study was relatively small (about 100 DOFs) and the real value of the formulation remains to be seen.

Hemez (1997b) also advocates the use of modal-based formulations to update large FE models. He targets at model sizes of 100 000 to 500 000 DOFs and employs a computationally more efficient implementation of modal expansion schemes. A limited number of modes (3 to 4) was then updated using an overall number of about 100 updating parameters. It is emphasised that the two most critical issues in updating large FE model is the incompleteness of the measurements and the localisation of erroneous elements. The paper propose parallel algorithm implementations and sub-structuring methods to update even larger models since the proposed procedure requires inversions of very large matrices.

A structural dynamics analysis platform has recently been developed for handling large industrial applications (Roy et al. 1997). The MATLAB-based code "PROTODYNAMIQUE" is the result of an industrial project within the framework of the European BRITE-EURAM project UPDYN. Special interest was placed on the integration of innovative FE validation and updating and to interface these with commercially available software packages.

To date, most reported model updating case studies of large FE models make use of modal-based formulations and these are often restricted to updating eigenvalues only. The computational requirements and the incompleteness of the measurements predominantly restrict the application FRF model updating formulations to models of equivalent sizes.

1.7 Objectives of Research

A common interest in model updating technology is to improve the reliability of FE models and the adjustment of these in a physically meaningful way so that the predictions come close to the measured dynamic properties. Currently, model validation and updating tools provide the only means to ensure that the level of FE approximations lie within reasonable bounds for otherwise continuous mechanical vibration problems.

As an alternative to many existing model updating techniques, the direct use of response measurements is particularly attractive as such data are free of modal identification errors and the FRFs disclose the correct damping information. However, the direct use of measurements often causes unexpected numerical problems over and above those already experienced with modal-based model updating techniques.

The overall objective of the research presented in this thesis is to improve the overall performance of FRF model updating techniques for general applications and particularly to find solutions to the problems associated with updating large FE models. The specific objectives relevant to this work were:

- to devise new correlation tools designed to quantify the level of correlation between the measured and predicted FRFs in a consistent manner,
- to analyse the mathematics of FRF model updating formulations and to explain the numerics of such algorithms,
- to identify potential limitations of current FRF model updating algorithms and develop possible solutions to these,
- to extend, or further develop, response-based formulations especially in the light of FE model applications of industrial size

The following outline of the thesis briefly summarises the content of each chapter. The order of the chapters largely follows with the progress made during research.

1.8 Outline of Thesis

Chapter 2 revisits FRF model updating techniques and identifies common features and assumptions in currently available algorithms. This discussion shows that the algorithms may be broadly categorised into methods based on *input* and *output* residuals, in analogy with the measured *force* and *displacement*. After discussing the relative merits of a frequently used error model, the p-value formulation, an improved error model is proposed which allows for true design parameter changes. The response function method (RFM) is then presented and discussed in detail and it is shown that, although initially derived from a mathematical identity, the RFM is a sensitivity-based model updating formulation, as many other techniques. Having identified and analysed the mathematical assumptions of FRF algorithms, the RFM is then critically evaluated and the detrimental effects of noise, incompleteness, model order differences and choice of updating frequencies is demonstrated. The mechanics of non-unique parameter estimates is then investigated and two analytically derived scenarios prove the existence of these in practical situations.

Chapter 3 directly addresses the problem of identifying appropriate FE model representations of large structures. It is proposed to make use of component mode synthesis methods (CMS) which allows one to reduce the system to an assembly of smaller FE model, each of which can be updated separately. Three different approaches are presented and are seen to effectively reduced the system size by using modal transformations whose transformation matrices are independent of frequency. The meaning of the so-called *component modes* employed is illustrated and interpreted in engineering terms. A numerical demonstration shows that such reduced FE models can give FRF predictions very close to those of the uncondensed model. Furthermore, the computational cost of reanalysing the FE model in an model updating exercise is considerably reduced as, in general, only design changes are introduced on a sub-structure level.

Chapter 4 addresses the issue of correlating measured responses directly with their analytical counterparts and introduces two FRF correlation coefficients. Both are derived with the objectives to formulate a correlation-based FRF model updating technique, the predictor-corrector (P-C) formulation. The first of the two correlation coefficients is closely related to the MAC (eqn. (1.18)) and is defined for any measured frequency point. The second of the two correlation coefficients also returns a value between zero and unity but is much more stringent as it is sensitive to any discrepancies between the measurements and their corresponding predictions. After presenting a computational more economical way of calculating FRF sensitivities, it is shown that these can be employed directly for calculating the sensitivities of both correlation functions. These and the correlation functions are the key ingredient of the P-C model updating formulation. This new FRF model updating technique does not require a one-to-one correspondence between measured and analytical DOFs, any explicit updating frequency point selection scheme and statistical approximations to obtain the weighting matrices for the proposed extended weighted least-square solution. A numerical validation of the method includes a case where the response of a FE model of 864 DOFs is improved by just using one measurement.

Chapter 5 is concerned with the location of errors in the FE model and can be considered as a logical extension the work presented in Chapter 4.Assuming that the FE model is capable of modelling the measured responses, it is argued that sensitivity-based procedures provide the only realistic means to locate erroneous elements in large FE models. The problem of estimating initial stiffnesses, however, shows that in general the erroneous design parameters must be sensitive for those methods to work. This is not always the case. After revisiting the classical eigenvalue sensitivities, the sensitivities of the predictor-corrector model updating formulation are employed to formulate an alternative error location procedure. The numerical case study included aims to localise known error locations and the proposed method is shown to produce better results than those obtained from an eigensensitivty study. However, the localisation of erroneous elements remains a difficult subject.

Chapter 6 discusses the issue of damping and its associated difficulties in model updating. It was found that many of the currently available FRF methods employ an undamped FE model and often assume that the measurement are from lightly damped structure. Only then does the resulting set of equations (eqn. (1.20)) remain real and the algorithm stable. Having realised these problems, a new identification procedures is derived. It benefits from the real nature of both correlation coefficients and their sensitivities introduced in Chapter 4 and employs two analytically derived damping sensitivities for proportionally

damped systems. The damping identification procedure involves no numerical approximations and computationally inexpensive. The concluding case study shows that the method converges very quickly and is able to adjust a structurally or viscously damped FE model within a few iterations.

Chapter 7 presents the application of the findings and developments to four different structural dynamic problems:

Clamped Beam Assembly, 648 DOFs: The first and smallest application is an assembly of three slender beams whose FE model has 648 DOFs. This numerical model was of particularly interesting as the number of measurements was limited ($n = 3$) and the clamping conditions were unknown. The boundary conditions were were successfully updated using the P-C model updating algorithm.

Benchmark S1203, 4044 DOFs: This particular case study has been the benchmark for developments in model updating at Imperial College, Dynamics Section, for many years. It is a structure consisting of three plates and two connecting beams and the measurements have shown that the response is a mixture between strong and weak modes as well as a balanced combination of well-separated and close modes. Compared to the clamped-beam assembly, the modal density was relatively high and the target frequency range was $0Hz$ to $800Hz$. This test case includes application of the error localisation procedure, the damping identification algorithm and , of course, the updating of mass and stiffness parameters] using the P-C method. With a relatively small number of 66 measurements, the response predictions of this 4044 DOFs model could be improved considerably.

Automotive Muffler, 13 176 DOFs: The last case study places emphasis on the incompleteness of measurements and shows on an industrial structure of 13 176 DOFs the ability of the P-C model updating technique. Using only a small number of 10 simulated measurements, the results presented demonstrate the ability of the P-C method to update large FE models.

Chapter 8 provides a summary of main achievements and conclusions of this thesis and tries to give some recommendations for future work. It concludes that updating of large FE models can be performed using the developments of this thesis and that the further studies should be performed using a computer program written in a low-level language. Other conclusions stress the need to further explore the problem of error localisation as this issues seems to the key for further progress in model updating technology.

Chapter 2

Frequency Response Function Model Updating

2.1 Introduction

Frequency response functions (FRFs) are typically the form of response measurements provided by a dynamic test and embody the reference data for subsequent FE model validation. The use of numerical correlation and model updating techniques has become increasingly popular over recent years and these are generally classified into modal-based and response-based methods. Modal-based FE model updating algorithms use the measured FRFs indirectly and rely on the results obtained from an experimental modal analysis, a process which inherently introduces errors and inaccuracies over and above those already present in the measured data.

In contrast, response-based model updating techniques utilise the measured FRFs directly to identify erroneous design parameters. This class of model updating methods is particularly appealing as the FE models are updated in view of the fully damped response and not an estimated set of modal properties. Also, the amount of available test data is not limited to a few identified eigenvalues and eigenvectors and, updating calculations can be performed at many more frequency points.

This chapter revisits the theory of standard FRF model updating techniques and highlights the underlying assumptions. The modelling of errors in FE models is addressed and the much-used p-value formulation is discussed. Based on the implicit assumptions of the p-value formulation, a physically representative error model is introduced. The **R**esponse **F**unction **M**ethod (RFM) proposed by Lin and Ewins (1990) is then introduced as a representative example of this class of model updating formulations and its underlying theoretical assumptions are discussed in some detail. Following two numerical case studies, the phenomenon of non-unique parameter estimates is analysed in the light of the conclusions drawn. Two families of correction matrices are then presented which do not indicate for any errors, $\{\varepsilon\}$, when solving the updating equations.

2.2 Theory of FRF Model Updating Techniques

The idea of using measured FRFs directly for model updating purposes is not a new one and probably started to crystallise with the paper by Natke (1977). Early works by Natke

(1983) and Cottin et al. (1984) already reflected the benefits over modal-based updating algorithms and Sestieri and D'Ambrogio (1989) stress that experimental modal analysis can introduce errors exceeding the level of accuracy required to update FE models. In particular, if the tested structure exhibits close modes or regions of high modal density, traditional updating tools will fail to give reliable results as the extracted modal properties are associated with a high level of inaccuracy.

The interest to further develop FRF model updating techniques has created a wealth of publications ever since. Comprehensive surveys are presented by Natke (1988), Imregun and Visser (1991) and Mottershead and Friswell (1993) provide a good introduction to the subject. Along with many other authors, the books by Friswell and Mottershead (1995) and Natke (1983) distinguish between FRF model updating methods based on *input residuals* and formulations based on *output residuals*. The terms "input" and "output" were probably adopted from the control engineering terminology where it is customary to use more abstract representations dynamic systems. The existence of residuals and their theoretical treatment rely on the assumption that the analytical FE model (A) and the experimental test specimen (X) can both be represented by:

$$[Z_X(\omega, \{\varphi\})]\{X_X(\omega)\} = \{F_X(\omega)\} \qquad [Z_A(\omega, \{\varphi\})]\{X_A(\omega)\} = \{F_A(\omega)\} \tag{2.1}$$

where $[Z(\omega, \{\varphi\})]$ is the dynamic stiffness matrix as a function of the excitation frequency, ω, and design parameters, $\{\varphi\}$, and $\{X\}$ and $\{F\}$ are the frequency dependent displacement (or output) and force (or input) vectors. It can be shown that all FRF model updating techniques are derived from these basic equations.

2.2.1 Minimisation of Input Residuals

Model updating algorithms derived from an input residual (or equation error) postulate an error function as the difference between the measured and predicted (input) forces in the form of:

$$\{\varepsilon_{input}\} = \{F_X(\omega_k)\} - \{F_A(\omega_k)\} \tag{2.2}$$

where the input residual vector $\{\varepsilon_{input}\}$ is defined at a selected measured frequency point ω_k. Using equation (2.1) and assuming the force vector of unit magnitude, the displacement can be replaced by the receptance (FRF) and the input residual may equivalently be defined as:

$$\{\varepsilon_{input}\} = [Z_A(\omega_k, \{\varphi\})]\{\alpha_{X_i}(\omega_k)\} - \{1\}_i \tag{2.3}$$

where $\{1\}_i$ is unity at excitation coordinate i and zero elsewhere. Now, if an appropriate error model is available and the experimental dynamic stiffness matrix is expressed as $[Z_X(\omega_k, \{\varphi\})] = [Z_A(\omega_k)] + [\Delta Z(\omega_k, \{\varphi\})]$, then the problem of minimising the error of the forces can be reduced to solving:

$$[S]\{\Delta\varphi\} = \{\varepsilon\} \tag{2.4}$$

which is a linear set of equations with coefficient (sensitivity) matrix $[S]$, design parameter changes $\{\Delta\varphi\}$ and residual $\{\varepsilon\}$. Frequently, $[S]$ has more rows than columns and a pseudo-inverse is employed to solve equation (2.4).

Input error formulations are distinctively different to many other FRF model updating formulations in the sense that linear design parameters (e.g. E, ρ) remain linear in the

updating formulation. Cottin et al. (1984), however, showed that these formulations tend to give more biased parameter estimates than those estimates computed from model updating formulations derived from output residuals.

More detailed discussions of methods based on input residuals were presented by Fritzen (1986) and Natke (1988). Other contributions were proposed by Link (1990), Larsson and Sas (1992), Ibrahim et al. (1992) and D'Ambrogio et al. (1993).

2.2.2 Minimisation of Output Residuals

An intuitive alternative to input residual methods is the minimisation of the output residual. Here, one seeks to minimise the difference between the measured and predicted displacements is sought to be minimised:

$$\{\varepsilon_{output}\} = \{X_X(\omega_k)\} - \{X_A(\omega_k)\} \tag{2.5}$$

Assuming, as before, a unit magnitude force at coordinate i and zero elsewhere, the output residual is equivalent to:

$$\{\varepsilon_{output}\} = \{\alpha_{X_i}(\omega_k)\} - [Z_A(\omega_k, \{\varphi\})]^{-1} \{1\}_i \tag{2.6}$$

which can only be minimised as $[Z_A]$ approaches $[Z_X]$. As a result, if the error is modelled as $[Z_X(\omega_k, \{\varphi\})] = [Z_A(\omega_k)] + [\Delta Z(\omega_k, \{\varphi\})]$, the output residual can be reduced in the same fashion as the input residual using a linearised set of equations represented by $[S]\{\Delta\varphi\} = \{\varepsilon\}$.

Unlike the input residual, equation (2.6) defines the error between the measured and predicted FRF directly. Less attractive in this kind of formulations, however, is the non-linearity of the updating parameters caused by the inverse relationship between the design parameters, $\{\varphi\}$, and the response matrix, $[Z_A(\omega_k, \{\varphi\})]^{-1}$.

Representative methods based on the output residuals were proposed by Lin and Ewins (1990) and a similar method by Fritzen (1992). Further work was presented by Imregun et al. (1995) concluding with an experimental case study of a medium sized (500 DOFs) FE model in a companion paper (Imregun et al. 1995).

2.2.3 Coordinate Incompatibility

The size of FE models must be relative large to make reliable response predictions in the measured frequency range and it is is good practice to ensure that all modes in the spectrum have converged. Unless such a convergence check is conducted (by successively refining the mesh density), the predicted responses may not be representative and any subsequent updating calculation will fail to be physically meaningful.

Assuming that a representative FE model is available, one will often find that the number of eventual analytical DOFs exceeds the number of measured coordinates and, as a result, that FRF formulations based on both the input-residual and the output-residual cannot be solved directly. The residuals lack information about the unmeasured coordinates. The incompatibility between the number of measured DOFs and the number of analytical DOFs necessitates either the measurement vector to be expanded to N DOFs or the FE model be reduced to n measured DOFs. No matter how sophisticated the expansion or

reduction schemes may be, the incompleteness aspect in FRF model updating introduces numerical errors into the algorithms as an inevitable consequence. Experience has shown that condensation tools are generally more successful than expansion schemes used for measured data (Gysin 1990; O'Callahan et al. 1989; Ziaei Rad 1997). To pinpoint the success rate of model updating procedures handling incomplete sets of measurements, let us therefore introduce the incompleteness ratio defined by:

$$\mathrm{i}_r = \frac{n}{N} \tag{2.7}$$

where n is the number of measurements and N the number of DOFs in the FE model.

Larsson and Sas (1992) and Lammens (1995) used an exact dynamic reduction of the dynamic stiffness and receptance matrix at ω_k together with an updating algorithm derived from the input residuals. The change of dynamic stiffness terms due to changes in design parameters could be determined up to a cut-off frequency. Beyond the cut-off frequency discontinuities became apparent and consequently, limited the applicability of the method. Ziaei Rad (1997) adopted the same condensation technique and pointed out that the discontinuities of dynamic stiffness terms move towards zero frequency with increasing levels of condensation. It was shown that the smaller i_r, the narrower the band-width on the frequency scale in which design changes could be introduced to the FE model without running into a discontinuity (singularity). Case studies presented by Ziaei Rad (1997) did not go beyond a level of reduction of $\mathrm{i}_r = 1/10$.

As part of this work, similar experience was made with the so-called "exact dynamic condensation". However, the limitations of this reduction scheme were much more serious, especially in the light of applications of industrial size. The approach requires the reduction of the system at each selected (updating) frequency point and the computation of matrix inverses whose size is equal to the number of unmeasured (slave) coordinates. These calculations make the reduction scheme not only inefficient but may well exceed the hardware requirements available on the local computer. Such a reduction scheme is not only computationally intensive but also inherently limits the applicability of the reduced system as the cut-off frequency progressively moves towards zero as i_r gets smaller.

2.3 Problems Associated with Large FRF Updating Problems

The analysis and updating of large FE models is computationally very expensive and involves the solutions of systems of many thousand DOFs. Often, it is the computer itself which restricts the analysis of larger models and the analyst is usually wary about increasing the size of the model.

A basic requirement of model updating formulations is the compatibility between the measured and predicted dynamic properties and is to retain the integrity of the constitutive updating equations. Modal-based updating formulations seek to minimise the differences between the measured and predicted eigenvalues and sometimes, eigenvectors. The minimisation of the differences is performed on a mode-by-mode basis it is usually relatively simple to comply with the data requirements of the updating equations. For instance, having identified the predicted mode corresponding to the measured one, the inverse eigensensitivity method can be used to formulate the updating equation without compromising the integrity of the formulation.

This is different for most FRF model updating formulations. The minimisation of response residuals usually requires a one-to-one correspondence between the number of DOFs in the FE model, N, and the number of measurements, n. From a practical point of view, however, this requirement is difficult to satisfy as not all analytical DOFs can be measured. In these cases, numerical expansion or condensation schemes must be employed to comply with the constitutive updating equations. The missing response measurements, therefore, violate the integrity of many FRF formulations and the incompleteness aspect has clearly much stronger implications than compared to modal-based formulations.

It is a characteristic feature of large applications that the FE models are usually large and, more importantly, the number of available measurements is comparatively small. For model updating problems of industrial size, it is not unusual to encounter an incompleteness ratio in the region of $\mathrm{i}_r = 1/1000$ or smaller (Grafe 1997d; Grafe 1997a). The real challenge of updating large FE models is not so much the size of the models, as these can be solved by ever more powerful computers, but rather small incompleteness ratios, as defined by equation (2.7).

2.4 Modelling the Errors in the FE Model

Elementary to the success of model updating exercises is the localisation and quantification of inaccurate design parameters in the initial FE model. Within the framework of updating procedures, the modelling of the errors plays an integral part and delineates the changes in response due to the changes in physical properties of the structure that is being updated.

In the following, the traditional p-value formulation is discussed and a more physically representative error model is introduced.

2.4.1 The p-value Formulation

This very simplistic error model associates each element with a modification factor. The modification factors, the so-called p-values, are applied to the elemental stiffness, mass and damping matrices and the global system matrices are obtained as:

$$[M] = \sum_{i=1}^{N_m} p_m^i \, [M_i^e] \qquad [K] = \sum_{i=1}^{N_k} p_k^i \, [K_i^e] \tag{2.8}$$

$$[C] = \sum_{i=1}^{N_c} p_c^i \, [C_i^e] \qquad [D] = \sum_{i=1}^{N_d} p_d^i \, [D_i^e] \tag{2.9}$$

where the summation sign denotes matrix building and, some authors, designate the total number of p-values by N_p, where $N_p = N_m + N_k + N_c + N_d$.

It is customary to linearise the updating problem using a truncated Taylor series expansion to define the error between the experimental and analytical models. Using, for instance, an elemental mass matrix, the error is expressed as:

$$[\Delta M^e] = [M_X^e] - [M_A^e] = \frac{\partial \, [M_A^e]}{\partial \varphi_i} \Delta \varphi_i + O(\varphi_i^2) \tag{2.10}$$

where φ_i is the design parameter under consideration.

Now, if the p-value formulation defined by equations (2.8) and (2.9) is adopted, then the error is assumed to vary with changes in p_i and $p_i = \varphi_i$ in equation (2.10). Differentiating equations (2.8) and (2.9), the equivalent errors of (2.10) of the system matrices are found to be:

$$[\Delta M] = \sum_{i=1}^{N_m} \Delta p_m^i \, [M_i^e] \qquad [\Delta K] = \sum_{i=1}^{N_k} \Delta p_k^i \, [K_i^e] \tag{2.11}$$

$$[\Delta C] = \sum_{i=1}^{N_c} \Delta p_c^i \, [C_i^e] \qquad [\Delta D] = \sum_{i=1}^{N_d} \Delta p_d^i \, [D_i^e] \tag{2.12}$$

The p-values differences in equations (2.11) and (2.12) represent absolute design changes and indicate the location, i, of erroneous elements with their corresponding values different from zero. In the literature, Δp is sometimes referred to as zero-based p-value. Absolute changes, however, may differ considerably in magnitude from one updating parameter to another (e.g. $\Delta p_m^1 = 100 \; kg/m^3$ and $\Delta p_k^{10} = 10\,000\,000\,000 \; N/m^2$) and updating calculations may become numerically unbalanced or even ill-conditioned.

By far the more appropriate error model is the use of unity-based p-values. These p-values are normalised (non-dimensionalised) and indicate with their values different from zero the percentage change in p. The derivative in equation (2.10) is accordingly replaced by $\left(\varphi_i \frac{\partial [M_A^e]}{\partial \varphi_i}\right) \left(\frac{\Delta \varphi_i}{\varphi_i}\right)$ and equations (2.11) and (2.12) become:

$$[\Delta M] = \sum_{i=1}^{N_m} (1 + \frac{\Delta p_m^i}{p_m^i}) \, [M_i^e] \qquad [\Delta K] = \sum_{i=1}^{N_k} (1 + \frac{\Delta p_k^i}{p_k^i}) \, [K_i^e] \tag{2.13}$$

$$[\Delta C] = \sum_{i=1}^{N_c} (1 + \frac{\Delta p_c^i}{p_c^i}) \, [C_i^e] \qquad [\Delta D] = \sum_{i=1}^{N_d} (1 + \frac{\Delta p_d^i}{p_d^i}) \, [D_i^e] \tag{2.14}$$

where the magnitudes of the unit-based modifications are generally more homogeneous than those of the zero-based p-values (e.g. $\frac{\Delta p_m^1}{p_m^1} = 0.11$ and $\frac{\Delta p_k^{10}}{p_k^{10}} = 0.13$) and $(1 + \frac{\Delta p^i}{p^i})$ is the actual updating parameter. It is noteworthy that both the zero-based and unity-based p-value formulations are identical in the first iteration as the $p's$ in equations (2.8) and (2.9) are initially unity.

The use of a simple p-value error model is computationally very efficient and easy to implement. No numerical differentiation is required as the derivative is simply the elemental matrix itself and the response changes are introduced by just scaling the finite element matrices. However, the identified p-values have no physical meaning, unless the design parameters are truly global to the element matrices (e.g. E,ρ), and allow model changes to be introduced which are physically not representative.

2.4.2 Physically Representative Error Modelling

In an attempt to formulate a more physically representative error model, Grafe et al. (1997) decomposed the elemental matrices into a number of sub-matrices, each representing the design parameter being considered and the order with which the element entries are changing. Although the number of unknowns generally increases, a case study has shown the method's ability and proven that simple p-values are not appropriate for some

more local design parameters, especially in higher frequency regions. The localisation of the sub-matrices, however, was computationally inefficient.

A simpler approach will be introduced here. It is based on the work presented by Friswell and Mottershead (1995) who addressed the problem of updating "physical parameters" by using the Taylor series expansion (2.10) directly, i.e. not replacing φ_i by p_i. Updating parameters may then represent any non-linear design parameter of the elemental matrices in a linearised fashion and the identified errors truly represent the required design changes $\{\Delta\varphi\}$.

For simple finite elements, the derivatives of such updating parameters may be analytically derived. In general, however, the derivative in (2.10) of the element matrices must be computed using a numerical approximation. Using a second order differentiation scheme (Press et al. 1992), the derivative for an elemental mass matrix, for example, is obtained by:

$$\frac{\partial\left[M^e(\varphi_i)\right]}{\partial\varphi_i} \approx \frac{\left[M^e(\varphi_i+h)\right]-\left[M^e(\varphi_i-h)\right]}{2h} \tag{2.15}$$

where h is the perturbation (or step-length) of design parameter φ_i. Good experience was gained by setting h to 0.001% of the current value of φ_i. Better numerical accuracy can be obtained by using automatic adaption schemes of h although these were not found to be essential and are computationally more expensive. The approximate derivative (2.15) has been implemented into MATLAB-based (Mathworks 1997) tool box OPTIMA (Grafe 1997c) and the available updating parameters are documented in Appendix C.

Error models simulate the characteristics of likely error sources and define an "updating parameter" by a collection of finite elements and an associated design parameters. Typically, computed design changes are introduced on an element-by-element level and often, these discriminate between the mass, stiffness and damping matrices of that element with different modification factors. See, for instance, equations (2.8) and (2.9).

Concluding the above remarks, it is therefore proposed to define the error in the analytical model by contemplating the dynamic stiffness matrix as a whole. Unlike Friswell and Mottershead (1995), who distinguished between mass and stiffness errors, the error formulation adopted in this thesis is:

$$\left[\Delta Z(\omega)\right] = \sum_{i=1}^{N_\varphi}\left(1+\frac{\Delta\varphi_i}{\varphi_i}\right)\frac{\partial\left[Z(\omega)\right]}{\partial\varphi_i}\varphi_i \tag{2.16}$$

where N_φ is the number of updating parameters.

The unity-based updating parameter changes $\left(1+\frac{\Delta\varphi_i}{\varphi_i}\right)$, obtained from equation (2.16), are then used to modify the design parameters, $\{\varphi\}$, and to re-evaluate the corresponding finite elements. Therefore, by changing the design parameters directly, any updated FE model can be reconstructed by simply performing a new FE analysis using the identified changes in $\{\varphi\}$. The changes are not introduced by simply scaling element matrices nor is the connectivity pattern of the FE model destroyed.

2.5 The Response Function Method (RFM)

Among many other FRF model updating techniques, the **R**esponse **F**unction **M**ethod (RFM) proposed by Lin and Ewins (1990) can be considered as a representative example

and will be presented in the following. Unlike the original paper, where the method is derived from a mathematical identity, a derivation based on the system's dynamic properties is presented using the error model introduced in the previous section. This is followed by a discussion of the underlying principles and two numerical case studies to evaluate the method's capabilities.

2.5.1 Derivation of the RFM Formulation

The quintessence of the RFM model updating formulation is the assumption that the system representation of the FE model ($[M_A], [K_A], \cdots$) can be modified with an appropriate set of design parameter changes ($[\Delta M], [\Delta K], \cdots$) and that these changes lead to an updated FE model whose predicted FRFs are identical to the corresponding measurements. Like other FRF model updating algorithms, if the updated system matrices are denoted by $[M_X], [K_X], \cdots$, then the relations between the initial and updated FE model:

$$[M_X] = [\Delta M] + [M_A] \qquad [K_X] = [\Delta K] + [K_A] \tag{2.17}$$

$$[C_X] = [\Delta C] + [C_A] \qquad [D_X] = [\Delta D] + [D_A] \tag{2.18}$$

form the basis of the RFM algorithm.

As a direct consequence of the assumptions made in equations (2.17) and (2.18), the hypothesis can easily be extended to the dynamic response of the system so that:

$$\Big\{1\Big\}_i = \Big[-\omega^2 \Big[M_A\Big] + \mathrm{i}\,\omega \Big[C_A\Big] + \mathrm{i}\Big[D_A\Big] + \Big[K_A\Big]\Big] \Big\{\alpha_{A_i}(\omega)\Big\} \tag{2.19}$$

$$\Big\{1\Big\}_i = \Big[-\omega^2 \Big[M_X\Big] + \mathrm{i}\,\omega \Big[C_X\Big] + \mathrm{i}\Big[D_X\Big] + \Big[K_X\Big]\Big] \Big\{\alpha_{X_i}(\omega)\Big\} \tag{2.20}$$

where $\{1\}_i$ is unity at excitation DOF, i, and zero elsewhere. Vectors $\{\alpha_{Xi}(\omega)\}$ and $\{\alpha_{Ai}(\omega)\}$ are the receptances at excitation frequency ω.

Substituting equations (2.17) and (2.18) into equation (2.20) and using equation (2.19) one arrives at:

$$\Big[\Delta Z(\omega)\Big]\Big\{\alpha_{X_i}(\omega)\Big\} = \Big[Z_A(\omega)\Big]\Big\{\Big\{\alpha_{A_i}(\omega)\Big\} - \Big\{\alpha_{X_i}(\omega)\Big\}\Big\} \tag{2.21}$$

Equation (2.21) relates the residual between the measured and predicted response to the updating matrices $[\Delta M], [\Delta K], \cdots$ and it is a typical example of an input-residual formulation. The updating equation proposed by Lin and Ewins (1990), however, assumes the more classical output-residual format. Pre-multiplying equation (2.21) with $[\alpha_A(\omega)]$ from the LHS leads to:

$$\Big[\alpha_A(\omega)\Big]\Big[\Delta Z(\omega)\Big]\Big\{\alpha_{X_i}(\omega)\Big\} = \Big\{\alpha_{A_i}(\omega)\Big\} - \Big\{\alpha_{X_i}(\omega)\Big\} \tag{2.22}$$

Equation (2.22) is the basic equation of the RFM updating algorithm and, together with an appropriate model for the error matrices $[\Delta M], [\Delta K], \cdots$, can be solved by:

$$\Big[S\Big]\Big\{\Delta\varphi\Big\} = \Big\{\varepsilon\Big\} \tag{2.23}$$

where the coefficient matrix $[S]$ has N_φ columns obtained by calculating the LHS of equation (2.22) for each design parameter separately. The residual vector $\{\varepsilon\}$ represents the RHS of equation (2.22) and its size depends on the number of updating frequencies, N_{f_u}, and the number of measured coordinates, n.

Equation (2.22) indicates that $[S]$ and $\{\varepsilon\}$ are complex due to the complex nature of the measurements and, if damping is considered in the FE model, the complexity of the system matrices. As real design parameter changes are sought, the linear system of equations must be partitioned into:

$$\begin{bmatrix} \Re\Big[S\Big] \\ \Im\Big[S\Big] \end{bmatrix} \Big\{\Delta\varphi\Big\} = \begin{Bmatrix} \Re\Big\{\varepsilon\Big\} \\ \Im\Big\{\varepsilon\Big\} \end{Bmatrix} \tag{2.24}$$

where operators $\Re(.)$ and $\Im(.)$ address the real and imaginary part of the coefficient matrix and the residual. Hence, equation (2.24) has twice as many equations as equation (2.22).

A number of publications have demonstrated the method's performance when applied to small undamped FE models. Other publications include experimental case studies of lightly damped structures and argue that a complex-to-real conversion of the measurements is justified. In both cases the updating problem was solved by equation (2.22) using a pseudo-inverse.

Visser and Imregun (1991) addressed the problem of updating complex responses and the inherent incompatibility between the number of DOFs in the FE model and the number of measured coordinates. Unlike other FRF updating formulations, they replaced the unmeasured receptances of the LHS of equation (2.22) by their analytical counterparts and, after assembling the linear set of equations, deleted corresponding rows from equation (2.23). The solution of equation (2.24), however, was critical and led to slower convergence.

2.5.2 Discussion of the RFM Theory

As in many theoretical studies the understanding of the underlying assumptions, on which the working theory is based is vital for a successful application of the equations involved. During the derivation of the updating equation in the previous section, the assumptions made can be summarised as follows:

- **Error Existence:** the error between the measured and the predicted responses must be expressable in the form of $[\Delta M], [\Delta K], \cdots$,
- **Error Representation:** the error model employed must be able to arrive at the existing errors $[\Delta M], [\Delta K], \cdots$,
- **Signal-Noise:** for equations (2.19) and (2.20) to be identical, the measurement vector $\{\alpha_{X_i}(\omega)\}$ must be free of noise,
- **Co-ordinate Completeness:** from equation (2.20) onwards, all FE co-ordinates are assumed to be measured (i.e. $n = N$),
- **Updating Frequencies:** any frequency point away from resonance solves updating equation (2.22).

The majority of assumptions outlined above are common to many FRF model updating methods. To date, it is not possible to ensure that the FE model representing the structure under test is *update-able*. Whereas the estimation of the *validity* of an analytical model is commonly performed by using numerical means such as correlation coefficients, there is no safeguard that the configuration of the FE model is sufficiently close to that of the real structure. Correlation measures **quantify** the validity of the FE model but are unable to disclose the **quality** of the computational model. Even if the initial correlation is satisfactory, the quality of the FE model may be poor and the mechanisms leading to discrepancies between the measurements and the predictions may not be present in the FE model. Any further "improvements" to the FE model are physically not representative in these cases.

Unlike some other FRF model updating techniques (Larsson and Sas 1992), the RFM requires a full measurement vector (Visser 1992). This requirement is unrealistic as there are many FE DOFs which cannot be measured sufficiently accurately (e.g. rotational DOFs) or that are physically not accessible on the test structure. The resulting incompleteness gives rise to a number of difficulties and, in common with other updating techniques, there is a need to reduce the size of the FE model or to expand the measurement vector.

Another noteworthy feature of updating equation (2.22) is the remarkable similarity of its LHS to the analytical sensitivity of the receptance matrix (see also p. 69),

$$\frac{\partial\left[\alpha_A(\omega)\right]}{\partial\varphi} = -\left[\alpha_A(\omega)\right]\frac{\partial\left[Z(\omega)\right]}{\partial\varphi}\left[\alpha_A(\omega)\right] \tag{2.25}$$

where the sensitivity is seen to be a function of the dynamic stiffness matrix and of the receptance matrix itself, as is the LHS of equation (2.22).

Now, if the error in the dynamic stiffness matrix (2.22) is linearised such that:

$$[\Delta Z] = [Z_X] - [Z_A] = \frac{\partial [Z(\omega)]}{\partial \varphi} \Delta\varphi \tag{2.26}$$

and one formulates the RFM for frequency point ω_k and response and excitation coordinates are i and j, then equations (2.22) and (2.26) lead to:

$$\frac{\left(\alpha_{X_{ij}}(\omega_k)\right) - \left(\alpha_{A_{ij}}(\omega_k)\right)}{\Delta\varphi} = -\left\{\alpha_{A_j}(\omega_k)\right\}^T \frac{\partial \left[Z(\omega_k)\right]}{\partial \varphi} \left\{\alpha_{X_i}(\omega_k)\right\} \tag{2.27}$$

whereas the analytical sensitivity of the receptance at the same coordinates and frequency point assumes:

$$\frac{\partial \left(\alpha_{A_{ij}}(\omega_k)\right)}{\partial \varphi} = -\left\{\alpha_{A_j}(\omega_k)\right\}^T \frac{\partial \left[Z(\omega_k)\right]}{\partial \varphi} \left\{\alpha_{A_i}(\omega_k)\right\} \tag{2.28}$$

Equations (2.27) and (2.28) are very similar in the sense that both sides of each equation represent the rate of the response change for a unit change in the design parameter φ. In fact, as $\Delta\varphi$ becomes infinitesimal small, $\alpha_{X_{ij}}(\omega_k) \rightarrow \alpha_{A_{ij}}(\omega_k)$ and the finite difference in equation (2.27) becomes the derivative of the analytical receptance. Similarly, as the error between the measurements and the predictions vanishes, equations (2.27) and (2.28) become identical.

The characteristic slope of the sensitivities defined in equations (2.27) and (2.28) is shown in figure 2.1. It is seen that the sensitivity of the RFM method (2.27) manifests as a secant approximation while the sensitivity of the analytical receptance (2.28) is a tangent approximation. As the distance between the initial and true design parameter diminishes, the secant progresses towards the tangent and, correspondingly, the sensitivity of the RFM includes the sensitivity of the analytical receptance as a special case when $\Delta\varphi = 0$.

In general, however, model updating procedures are designed to minimise $\Delta\varphi$ and the difference is not so small that equations (2.27) and (2.28) are identical. Yet, from the definition of equations (2.27) and (2.28) some conclusions may be drawn about the convergence properties.

The use of sensitivities such as $\frac{\partial \alpha_{ij}(\varphi)}{\partial \varphi}$ may well be hindered by local irregularities. As $\alpha_{ij}(\varphi)$ approaches a resonant frequency, the secant approximation may pass through such uneven features and tends to converge faster. The characteristics of the secant method (RFM method) could explain erratic design parameter changes and the algorithm may allow jumps across local minima. The analytical sensitivities, on the other hand, could exhibit slower convergence properties with less erratic parameter changes in intermediate iterations. They also may come to rest at local minima.

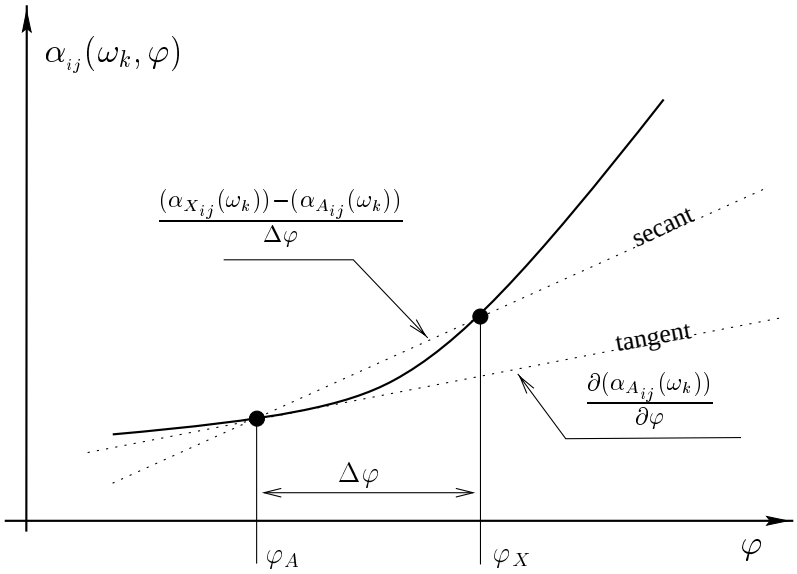

Figure 2.1: Geometrical interpretation of sensitivity used for the RFM updating approach (secant) and the ordinary FRF sensitivity (tangent)

2.5.3 Case Study: A Simple 4 DOFs Spring-Mass System

The 4 DOFs spring-mass system of figure 2.2 was analysed first and used to verify the theory of the RFM as well as to study the effects when the conformity of the basic updating equation is violated. Two nominally identical models were generated to simulate the *measurements* and the *FE model* respectively. All springs assumed a stiffness of 10 000 N/m^2 and the masses of both models were identically set to 1 kg except $m_2 = 1.3\ kg$ for the *analytical* model.

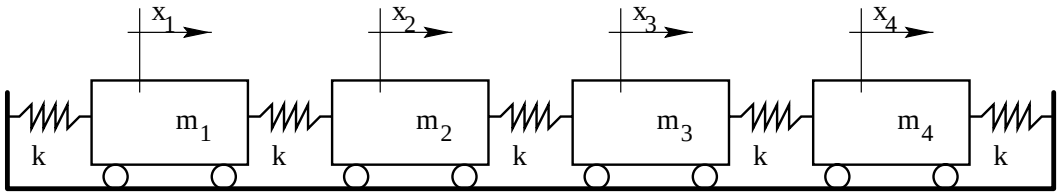

Figure 2.2: A simple 4 DOFs spring-mass system

The differences of the point receptances $\alpha_{11}(\omega)$ in the frequency range from $0\,Hz$ to $40\,Hz$ are displayed in figure 2.3.

Imposing no noise on the *measurements* and simulating all four receptances using a full-model solution ($[\alpha] = [Z]^{-1}$), it was found that, irrespective of the number and location of updating frequencies, the RFM correctly identified all masses of the *analytical* model to be unity. This does not include frequency points at resonances, as the response is not defined at these points.

In advancing the simulation towards more realistic data, the measurements were contaminated with $p = 5\%$ and $p = 10\%$ noise ε with a uniform distribution on the interval [0 , 1] such that:

$$\alpha_X(\omega) = \alpha_X(\omega)(1 + p \times \varepsilon) \quad \text{where} \quad p = 0.05, 0.10 \tag{2.29}$$

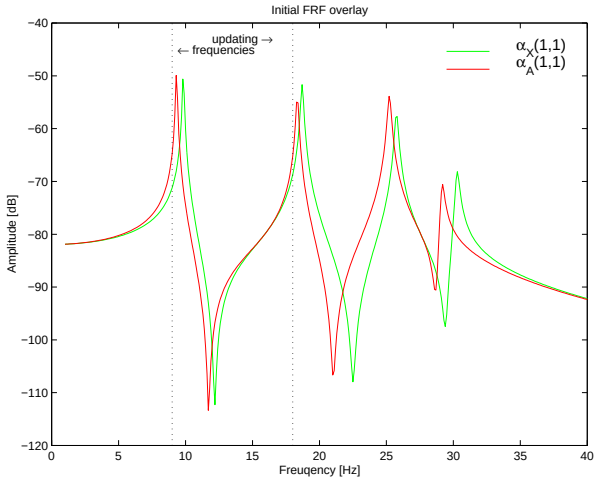

Figure 2.3: Initial FRF overlay of full 4 DOFs mass-spring system without noise

Figure 2.4 shows the computed changes in mass and it is seen that, although all four modes participate and all coordinates are included, the updated masses vary in magnitude from one noise level to another.

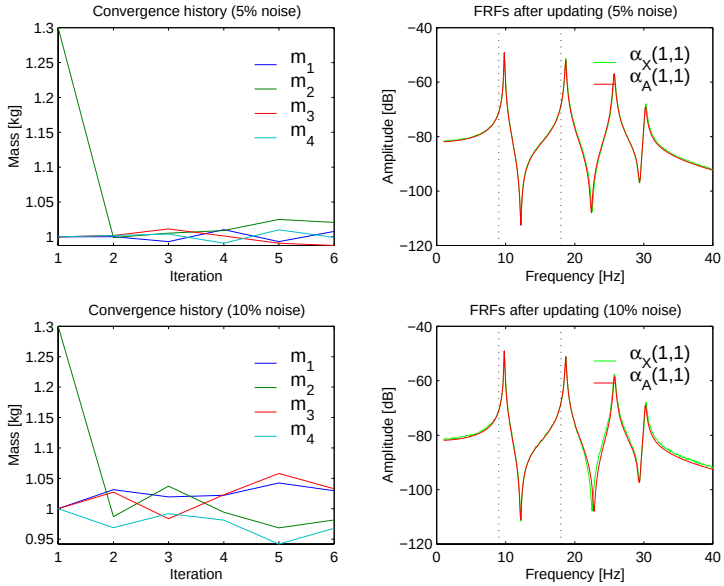

Figure 2.4: Updated 4 DOFs mass-spring system using a noise-contaminated and complete *measurements*

A second run reverted to noise-free data and the consequences of incomplete *measurements* were investigated. As before, two separate settings were explored. The first, and more complete, case was to see the effect of using three ($i_r = 3/4$) *measurements* and the second was to use just two *measurements* ($i_r = 1/2$). The results are presented in figure 2.5 and indicate, as for the previous case, non-unique parameter estimates especially for the case of $i_r = 1/2$.

As a third study, a complete and noise-free set of *measurements* was computed from a truncated number of modes. Again, the effect on the identification results was investigated

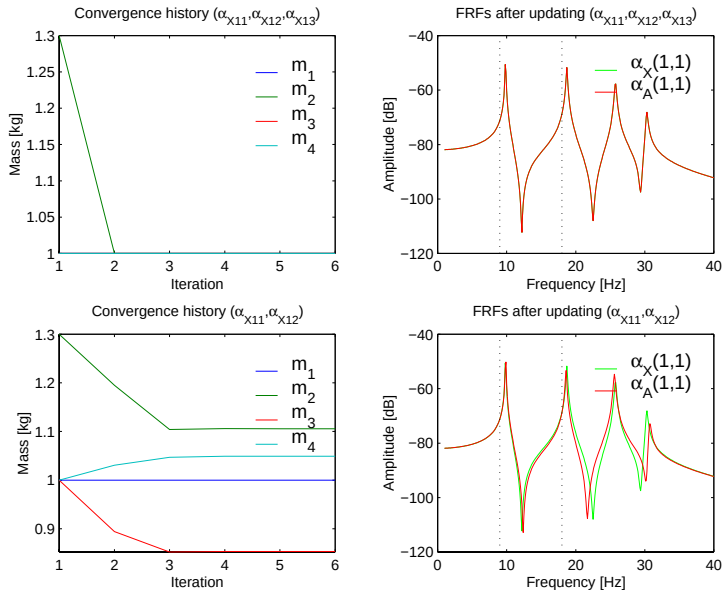

Figure 2.5: Updated 4 DOFs mass-spring system using noise-free and incomplete *measurements*

for two different conditions. In the first case, the *experimental* FRFs were computed from just two modes and the response was computed from three modes in the second study. In both cases, differences in the identified masses existed (fig. 2.6). This particular mechanism is further discussed in Section 2.6.

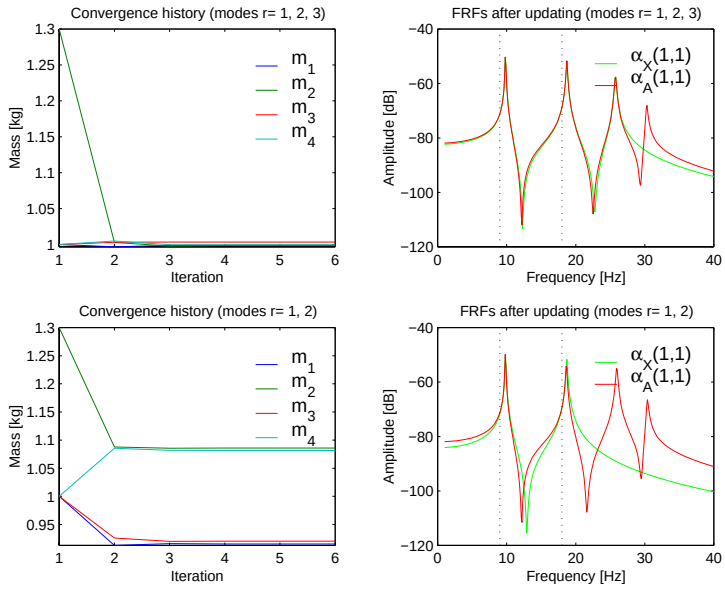

Figure 2.6: Updated 4 DOFs mass-spring system using noise free and complete *measurements* generated from a limited number of modes ($r < 4$)

A concluding case was run in which the combined effect of noise, incompleteness and model-order differences was analysed with respect to changing the updating frequencies. As a rule of thumb, many authors propose selecting updating frequencies close to resonances

(Ziaei Rad 1997; Visser 1992). Since both updating frequencies used so far were before the first two resonances, another case was run in which both of the updating frequencies were deliberately placed just after the resonances. In either case, the results, shown in figure 2.7, display dramatic changes in mass even though both frequency points are still around the resonances.

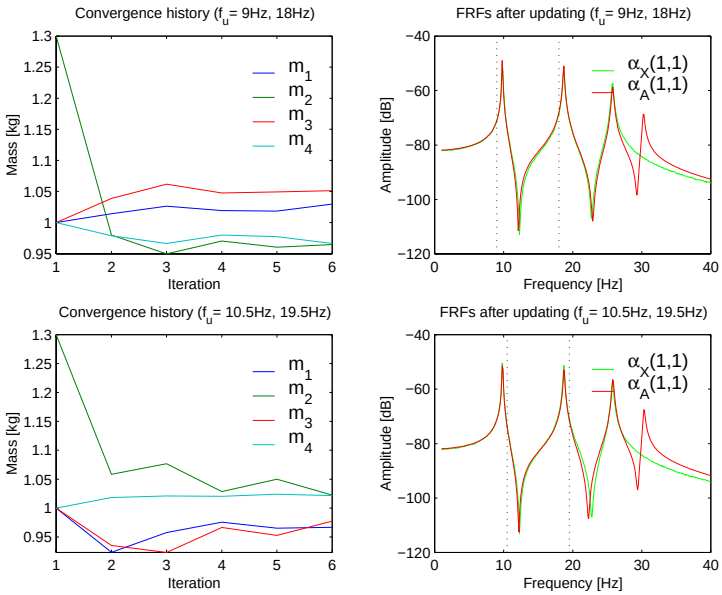

Figure 2.7: Updated 4 DOFs mass-spring system using three *measurements* $(\alpha_{X_1}1, \alpha_{X_1}2, \alpha_{X_1}3)$ generated from a three modes and contaminated with 5% noise: the affect of changing updating frequencies

All four cases have produced non-unique design parameter estimates resulting from the simulated imperfections of real measurements. The four updating parameters naturally led to a sensitivity matrix of mutually independent columns (because of the diagonal mass matrix) and have therefore not introduced biased parameter estimates resulting from a ill-conditioned sensitivity matrices. In more realistic circumstances, the updating parameters may be linearly dependent and further contribute to the non-uniqueness aspect in model updating.

2.5.4 Case Study: A Bent Plate with a Stiffening Bar

In closing the gap towards more realistic updating problems, a simple FE model of a bent plate with a strengthening bar was considered next. Figure 2.8 shows the FE model and its physical dimensions. For reasons of consistency, this particular FE model will be used throughout the thesis to benchmark further developments introduced in the following chapters.

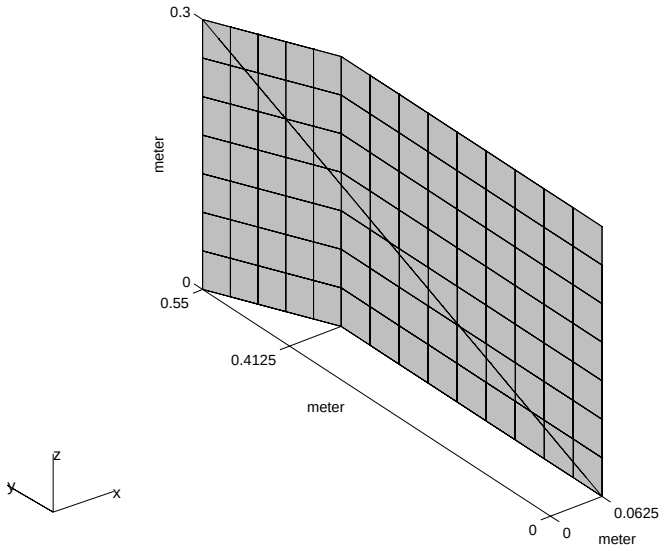

Figure 2.8: FE model of crooked plate with strengthening bar across diagonal and opposite corners

Type of Elements	E	ν	ρ	$t$hickness/$w$idth
98 quadrilateral shell elements	$2.11 \times 10^{11} \frac{N}{m^2}$	0.3	$7900 \frac{kg}{m^3}$	$t = 1.4\,mm$
25 Timoshenko beam elements	$2.11 \times 10^{11} \frac{N}{m^2}$	0.3	$7900 \frac{kg}{m^3}$	$w = 5.5\,mm$

Table 2.1: Material property table of FE model with shell elements of constant thickness t and Timoshenko beams with square cross-sectional area of width w

The discretised model of the structure shown in figure 2.8 has 864 DOFs and consists of 25 Timoshenko beam elements with a square cross-section and 98 4-noded shell elements of constant thickness. The nominal properties of the shell and beam elements are given in table 2.1 and serve as that of the *measured* structure.

The Young's modulus, E, of selected shell elements was increased by 30% for the erroneous FE model. In all, there were $N_\varphi = 14$ updating parameters of which each is pointing at a strip of seven shell elements together with material property E. Both, the erroneous shell elements and the location of the $N_\varphi = 14$ design parameters are shown in figure 2.9.

Concluding the discussion of the RFM in Section 2.5.2, the initial objective was to validate the RFM with a complete set of noise-free *measurements* on this structure. The FRFs were computed from a full modal solution and any selected frequency point (except resonance) correctly identified and quantified the erroneous shell elements. The theoretical framework of the RFM has therefore proven to be correct as long as none of the restrictions listed in Section 2.5.2 are encountered.

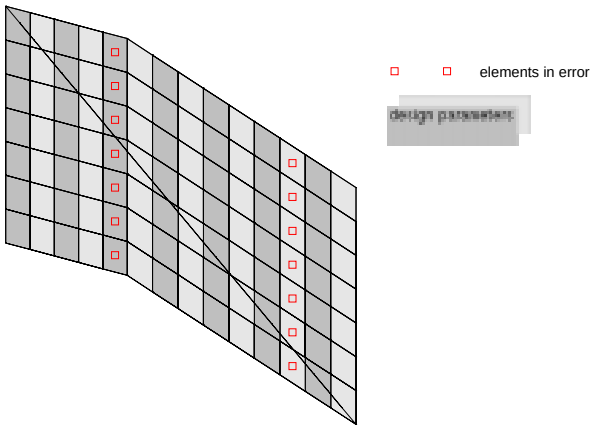

Figure 2.9: Location of updating parameters and of elements in error

Without changing the parameters of the initial *measurement* and *analytical* model, the same study was repeated. This time, however, 30% perturbation in thickness of the shell elements was introduced and, accordingly, it was sought to identify the thickness of $N_\varphi = 14$ groups of shell elements. Using the improved error model representation, as introduced with equation (2.16), the errors were again correctly identified. This time, however, full convergence was reached after only two iterations.

Under perfect conditions, therefore, the RFM is able to identify the erroneous shell elements. When perturbing and updating Young's modulus E, the updating algorithm converged immediately. If, however, the selected design parameter changes the dynamic stiffness matrix non-linearly, the updating computations take more than one iteration. For non-linear design parameters, such as the shell element thickness t, the number of iterations to convergence is a function of the level of perturbation between the initial and correct model.

Figure 2.10 shows the initial FRF overlay between *measurement* $\alpha_{X_{11}}(\omega)$ and *prediction* $\alpha_{A_{11}}(\omega)$ for a perturbation of 30% in Young's modulus E at the elements indicated in figure 2.9 (see figure 2.12 for the position of coordinate number 1). The FRF overlay shows that both responses correlate exceptionally well. In fact, one may be tempted to assume that the differences in spatial properties are insignificant and convergence be achieved easily.

Based on these relatively small perturbations in response, the coordinate incompleteness aspect was investigated next. The measurements were restricted to the DOFs in the x-direction, and since every node has 6 DOFs, only $\mathrm{i}_r = 1/6$ of the complete *measurement* vector was provided. No other restrictions were placed on the *measurements* and a updating frequency was arbitrarily selected at $40\,Hz$.

The updating computation were stopped after ten iterations and the results of the computations can be seen in figure 2.11. After seven iterations, the computations had converged and subsequent changes to the updating parameters were of negligible magnitude. The updated FRF $\alpha_{A_{11}}(\omega)$ is very close to its *measured* counterpart and the response has been successfully improved. However, the identified design parameter changes are biased and none of the updating parameters is close to the correct values. It was observed that some

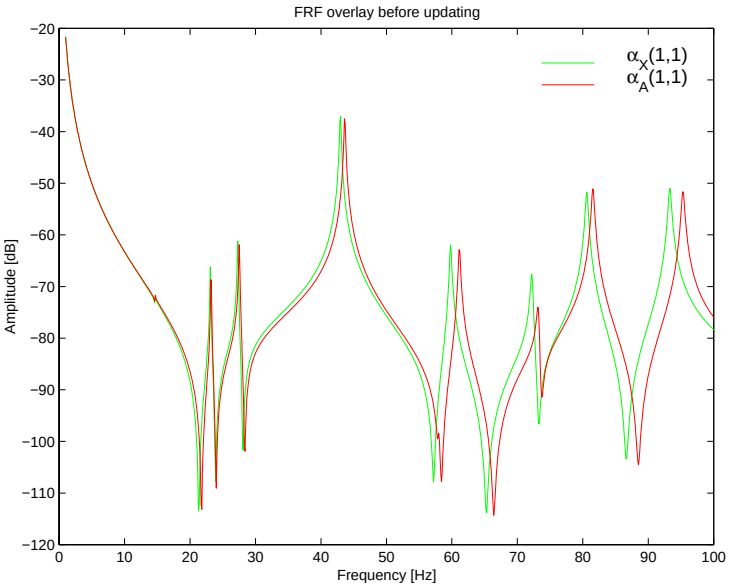

Figure 2.10: Initial FRF overlay of *measured* and *predicted* responses of the structure shown in figure 2.8 (30% perturbation in E)

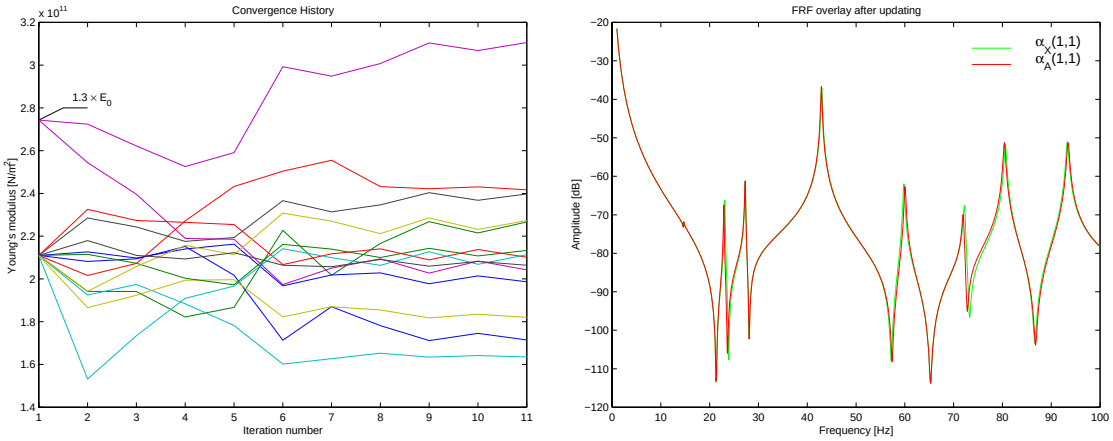

Figure 2.11: Overlay of point FRFs and convergence history after updating the *analytical* model using all *measured* DOFs in x-direction

of the "corrected" updating parameters were in error by up to 50% in comparison with the nominal value.

Since the incompleteness aspect is a dominant factor for problems of industrial size, the same computations were repeated with an even smaller number of *measurements*. This time, a total of 30 DOFs in the x-direction was used, the locations being shown in figure 2.12.

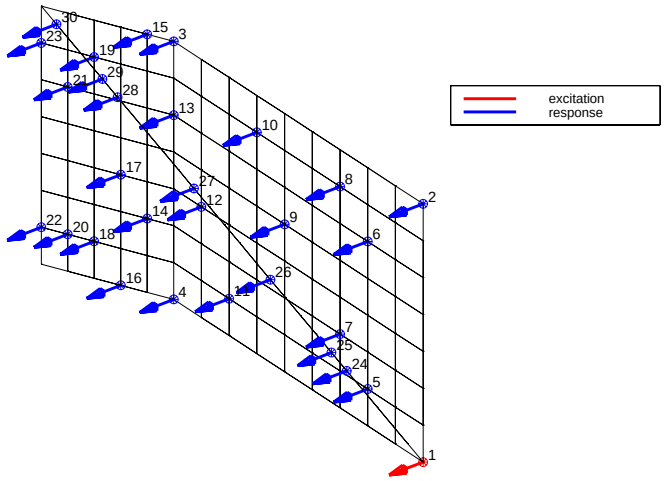

Figure 2.12: 30 arbitrarily selected *measurement* DOFs in x-direction

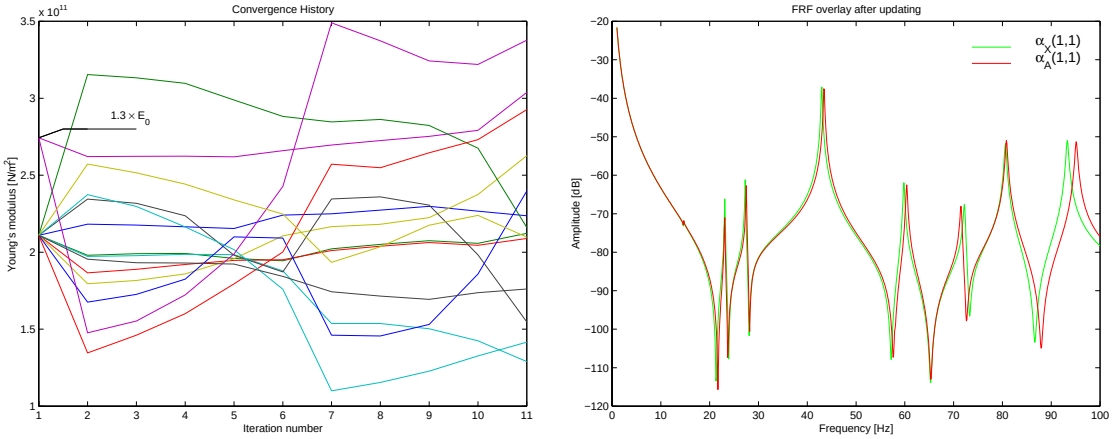

Figure 2.13: Overlay of point FRFs and convergence history after updating the *analytical* model using 30 *measurements* in x-direction

As before, the updating calculation were performed at one frequency point (40 Hz) and the Young's modulus was sought to be identified for $N_\varphi = 14$ design parameters. After ten iterations the solution to this over-determined problem ($[S]_{m\times n} : m = 30, n = 14$) was stopped and the results are displayed in figure 2.13.

A deterioration from the previous case of 144 *measurements* was expected for incompleteness ratio of $i_r \approx 1/30$. In this particular case, where the initial correlation was very good, better estimates might have been achieved simply by selecting more frequency points. The selection of frequency points, however, is itself a difficult subject and was disregarded here

since it is still unknown what particular frequency points are better suited in FRF model updating. However, the second simulation confirms that, in general, more measurements lead to less biased estimation results.

In line with the above conclusions, it is therefore not surprising to see that the FRF overlay is not as good as for the previous case; nor are the design parameters any closer to the correct setting of the *measurement* model. The convergence history indicates that the parameters never converge and, even after nine iterations, significant changes are still visible. Extrapolating this finding, the number of included *measurements* is not only crucial for the quality of estimation results but can also stop the algorithm from converging altogether if the incompleteness ratio n/N is too small.

In fact, the application of the RFM on industrial-sized problems was reported by Grafe (1997d) and Grafe (1997a) and it was found that neither convergence nor any improvement in response were obtained for an incompleteness ratio of about $\mathrm{i}_r = 1/1000$. Imregun et al. (1995) came to the same conclusions on a much smaller case study of 90 DOFs using 15 beam elements. It was shown that if $\mathrm{i}_r < 5/90$, the solution is unstable and the simulated error cannot be identified.

2.6 Non-Unique Parameter Estimations

The previous two case studies have shown that simulated test data lead to case-dependent parameter estimates. Even when data incompleteness, noise contamination and the band-limited nature of measurements were simulated in isolation from each other, the computations resulted in different parameter estimates, i.e. the parameter estimates were not unique.

For a given set of measurements, updating parameter estimates will also vary with:

- the location of the measured DOFs (while n is constant)
- the location and/or number of updating frequencies
- the location and/or number of updating parameters

This section investigates this non-uniqueness of results in a mathematical context. The derivations show that there is usually an unlimited number of solutions to updating problems resulting from:

- ill-conditioned sensitivity matrices $[S]$
- band-limited measurements

In either case, the non-uniqueness of the parameter estimates can be expressed as the sum of the actual solution obtained and a family of non-unique corrections.

2.6.1 The Conditions Leading to Non-Unique Solutions

In the preceding sections, the model updating problem was discussed for general FE models and the RFM formulation was introduced as:

$$\big[\alpha_A(\omega)\big]\big[\Delta Z(\omega)\big]\big\{\alpha_{X_i}(\omega)\big\} = \big\{\alpha_{A_i}(\omega)\big\} - \big\{\alpha_{X_i}(\omega)\big\} \tag{2.30}$$

where, as before, an N-DOF FE model is excited at co-ordinate, i, and $\big[\Delta Z(\omega)\big]$ is the error in terms of the dynamic stiffness matrix.

Condition 1

Assuming there exist a family of non-zero matrices $[\hat{Z}]$ which can be added to $[\Delta Z(\omega)]$ without changing the validity of equation (2.30), one can write:

$$[\alpha_A(\omega)][\hat{Z}]\{\alpha_{X_i}(\omega)\} = \{0\} \tag{2.31}$$

The non-trivial solutions of equation (2.31) can therefore be stated as:

$$[\alpha_A(\omega)][\hat{Z}] = [0] \quad \text{and} \quad [\hat{Z}]\{\alpha_{X_i}(\omega)\} = \{0\} \tag{2.32}$$

Condition 2

Equation (2.30) yields a set of linear equations of the form:

$$[S]\{\Delta p\} = \{\varepsilon\} \tag{2.33}$$

where the size of the coefficient matrix, $[S]$, is a function of the number of p-values, N_p, the number of measurements included, n, and the number of updating frequency points considered, N_{f_u}. Equation (2.33) expresses the errors in the FE model by the differences in the p-values, $\{\Delta p\}$.

In line with the first condition, the solution of equation (2.33) does also not necessarily produce "the" answer to the updating problem. This is the case if there exist a family of non-zero parameter changes, $\{\hat{p}\}$, satisfying the equation:

$$[S]\{\hat{p}\} = \{0\} \tag{2.34}$$

As for Condition 1, $\{\hat{p}\}$ can be added to $\{\Delta p\}$ and equation (2.33) will still be satisfied.

2.6.2 The Nullspace of the Sensitivity Matrix - Condition 1

It is widely known that the coefficient matrix $[S]$ in equation (2.33) is prone to ill-conditioning and that this set of linear equations is frequently over-determined. Among other techniques, equation (2.33) can be solved by using the **S**ingular **V**alue **D**ecomposition (SVD),

$$[S] = [U][\Sigma][V]^T \tag{2.35}$$

such that,

$$\{\Delta p\} = \left[[V][\Sigma]^{-1}[U]^T\right]\{\varepsilon\} \tag{2.36}$$

The SVD distinguishes itself from many other methods for solving linear least-squares problems with its diagnostic capabilities of rank-deficient systems (Press et al, 1992).

For rank-deficient systems (rank $r \ll N_p$), the complementary space of the range is called *nullspace*. The nullspace can be thought of as the subspace of $\{\Delta p\}$ that is mapped to zero. Since the SVD explicitly constructs an orthonormal basis for the nullspace with the columns of $[V]$ whose same numbered singular values σ_j of the spectral matrix $[\Sigma]$ are zero (or close to zero), any such vector $\{v_j\}$ is mapped by $[S]$ to zero:

$$[S]\{v_j\} = \{0\} \quad \text{for} \quad j = r+1, r+2, \cdots N_p \tag{2.37}$$

where, as before, r is the rank of $[S]$ and N_p the number of columns (p-values).

Therefore, for poorly conditioned and singular sensitivity matrices, $[S]$, the condition expressed by (2.34) can be readily associated with:

$$\{\hat{p}\} = \sum_{j=r+1}^{N_p} \kappa_j \{v_j\} \tag{2.38}$$

where κ_j is a scalar constant. Equation (2.38) expresses an infinite number of solutions to equation (2.33) and therefore identifies the sub-space which leads to non-unique parameters estimates if sensitivity matrix $[S]$ is ill-conditioned.

This purely numerical aspect of ill-conditioning, typically found in inverse problems, does not explain the existence of non-unique parameter estimates entirely. The following section discusses argument from an engineering point of view, namely the fact that updating is performed on a band-limited frequency range.

2.6.3 Band-Limited Updating Analysis - Condition 2

Updating is performed in a pre-defined frequency range and the response is dominated by the modes residing in this spectrum but it is also affected by some out-of-range modes. If the number of modes contributing to the measured and predicted response are designated by m_X and m_A respectively, and the receptances in equations (2.32) are expressed by equivalent modal summations then,

$$\left[\sum_{j=1}^{m_A} \frac{1}{\omega_{A_j}^2 - \omega^2} \left[\{\phi_A^R\}_j \{\phi_A^R\}_j^T\right]\right] \left[\hat{Z}\right] = [0] \tag{2.39}$$

and

$$\left[\hat{Z}\right] \left\{ \left[\Phi_X^R\right] \left\{ \frac{\phi_{X_{i1}}^R}{\omega_{X_1}^2 - \omega^2}, \cdots \frac{\phi_{X_{ij}}^R}{\omega_{X_j}^2 - \omega^2}, \cdots \frac{\phi_{X_{im_X}}^R}{\omega_{X_{m_X}}^2 - \omega^2} \right\}_{1\times m_X}^T \right\} = \{0\} \tag{2.40}$$

using the right eigenvector matrices of the analytical and experimental models, $[\Phi_X^R]$ and $[\Phi_A^R]$. The band-limited nature of updating problems is represented by m_X and m_A.

A formal definition of left and right eigenvectors is given in Appendix A.2 and shows that these always obey the orthogonal relationship:

$$\left[\Phi^R\right]^T \left[\Phi^L\right] = \left[\begin{smallmatrix} & \\ & I \end{smallmatrix}\right] \tag{2.41}$$

where $[\Phi]$ designates the mass-normalised eigenvector matrix.

Using the orthogonality properties of the identified mode shapes:

$$\left[\Phi^R\right]^T \left[M\right] \left[\Phi^R\right] = \left[\begin{smallmatrix} & \\ & I \end{smallmatrix}\right] \tag{2.42}$$

the left eigenvectors are identified as:

$$\left[\Phi^L\right] = \left[M\right] \left[\Phi^R\right] \tag{2.43}$$

In other words, the eigenvectors of the system are said to be "orthogonal with respect to mass" (Ewins 1984).

Because of this inverse relationship between the left and right eigenvectors, both conditions, (2.39) and (2.40), can be satisfied by using the sub-space spanned by the left eigenvectors. That is, if $[\hat{Z}]$ is expressed by the left eigenvectors of the out of range modes and substituted into equation (2.39):

$$\left[\sum_{j=1}^{m_A} \frac{1}{\omega_{A_j}^2 - \omega^2} \left[\left\{\phi_A^R\right\}_j \left\{\phi_A^R\right\}_j^T\right]\right] \left[\sum_{i=m_A+1}^{N} \left\{\phi_A^L\right\}_i \left\{\phi_A^L\right\}_i^T\right] = [0] \tag{2.44}$$

and equation (2.40) becomes accordingly:

$$\left[\sum_{i=m_X+1}^{\infty} \left\{\phi_X^L\right\}_i \left\{\phi_X^L\right\}_i^T\right] \left\{\left[\Phi_X^R\right] \left\{\frac{\phi_{X_{i1}}^R}{\omega_{X_1}^2 - \omega^2}, \cdots \frac{\phi_{X_{im_X}}^R}{\omega_{X_{m_X}}^2 - \omega^2}\right\}_{1\times m_X}^T\right\} = \{0\} \tag{2.45}$$

where the operations $\left\{\phi^L\right\}_i^T \left\{\phi^R\right\}_j$ are seen to equate to zero as $i \neq j$.

If the non-unique correction matrices of equation (2.44) and (2.45) are further distinguished by $[\hat{Z}]_1$ and $[\hat{Z}]_2$:

$$\left[\hat{Z}\right]_1 = \left[\sum_{i=m_A+1}^{N} \kappa_i \left\{\phi_A^L\right\}_i \left\{\phi_A^L\right\}_i^T\right] \tag{2.46}$$

$$\left[\hat{Z}\right]_2 = \left[\sum_{i=m_X+1}^{\infty} \kappa_i \left\{\phi_X^L\right\}_i \left\{\phi_X^L\right\}_i^T\right] \tag{2.47}$$

then (2.46) accounts for the truncation error of the analytical model and (2.47) reflects the non-unique parameter estimates caused by the band-limited nature of measurements. The scalar constant κ_i indicates the existence of a multiplicity of solutions. Therefore, a similar nullspace has been identified which leads to a multiplicity of solutions, as in equation (2.38).

At this stage, it is interesting to reflect on the discussion about "uniqueness" in the book by Friswell and Mottershead (1995). Here the question is raised of whether the existence of a solution necessarily results in physically meaningful parameter estimates. Using the system stiffness matrix as an example, they showed that:

$$[K]^{-1} = \sum_r \frac{1}{\omega_r^2} \left\{\phi_r^R\right\} \left\{\phi_r^R\right\}^T \qquad [K] = \sum_r \omega_r^2 [M] \left\{\phi_r^R\right\} \left\{\phi_r^R\right\}^T [M] \tag{2.48}$$

where the second equation of (2.48) demonstrates that $[K]$ is constructed from the left eigenvectors (eqn. (2.43)). Although the flexibility terms may be estimated very accurately by just using the lower modes, the stiffness matrix is dominated by the higher modes which are, in general, not available. Therefore, unless all modes are included, the stiffness matrix cannot be uniquely identified.

2.6.4 Numerical Demonstration of Phenomena

A small numerical example will be used to demonstrate the detrimental effect of truncation error on the uniqueness of the updating results. The 4 DOF system pictured in figure 2.2 has four masses of $1kg$ in magnitude. The simulated experimental responses were computed from the same nominal model but with $m_2 = 1.3kg$. Four successive initial estimates of the error in mass between the analytical and *experimental* model were then computed. Each time, the four *measurements* were computed from a decreasing number of modes ($m = 4, 3, 2, 1$) whereas the analytical predictions were computed from a full modal solution. The results of this case study are presented in figure 2.2.

In the context of the above outlined error mechanism, the frequency region of interest was presumed to be from $0Hz$ to about $12Hz$ and embodied the band-limited nature of the model updating calculation. All remaining modes beyond 12 Hz should be thought of as being modes which participate very weakly in the *measured* FRFs. This assumption is, of course, not realistic for such a low order-model but it serves the purpose to demonstrate the effect of the out-of-range modes on the parameter estimation results.

Throughout the numerical simulation of the phenomena, the results have confirmed the previously derived model for non-unique parameter estimates. The fewer modes which were included for simulating $\alpha_X(1,1)$ the worse were the parameter estimates after one iteration. Only when the complete *measurement* was used, i.e. there were no "free" left eigenvectors whose corresponding right eigenvectors did not participate in the response, a **unique** result was obtained in the form of a correct initial estimate.

Probably the most illustrative is the case where $\alpha_X(1,1)$ is composed of three (right) modes. In this case, very little difference is visible in the "complete" *measurement* and it is not obvious why the results should not be liberated from the effects of the out-of-band modes. Yet, the computed design changes were not unique because of the presence of the updating matrix $[\Delta Z]_2$, as discussed before.

It should be noted that this particular numerical example addresses the effects of band-limited *measurements* only. The resulting non-unique updating matrices have been designated by $[\Delta Z]_2$ (eqn. (2.47)) and lead to biased design parameter estimates without the effect of $[\Delta Z]_1$ (eqn. (2.46)). To illustrate the combined effect of both $[\Delta Z]_1$ and $[\Delta Z]_2$, the changes in mass were estimated from the *measurements*, $\alpha_X(1,1)$, and *predictions*, $\alpha_A(1,1)$, by computing them from 3 modes only. The identified changes in mass were found to be:

$$[\Delta Z] = \begin{bmatrix} -0.08 & 0 & 0 & 0 \\ 0 & -0.22 & 0 & 0 \\ 0 & 0 & -0.07 & 0 \\ 0 & 0 & 0 & +0.03 \end{bmatrix} \tag{2.49}$$

instead of the correct differences in the diagonal elements $\Delta m_1 = 0.0$,
$\Delta m_2 = -0.3$, $\Delta m_3 = 0.0$, $\Delta m_4 = 0.0$.

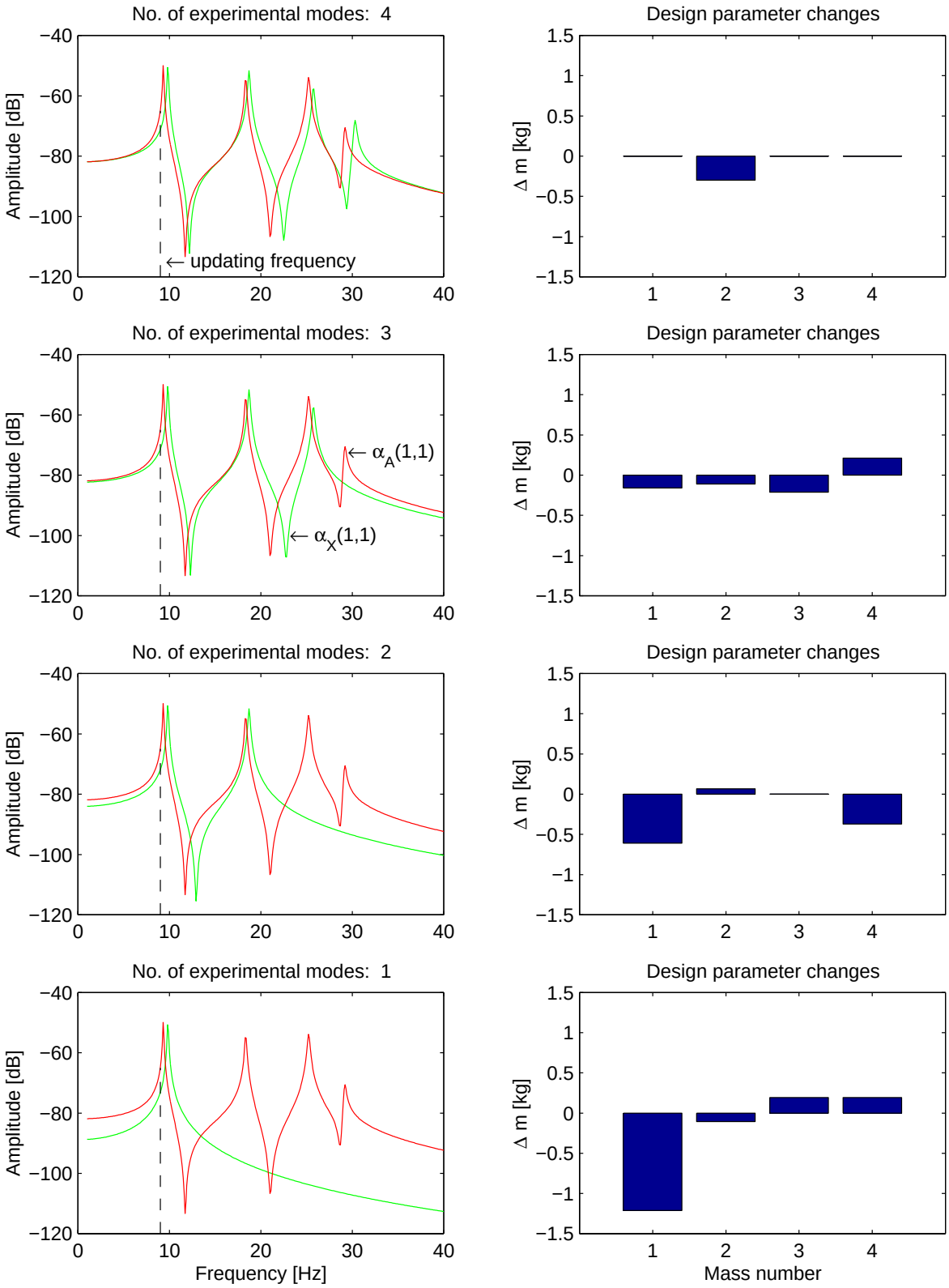

Figure 2.14: Simulation of band-limited measurements and the resulting non-unique design parameter estimates due to the effect of left out-of-band modes

2.7 Concluding Remarks

- The general principles of FRF model updating algorithms were discussed and classified into methods based on *input-residuals* and *output-residuals*. The discussion of the algorithms showed that the demands put on measurements are difficult, if not impossible, to meet. The incompleteness ratio (eqn. (2.7)) was introduced to measure the performance of various techniques and the literature showed that the success rate of FRF model updating techniques deteriorates with decreasing incompleteness ratio as an increasing level of information information is missing.
- The more traditional p-value formulation to model the errors in the FE model was reviewed and it was argued that such an error representation inherently fails to introduce model changes in a physically representative manner. As a result of the insufficiency of the p-values, is was suggested to employ a physically representative parameterisation which is closely in line with the one proposed by Friswell and Mottershead (1995). Instead of using design parameters associated with mass, stiffness and damping matrices, the proposed representation necessitates the calculation of numerical sensitivities of the dynamic stiffness matrix and recomputes new finite elements after each iteration.
- The RFM was presented as a representative response-based updating technique. During the derivation, both types of *input-residual* and *output-residual* formats were identified. Although the RFM was originally derived from a mathematical identity, the method was identified to be a sensitivity-based FRF algorithm and the sensitivities represent a secant approximation. A systematic analysis of the method's ability to update a FE model followed and the incompleteness aspect was identified as the most limiting factor. All other possible imperfections in measurements also led to non-unique parameter estimates.
- In an attempt to explain the non-uniqueness aspect of computed design parameter changes, three possible mechanisms were derived which lead to an infinite number of solutions. Non-unique parameter estimates are not only obtained for ill-conditioned sensitivity matrices $[S]$, for a selection of linearly dependent updating parameters, but also in cases where band-limited measurements are employed and/or a truncated modal model is used to construct the response matrix. All three of the origins are almost bound to happen when applying the RFM to (large) FE models.

Chapter 3

Substructuring and Component Mode Synthesis

3.1 Introduction

With the advent of digital computers, an increasing number of engineering structures are routinely analysed using numerical tools such as the finite element method. Ever-increasing computing power permits the solution of continuously larger FE models. As computer performance advances rapidly, there is a growing interest in solving even larger problems, such as an FE model of a whole automotive car assembly, and the demand put on computers seems to out-pace the hardware advances. Comprehensive models may contain so many DOFs that they cannot be handled directly on even the largest of modern computers.

Modern design cycles are of an iterative nature and FE models frequently go through several cycles of adjustments before the design meets pre-set criteria. In the initial stages of the design process, adjustments commonly incorporate local design changes, such as mesh refinements, and improvements are often based on engineering judgement and experience. As the mathematical design progresses, more elaborate tools are facilitated to validate and improve the quality of the FE model involving numerous re-analysis computations.

Substructuring and modal synthesis methods allow considerable reduction of the system's size and approximation of the system response by analysing a number of much smaller problems. Repetitive computations of sub-structured models are more economical and only take a fraction of the time required for a direct solution. Modal synthesis methods also allow the analysis of much bigger problems which could not have been solved otherwise on the computer available.

Irrespective of the computational benefits of modal synthesis techniques, it will be shown that these numerical tools can be used to satisfy a key requirement in FRF model updating, namely the need to bring about the incompleteness ratio i_r (eqn. 2.7, p. 23) closer to unity while retaining a good level of accuracy of the predicted responses. A systematic derivation of classical modal synthesis methods will highlight the physical meaning of the component modes used to reduce individual sub-structures and the presentation of three modal synthesis methods demonstrates the method's ability to condense large FE models which are otherwise very expensive, if not impossible, to reduce using conventional condensation schemes (Guyan 1965).

3.2 Motivation of Substructuring Techniques

Although substructuring and component mode synthesis (CMS) techniques are primarily employed for improved computational efficiency these days, substructuring techniques find their origin in the problem of coupling components of FE models. In the early 1960s, many sub-components of structures were designed and analysed separately (e.g. different companies/analysts/computers) but increasing interest was placed on the overall performance of the full assembly. Since no tools were available to analyse the structure as a whole at that time (Seshu 1997), techniques started to emerge to interface individual components on a much reduced basis to accommodate the limited computer capabilities and platforms. Originally, therefore, sub-structures were physically independent components and only part of a larger assembly. Generally, however, the partitions may be induced from a mathematical point of view, e.g. a group of finite elements, and an overall system reduction is achieved by analysing and reducing each individual sub-structure. Such mathematically induced partitions, for instance, could represents those parts of an FE model which need to be updated.

Apart from the obvious computational advantages of reduced FE models, the need to analyse each sub-structure independently from each other makes the computation ideally suitable for parallel processing (Hemez 1997a). As the majority of CPU time is consumed by analysing the individual sub-structures (approximately 90 % of the full analysis time), a parallelisation of the computation would further reduce the computation time.

Other advantages include the possible inclusion of non-linear finite elements at designated coordinates located on the interfaces between two adjacent components. By doing this, the required non-linear computation is kept to a minimum while the remaining structure, i.e. the sub-structures, are solved in linear fashion.

Because CMS techniques have primarily been developed as a tool to interface different FE models on the basis of computed dynamic properties, most methods allow the direct integration of dynamic testing results also. The reduced model representation does not need to be purely analytical.

3.3 Underlying Theoretical Principles

Substructuring and component mode synthesis (CMS) methods consist of three fundamental steps: **1**) the definition of the sub-structures, **2**) the definition of the component modes, and **3**) the coupling of the reduced components to represent the full system. Before any detailed analysis can be performed, a formal distinction is made between different sets of co-ordinates which will be defined in the following.

Sub-structures, or components (Craig Jr. 1987), are connected to one or more adjacent sub-structures at a number of *junction* DOFs (JDOFs). The remaining set of co-ordinates are referred to *internal* or *interior* DOFs (IDOFs) and do not interact with any other part of the FE model, as can be seen in figure 3.1.

Junction DOFs are those co-ordinates at which the sub-structures interact and compatibility constraints must be obeyed. Specifically, the compatibility constraints have to be satisfied at those JDOFs which interface a common number of components. These sections of interfaces are accordingly treated as a separate mathematical entity and referred to as *boundaries*. In line with the annotation of figure 3.1, it is convenient to designate N_s as the total number of sub-structures in the assembly and N_b as the number of boundaries.

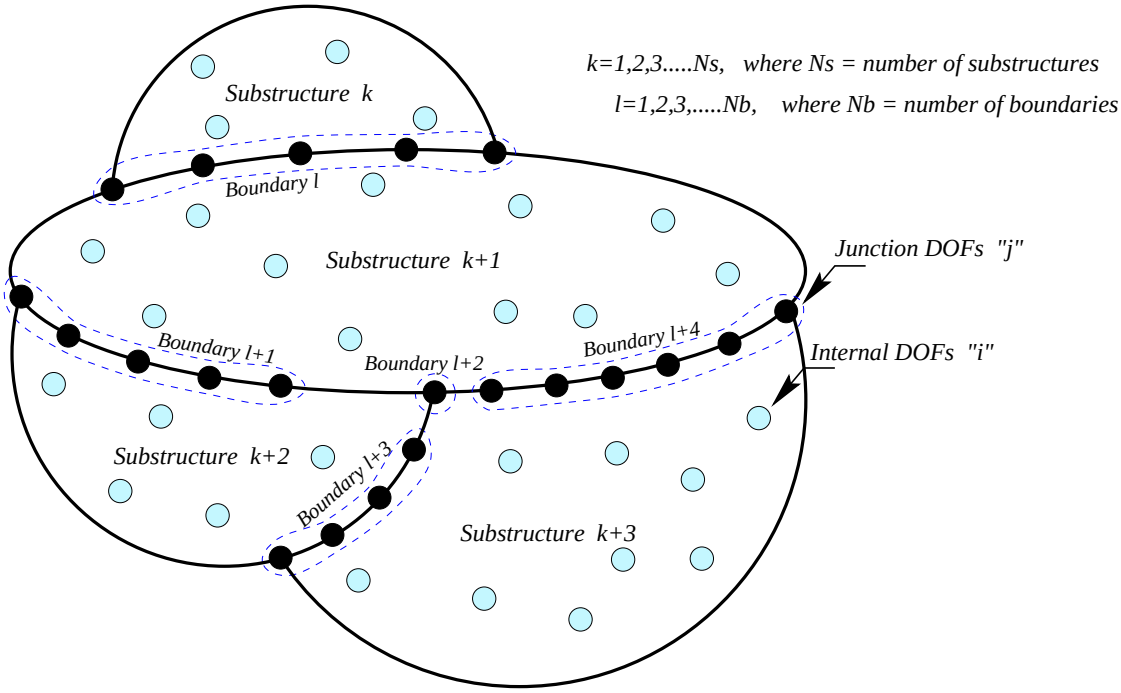

Figure 3.1: Abstract representation of sub-structures, boundaries, internal and junction DOFs for the mathematical treatment of CMS techniques

Having identified the above-defined sets of co-ordinates, each component k can then be analysed. Assuming a linear equation of motion,

$$\left[M^k\right]\left\{\ddot{x}^k(t)\right\} + \left[C^k\right]\left\{\dot{x}^k(t)\right\} + \left(\left[K^k\right] + \left[D^k\right]\mathrm{i}\right)\left\{x^k(t)\right\} = \left\{f^k(t)\right\} \tag{3.1}$$

where a general damping model is considered using viscous damping matrix $[C]$ and structural damping matrix $[D]$. The total number of physical DOFs of component k is denoted by N^k and the dynamic equilibrium in equation (3.1) is conveniently partitioned into internal DOFs, i, and junction DOFs, j, using the following matrix notation,

$$\begin{bmatrix} \left[Z^k_{jj}\right] & \left[Z^k_{ji}\right] \\ \left[Z^k_{ij}\right] & \left[Z^k_{ii}\right] \end{bmatrix} \begin{Bmatrix} \{X^k_j\} \\ \{X^k_i\} \end{Bmatrix} = \begin{Bmatrix} \{F^k_j\} \\ \{0\} \end{Bmatrix} \tag{3.2}$$

where $[Z]$ is the dynamic stiffness matrix and, $\{X\}$ and $\{F\}$ are the frequency dependent displacement and force vectors. Since no external force is assumed, equation (3.2) indicates no internal forces and only junction forces arising from the interaction between adjacent components.

3.3.1 Classification of Component Modes

Critical to the success of CMS methods is the choice of the so-called *component modes*. Component modes may be derived from a variety of physical interpretations of the interactions between IDOFs and JDOFs and allow the formation of a transformation matrix in the form of,

$$\left\{x^k(t)\right\} = \left[\Psi^k\right]\left\{q^k(t)\right\} \tag{3.3}$$

where the columns of $[\Psi^k]$ contain a selected set of component modes and $\{q(t)\}$ is a set of generalised co-ordinates. The terminology of "modes", however, can be misleading since they refer to a basis of vectors and not necessarily to normal modes.

Craig Jr. (1987) provides a good introduction to the subject of CMS methods and reiterates the definition of varies types of component modes. The review classifies a broad spectrum of CMS methods, which have been published since the early 1960s, into techniques based on normal modes, attachment modes, constraint modes, rigid-body modes and inertia-relief modes. These may be briefly defined as,

- **Normal modes** describe the free vibration of the component. The boundaries of component k may either be clamped, free or a mixture of both and the corresponding eigenvectors represent the normal modes. Loaded-interface modes fall also into this category and are obtained by placing extra mass on a set of JDOFs (Craig Jr. 1987).

- **Rigid-body modes** define the rigid-body response of the component and are obtained by imposing an arbitrary displacement on one rigid-body DOF at a time (Hintz 1975).
- **Constraint modes** are defined as the response of the component due to the successive unit displacement of the JDOFs, while all other JDOFs are constrained (Hurty 1965; Craig Jr. and Bampton 1968).
- **Attachment modes** are the displacements resulting from applying a unit force to a selected JDOF and zero forces elsewhere. If the component has rigid-body DOFs, the component is temporarily fixed and the resulting component modes are called *inertia-relief modes* (Rubin 1975).

Depending on the CMS method employed, a truncated set of normal modes and a selection of other component modes permits the transformation as described by equation (3.3). For purely static problems, $[M] = [0]$ and normal modes are redundant.

3.3.2 Compatibility Requirements Between Components

When CMS methods are applied to large FE models, physically large regions are discretised into many finite elements and the choice of sub-structures may not be straightforward. Sub-structures are then made up of partitions whose choice is purely based on numerical/mathematical aspects such as the size of components (N^k), location of boundary nodes and, if a model updating exercise is to follow, the level of uncertainty related to certain regions in the FE model.

Upon completion of computing the sets of modes for N_s components, the sub-structures are condensed to a reduced set of generalised co-ordinates using transformation equation (3.3) and assembled to form the overall system. As with the choice of component modes, assembly procedures are not unique and other elements may be introduced, such as the inclusion of local damping elements and non-linear spring elements.

Common to all coupling procedures are the compatibility constraints of forces and displacements at any one JDOF. Specifically, at boundary l, the displacements and forces

must comply with:

$$l = 1, 2, 3, \cdots, N_b \quad \begin{cases} \{{}_l x^k\} = \{{}_l x^{k+1}\} = \{{}_l x^{k+2}\} = \cdots = \{{}_l x^{n^k}\} \\ \{{}_l f^k\} + \{{}_l f^{k+1}\} + \{{}_l f^{k+2}\} + \cdots + \{{}_l f^{n^k}\} = \{0\} \end{cases} \tag{3.4}$$

where n^k is the number of sub-structures sharing boundary number l.

3.4 Modal Synthesis with Constraint Interfaces

Craig Jr. and Bampton (1968) proposed one of the classic CMS methods and this technique has found many followers since. It is still widely praised as easy to use and numerically stable. The method is based on finding a truncated set of normal modes with fixed interface co-ordinates and a set of constraint modes. As there are usually many more junction DOFs than there are rigid-body DOFs, both component mode sets are straightforward to compute, as will be seen in the following.

3.4.1 Definition of Constraint Modes

The constraint modes are determined by successively imposing a unit displacement on one boundary co-ordinate (JDOFs) while the others remain zero. By placing these conditions on the equation of motion, the following equilibrium must be satisfied:

$$\begin{bmatrix} [K_{jj}] & [K_{ji}] \\ [K_{ij}] & [K_{ii}] \end{bmatrix} \begin{bmatrix} \begin{bmatrix} \diagdown I \diagdown \end{bmatrix} \\ [\Phi_i^c] \end{bmatrix} = \begin{bmatrix} [F_j] \\ [0] \end{bmatrix} \tag{3.5}$$

where $[F_j]$ is the matrix of reaction forces at the junction DOFs and superscript k has been dropped as a matter of convenience. Using the second row of matrix identity (3.5), the set of constraint modes $[\Phi^c]$ defined at internal DOFs results in:

$$[\Phi_i^c] = -\left[K_{ii}\right]^{-1}\left[K_{ij}\right] \tag{3.6}$$

Therefore, by expanding $[\Phi_i^c]$, the matrix of constraint modes is defined by,

$$[\Phi^c] = \begin{bmatrix} \begin{bmatrix} \diagdown I \diagdown \end{bmatrix} \\ \left[-\left[K_{ii}\right]^{-1}\left[K_{ij}\right]\right] \end{bmatrix} = \begin{bmatrix} \begin{bmatrix} \diagdown I \diagdown \end{bmatrix} \\ [\Phi_i^c] \end{bmatrix}_{N^k \times n^j} \tag{3.7}$$

where n^j denotes the number of JDOFs of component k.

Contrary to the definition of constraint modes, it is helpful to the understanding of component modes that the columns of $[K_{ii}]$ are the forces at internal DOFs due to a unit displacement at one internal DOF while the remaining ones are zero.

3.4.2 Constraint-Interface System Order Reduction

In accordance with the name of the CMS method, Craig Jr. and Bampton (1968) proposed to constrain the junction DOFs and extract the normal modes from a reduced eigenvalue problem. Therefore, the reduced equation of motion of size n^i,

$$\left(-\omega_r^2\left[M_{ii}^k\right] + \left[K_{ii}^k\right]\right)\{\phi^n\}_r = \{0\} \tag{3.8}$$

can generally be solved for n^i normal modes. Assuming the number of internal DOFs, n^i, is reasonably large, a good approximation of the component's response can be obtained by using a truncated set of normal modes only. If the truncated number of normal modes is designated by integer m, then

$$\begin{aligned} \left[\ \Phi_i^n\ \right] &= \Big[\underbrace{\{\phi_1\}\,\{\phi_2\}\,\{\phi_3\}\cdots}_{m}\Big|\cdots\{\phi_{n^i}\}\Big]_{n^i \times n^i} \\ \left[\Phi_i^n\right] &= \left[\Phi\right]_{n^i \times m} \end{aligned} \tag{3.9}$$

where m usually accounts for all modes in the frequency spectrum of interest and a number of out-of-band modes. For large FE models, therefore, $m \ll N^k$.

Based on the identified constraint and normal modes, the displacement of the internal DOFs is approximated via,

$$\left\{x_i^k\right\} = \left[\Phi_i^c\right]\left\{x_j^k\right\} + \left[\Phi_i^n\right]\{q_n\} \tag{3.10}$$

The initial N^k DOFs of component k can therefore be reduced to $(n^j + m)$ hybrid co-ordinates using the following transformation:

$$\left\{\begin{Bmatrix} x_j^k \\ x_i^k \end{Bmatrix}\right\} = \begin{bmatrix} \begin{bmatrix} \diagdown I \diagdown \end{bmatrix} & [0] \\ \left[\Phi_i^c\right] & \left[\Phi_i^n\right] \end{bmatrix} \left\{\begin{Bmatrix} x_j^k \\ q_n \end{Bmatrix}\right\} \tag{3.11}$$

or

$$\left\{\begin{Bmatrix} x_j^k \\ x_i^k \end{Bmatrix}\right\} = \begin{bmatrix} \begin{bmatrix} \diagdown I \diagdown \end{bmatrix} & [0] \\ \left[-\left[K_{ii}\right]^{-1}\left[K_{ij}\right]\right] & \left[\Phi_i^n\right] \end{bmatrix} \left\{\begin{Bmatrix} x_j^k \\ q_n \end{Bmatrix}\right\} \tag{3.12}$$

$$\left\{x^k(t)\right\} = \left[T^k\right]\left\{q^k(t)\right\} \tag{3.13}$$

As the junction DOFs are retained for each component, the N_s reduced components assembled as follows:

$$\left[Z_c(\omega)\right] = \sum_{k=1}^{N_s} \left[T^k\right]^T \left[Z^k(\omega)\right] \left[T^k\right] \tag{3.14}$$

where the summation designates matrix building at common co-ordinates of boundaries l and the assembly procedure implicitly satisfies compatibility conditions (3.4).

The first column of the transformation matrix $[T]$ is that of a simple static condensation (Guyan 1965) and the full transformation can be said to be a mixture between static and dynamic condensation (Gasch and Knothe 1987).

3.5 Modal Synthesis with Free Interfaces

The key to the success of the CMS methods is to find a good approximation to the component's local displacement/vibration when the components are analysed in complete isolation from each other. The boundary conditions at the junction DOFs are unknown and it is critical to model the dynamic interaction accurately.

Instead of grounding the junction DOFs, the so-called *free-interface* methods analyse each individual component with unconstrained boundary conditions. That is, if no external co-ordinates are fixed (i.e. co-ordinates other than the interface co-ordinates), a truncated set of normal modes of a free-free structure (free-interface normal modes) serves as prime basis to approximate the overall displacement of the component. Early articles by MacNeal (1971), Rubin (1975) and Hintz (1975) have reported on pioneering work and proposed the mathematical framework of free-interface techniques which are still used to date. As for constraint interface methods, it is common to use a complementary set of component modes in the form of rigid-body modes and attachment modes.

3.5.1 Definition of Attachment Modes

An attachment mode is the static displacement obtained by imposing a unit force at one interface co-ordinate and zero forces at the remaining junction DOFs. For a restraint component, attachment modes $[\Phi^a]$ are defined as:

$$\begin{bmatrix}[K_{jj}] & [K_{ji}]\\ [K_{ij}] & [K_{ii}]\end{bmatrix}\begin{bmatrix}\begin{bmatrix}\Phi^a_j\end{bmatrix}\\ [\Phi^a_i]\end{bmatrix} = \begin{bmatrix}\begin{bmatrix}\diagdown I \diagdown\end{bmatrix}\\ [0]\end{bmatrix} = [F]_{N^k \times n^j} \tag{3.15}$$

where the matrix equation has been partitioned into IDOFs, i, and JDOFs, j, for simplicity.

Non-Singular Stiffness Matrix

From equation (3.15) it becomes immediately clear that the inversion of the stiffness matrix is only possible if the structure is grounded, i.e. non-singular. In this case, the inverse relationship between the stiffness matrix $[K]$ and the flexibility matrix $[G]$,

$$\begin{bmatrix}[K_{jj}] & [K_{ji}]\\ [K_{ij}] & [K_{ii}]\end{bmatrix}\begin{bmatrix}[G_{jj}] & [G_{ji}]\\ [G_{ij}] & [G_{ii}]\end{bmatrix} = \begin{bmatrix}\begin{bmatrix}\diagdown I \diagdown\end{bmatrix} & [0]\\ [0] & \begin{bmatrix}\diagdown I \diagdown\end{bmatrix}\end{bmatrix} \tag{3.16}$$

may be employed to solve equation (3.15) for the attachment modes as:

$$\begin{bmatrix}\begin{bmatrix}\Phi^a_j\end{bmatrix}\\ [\Phi^a_i]\end{bmatrix} = \begin{bmatrix}[K_{jj}] & [K_{ji}]\\ [K_{ij}] & [K_{ii}]\end{bmatrix}^{-1}\begin{bmatrix}\begin{bmatrix}\diagdown I \diagdown\end{bmatrix}\\ [0]\end{bmatrix} \tag{3.17}$$

$$\begin{bmatrix}\Phi^a\end{bmatrix} = \begin{bmatrix}[G_{jj}]\\ [G_{ij}]\end{bmatrix} \tag{3.18}$$

Since the attachment modes (eqn. (3.15)) and the constraint modes (eqn. (3.5)) are both defined for the interface co-ordinates, Craig Jr. (1987) has identified an interesting relationship between both component mode sets. The matrix identity (3.16) states that,

$$[G_{ij}] = -[K_{ii}]^{-1}[K_{ij}][G_{jj}] \tag{3.19}$$

which is seen to contain the constraint modes defined by equation (3.6). Substituting, therefore, the above flexibility term into equation (3.18), the following relationship between the constraint and attachment modes is obtained:

$$\begin{bmatrix}\Phi_a\end{bmatrix} = \begin{bmatrix}\begin{bmatrix}\diagdown I \diagdown\end{bmatrix}\\ -[K_{ii}]^{-1}[K_{ij}]\end{bmatrix}[G_{jj}] \tag{3.20}$$

$$\begin{bmatrix}\Phi^a\end{bmatrix} = \begin{bmatrix}\Phi^c\end{bmatrix}[G_{jj}] \tag{3.21}$$

In other words, the columns of the attachment modes are linear combinations of the columns of the constraint modes.

Singular Stiffness Matrix

When component k is unrestrained, equation (3.15) may no longer be used to solve for the attachment modes as the component stiffness matrix is singular. Hintz (1975), proposed an alternative solution for this indeterminate case and showed that by imposing inertia-forces due to a uniformly accelerating system, an inertia-relief loading matrix can be used to gain access to the attachment modes. The complete derivation of inertia-relief loading matrix $[P]$ is presented in Appendix A and its use will be briefly summarised in the following.

Assuming that there are r rigid-body DOFs, an appropriate set of r co-ordinates can be found to temporarily fix the component. After deleting the corresponding rows and columns in $[K]$, the reduced stiffness matrix $[\tilde{K}]$ is of size $(N^k - r) \times (N^k - r)$. As $[\tilde{K}]$ is non-singular, one may then assemble a flexibility matrix in the form of:

$$[G] = \begin{bmatrix} [\tilde{K}]^{-1}_{(N^k-r)\times(N^k-r)} & [0]_{(N^k-r)\times(r)} \\ [0]_{(r)\times(N^k-r)} & [0]_{(r)\times(r)} \end{bmatrix}_{N^k \times N^k} \tag{3.22}$$

where $[G]$ is as singular as $[K]$ and the null-matrices symbolise the insertion of zero rows and columns at the fixed co-ordinates.

The inertia-relief loading matrix $[P]$ may then be used together with the force matrix (eqn. (3.15)) to derive an equivalent definition of the components flexibility terms as:

$$\begin{aligned} \left[\Phi^a\right] &= \left[P\right]^T \left[G\right] \left[P\right] \left[F\right] && (3.23) \\ &= \left[G^e\right] \left[F\right] && (3.24) \\ &= \begin{bmatrix} \left[G^e_{jj}\right] \\ \left[G^e_{ij}\right] \end{bmatrix} && (3.25) \end{aligned}$$

The elastic flexibility matrix $[G^e]$ serves as an inverse of the singular stiffness matrix and hence, constitutes the attachment modes with its columns corresponding to the junction DOFs. Brahmi et al. (1995b) referred to the inertia-relief load matrix, as a filtering matrix as it effectively "frees" the stiffness matrix from temporarily imposed boundary conditions. The filtering ability of $[P]$ is demonstrated in Appendix A using a numerical example and it is shown that, regardless what co-ordinates are temporarily grounded, the resulting attachment modes are identical.

3.5.2 Accounting for the Effects of Higher-Order Residuals

The real value of the attachment modes defined earlier becomes obvious with the introduction of the so-called *residual flexibility* matrix. Any CMS method employs a truncated set of normal modes and a complementary set of component modes derived from the elastic properties of the component. As has been shown above, the attachment modes are a selected set of columns of the flexibility matrix which may be obtained from equation (3.17), for the statically determinate case, or from equation (3.24), for singular stiffness matrices. In either case, a full inverse of the stiffness matrix has been identified.

An alternative way of expressing the flexibility matrix can be derived from the orthogonality conditions between system's normal modes and the stiffness matrix:

$$\left[\Phi^n\right]^T \left[K\right] \left[\Phi^n\right] = \left[\lambda_r\right]_{N^k \times N^k} \tag{3.26}$$

which may be solved for the flexibility matrix as,

$$\big[K\big]^{-1} = \Big[\Phi^n\Big]_l \Big[\lambda\Big]_l^{-1} \Big[\Phi^n\Big]_l^T + \Big[\Phi^n\Big]_h \Big[\lambda\Big]_h^{-1} \Big[\Phi^n\Big]_h^T \tag{3.27}$$

where index l addresses the modes in the lower frequency region, and h the remaining modes from $m+1$ to N^k. The above summation of the flexibility matrices indicates that the first m modes are not only represented as a set of truncated normal modes in the free-interface CMS method, but also actively contribute to the flexibility matrix (i.e. attachment modes). Since an approximate deflection for the component is either determined by $[G]$ or $[G^e]$, the contribution of the m retained normal modes to the flexibility matrix can be removed. Specifically, the influence of the higher modes h on the flexibility matrix is directly accessible because,

$$\Big[\Phi\Big]_h \Big[\lambda\Big]_h^{-1} \Big[\Phi\Big]_h^T = \big[K\big]^{-1} - \Big[\Phi\Big]_l \Big[\lambda\Big]_l^{-1} \Big[\Phi\Big]_l^T \tag{3.28}$$

$$[R] = \big[K\big]^{-1} - \Big[\Phi\Big]_l \Big[\lambda\Big]_l^{-1} \Big[\Phi\Big]_l^T \tag{3.29}$$

where $[R]$ is the so-called *residual flexibility* matrix.

Based on the definition of the residual flexibility matrix in equation (3.29), the objective to represent the contribution of higher modes is consequently achieved by employing the first m normal modes and the inverse of the stiffness matrix. If the structure is statically determinate:

$$[R] = \big[G\big] - \Big[\Phi\Big]_l \Big[\lambda\Big]_l^{-1} \Big[\Phi\Big]_l^T \tag{3.30}$$

whereas for singular stiffness matrices:

$$[R] = \big[G^e\big] - \Big[\Phi\Big]_l \Big[\lambda\Big]_l^{-1} \Big[\Phi\Big]_l^T \tag{3.31}$$

Concluding the above derivation, the residual flexibility matrix embodies the contribution of the higher modes, h, to the flexibility matrix $[G]$ (or $[G^e]$) without actually having to calculate them.

3.5.3 Free-Interface System Order Reduction

As mentioned before, an essential ingredient in any CMS method is the use of normal modes to approximate the component's displacement. For free-interface methods, no explicit boundary conditions are prescribed on the interface co-ordinates and the normal modes are extracted from the following eigenvalue problem:

$$\left(-\omega_r^2 \left[M^k\right] + \left[K^k\right]\right) \{\phi^n\}_r = \{0\} \tag{3.32}$$

A partial solution of the eigenvalue problem is usually sufficient to find an appropriate level of approximation of the physical displacement at the IDOFs and JDOFs. By including the first m modes only, the normal mode matrix $[\Phi^n]$ is:

$$\begin{aligned} \left[\ \Phi\ \right]^k &= \Big[\underbrace{\{\phi_1\}\,\{\phi_2\}\,\{\phi_3\}\cdots}_{m}\Big|\cdots\{\phi_{N^k}\}\Big]_{N_k \times N_k} \\ \left[\Phi^n\right] &= \left[\Phi\right]_{N^k \times m} \end{aligned} \tag{3.33}$$

where m should be higher than the highest mode in the frequency range of interest. Past experience has shown that satisfactory results are obtained if the maximum natural frequency ($\omega_r,\ r = m$) is 2 to $1\frac{1}{2}$ times the highest frequency point in the spectrum.

Having evaluated the residual flexibility matrix $[R]$ as the difference between the flexibility of the full elastic body and the flexibility contribution of lower modes, the displacement of sub-structure k is now approximated using the identified normal modes as:

$$\left\{x^k\right\} = \left[\Phi^n\right]\left\{q_n\right\} + \left[R\right]\left\{F\right\} \tag{3.34}$$

or in partitioned format:

$$\begin{Bmatrix} \{x_j^k\} \\ \{x_i^k\} \end{Bmatrix} = \begin{bmatrix} [\Phi_j^n] \\ [\Phi_i^n] \end{bmatrix} \{q_n\} + \begin{bmatrix} [R_{jj}] & [R_{ji}] \\ [R_{ij}] & [R_{ii}] \end{bmatrix} \begin{Bmatrix} \{F_j\} \\ \{0\} \end{Bmatrix} \tag{3.35}$$

where $\{q_n\}$ are m generalised co-ordinates and $\{F_j\}$ denotes the forces at the interface co-ordinates. Similar to the definition of the attachment modes, it is seen that only the first n^j columns of $[R]$ at the junctions DOFs come into effect.

By expressing the unknown junction forces $\{F_j\}$ in terms of the displacement of the interface co-ordinates using the first row of equation (3.35):

$$\left\{F_j\right\} = \left[R_{jj}\right]^{-1}\Big(\left\{x_j^k\right\} - \left[\Phi_j^n\right]\left\{q_n\right\}\Big) \tag{3.36}$$

which may then be back-substituted into the second row of equation (3.35) to find the displacements of the IDOFs as a function of the JDOFs:

$$\left\{x_i^k\right\} = \Big(\left[\Phi_i^n\right] - \left[R_{ij}\right]\left[R_{jj}\right]^{-1}\left[\Phi_j^n\right]\Big)\{q_n\} + \left[R_{ij}\right]\left[R_{jj}\right]^{-1}\left\{x_j^k\right\} \tag{3.37}$$

As a result, component k of the assembly can be condensed to a reduced number of hybrid co-ordinates as:

$$\begin{Bmatrix} \{x_j^k\} \\ \{x_i^k\} \end{Bmatrix} = \begin{bmatrix} \left[\ I\ \right] & \vdots & [\ 0\ ] \\ \cdots\cdots & \cdots & \cdots\cdots \\ \left[R_{ij}\right]\left[R_{jj}\right]^{-1} & \vdots & \Big(\left[\Phi_i^n\right] - \left[R_{ij}\right]\left[R_{jj}\right]^{-1}\left[\Phi_j^n\right]\Big) \end{bmatrix} \begin{Bmatrix} \{x_j^k\} \\ \{q_n\} \end{Bmatrix} \tag{3.38}$$

$$\left\{x^k(t)\right\} = \left[T^k\right]\left\{q^k(t)\right\} \tag{3.39}$$

where transformation matrix $[T^k]$ enables to perform a reduction from N^k DOFs to $(m + n^j)$ DOFs. As for the constraint-interface method, the reduced components are then assembled at the junction DOFs using the matrix building denoted by equation (3.14).

3.5.4 A Reduced Model Order in Physical Coordinates

The two classical CMS methods presented earlier use either free- or fixed-interfaces and generally lead to a condensed model whose displacements are expressed in hybrid coordinates. The interface coordinates (JDOFs) are retained to allow subsequent coupling of the components and the internal DOFs (IDOFs) of each individual component are approximated using the displacements of the junction DOFs and a reduced set of modal co-ordinates. Depending on the nature of the problem, the size of the final condensed system can still be large due to a large number of junction DOFs. Attempts to solve this kind of problem have been made by Brahmi et al. (1995a) and Brahmi et al. (1995b) and an extra level of condensation was shown to be possible. In the techniques proposed, one boundary at a time was contemplated and a common basis of interface modes identified. These were then applied to each neighbouring sub-structure to allow for a further reduction in the overall number of modal co-ordinates. However, the success of the method depends on the quality of the common modal base, which is not straightforward to compute, and comes only at the expense of extra CPU time.

An alternative technique was recently proposed by Lombard et al. (1997) and is closely related to the free-interface method proposed by MacNeal (1971). It employs a distinctly different coupling procedure and potentially makes all junction DOFs redundant using a junction force coupling procedure. In effect, the CMS method leads to a reduced system equation in physical coordinates only and makes the presence of modal coordinates redundant.

Based on equation (3.35), the internal DOFs, i, are generally divided into *slave* DOFs (SDOFs) and *master* DOFs (MDOFs) so that the N^k physical DOFs of component k are approximated as:

$$\begin{Bmatrix} \{x_j^k\} \\ \{x_m^k\} \\ \{x_s^k\} \end{Bmatrix} = \begin{bmatrix} [\Phi_j^n] \\ [\Phi_m^n] \\ [\Phi_s^n] \end{bmatrix} \{q_n\} + \begin{bmatrix} [R_{jj}] \\ [R_{mj}] \\ [R_{sj}] \end{bmatrix} \{F_j\} \tag{3.40}$$

Unlike the classical free interface method where (3.40) would be solved for the junction forces and a transformation induced to a set of physical and modal coordinates, the middle row of equation (3.40) is now solved for the modal coordinates first and yields:

$$\left\{q_n^k\right\} = \left[\Phi_m^n\right]^+ \left(\left\{x_m^k\right\} - \left[R_{mj}\right]\left\{F_j\right\}\right) \tag{3.41}$$

Substituting (3.41) back into equation (3.40), then:

$$\begin{Bmatrix} \{x_j^k\} \\ \{x_m^k\} \\ \{x_s^k\} \end{Bmatrix} = \begin{bmatrix} \left[[R_{jj}] - [\Phi_j^n][\Phi_m^n]^+[R_{mj}]\right] & \left[[\Phi_j^n][\Phi_m^n]^+\right] \\ \begin{bmatrix} 0 \end{bmatrix} & \begin{bmatrix} \searrow I \searrow \end{bmatrix} \\ \left[[R_{sj}] - [\Phi_s^n][\Phi_m^n]^+[R_{mj}]\right] & \left[[\Phi_s^n][\Phi_m^n]^+\right] \end{bmatrix} \begin{Bmatrix} \{F_j\} \\ \{x_m^k\} \end{Bmatrix} \tag{3.42}$$

or in a more compact notation,

$$\begin{Bmatrix} \{x_j^k\} \\ \{x_m^k\} \\ \{x_s^k\} \end{Bmatrix} = \begin{bmatrix} [T_{jj}^k] & [T_{jm}^k] \\ [\,0\,] & \begin{bmatrix} \searrow I \searrow \end{bmatrix} \\ [T_{mj}^k] & [T_{mm}^k] \end{bmatrix} \begin{Bmatrix} \{F_j^k\} \\ \{x_m^k\} \end{Bmatrix} \tag{3.43}$$

which transforms the original N^k DOFs to the junction forces and the displacements at a selected number of MDOFs.

It should be realised that the number and location of the selected MDOFs is critical for the successful determination of $[\Phi_m^n]^+$. That is, there must be at least as many MDOFs as there are computed normal modes, m, for that component and the physical distribution of the MDOFs must render $[\Phi_m^n]$ to be numerically well-conditioned. Since MDOFs are typically linked to measurement coordinates, this condition is rarely met and usually a higher number of coordinates is considered initially (hence, a pseudo-inverse is used in the general case). It is therefore appropriate to precede the condensation by numerical measures to identify suitable measurement locations. Techniques like the Effective Independence can be successfully employed in these cases (Kammer 1992; Chatterje and Hadi 1988). Given a number of modes, say m, this algorithm analyses the eigenvector matrix and identifies a collection of DOFs whose number and location best describe the number of modes included.

Force Coupling

To explain the force coupling procedure of this free-interface CMS method, let us initially assume a simple assembly of two sub-structures connected at one boundary l, as defined in figure 3.1. The junction forces of component k are found from equation (3.43) and are given by:

$$\{F_j^k\} = [T_{jj}^k]^{-1}\Big\{\{x_j^k\} - [T_{jm}^k]\{x_m^k\}\Big\} \tag{3.44}$$

From the compatibility conditions in (3.4), the N_s components must be in equilibrium and,

$$\sum_{k=1}^{N_s}\{F_j^k\} = \sum_{k=1}^{N_s}[T_{jj}^k]^{-1}\Big\{\{x_j^k\} - [T_{jm}^k]\{x_m^k\}\Big\} = \{0\} \tag{3.45}$$

while the displacements at JDOFs must be compatible. If a common vector of displacements is denoted by $\{x_j\}$, then $\{x_j\} = \left\{x_j^1\right\} = \left\{x_j^2\right\}$ and from equation (3.45) we obtain:

$$\{x_j\} = \left[\sum_{k=1}^{N_s}[T_{jj}^k]^{-1}\right]^{-1}\sum_{k=1}^{N_s}\Big\{[T_{jj}^k]^{-1}[T_{jm}^k]\{x_m^k\}\Big\} \tag{3.46}$$

Combining equations (3.46) and (3.44), the junction forces in equation (3.43) can finally expressed as:

$$\{F_j^k\} = [T_{jj}^k]^{-1}\left[\left[\sum_{i=1}^{N_s}[T_{jj}^i]^{-1}\right]^{-1}\sum_{i=1}^{N_s}[T_{jj}^i]^{-1}[T_{jm}^i]\{x_m^i\} - [T_{jm}^k]\{x_m^k\}\right] \tag{3.47}$$

Re-arranging equation (3.47) into a matrix/vector notation, the RHS of equation (3.43) becomes:

$$\begin{Bmatrix}\{F_j^k\}\\ \{x_m^k\}\end{Bmatrix} = \begin{bmatrix}[T_f^k]\\ [B^k]\end{bmatrix}\begin{Bmatrix}\{x_m^1\}\\ \{x_m^2\}\\ \{x_m^3\}\\ \vdots\\ \{x_m^{N_s}\}\end{Bmatrix} \tag{3.48}$$

where N_s is the number of components (at that boundary) and matrix $[B]$ is a Boolean matrix with unit entries at locations corresponding to the master DOFs, $\{x_m^k\}$, and zeros elsewhere.

Using both consecutive transformations, an overall transformation matrix is found in equations (3.43) and (3.48) combined and results in:

$$\begin{Bmatrix} \{x_j^k\} \\ \{x_m^k\} \\ \{x_s^k\} \end{Bmatrix} = \left[T^k\right] \begin{Bmatrix} \{x_m^1\} \\ \{x_m^2\} \\ \{x_m^3\} \\ \vdots \\ \{x_m^{N_k}\} \end{Bmatrix} \tag{3.49}$$

$$\{x^k(t)\} = \left[T^k\right] \{q^k(t)\} \tag{3.50}$$

The full transformation achieved in equation (3.50) uniquely differs from the classical CMS methods discussed earlier. Each sub-structure is immediately mapped to all remaining master DOFs and therefore does not necessarily provide a condensation on the component level. Each component is of the same size after "condensation" and the assembly of the system simply reduces to a straight summation of the component's "reduced" system matrices:

$$[Z_c] = \sum_{k=1}^{N_s} \left[T^k\right]^T \left[Z^k\right] \left[T^k\right] \tag{3.51}$$

which is unlike equation (3.14) where the assembly is performed at common interface coordinates to comply with the compatibility conditions (3.4).

So far, the presence of just one boundary l has been considered. This assumption has clearly no practical relevance as one frequently encounters a number of different interfaces with a varying number of junction DOFs and sub-structures attached to it. In general, each of those boundaries must be treated separately and the complete vector of junction forces divided into sets of coordinates with common boundaries. In fact, before the local transformation matrices are computed, the total number of remaining coordinates must be determined since a mapping is performed to the full set of MDOFs and some sub-structures may not be connected to others. To clarify the working principles of this unique assembly procedure, Appendix A demonstrates the use of equation (3.48) on a hypothetical case of five sub-structures.

Second Level Condensation

In some instances, one may want to reduce the system even further as a larger number of MDOFs might have been retained to ensure a numerically well-conditioned modal matrix $[\Phi_m^n]$ (eqn. (3.42)). Case studies have shown, supporting the findings of Lombard et al. (1997), that a second level of condensation can readily be achieved. If the new displacement vector $\{x_m\}$ of the condensed system is further divided into,

$$[Z_c] \begin{Bmatrix} \{x_{m1}\} \\ \{x_{m2}\} \end{Bmatrix} = \{0\} \tag{3.52}$$

and an eigensolution of the reduced system is used to approximate $\{x_m\} = [\Phi^n]\{q\}$ using a limited number of modes, then a further reduction may be performed simply by,

$$\begin{Bmatrix}\{x_{m1}\}\\ \{x_{m2}\}\end{Bmatrix} = \begin{bmatrix} \begin{bmatrix} I \end{bmatrix} \\ [\Phi_{m2}]\,[\Phi_{m1}]^{+} \end{bmatrix} \{x_{m1}\} \tag{3.53}$$

which subscripts $m1$ and $m2$ denote the retained and condensed coordinates respectively.

3.6 Validation of Modal Synthesis Methods

Finite element analysis tends to be economically inefficient for large structural dynamics problems and three reduction schemes have been introduced to address this problem. The handling of boundary conditions at the interface coordinates seems to be the key to the success of these methods and has given rise to a number of different CMS techniques. In order to weight the method's abilities against each other, and hence the validity of the model of dynamic boundary conditions at the interface co-ordinates, in the following the results of a validation and comparison study are presented. Here, particular attention was paid to 1) the quality of the FRF predictions, 2) the ease of use and 3) the level of reduction which can be achieved in relation to the amount of computation required.

As with all the developments presented in this thesis, the various algorithms were implemented into the code OPTIMA (Grafe 1997c) using the MATLAB language (Mathworks 1997). The suite of standard dynamic analysis tools was considerably extended and FE libraries were implemented for this purpose. The original finite element definitions were developed by University of Kassel (MATFEM 1997) and integrated into a more general platform for analysing sub-structured FE models. The input-definition file for FE analysis and updating computations may be found in Appendix C.

The test structure considered was a simple two-plate assembly and the size of the full FE model was 720 DOFs. With the primary objective of retaining a good quality of predicted FRFs, an arbitrary FRF from the full model was compared against the same FRF from the condensed models. The results of this study are shown in figure 3.2 and present the post-processing results of the FE analysis using OPTIMA and an overlay between the reference FRFs of the condensed and uncondensed FE models shown. The FRFs pictured in figure 3.2 were computed from the first 20 modes of each corresponding model and over an extended frequency range from $0Hz$ to $250Hz$. A constant structural damping factor of 2% was used throughout the study.

In all three analyses presented, the validity range of the condensation procedures was set to $100Hz$ and, correspondingly, all modes within $0Hz$ and $200Hz$ were included in the normal mode matrix $[\Phi^n]$ to condense each component. The classical constraint- and free-interface methods produced reduced model sizes of 61 DOFs and 71 DOFs (hybrid coordinates) respectively whereas the free-interface method together with the force assembly procedure led to a reduced model order of 27 DOFs in physical coordinates only. Hence, both the $100Hz$ and $200Hz$ thresholds are included as well as 50 frequency points beyond $200Hz$ in figure 3.2.

Table 3.1 summarises the numerical experiment shown in figure 3.2. The three CMS methods tested introduce a considerable degree of reduction and up to $100Hz$, the predicted FRFs are in good agreement with those obtained from the full model. Beyond the range of validity, the correlation becomes increasingly worse and is non-existent after $200Hz$ for the chosen response location.

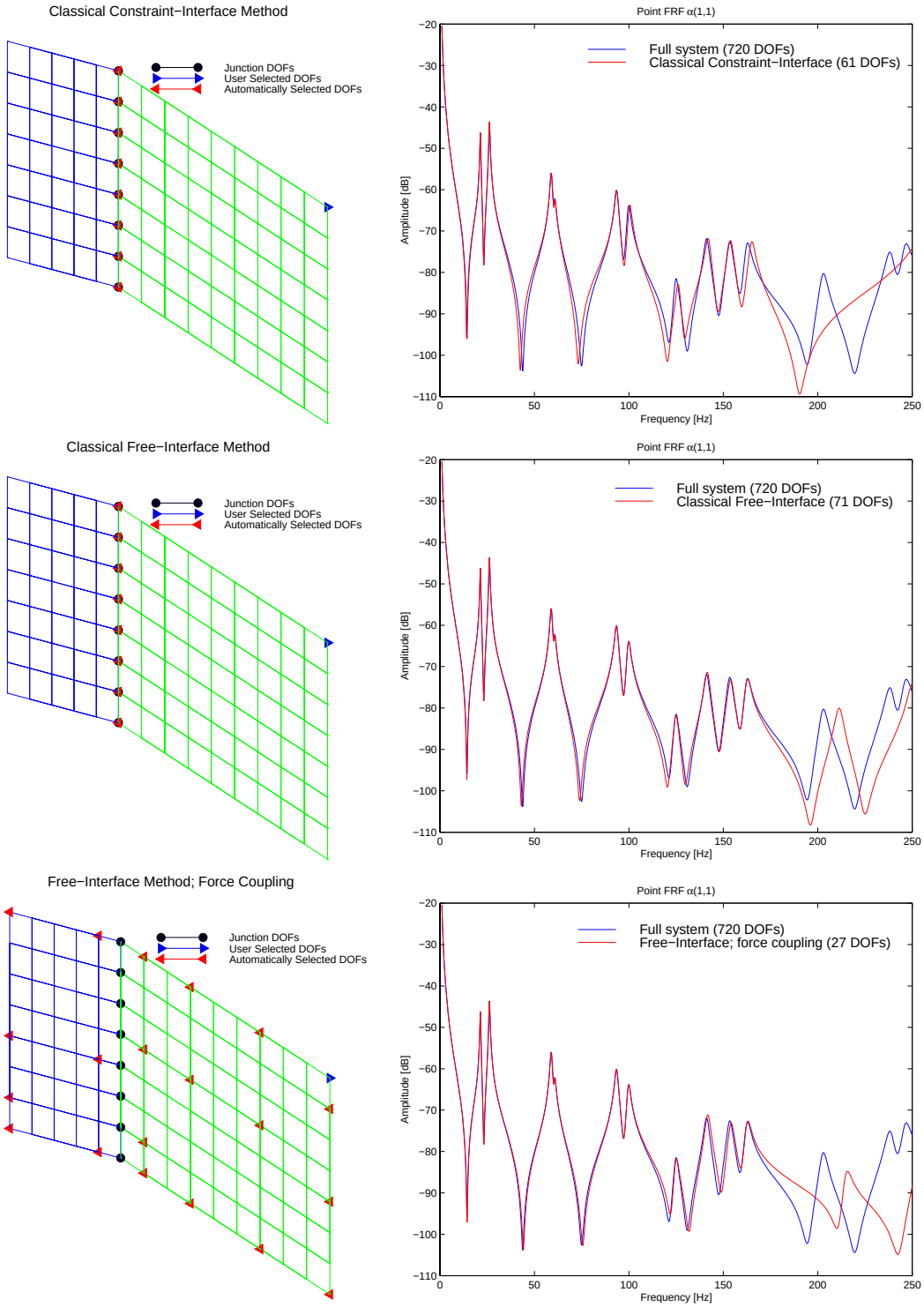

Figure 3.2: Test FE model condensed with CMS techniques and overlay of point FRFs ("User selected DOF") between full solution and corresponding reduced system representation

	Classical Constraint-Interface	Classical Free-Interface	Free-Interface; Force Coupling	Uncondensed FE Model
Number of shell elements	63 / 35	63 / 35	63 / 35	98
Frequency range of model validity	$100Hz$	$100Hz$	$100Hz$	not applicable
Number of modal coordinates	13	23	0	not applicable
Number of physical coordinates	48	48	27	720
Total number of DOFs	61	71	27	720
Number of modes included for FRF computations	20	20	20	20
Highest natural frequency	$f_{20} = 394Hz$	$f_{20} = 378Hz$	$f_{20} = 411Hz$	$f_{20} = 246Hz$

Table 3.1: Specifications of sub-structured FE model and computed results after condensation using CMS methods

The number and location of retained co-ordinates shown in figure 3.2 and table 3.1 also indicate the unique characteristics of the three CMS methods presented. Both *classical* methods must retain the junction DOFs for assembly, whereas the free-interface method based on force assembly excludes these and relies on automatically selected physical DOFs which best represent the truncated modal space used ($[\Phi_m^n]$). The latter CMS procedure produces a condensed FE model representation in physical co-ordinates only. Both *classical* CMS techniques include a truncated number of modal coordinates.

In this case, the closeness of the FRFs is implicitly a function of the level of correlation between the predicted eigenvalues and eigenvectors of the full model and the ones equivalent to its condensed representation. As a supplementary correlation analysis, therefore, the relative differences between the eigenvalues, defined by,

$$\epsilon = \frac{|\lambda_{condensed} - \lambda_{full}|}{\lambda_{full}} \times 100 \tag{3.54}$$

were calculated for all three cases and the results are shown in figure 3.3.

The free-interface methods proposed by MacNeal (1971) and Lombard et al. (1997) achieve about the same quality of reduction while the constraint interface method appears to be less accurate. All three models, however, yield errors in eigenvalues of less than 1% for the modes residing within $0Hz$ and $200Hz$. From a practical point of view, by far the most attractive model is the one obtained by the free-interface method using a force coupling procedure. It is not only the smallest of all three models but also only contains physical DOFs. Yet, from a computational point of view, the condensed model representation has lost its component independence discussed earlier and consequently, any changes introduced to the FE model necessitates the reanalysis of all sub-structures. This is not the case for both *classical* CMS techniques which, however, suffer from the need to retain their junction DOFs.

This numerical case study has shown that the easiest and fasted method is the classical

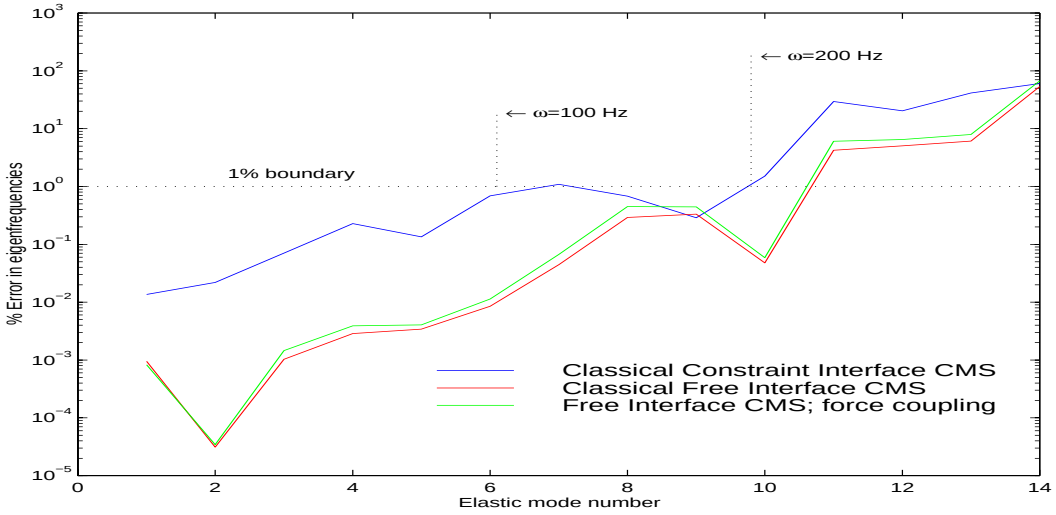

Figure 3.3: Analytically computed differences in natural frequencies between full model solution and reduced representation using three CMS condensation schemes

fixed-interface method. It is not only relatively easy to implement but also numerically very stable (no inversion of $[\Phi_m^n]$ required). In particular, the free-interface methods have been shown to be computationally very expensive especially in the case of components with rigid-body DOFs. Here, the inertia-relief mode matrix (eqn. (3.23)) needs to be computed and the attachment modes are only available through the computationally expensive matrix product, $[P]^T[G][P]$, of three square matrices.

In contrast to the findings of this particular case study, Lombard et al. (1997) have shown their method's performance to be superior to its predecessor proposed by MacNeal (1971) when all sub-structures are clamped, i.e. none of component's stiffness matrices are singular.

3.7 A New Perspective in FRF Model Updating

The subject of FRF model updating has been studied for the past 20 years and the techniques are widely accepted as a promising means to adjust and validate analytical models in the light of the true damped structural response. Previous work has shown that the direct use of measurements may cause numerically ill-conditioned sensitivity matrices $[S]$ (eqn. (1.20), p. 12) and that FRF model updating algorithms require a one-to-one correspondence between the number of measured coordinates and the number of DOFs in the FE model. A typical example of such an updating formulation is the one proposed by Lin and Ewins (1990). Here, a selected number of design parameters changes, $\Delta\varphi$, is determined from:

$$\big[H_A(\omega)\big]\big[\frac{\partial Z(\omega)}{\partial\varphi}\Delta\varphi\big]\big\{H_{X_i}(\omega)\big\} = \big\{H_{A_i}(\omega)\big\} - \big\{H_{X_i}(\omega)\big\} \tag{3.55}$$

where subscripts A and X designate the *analytical* and *experimental* responses and i the excitation DOF.

The need for matching the number of coordinates is evident on both sides of equation (3.55) and consequently, N measurements must be available before a least-square solution for

$\Delta\varphi$ is available. Any number of parameters exceeding N, i.e. $N_\varphi > N$, resolves updating equation (3.55) into an under-determined problem.

Past experience has shown, however, that the number of updating parameters is generally smaller than N, i.e. $N_\varphi < N$, and the success of the updating calculation primarily depends on the choice of updating parameters and the number of measurements, n, provided. That is to say, the more measurements are provided, the better the resulting parameter estimation and ideally there exists a one-to-one correspondence ($N = n$).

As has been discussed in Chapter 2, one-to-one correspondence may be established by either expansion schemes or FE model reduction techniques. Traditionally, these involve the full system solution and if a condensation technique is contemplated, inverses of the size equal to the number of "deleted" co-ordinates are required (Gasch and Knothe 1989). Conventional reduction schemes and substructuring techniques use a transformation matrix $[T]$ to reduce the system to:

$$\left[Z_c(\omega)\right] = \sum_{k=1}^{N_s} \left[T^k\right]^T \left[Z^k(\omega)\right] \left[T^k\right] \tag{3.56}$$

where $[Z_c]$ is the reduced order dynamic stiffness matrix and N_s the number of sub-structures. If $N_s = 1$ and a conventional dynamic condensation scheme is employed, $[T] = [T(\omega)]$ (Friswell and Mottershead 1995) and a new transformation matrix must be computed for each required frequency point. Transformation matrices obtained from CMS methods, on the contrary, are frequency-independent.

A similar argument holds true for the size of $[T]$. Unlike conventional dynamic reduction schemes, large FE models can be divided into partitions of manageable size and each of the N_s sub-structures is condensed with less computational effort since $N^k \ll N$. The computational effort of conventional reduction techniques, on the other hand, quickly increases as the operation count for inverting square matrices is proportional to N^3 (Press et al. 1992).

Sub-structured FE models and CMS methods also present a suitable analysis environment for model updating. Any computed parameter changes are confined to the reanalysis of the associated component and in particular, the required FRF matrix is simply the inverse of equation (3.56), namely:

$$\left[H_A(\omega)\right]_c = \left[\sum_{k=1}^{N_s} \left[T^k\right]^T \left[Z^k(\omega)\right] \left[T^k\right]\right]^{-1} \tag{3.57}$$

which is usually orders of magnitude smaller than the full system size N. If one of the classical free- or constraint-interface methods is to be used, the condensed system will take the form of:

$$\begin{bmatrix} \left[Z_{xx}\right] & \left[Z_{xq}\right] \\ \left[Z_{qx}\right] & \left[Z_{qq}\right] \end{bmatrix} = \begin{bmatrix} \left[H_{xx}\right] & \left[H_{xq}\right] \\ \left[H_{qx}\right] & \left[H_{qq}\right] \end{bmatrix}^{-1} \tag{3.58}$$

where indices x and q address the columns/rows of corresponding physical and modal co-ordinates. Since, however, no information may be available from tests regarding the modal co-ordinates, only the partial matrices in physical coordinates, namely $\left[H_{xx}\right]$ and $\left[Z_{xx}\right]$, are used to formulate equation (3.55).

To complete the model updating formulation in equation (3.55), the derivative is obtained by:

$$\left[\frac{\partial Z_c(\omega)}{\partial \varphi_i}\right] = \left[T^i\right]^T \left[\frac{\partial Z^i(\omega)}{\partial \varphi_i}\right] \left[T^i\right] \tag{3.59}$$

where i denotes the design parameter number and its associated sub-structure. As the chosen design parameter is directly related to one particular substructure, there is no need to perform the (matrix building) summation of equation (3.56) and only the derivative of the full dynamic stiffness matrix of component i is to be transformed.

Once the FE model has been reduced to the number of measurement locations, n, and a few other physical DOFs, the incompleteness ratio defined by $\mathrm{i}_r = n/N$ has improved and lies closer to unity. A second level of reduction, as outlined in Section 3.5.4, may then be employed to further reduce the FE model to just the n measurement locations or any other condensation can then be employed much more efficiently. If the model updating formulation proposed by Lin and Ewins (1990) (eqn. (3.55)) is considered, the unmeasured DOFs are replaced by their analytical counterpart. But also the use of analytical expansion schemes, like SEREP (O'Callahan et al. 1989), can be performed more accurately as $\mathrm{i}_r = n/N$ is closer to unity.

Hemez (1997b) targeted FE model sizes of 100 000 to 500 000 DOFs and pointed out that in extreme situations, where the model is very large and the number of measurements limited, an FE model of intermediate size is best suited for subsequent condensation/expansion procedures. In his companion paper (Hemez 1997a) he uses a sub-structured FE model along with an eigensensitivity-based model updating algorithm and stresses that the identification of modelling errors can easily be concentrated on the sub-domains/components only. The size of the model updating problem was therefore only a fraction of the original problem size. The same philosophy was presented in a paper by Link (1998).

3.8 Concluding Remarks

- Substructuring and component mode synthesis methods have been presented in a consistent and uniform manner and it was attempted to illustrate the physical meaning of the component modes, a key parameter in both free- and fixed-interface methods.
- All three CMS methods have been shown to be able to reduce FE models considerably and allow the estimation of the dynamic properties of the system with a good level of accuracy. Free-interface methods performed better than the fixed-interface methods and it was observed that the superior performance of free-interface methods is at the expense of an increased computational load and, more importantly, numerically less well defined eigenvalue problems.
- As an alternative to traditional CMS coupling procedure, a recently proposed coupling routine was also validated. Although the results were of the same quality as its predecessor and the number of retained coordinates was much smaller, the technique violates the component independence. When changes are to be introduced to local substructures, all adjacent substructures must be re-analysed as well. This extra computation makes it generally less suitable for model updating procedures. However, for applications other than model updating, this CMS method is attractive as it only retains physical DOFs.
- Common to all CMS methods presented is the need to perform an independent modal analysis of each component and hence, the algorithms may be implemented into a parallel processing environment, as may be many computational elements of the updating computations itself. There are N_f independent response computations, N_φ sensitivity calculations and at least N_φ design changes to be introduced after each iteration. Thus, the computationally most expensive elements in a "CMS-updating" algorithm are paralleliseable.
- Section 3.7 explains the use of sub-structured FE models in model updating and highlights that the transformation matrices are frequency-independent. It was shown that the sensitivity computations of the reduced system do not introduce extra non-linearities and can be performed by transforming the component's uncondensed sensitivity matrix using these transformation matrices.

Chapter 4

A Predictor-Corrector Model Updating Technique

4.1 Introduction

Various aspects of FRF updating algorithms have been discussed in the previous chapters and it was highlighted that an increasing number of unmeasured FE DOFs increasingly limits the applicability of such methods. Whereas modal-based algorithms rely on a well-distributed set of response co-ordinates (or actuator/sensor architecture) for mode pairing purposes, FRF-based model updating techniques integrate the measurements directly into the equation of motion and require a one-to-one correspondence between the number of measured DOFs and the number of DOFs in the FE model. In both cases the number and location of the measurements is consequently not independent of the size of the FE model.

Usually, the number of measurements is much smaller than the number of DOFs of the FE model (i.e. $n \ll N$) and the incompleteness ratio, i_r (eqn. (2.7), p. 23), generally decreases for larger FE models. Chapter 3 has demonstrated that the model size may be considerably reduced using modal synthesis methods but one may raise the question as to why response-based model updating techniques require a one-to-one correspondence and how this requirement is physically justified.

This chapter introduces a new response-based model updating technique using two FRF correlation functions. Response sensitivities are approximated using a truncated modal solution and are derived for FRFs in linear and logarithmic scale. After formulating the derivatives of the correlation coefficients, the updating equations are then shown to be uniquely different to many other FRF model updating algorithms. The **P**redictor-**C**orrector (P-C) method effectively removes the built-in requirement of a one-to-one correspondence between the number of measurements and the number of DOFs in the FE model and the need to explicitly select updating frequency points.

4.2 Frequency Response Function Sensitivities

Optimisation and model updating techniques usually linearise non-linear problems and seek a solution in an iterative fashion. A key parameter during the iterations is the gradient or sensitivity of the system with respect to the variables concerned. The variables in

model updating problems are the design parameters of the structure, $\{\varphi\}$, and the system properties to be adjusted are the response predictions, $[H]$, for FRF model updating techniques.

Depending on the error representation in the FE model, there are a number of ways of computing such response sensitivities. All of them require the derivative of the dynamic stiffness matrix in one way or another. In Chapter 2, a physically representative error model was adopted which allows the introduction of any design modification into the FE property tables. Since analytical derivatives are not available for finite elements other than for the very simplest, a numerical approximation (eqn. (2.15), p. 26) was found to be sufficient to identify the derivative of the system's dynamic stiffness matrix.

In the following, the theoretical framework for computing FRF sensitivities is outlined and it is shown that the computation of these can be reduced considerably if the FE model is condensed by CMS methods. Instead of using the response quantities directly, it is shown how the response sensitivities can be computed from the derivatives of dynamic stiffness terms. This section also introduces the notion of logarithmic FRF sensitivities and shows that these too may be derived in the same way.

4.2.1 Linear Response Sensitivities

The response matrix is the inverse of the dynamic stiffness matrix, $[Z]$, and both are uniquely described by a string of design parameters, $\{\varphi\}$, and the excitation frequency, ω:

$$[\alpha(\omega, \{\varphi\})] = [Z(\omega, \{\varphi\})]^{-1} = \left[-\omega^2[M(\{\varphi\})] + [K(\{\varphi\})]\right]^{-1} \tag{4.1}$$

where $[\alpha]$ is the receptance matrix.

The response may equally well be written in terms of mobility matrix, $[Y]$, or inertance matrix, $[A]$, as these are directly proportional to the velocity and acceleration respectively. Without losing generality, the FRF matrix will therefore be represented by the response matrix $[H]$ in the following.

The first derivative of the response matrix is obtained by multiplying the response by the identity matrix and successively differentiating the expression by parts, as shown below:

$$\begin{aligned}
\frac{\partial\,[H]}{\partial\varphi} &= \frac{\partial[H][Z][H]}{\partial\varphi} \\
&= \frac{\partial[H]}{\partial\varphi}[Z][H] + [H]\frac{\partial[Z]}{\partial\varphi}[H] + [H][Z]\frac{\partial[H]}{\partial\varphi} \\
&= 2\frac{\partial\,[H]}{\partial\varphi} + [H]\frac{\partial[Z]}{\partial\varphi}[H] \\
&= -[H]\frac{\partial[Z]}{\partial\varphi}[H]
\end{aligned} \tag{4.2}$$

Equation 4.2 is valid for generally damped systems yielding complex responses and reduces the computational effort to the evaluation of dynamic stiffness derivative. As a result, the response matrices need only be evaluated once at the excitation frequency ω and the response sensitivities are calculated from the derivatives of $[Z]$, which are easier and more accurate to compute (eqn. (2.15), p. 26) than $\partial[H]/\partial\varphi$ directly.

Updating computations are frequently carried out at a number of discrete frequency points and equation 4.2 typically needs to be evaluated at a number ω's. Response calculations

are expensive for larger FE models and if the response matrix is computed from the direct inverse of the dynamic stiffness matrix (eqn. (4.1)), then the computations are also very inefficient as the direct inverse of a system is required.

Large FE models have typically many more DOFs than there are modes residing in the frequency range of interest, m. The validation of CMS methods in Chapter 3 showed that the predicted response of an uncondensed system can sufficiently be approximated by using a truncated number of modes. Based on these findings, it is therefore proposed to use a truncated modal solution of $2m$ modes to approximate the response matrix $[H]$:

$$[H(\omega)] \approx [\Phi]_{N\times 2m} \left[\lambda_r - \omega^2 \right]^{-1} [\Phi]^H_{N\times 2m} \tag{4.3}$$

By employing equation (4.3), the need to calculate a direct inverse of the dynamic stiffness matrix has been reduced to an inverse of the diagonal spectral matrix. Although a modal solution of $2m$ modes is needed, the resulting response matrix calculations are more efficient for large FE models.

The response calculations (4.3) can also accommodate a proportional damping model (by replacing the λ_r's with the corresponding complex eigenvalues), in which case the elements of the response matrix become complex:

$$H_{ij} \quad = \quad \Re(H_{ij}) + \Im(H_{ij})\,\mathrm{i} \tag{4.4}$$

where $\Re()$ and $\Im()$ designate the real and imaginary part. Similarly, the sensitivities of equation (4.2) can be written in real and imaginary parts:

$$\frac{\partial H_{ij}}{\partial \varphi} \quad = \quad \frac{\partial \Re(H_{ij})}{\partial \varphi} + \frac{\partial \Im(H_{ij})}{\partial \varphi}\,\mathrm{i} \tag{4.5}$$

4.2.2 Logarithmic Response Sensitivities

Arruda and Duarte (1990) and later Balmes (1993b) minimised the difference between the measurements and the predictions using a norm in the form of:

$$J(\{\varphi\}) = \|20\log_{10}|\{H_{Aij}(\omega,\{\varphi\})\}| - 20\log_{10}|\{H_{Xij}(\omega)\}|\,\| \tag{4.6}$$

where $\{H_{ij}(\omega)\}$ designates a FRF at all measured frequency points, ω, and response and excitation co-ordinates i,j. Indices A and X denote the predicted and measured quantities respectively.

As with the derivatives introduced in the previous section, the derivative of logarithmic FRFs (here in dB scale) can also be derived from just the knowledge of the derivative of the dynamic stiffness matrix and the response matrix itself. This is best demonstrated by considering the predicted response $\{H_{Aij}(\omega,\{\varphi\})\}$ at an arbitrary frequency point $H_{ij} = H_{Aij}(\omega_k,\{\varphi\})$. Using the notation of (4.5) and (4.4), the logarithmic sensitivity becomes:

$$\begin{aligned}
\frac{\partial\left(20\log_{10}|H_{ij}|\right)}{\partial\varphi} &= \frac{\partial\left(20\log_{10}\sqrt{\Re(H_{ij})^2+\Im(H_{ij})^2}\right)}{\partial\varphi} \\
&= \frac{20}{\log_e(10)}\left(\frac{\Re(H_{ij})\frac{\partial\Re(H_{ij})}{\partial\varphi}+\Im(H_{ij})\frac{\partial\Im(H_{ij})}{\partial\varphi}}{\Re(H_{ij})^2+\Im(H_{ij})^2}\right) \\
&\approx 8.6859\left(\frac{\Re(H_{ij})\frac{\partial\Re(H_{ij})}{\partial\varphi}+\Im(H_{ij})\frac{\partial\Im(H_{ij})}{\partial\varphi}}{\Re(H_{ij})^2+\Im(H_{ij})^2}\right)
\end{aligned} \tag{4.7}$$

where the last equation (approximation) in (4.7) is identical to the one identified by Arruda and Duarte (1990).

The logarithmic least-squares cost function (4.6) was found to be locally convex in much larger regions than the equivalent linear least-squares objective function (Balmes 1993b). Since the level of response change in dB scale is naturally much smaller than that in a linear scale, the logarithmic sensitivities will be smaller in magnitude. However, linear sensitivities are complex and relatively difficult to interpret in terms of their physical significance. Logarithmic sensitivities are real and more accessible to physical interpretation.

4.3 Response Correlation Coefficients

The success of any model updating procedure is largely determined by the quality of measurements and by the suitability of the FE model to represent the measured dynamic properties. Both aspects have been investigated in the light of their effect on updating results (Mottershead et al. 1995; Ziaei-Rad and Imregun 1996) and it was found that an inadequate mesh density and choice of finite elements, for instance, can have a detrimental effect on the updating results.

However, neither the incapacity of the FE model nor the inadequacy of the measurements can be identified by systematic data analysis. Although such numerical tools would be highly desirable, to date it is common practice to asses the closeness between measurements and predictions using correlation measures and draw conclusions from the level of correlation obtained. Often, it is implicitly assumed that if both the test data and the

FE model exhibit a good level of initial correlation, the FE model describes the physical system appropriately.

The majority of correlation techniques employ the measured and predicted mode shapes, of which the MAC (Allemang and Brown 1982)(eqn. (1.18), p. 9) is probably known best. The direct comparisons between measured and predicted FRFs, on the other hand, are less developed. For many years, it has been common practice to overlay the computed FRFs and their measured counterparts and thus visually assessing the level of correlation. Although convincing from an engineering point of view, this means of correlation is subjective and two alternatives will be introduced in the following.

Measurements are generally believed to be more accurate than predictions and represent the reference data in model updating. Assuming the measurements come in the form of measured FRFs, then these and an equal number of corresponding predictions constitute the basic data for any further correlation analysis. Either set of FRFs are uniquely described by common frequency points, their corresponding phase and amplitude, and the location of the response and excitation co-ordinates. A typical scenario in which four measurements are considered and compared in dB scale with their analytical counterparts can be seen in figure 4.1.

Figure 4.1 highlights two projection planes and suggests that these can be conveniently used to categorise most correlation techniques and even most of the existing model updating techniques.

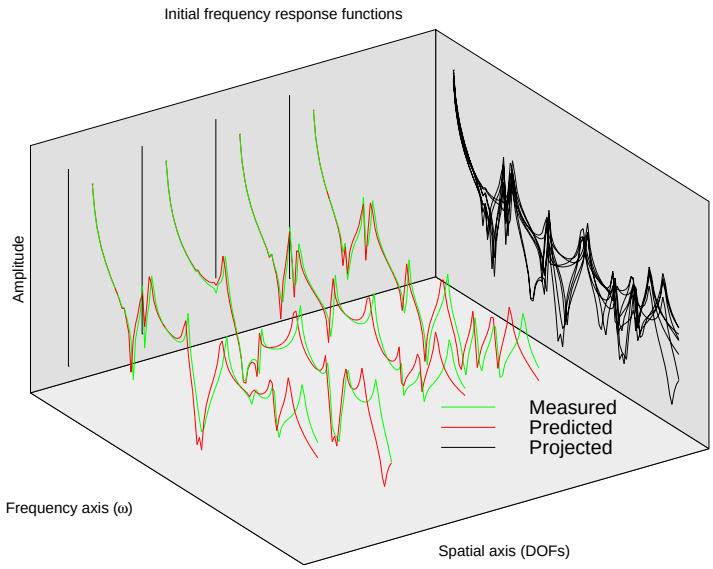

Figure 4.1: FRF overlays projected onto "amplitude-frequency plane" and "amplitude-coordinate plane"

The first plane may be called the "amplitude-frequency plane" and integrates the excitation/response location while retaining the amplitude and frequency axis. Correlation techniques using this plane therefore measure the closeness between the measured and predicted responses across the spatial axis. Such techniques can be classified as "global" correlation measures.

The second plane may be called the "coordinate-amplitude plane" and integrates the full frequency spectrum while retaining the amplitude and spatial axis. This domain permits

"local" correlation to be exercised at common excitation/response co-ordinates.

Generally, it is more desirable to get a global picture of correlation and, based on the above considerations, one such global correlation coefficient may thus be derived from the MAC for any measured frequency point, ω_k, as:

$$\chi_s(\omega_k) = \frac{\left|\{H_X(\omega_k)\}^H \{H_A(\omega_k)\}\right|^2}{(\{H_X(\omega_k)\}^H \{H_X(\omega_k)\})(\{H_A(\omega_k)\}^H \{H_A(\omega_k)\})} \tag{4.8}$$

where $\{H_X(\omega_k)\}$ and $\{H_A(\omega_k)\}$ are the measured and predicted response vectors at matching excitation/response locations. As the MAC value, $\chi_s(\omega_k)$ assumes a value between zero and unity and indicates perfect correlation with $\chi_s(\omega_k) = 1$. For $\chi_s(\omega_k) = 0$, no correlation exists. Similar to the MAC, $\chi_s(\omega_k)$ is unable to detect scaling errors and is only sensitive to discrepancies in the overall deflection shape of the structure. To emphasis this characteristic, $\chi_s(\omega_k)$ is accordingly called the *shape correlation coefficient* (Grafe 1995).

The lack of sensitivity to scaling of the shape correlation coefficient does not allow the identification of identical FRFs. This insufficiency becomes even more dramatic if just one measurement and its corresponding prediction are correlated. In this case, the column vectors reduce to scalars and $H_A(\omega_k) = \kappa H_X(\omega_k)$ is always satisfied (constant κ may be complex), therefore leading to $\chi_s = 1$ across the full frequency spectrum for uncorrelated FRFs.

As a result, a supplementary correlation coefficient, $\chi_a(\omega_k)$, is proposed by targeting the discrepancies in amplitude. The *amplitude correlation coefficient* is defined as:

$$\chi_a(\omega_k) = \frac{2\left|\{H_X(\omega_k)\}^H \{H_A(\omega_k)\}\right|}{\{H_X(\omega_k)\}^H \{H_X(\omega_k)\} + \{H_A(\omega_k)\}^H \{H_A(\omega_k)\}} \tag{4.9}$$

where the response vectors are identical to those used for $\chi_s(\omega_k)$. As for the shape correlation coefficient, $\chi_a(\omega_k)$ is defined to lie between zero and unity. This time, however, the correlation measure is more stringent and only becomes unity if $\{H_A(\omega_k)\} = \{H_X(\omega_k)\}$. That is to say, all elements of the response vectors must be identical in both phase and amplitude even if only one measurement is considered. Equation (4.9) may be understood as a variant of the Cauchy-Schwartz inequality (Golub and van Loan 1996).

In the context of the correlation planes shown in figure 4.1, both χ_s and χ_a are global correlation measures and integrate as much information as there is provided along the spatial axis. Because both correlations coefficients always return a scalar between zero and unity, the complex responses are uniquely mapped into real space.

Unlike $\chi_s(\omega_k)$ and $\chi_a(\omega_k)$, the FRAC (eqn. (1.19), p. 9) can be thought of as a local correlation measure. It operates in the amplitude-frequency plane and correlates one measurement and its corresponding prediction at a time. The correlation measures used in the objective functions proposed by Arruda and Duarte (1990) and Balmes (1993b) also fall into this category.

4.4 Sensitivities of FRF Correlation Coefficients

The mathematical design of dynamic structures is in some cases advantageously supported by a sensitivity analysis of a targeted dynamic property with respect to a number of selected design parameters (FEMtools 1995). A good example is the use of eigenvalue

sensitivities of a selected number of modes. Here, normalised sensitivities of different design parameters are typically compared to each other and design parameters are identified which tune the system most effectively.

Design sensitivities are not only useful for the understanding of the structure but they also allow to formulation of sensitivity-based model updating algorithms. With the aim of developing a correlation-based updating technique, this section presents the derivation of a closed-form solution to $\partial\chi_s(\omega_k)/\partial\varphi$ and $\partial\chi_a(\omega_k)/\partial\varphi$. Starting with equations (4.8) and (4.9), the following derivatives must be solved:

$$\begin{aligned}\frac{\partial\chi_s(\omega_k)}{\partial\varphi} = &\frac{\partial\left|\{H_X\}^H\{H_A\}\right|^2}{\partial\varphi}\frac{(\{H_X\}^H\{H_X\})(\{H_A\}^H\{H_A\})}{(\{H_X\}^H\{H_X\})^2(\{H_A\}^H\{H_A\})^2}\\ &-\frac{\partial(\{H_X\}^H\{H_X\})(\{H_A\}^H\{H_A\})}{\partial\varphi}\frac{\left|\{H_X\}^H\{H_A\}\right|^2}{(\{H_X\}^H\{H_X\})^2(\{H_A\}^H\{H_A\})^2}\end{aligned} \tag{4.10}$$

$$\begin{aligned}\frac{\partial\chi_a(\omega_k)}{\partial\varphi} = &2\frac{\partial\left|\{H_X\}^H\{H_A\}\right|}{\partial\varphi}\frac{(\{H_X\}^H\{H_X\}+\{H_A\}^H\{H_A\})}{(\{H_X\}^H\{H_X\}+\{H_A\}^H\{H_A\})^2}\\ &-2\frac{\partial\left(\{H_A\}^H\{H_A\}\right)}{\partial\varphi}\frac{\left|\{H_X\}^H\{H_A\}\right|}{(\{H_X\}^H\{H_X\}+\{H_A\}^H\{H_A\})^2}\end{aligned} \tag{4.11}$$

where $\{H_A\} = \{H_A(\omega_k,\{\varphi\})\}$ and $\{H_X\} = \{H_X(\omega_k)\}$, as before.

In the following, the individual derivatives of equation (4.10) and (4.11) are derived for real responses ($\{H_A\}$ and $\{H_X\}$ are undamped, realised or in dB scale) and for generally complex responses.

4.4.1 Sensitivities for Real Responses

For real responses, the algebra for deriving the sensitivities is largely simplified. Specifically, the Hermitian transpose becomes the transpose of real vectors leading to the following simplifications of the derivatives:

$$\begin{aligned}\frac{\partial\left|\{H_X\}^H\{H_A\}\right|^2}{\partial\varphi} &= \frac{\partial\left(\{H_X\}^T\{H_A\}\right)^2}{\partial\varphi}\\ &= 2\left(\{H_X\}^T\{H_A\}\right)\left(\{H_X\}^T\frac{\partial\{H_A\}}{\partial\varphi}\right)\\ \frac{\partial\left|\{H_X\}^H\{H_A\}\right|}{\partial\varphi} &= \left(\{H_X\}^T\frac{\partial\{H_A\}}{\partial\varphi}\right)\left(\frac{\left|\{H_X\}^T\{H_A\}\right|}{\left(\{H_X\}^T\{H_A\}\right)}\right)\\ \frac{\partial\left(\{H_A\}^H\{H_A\}\right)}{\partial\varphi} &= 2\left(\{H_A\}^T\frac{\partial\{H_A\}}{\partial\varphi}\right)\end{aligned}$$

As can be seen from the RHS of the above expressions, the differentiation by parts has led to terms which are functions of the FRF sensitivities (4.5) only and that these are now mixed with the measured data. Upon substitution of these individual terms into (4.10)

and (4.11), the design sensitivities of $\chi_s(\omega_k)$ and $\chi_a(\omega_k)$ are found to be:

$$\begin{aligned}\frac{\partial \chi_s(\omega_k)}{\partial \varphi} = &\left(\{H_X\}^T \frac{\partial \{H_A\}}{\partial \varphi}\right) \frac{2\left(\{H_X\}^T \{H_A\}\right)}{\left(\{H_X\}^T \{H_X\}\right)\left(\{H_A\}^T \{H_A\}\right)} \\ &- \left(\{H_A\}^T \frac{\partial \{H_A\}}{\partial \varphi}\right) \frac{2\left(\{H_X\}^T \{H_A\}\right)^2}{\left(\{H_X\}^T \{H_X\}\right)\left(\{H_A\}^T \{H_A\}\right)^2}\end{aligned} \tag{4.12}$$

and

$$\begin{aligned}\frac{\partial \chi_a(\omega_k)}{\partial \varphi} = &\left(\{H_X\}^T \frac{\partial \{H_A\}}{\partial \varphi}\right) \frac{2\left|\{H_X\}^T \{H_A\}\right|}{\left(\{H_X\}^T \{H_X\} + \{H_A\}^T \{H_A\}\right)\left(\{H_X\}^T \{H_A\}\right)} \\ &- \left(\{H_A\}^T \frac{\partial \{H_A\}}{\partial \varphi}\right) \frac{4\left|\{H_X\}^T \{H_A\}\right|}{\left(\{H_X\}^T \{H_X\} + \{H_A\}^T \{H_A\}\right)^2}\end{aligned} \tag{4.13}$$

The sensitivities in equations (4.12) and (4.13) are valid for real FRFs and are evaluated by using the real sensitivities of the analytical response, as denoted by equation (4.5). Therefore, the accuracy of both sensitivities depends on that of the dynamic stiffness derivatives.

4.4.2 Sensitivities for Complex Responses

In cases where the measurements are used directly and/or a damped FE solution is available, the responses will be complex and the derivation of $\partial\chi_s(\omega_k)/\partial\varphi$ and $\partial\chi_a(\omega_k)/\partial\varphi$ becomes more elaborate. Although both correlation coefficients $\chi_s(\omega_k)$ and $\chi_a(\omega_k)$ are still valid and will return a real value, particular attention must be paid to the real ($\Re$) and imaginary ($\Im$) parts of the responses. In line with the previous section, the derivatives of the following terms are found to be:

$$\begin{aligned}\frac{\partial \left|\{H_X\}^H \{H_A\}\right|^2}{\partial \varphi} = &2\left[\Im\{H_X\}^H \left(\frac{\partial \Re\{H_A\}}{\partial \varphi}\Im\left(\{H_X\}^H \{H_A\}\right) - \frac{\partial \Im\{H_A\}}{\partial \varphi}\Re\left(\{H_X\}^H \{H_A\}\right)\right)\right. \\ &\left. + \Re\{H_X\}^H \left(\frac{\partial \Re\{H_A\}}{\partial \varphi}\Re\left(\{H_X\}^H \{H_A\}\right) + \frac{\partial \Im\{H_A\}}{\partial \varphi}\Im\left(\{H_X\}^H \{H_A\}\right)\right)\right]\end{aligned}$$

$$\begin{aligned}\frac{\partial \left|\{H_X\}^H \{H_A\}\right|}{\partial \varphi} = &\frac{1}{\left|\{H_X\}^H \{H_A\}\right|} \\ &\cdot \left[\Re\left(\{H_X\}^H \{H_A\}\right)\left(\Re\{H_X\}^H \frac{\partial \Re\{H_A\}}{\partial \varphi} - \Im\{H_X\}^H \frac{\partial \Im\{H_A\}}{\partial \varphi}\right)\right. \\ &\left. + \Im\left(\{H_X\}^H \{H_A\}\right)\left(\Re\{H_X\}^H \frac{\partial \Im\{H_A\}}{\partial \varphi} + \Im\{H_X\}^H \frac{\partial \Im\{H_A\}}{\partial \varphi}\right)\right]\end{aligned}$$

$$\frac{\partial \left(\{H_A\}^H \{H_A\}\right)}{\partial \varphi} = 2\left(\Re\{H_A\}^H \frac{\partial \Re\{H_A\}}{\partial \varphi} - \Im\{H_A^H\} \frac{\partial \Im\{H_A\}}{\partial \varphi}\right)$$

It should be noted, that the three derivatives above return real scalars, as the sensitivities of $\chi_s(\omega_k)$ and $\chi_a(\omega_k)$ are real by definition. By substituting the above expressions into

equation (4.10) and (4.11), the derivatives for complex responses are obtained as:

$$\begin{aligned}\frac{\partial \chi_s(\omega_k)}{\partial \varphi} = & \frac{2}{\left(\{H_X\}^H \{H_X\}\right)\left(\{H_A\}^H \{H_A\}\right)} \\ & \cdot \Bigg[\Re\left(\{H_X\}^H \{H_A\}\right)\left(\Re\{H_X\}^H \frac{\partial \Re\{H_A\}}{\partial \varphi} - \Im\{H_X\}^H \frac{\partial \Im\{H_A\}}{\partial \varphi}\right) \\ & + \Im\left(\{H_X\}^H \{H_A\}\right)\left(\Re\{H_X\}^H \frac{\partial \Im\{H_A\}}{\partial \varphi} + \Im\{H_X\}^H \frac{\partial \Re\{H_A\}}{\partial \varphi}\right) \\ & + \frac{\left|\{H_X\}^H \{H_A\}\right|^2}{\{H_A\}^H \{H_A\}}\left(\Im\{H_A\}^H \frac{\partial \Im\{H_A\}}{\partial \varphi} - \Re\{H_A\}^H \frac{\partial \Re\{H_A\}}{\partial \varphi}\right)\Bigg]\end{aligned} \tag{4.14}$$

and

$$\begin{aligned}\frac{\partial \chi_a(\omega_k)}{\partial \varphi} = & \frac{2}{\left|\{H_X\}^H \{H_A\}\right|\left(\{H_X\}^H \{H_X\} + \{H_A\}^H \{H_A\}\right)} \\ & \cdot \Bigg[\Re\left(\{H_X\}^H \{H_A\}\right)\left(\Re\{H_X\}^H \frac{\partial \Re\{H_A\}}{\partial \varphi} - \Im\{H_X\}^H \frac{\partial \Im\{H_A\}}{\partial \varphi}\right) \\ & + \Im\left(\{H_X\}^H \{H_A\}\right)\left(\Re\{H_X\}^H \frac{\partial \Im\{H_A\}}{\partial \varphi} + \Im\{H_X\}^H \frac{\partial \Re\{H_A\}}{\partial \varphi}\right) \\ & + \frac{2\left|\{H_X\}^H \{H_A\}\right|^2}{\left(\{H_X\}^H \{H_X\} + \{H_A\}^H \{H_A\}\right)}\left(\Im\{H_A\}^H \frac{\partial \Im\{H_A\}}{\partial \varphi} - \Re\{H_A\}^H \frac{\partial \Re\{H_A\}}{\partial \varphi}\right)\Bigg]\end{aligned} \tag{4.15}$$

The shape-correlation coefficient (eqn. (4.8)) and the amplitude-correlation coefficient (eqn. (4.9)) have been evaluated for a number of parameter values, each separated by a small level of perturbation. The resulting non-linear function in φ was then used to validate the sensitivities at a number of design values. The MATLAB functions used can be found in Appendix B.

4.5 A Correlation-Based FRF Updating Technique

4.5.1 Motivation for New Algorithm

The success of many response-based model updating techniques depends upon the quality of condensation or expansion tools, as the formulations inherently require a one-to-one correspondence between the number of measurements and the number of DOFs of the FE model. For large FE models, the incompleteness ratio (2.7) is usually very small and techniques to expand the measurement vector to all FE DOFs tend to be less reliable (Ziaei Rad 1997). Model updating algorithms together with reduced FE models generally produce better results. However, conventional condensation schemes, like the one proposed by Guyan (1965), are only applicable if the FE model is relatively small and the number of measurements exceeds the number of modes in the frequency spectrum of interest[1]. Moreover, FRF model updating formulations relying on a matching number of co-ordinates and reduction or condensation methods introduce numerical errors whose magnitude may be above that required in the constitutive equations.

[1] one cannot reduce an FE model to 3 (measurement) DOFs and predict 4 modes

It is not only difficult to satisfy the data requirements of response-based updating equations but their working principle may also be difficult to handle. The input and output residual formulations presented in Chapter 2 update each individual co-ordinate separately at a number of selected frequency points. In correspondence with figure 4.1, the required responses are located in a plane parallel to the amplitude-coordinate plane at discrete frequency points. It is well understood that the selected frequency points influence the updating results, usually leading to non-unique design parameter estimates. To date, little is known about the number and location of frequency points which are most appropriate.

From an FE modelling point of view, the level of discretisation is frequently increased to ensure that the targeted modes have converged. An increased number of DOFs in the FE model, N, calls for an increased number of response measurements to comply with the FRF updating algorithms. However, the fact that the size of the FE model (DOFs) governs the number of measurements required to update the model is unreasonable from an engineering perspective. Irrespective of the amount of test data provided, the system's response is uniquely described by any measurement. In fact, it is not easy to see why one should not be able to update just one FRF over a frequency range with many more modes.

The above-addressed shortcomings of FRF model updating algorithms were the focal point in the development of the predictor-corrector model updating algorithm, which is presented in the following.

4.5.2 The Predictor-Corrector Updating Formulation

Both $\chi_s(\omega_k)$ and $\chi_a(\omega_k)$ project the measured and predicted responses to a unique correlation coefficient between zero and unity at frequency point ω_k. Using all N_f measured frequency points, the resulting two correlation curves then uniquely combine the information provided by any number of measurements and their corresponding predictions. Therefore, instead of updating the predicted response(s) directly, the objectives of FRF model updating can be re-defined to seeking unit correlation.

As has been shown before, the shape-correlation coefficient $\chi_s(\omega_k)$ defined by equation (4.8) is insensitive to scaling and is unable to localise response errors other than those detected in the relative displacements of measured co-ordinates. Its corresponding sensitivities (4.10) can therefore only be used to minimise the error in the overall deflection shape.

Unlike $\chi_s(\omega_k)$, the amplitude-correlation coefficient $\chi_a(\omega_k)$ defined by equation (4.9) is sensitive to global and local errors and its sensitivities (4.11) are accordingly responsive to any kind of discrepancies.

Assuming the responses H_{ij} of (4.4) and their derivatives $\partial H_{ij}/\partial\varphi$ in (4.5) have been computed from a reduced system representation, then the evaluation of both correlation coefficients and their sensitivities is computationally inexpensive (no matrix operations involved). It is therefore proposed to make use of $\chi_s(\omega_k)$ and $\chi_a(\omega_k)$ and their sensitivities in a combined manner to improve the overall level of correlation. Based on a truncated Taylor series expansion, one can write therefore two equations for frequency point ω_k:

$$\left\{ \begin{array}{c} 1-\chi_s(\omega_k) \\ 1-\chi_a(\omega_k) \end{array} \right\} = \left[\begin{array}{cccc} \frac{\partial\chi_s(\omega_k)}{\partial\varphi_1} & \frac{\partial\chi_s(\omega_k)}{\partial\varphi_2} & \cdots & \frac{\partial\chi_s(\omega_k)}{\partial\varphi_{N_\varphi}} \\ \frac{\partial\chi_a(\omega_k)}{\partial\varphi_1} & \frac{\partial\chi_a(\omega_k)}{\partial\varphi_2} & \cdots & \frac{\partial\chi_a(\omega_k)}{\partial\varphi_{N_\varphi}} \end{array} \right]_{2\times N_\varphi} \left\{ \Delta\varphi \right\} \tag{4.16}$$

where N_φ is the number of updating parameters and equation (4.16) is recognised to be in the standard form of sensitivity-based model updating formulations:

$$\{\varepsilon\} = [S]\{\Delta\varphi\} \tag{4.17}$$

The first of the two equations in (4.16) anticipates, or *predicts*, the change in $\{\varphi\}$ necessary to correct the discrepancy in the overall deflection pattern whereas the second equation adjusts, or *corrects*, the parameter estimates obtained from the first equation. As both equations interact with each other and the amplitude-correlation coefficient is more stringent than the shape-correlation coefficient, the formulation will be referred to as the **P**redictor-**C**orrector (P-C) method in the following.

As opposed to many other FRF updating formulations, the elements of residual $\{\varepsilon\}$ are bound to lie between zero and unity. Isolated elements of response residuals, on the other hand, may be orders-of-magnitude apart and bias the linear least-square solution. In linear regression, such points are called "outliers" (Chatterje and Hadi 1988).

Equation (4.16) can be readily turned into an over-determined system of equations by considering a number of frequency points. Assuming N_{f_u} is the selected number of frequency points and $2N_{f_u} > N_\varphi$, then a solution is available. In the following, an extended weighted least-square approach is proposed which minimises:

$$J(\{\varphi\}) = \{\varepsilon\}^T \left\lceil W_{f_\searrow} \right\rfloor \{\varepsilon\} + \{\Delta\varphi\}^T \left\lceil W_{\varphi_\searrow} \right\rfloor \{\Delta\varphi\} \tag{4.18}$$

where $\left\lceil W_{f_\searrow} \right\rfloor$ and $\left\lceil W_{\varphi_\searrow} \right\rfloor$ are diagonal weighting matrices for the frequency points and updating parameters respectively.

Equation (4.18) can be solved for the updating parameter changes by Link (1998):

$$\{\Delta\varphi\} = \left[[S]^T \left\lceil W_{f_\searrow} \right\rfloor [S] + \left\lceil W_{\varphi_\searrow} \right\rfloor \right]^{-1} [S]^T \left\lceil W_{f_\searrow} \right\rfloor \{\Delta\varepsilon\} \tag{4.19}$$

4.5.3 Frequency Point Selection

A novel feature of the proposed predictor-corrector model updating method is that no explicit frequency point selection scheme needs to be employed. In general, all N_f measured frequency points should be considered. The resulting sensitivity matrix $[S]$ is then of dimension $2N_f \times N_\varphi$ where usually $2N_f > N_\varphi$.

However, some of the N_f frequency points should be excluded. The predictor and the corrector equations in (4.16) are implicitly functions of the predicted FRFs H_{ij} and their sensitivities $\partial H_{ij}/\partial\varphi$. These are not defined at resonances and care should be taken to avoid them. As the updating computations progress, updating parameter changes may lead to changes in natural frequencies and therefore, the frequency points to be excluded generally vary from one iteration to another.

For computational efficiency, it is recommended to concentrate only on those frequency regions where the level of correlation needs to be improved while ignoring the others. When both correlation coefficients $\chi_s(\omega_k)$ and $\chi_a(\omega_k)$ are computed for all N_f frequency points, i.e. $\chi_s(\omega)$ and $\chi_a(\omega)$ where $\omega = \omega_1, \omega_2 \cdots \omega_k \cdots \omega_{N_f}$, then those ω_k may be excluded which, for example, satisfy:

$$\omega_k = \omega_i \quad \text{if} \quad \frac{\chi_s(\omega_i) + \chi_a(\omega_i)}{2} > \kappa \tag{4.20}$$

where typically $0.9 < \kappa < 1.0$.

As before, the eventual number and location of updating frequencies N_{f_u} may vary from one iteration to the next as the computation progresses and $\chi_s(\omega)$ and $\chi_a(\omega)$ change. In fact, selection procedure (4.20) serves also as a stopping criterion for the updating computations and reveals with its number of excluded frequency points the level of improvement achieved after each iteration.

4.5.4 Choice of Weighting Matrices

After the identification of a reduced number of updating frequency points N_{f_u}, where $N_{f_u} < N_f$, the weighting matrices in equation (4.19) remain to be determined. Each diagonal element of the weighting matrices may be considered as the level of confidence one has in the frequency points addressed by $\{\varepsilon\}$ and the design parameter changes denoted by $\{\Delta\varphi\}$ in equation (4.18). Therefore, the higher the weighting, the more leverage is placed on that particular equation. That is to say, "accurate" elements should experience little change.

The identification of weighting matrices is a difficult subject and often, estimated statistical properties are employed (Friswell and Mottershead 1995). In the solution procedure suggested here, no explicit statistical calculations of the weighting factors are required as the correlation coefficients $\chi_s(\omega)$ and $\chi_a(\omega)$ may be used directly. By using:

$$\left[W_f \right] = \begin{bmatrix} \left[\chi_s(\omega) \right] & 0 \\ 0 & \left[\chi_a(\omega) \right] \end{bmatrix}_{2N_{f_u} \times 2N_{f_u}} \tag{4.21}$$

the weighting factors vary between zero and unity and more confidence is placed on equations whose corresponding frequency points are better correlated.

The second term in equation (4.18) constrains the rate of change in the design parameters and damps out excessive parameter variations. This is done by assigning a weight to all the included design parameters. Similar to the approach proposed by Link (1998), good experience was made by defining the updating parameter weighing matrix as:

$$[w_\varphi] = \left[[S]^T \left[W_f \right] [S] \right]^{-1}$$

$$\left[W_\varphi \right] = \frac{\| [w_\varphi] \|_2}{max(diag([w_\varphi]))} \left[diag([w_\varphi]) \right]_{N_\varphi \times N_\varphi} \tag{4.22}$$

where the weighting matrix varies from one iteration to the next.

When (4.22) is zero, the solution of equation (4.18) represents the standard weighted least-square solution. In all other cases, the diagonal elements constrain their corresponding updating parameters in proportion to their sensitivity. Therefore, a parameter remains unchanged if its corresponding sensitivity approaches zero. An alternative definition of weighting matrix (4.22) was proposed by (Mottershead and Foster 1991).

4.6 Numerical Example

The theory of the predictor-corrector model updating formulation was checked on the 2-plate, 1-beam FE model introduced in Chapter 2 whose geometry (fig. 2.8, p. 35) and finite element properties (tab. 2.1, p. 35) remained unchanged.

In order to explore the novel features of the P-C method, the number of simulated measurements was chosen to be less than the number of modes within a given frequency spectrum of interest (i.e. $n < m$) and much smaller than the number DOFs in the FE model (i.e. $n \ll N$). By choosing three arbitrary measurement points, shown in figure 4.2, and the frequency range of the first seven modes between $0Hz$ and $100Hz$, both testing constraints were achieved. As the FE model has 864 DOFs, the resulting incompleteness ratio, defined by equation (2.7) (p. 23), was therefore $i_r \approx 1/300$.

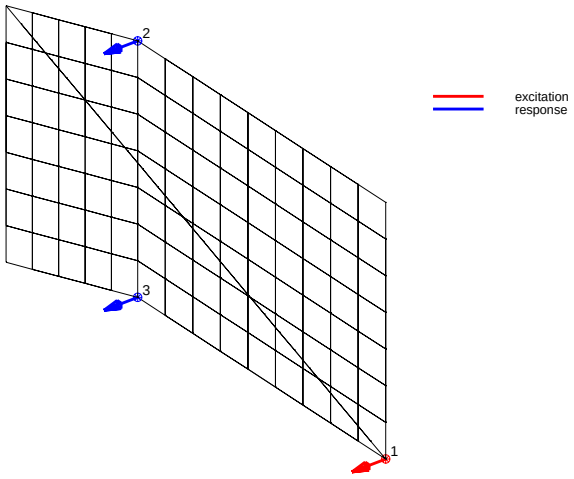

Figure 4.2: FE model and locations of excitation and response co-ordinates

Two nominal FE models were considered separately to represent the *measured* structure and the FE model to be validated. A full eigensolution of the complete *measured* structure, i.e. 864 DOFs, was employed to compute the three *measurements*. As in Chapter 2, the *measurements* were then contaminated by 15% so that

$$H_{Xij}(\omega_k) \rightarrow H_{Xij}(\omega_k)\Big(1 + 0.15\varepsilon\Big)$$

where ε is a random number between 0 and 1.

In contrast to the *measurement* model, the thickness of seven shell elements in the initial FE model were perturbed to $0.80mm$, which amounts to an error of 75% over the *measured* structure. In all, nine updating parameters were considered, each representing the shell thickness t and a group of seven shell elements. The location of the erroneous elements and the updating parameters is shown in figure 4.3.

The FE model predictions were computed from a condensed system representation. Using the fixed-interface CMS method of Craig-Bampton introduced in Chapter 3, the full model was partitioned into three sub-structures (two plates, one beam) and the condensation was performed to be valid within $0Hz$ and $100Hz$. After reducing each sub-structure, the condensed FE model had 77 (hybrid) DOFs.

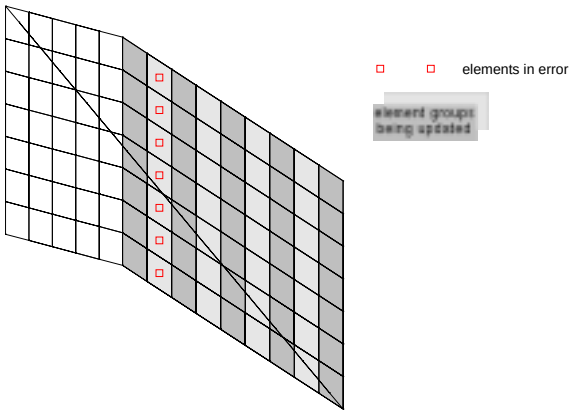

Figure 4.3: Erroneous shell elements (thickness t) and groups of shell elements as updating parameters

The *measurements* and the predictions included $\eta = 1\%$ structural damping. The initial level of correlation is shown in figure 4.4. At this point it should be noted that the predicted FRFs were computed from a condensed FE model using a truncated number of modes residing between $0Hz$ and $200Hz$. Therefore, as the *measurements* are not subject to any truncation errors, there also exist model order differences.

Although FRF correlation functions $\chi_s(\omega)$ and $\chi_a(\omega)$ are similar in that particular frequency range, the plots in figure 4.4 confirm that the amplitude-related correlation function, $\chi_a(\omega)$, is more stringent than $\chi_s(\omega)$. In particular, the discrepancies in the $0Hz$ to $50Hz$ frequency range are less well captured by $\chi_s(\omega)$.

Based on the above-described *measurements* and response predictions, the updating computations were then performed and the element thickness of the nine super-elements was updated using the P-C formulation as introduced in Section 4.5. As a result, $N_\varphi = 9$ free parameters were adjusted from $n = 3$ simulated measurements. In all there were $m = 7$ modes in updating frequency range of $0Hz$ and $100Hz$ with an frequency increment of $1Hz$, which is equivalent to $N_f = 100$.

Figure 4.5 displays the changes in element thickness over the number of iterations and table 4.1 lists the updated thicknesses. The computations converged after six iterations using the following stopping criterion:

$$\text{model updating} \rightarrow \begin{cases} \text{stop} & \text{if} \quad \left(\sum_{k=1}^{N_f} \frac{\chi_s(\omega_k)+\chi_a(\omega_k)}{2} \right) \geq 0.99 \\ \text{continue} & \text{if} \quad \left(\sum_{k=1}^{N_f} \frac{\chi_s(\omega_k)+\chi_a(\omega_k)}{2} \right) < 0.99 \end{cases} \tag{4.23}$$

It is apparent that major changes were introduced to the element thicknesses of groups 1 and 2 (both adjacent to the interface between the plates), of which group 2 was genuinely in error. An initial decrease of t of the elements in group 1 is compensated in the following iterations. The element thickness of group 2, however, consistently increases. All remaining updating parameters remain largely unchanged throughout the computations.

It is seen that the error in element group 2 has largely been identified and corrected to yield an element thickness of $1.36mm$. Element group 1 has converged to an element thickness of $1.42mm$ which is an over-estimate, unlike element group 2. As already observed from

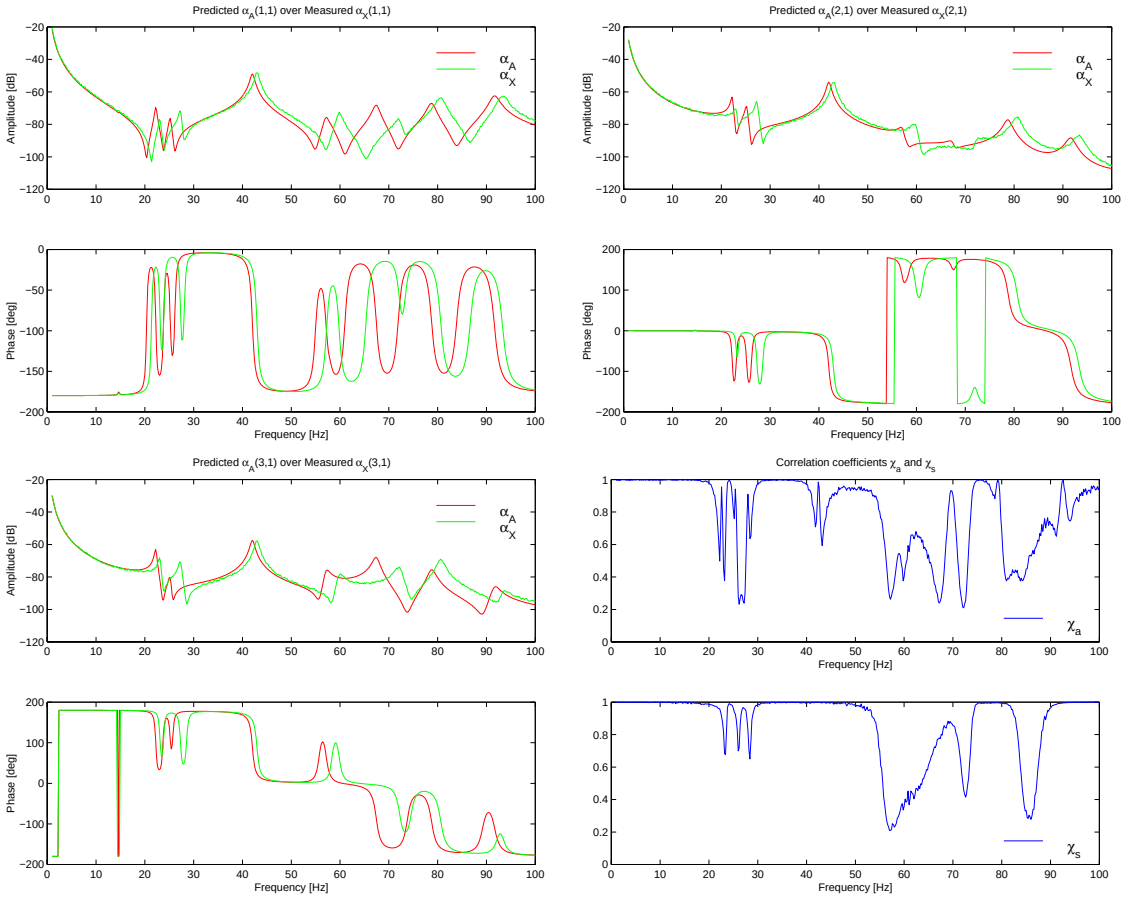

Figure 4.4: FRF overlays of three *measurements* (fig. 4.2) and associated FRF correlation coefficients

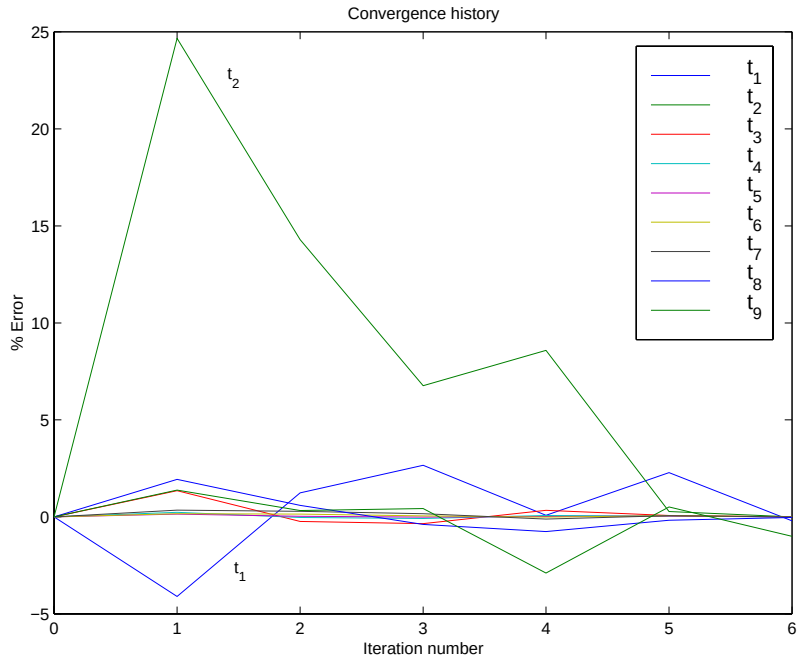

Figure 4.5: Computed changes of element thicknesses during updating of three FRFs

	Element Thickness t $[mm]$								
Group	1	2	3	4	5	6	7	8	9
Correct t	1.40	1.40	1.40	1.40	1.40	1.40	1.40	1.40	1.40
Initial t	1.40	0.800	1.40	1.40	1.40	1.40	1.40	1.40	1.40
Updated t	1.42	1.36	1.41	1.40	1.40	1.40	1.41	1.41	1.39

Table 4.1: Computed changes in element thicknesses after converged updating computations using three *measurements*

the convergence history, the remaining elements remain largely unchanged. Based on these updated element thicknesses, the level of improvement achieved in the response predictions can be seen in figure 4.6.

Figure 4.6 suggests that the differences to the nominal shell element thicknesses of $1.40mm$ do not seem to affect the updated responses. In fact, the updated FRFs exhibit a high level of correlation and the correlation coefficients are adversely affected by the noise added to corrupt the simulated measurements. Since the P-C method updates $\chi_s(\omega)$ and $\chi_a(\omega)$ directly, any further improvement may therefore prove difficult. As a direct result, the method is directly limited by the level of noise contained in the measurements and the numerical conditioning of the updating computations seemed unaffected even with a relatively high level of noise.

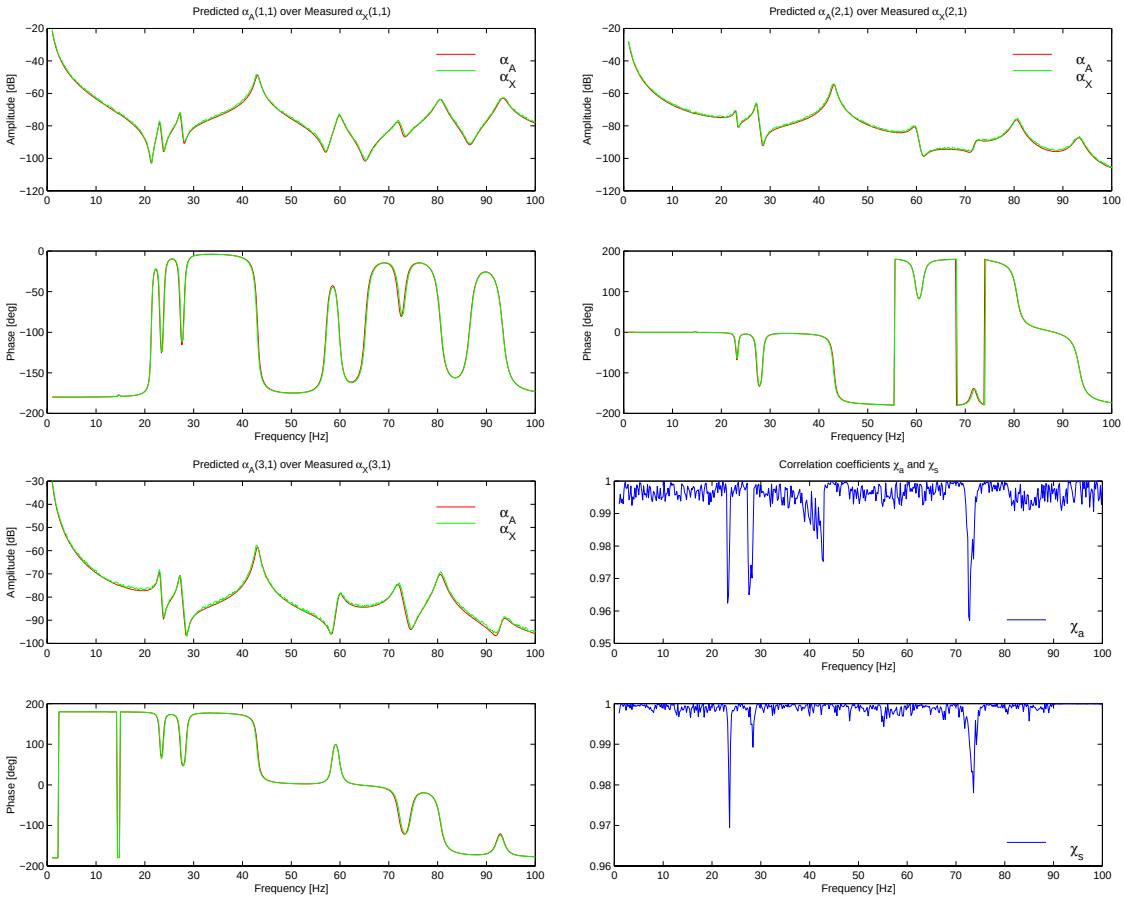

Figure 4.6: Correlation of updated FE model predictions and three measurements

Based on this encouraging result, the case study was extended to the case of just considering one simulated measurement. Both the number of updating parameters (nine strips of shell elements) as well as the initial FE model remained unchanged. This time, only *measurement* $\alpha_X(1,1)$ was included and the other two excluded.

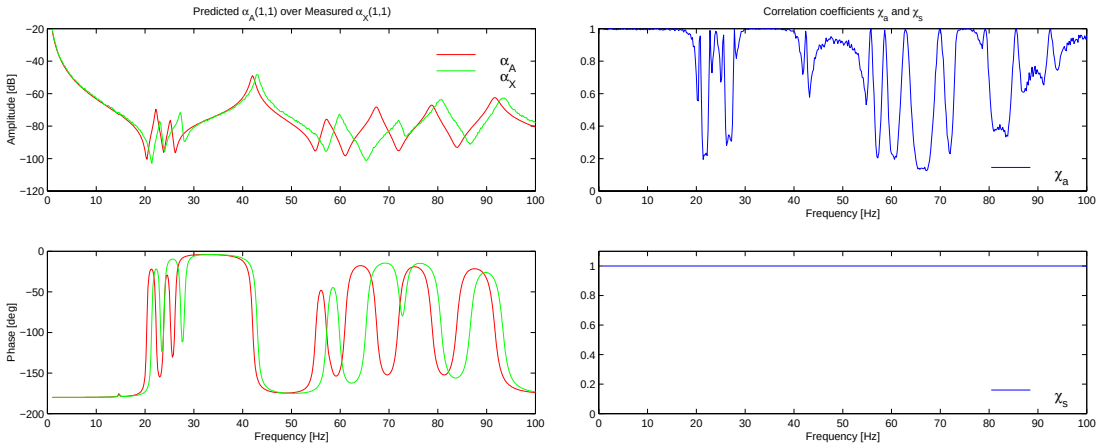

Figure 4.7: FRF overlay of one *measurement* (fig. 4.2) and associated FRF correlation coefficients

The initial correlation between the simulated measurement and its predicted counterpart is significantly different from the case with three *measurements*. Whereas the *shape*-sensitive correlation function $\chi_s(\omega)$ is unity across the full spectrum (i.e. it is immune to scaling), the *amplitude*-sensitive correlation function $\chi_a(\omega)$ still exhibits considerable discrepancies. In this particular circumstance, $\chi_s(\omega)$ and $\frac{\partial \chi_s(\omega)}{\partial \varphi}$ are redundant in the updating formulation. The updating formulation is solely based on the information provided by $\chi_a(\omega)$.

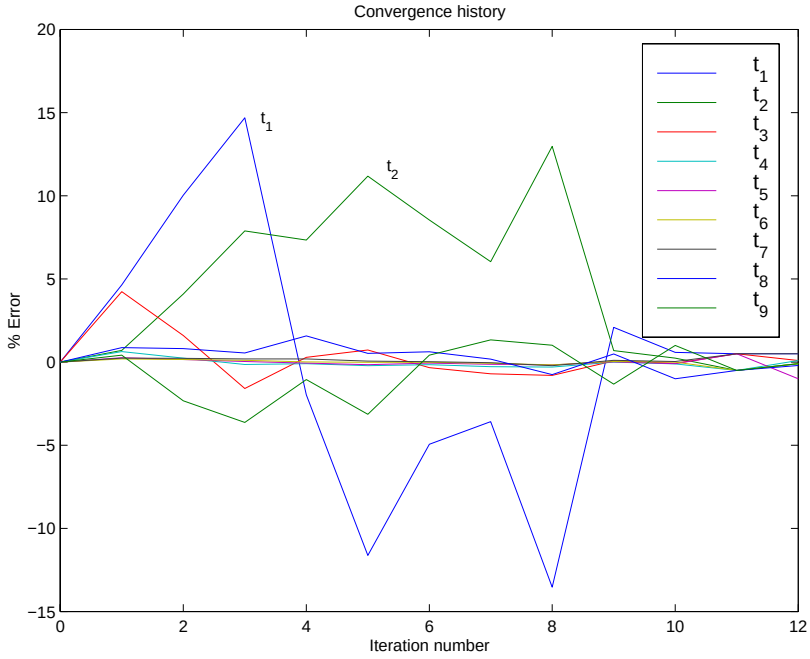

Figure 4.8: Computed changes of element thicknesses during updating of one FRF

	Element Thickness t $[mm]$								
Group	1	2	3	4	5	6	7	8	9
Correct t	1.40	1.40	1.40	1.40	1.40	1.40	1.40	1.40	1.40
Initial t	1.40	0.800	1.40	1.40	1.40	1.40	1.40	1.40	1.40
Updated t	1.35	1.40	1.44	1.39	1.40	1.40	1.37	1.45	1.36

Table 4.2: Computed changes in element thicknesses after converged updating computations using one *measurement*

During the updating computations shown in figure 4.8, the same pattern of convergence was observed as for the case of updating three FRFs. The order of magnitude by which parameters 1 and 2 changed was dominant again. This time, however, other groups of elements were exposed to higher changes, too. These were element groups 3,7,8 and 9 which, together with parameters 1 and 2, are the first and last three strips of shell elements in sub-structure 1. In both updating exercises, therefore, these boundary elements appear to be more responsive than the shell elements in the middle of the structure.

Table 4.2 shows the actual changes in thickness and indicates that some differences exist between the true thicknesses and the updated thicknesses. Since the computation converged and the stopping criterion (4.23) was satisfied, a new solution of the updated FE model was computed and its response function was correlated. As shown in figure 4.9, the adjustments introduced to the model have led to a high level of correlation and the amplitude correlation coefficient is again largely controlled by the 15% noise used to contaminate the simulated measurement.

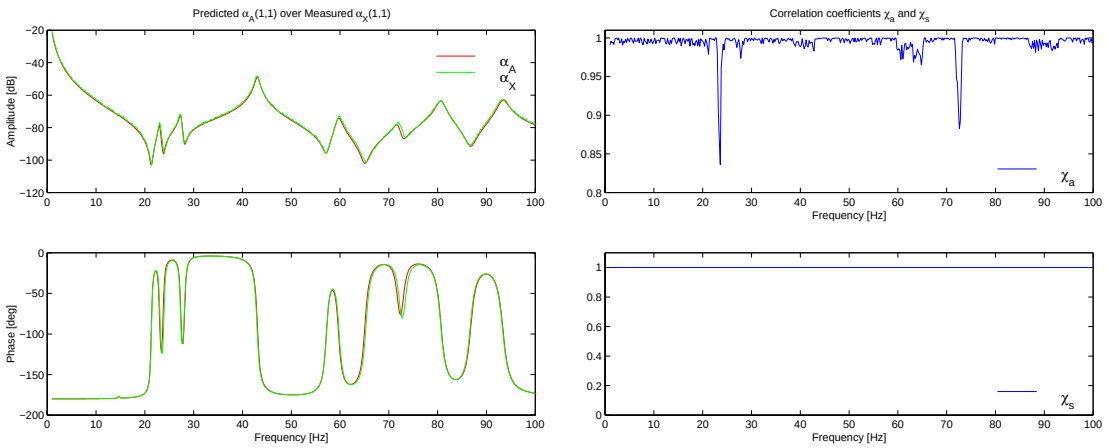

Figure 4.9: Correlation of updated FE model predictions and one measurement

4.7 Concluding Remarks

- A new updating procedure has been introduced and tested on a numerical example. It distinguishes itself from many other FRF model updating techniques by updating two correlation functions, defined across the full measured spectrum, rather than the analytical responses directly. This way, the constitutive equations of the P-C method can be satisfied for any number of measurements of any response/excitation pairing. One does not need a one-to-one correspondence between the number of measurements and the number of DOFs in the FE model.
- The need to specifically select a number of frequency points is often a basic requirement in other FRF updating algorithms. In the proposed procedure, all N_f frequency points are initially considered. After identifying the measured ω_k's which are associated with a high level of correlation and are located at resonance frequencies, N_f is reduced to the actual number of updating frequencies N_{f_u}. No explicit statistical means are required to solve the proposed extended weighted least-square problem as the correlation coefficients also serve as weights. In general, the number and location of the N_{f_u} frequency points changes from one iteration to the next.
- Both the correlation functions and their corresponding sensitivities return real values and are functions of the predicted and measured responses. Since the sensitivities are not purely analytical expressions, the the computed design parameter changes derive from both the information provided by the measurements and the FE predictions. As both quantities are also real, there is no need to partition the sensitivity equation into real and imaginary parts (eqn. (2.24), p. 28).
- The elements of the residual in the new P-C model updating technique are bound to lie between zero and unity. Unlike the differences between measured and predicted responses, the residual is much more homogeneous and is prevented from large jumps in magnitude. This property is beneficial for the least-square solution proposed.
- A high percentage of noise (15%) was used to contaminate the simulated measurements. The level of noise did not corrupt the integrity of the formulation and still led to reasonable convergence properties and updating parameter results. This level of insensitivity against noise can be explained by the formulation of the updating equations itself. Whereas many other FRF model updating techniques treat the predictions and the measurements as two separate entities, usually in the form of $[(FE) \times (\text{raw measurements})]$, both the correlation coefficients and the sensitivities are by definition a function of the measurements and the predictions.
- The updated FRFs and the measurements match almost perfectly, although the computed design parameter changes were less perfect. This is because of the discrepancy in model size ($N_{EXP} = 864$ DOFs, $N_{FE} = 77$ DOFs) and the truncated number of modes used to compute the predictions. Another possible reason is the limited number of measurements used (i.e. $n = 3$ and then $n = 1$). These aspects cannot be avoided in normal circumstances and the P-C method produces non-unique results also.
- The cost of running such an algorithm is determined by the efficiency of calculating the response sensitivities ($\partial H_{ij}(\omega)/\partial\varphi$, eqn. (4.5)). The presented case study has shown that a truncated modal solution for calculating the response matrix at every measured frequency point is sufficient for this algorithm. Although a new eigen-

solution is required after each iteration (of appropriate sub-structures), the computational cost can be low if the reanalysis is done on a sub-structured FE model (Chapter 3).

Chapter 5

Selection of Updating Parameters

5.1 Introduction

The mathematical design of dynamic structures is usually of an iterative nature and the FE model normally goes through several cycles of manual adjustments. Mesh refinements may be introduced, types of finite elements altered or extra mechanical components added whose significance to the dynamic behaviour becomes clearer during the design process. Once the FE model has been created to the best of the engineer's ability, model updating procedures are frequently employed to improve the initial, and often insufficient, level of correlation between the measurements and the predictions.

The inclusion of the right design parameters of appropriate finite elements, the updating parameters, is the key to success for any model updating algorithm. Assuming these elements and an associated element properties coincide with the error sources in the FE model, the remaining discrepancies between the FE predictions and the measurements are usually successfully reduced and a definite improvement of the correlation measures is achieved. In realistic model updating problems however, it is difficult to localise erroneous finite elements and numerical error localisation procedures are needed.

To date, there are no means available to ensure that the origins of the errors are featured in the FE model. That is to say, unless the mesh density and choice of elements of the FE model is able to reproduce the measurements by modifying appropriate design parameters, any numerical error localisation operation is destined to fail. In this chapter, it is assumed that the configuration of the FE model is adequate and error localisation procedures will be addressed on this basis.

By far the most straightforward design parameter selection-process is the inclusion of finite elements whose properties are associated with a high level of uncertainty (joints etc.). The selection of such elements is thus entirely based on engineering judgement and these uncertainties should ideally be identified also by numerical identification routines.

A strict mathematical approach to the problem of localising errors in FE models is less straightforward and the systematic identification of erroneous regions has been the subject of research in its own right over recent years. Error-localisation procedures generally analyse a number of pre-selected design parameters and allow a relative comparison between each parameter's "strength" to minimise existing discrepancies. It is then assumed that the *stronger* design parameters are associated with erroneous regions in the FE model. A related subject known as *damage detection* is similar in its objective: here, two different

states of a system are compared, one of which is the damaged structure, i.e. the erroneous one.

In the following, the principles of sensitivity-based error localisation procedures are explained and the eigenvalue-sensitivity is introduced. Contrary to modal-based sensitivity formulations, a similar procedure is then derived using the sensitivities of the P-C model updating technique. Following a discussion on the intrinsic limitations of sensitivity studies, the ability of the new algorithm is then assessed using a numerical case study.

5.2 Sensitivity-Based Error Location Procedures

Model updating algorithms are inverse processes. Given a set of measured responses and an initial FE model of the structure, the objective is to adjust the spatial parameters of the analytical model, $[M], [K] \cdots$, using measurements. Because of this non-linear relationship between the spatial parameters of the FE model and the dynamic properties of the system, the problem of finding appropriate design parameter changes is usually simplified to an algorithm of successive solutions to a linearised problem, namely $[S]\{\Delta\varphi\} = \{\varepsilon\}$.

A large family of error localisation procedures concentrate on the sensitivity matrix $[S]$ only and evaluate the level of linear-independence of each single updating parameter (column in $[S]$). More linearly-independent updating parameters are subsequently included and assumed to more erroneous. These methods make regularly use of matrix decomposition techniques such as the SVD or QR decomposition and a representative example was proposed by Yang and Brown (1997). Algorithms which also take account of the information provided by residual $\{\varepsilon\}$ have been reviewed by Friswell et al. (1997). They proposed an alternative method and contemplated group of updating parameters rather than weighting the efficiency of single parameters in isolation from each other.

The strategy of analysing the linear set of equations, $[S]\{\Delta\varphi\} = \{\varepsilon\}$, implicitly assumes that all individual finite elements have been included to retain the generality of error localisation. Since there are usually very many design parameters, the computation and subsequent decomposition of $[S]$ leads generally to excessive computational requirements for large systems.

An alternative to these procedures is the sensitivity analysis approach, i.e. the computation of sensitivities of response propertied with respect to changes in design parameters. Contrary to matrix decomposition methods where all design parameters participate at the same time, a classical sensitivity analysis contemplates each individual design parameter independently and does not "see" what the remaining parameters "do". In sensitivity studies of this kind, it is maintained that more sensitive design parameters will predominantly be able to change the response properties and that these are also indicating the elements in error. Less sensitive design parameters, on the other hand, are customarily excluded from further updating calculations.

5.2.1 Eigenvalue Sensitivity

A widely used means of identifying potential error locations in the FE model is the use of eigenvalue-sensitivities. These frequently accompany parameter studies of dynamic structures (FEMtools 1995) and represent the rate of change in λ_r for a unit change of a given design parameter, φ_i. Normally, the sensitivities of each finite element associated with a selected design parameter are computed and compared. Based on this comparison,

the analyst may then select the most sensitive elements as updating parameters. For the undamped structure, the eigenvalue-sensitivities can be derived from:

$$([K] - \lambda_r [M]) \{\phi\}_r = \{0\} \tag{5.1}$$

where $w_r^2 = \lambda_r$. Differentiating equation (5.1) with respect to a given design parameter, φ_i, then:

$$([K] - \lambda_r [M]) \frac{\partial \{\phi\}_r}{\partial \varphi_i} + \left(\frac{\partial [K]}{\partial \varphi_i} - \lambda_r \frac{\partial [M]}{\partial \varphi_i} - \frac{\partial \lambda_r}{\partial \varphi_i} [M] \right) \{\phi\}_r = \{0\} \tag{5.2}$$

Pre-multiplying equation (5.2) by $\{\phi\}_r^T$ and assuming that the mode shapes are mass-normalised so that,

$$\{\phi\}_r^T [M] \{\phi\}_r = 1$$

then the eigenvalue-sensitivity of mode r with respect to design parameter i is obtained together with the transpose of equation (5.1) as,

$$\frac{\partial \lambda_r}{\partial \varphi_i} = \{\phi\}_r^T \left(\frac{\partial [K]}{\partial \varphi_i} - \lambda_r \frac{\partial [M]}{\partial \varphi_i} \right) \{\phi\}_r \tag{5.3}$$

where the sensitivity of λ_r is seen to be just a function of the global mass and stiffness matrices and the eigenvalue and mode shape of mode r. As has been observed before, the accuracy of this sensitivity is also determined by the accuracy of the derivative of the dynamic stiffness matrix and it should be noted that this kind of sensitivity is naturally linked to modal-based updating methods.

Customarily, the sensitivities of a number of modes are analysed with respect to a selected set of design parameters. Unless only one particular mode is under scrutiny, the process of locating the errors (i.e. identifying highly sensitive regions) consists of as many sensitivity studies as there are modes of concern. However, the use of eigenvalue-sensitivities for localising miss-modelled elements must be handled with care. The sensitivity term defined in equation (5.3) ignores the measured information and is a purely analytical expression. This is somewhat contradictory as it is aimed at identifying elements which are potentially able to minimise the discrepancy between the measurements and the predictions. Therefore, highly sensitive design parameters do not necessarily bring about the response changes that actually minimise the errors. Or in other words, equation (5.3) is insensitive to the direction to which the predicted eigenvalue, r, should change. The terminology of *error localisation*, together with a purely analytical sensitivity 5.3, is therefore inappropriate.

5.2.2 Predictor-Corrector (P-C) Sensitivities

In Chapter 4, the newly developed P-C model updating method was derived from two correlation coefficients and it was shown that, together with their sensitivities, an FE model can be updated with a minimum number of available measurements. It is a sensitivity-based updating formulation and the correlation coefficients uniquely combine the information provided by the measurements and the predictions at corresponding frequency points. The sensitivities of the P-C model updating formulation may be described as "mixed" sensitivities.

Whatever the complexity of the measurements (and predictions), the sensitivities of the correlation coefficients always compute to real-valued quantities. Also distinctly different to the eigenvalue-sensitivities is the frequency spectrum covered. Instead of analysing sensitivities of particular modes, the P-C method may cover the full measured frequency spectrum. Since for most applications predominant attention is paid to a critical frequency range of interest, and real sensitivities are more amenable to physical interpretation than complex quantities, the sensitivities of the P-C method are attractive for an error localisation procedure.

In line with the algorithm proposed by Friswell et al. (1997), it is proposed to select those design parameters which minimise best residual $\{\varepsilon\}$. Assuming that one design parameter is selected, then from equation (4.16) (p. 77) the change in design parameter, $\Delta\varphi_i$, is obtained from the linearised problem:

$$\begin{Bmatrix}\{1\}\\ \{1\}\end{Bmatrix} - \begin{Bmatrix}\{\chi_s\}\\ \{\chi_a\}\end{Bmatrix}_{2N_{f_u}\times 1} = \begin{Bmatrix}\left\{\frac{\partial\chi_s}{\partial\varphi_i}\right\}\\ \left\{\frac{\partial\chi_a}{\partial\varphi_i}\right\}\end{Bmatrix}\Delta\varphi_i \tag{5.4}$$

where N_{f_u} is the number of updating frequencies. Re-writing equation (5.4) to,

$$\{\varepsilon\} = \{S_i\}\,\Delta\varphi_i \tag{5.5}$$

then the change in parameter of design variable i is simply,

$$\Delta\varphi_i = \frac{\{\varepsilon\}^T\{S_i\}}{\{\varepsilon\}^T\{\varepsilon\}} \tag{5.6}$$

which is a pseudo-inverse approximation. One possible measure to assess the *strength* of design parameter i in minimising residual $\{\varepsilon\}$ is to find those design parameter changes $\Delta\varphi_i$ which minimises an objective function $J(\{\varphi\})$ better than others. Using the equation error of the estimation problem, then this objective function could be:

$$J(\varphi_i) = \left\|\{\varepsilon\} - \{S_i\}\,\Delta\varphi_i\right\|^2 \tag{5.7}$$

which is equivalent to,

$$J(\varphi_i) = \{\varepsilon\}^T\{\varepsilon\} - \frac{\left(\{S_i\}^T\{\varepsilon\}\right)^2}{\{S_i\}^T\{S_i\}} \tag{5.8}$$

using equation (5.6). Both terms in equation (5.8) are positive and, consequently, preference should be given to those design parameters i which maximise:

$$L_i = \frac{\left(\{S_i\}^T\{\varepsilon\}\right)^2}{\{S_i\}^T\{S_i\}} \tag{5.9}$$

The function L_i is conveniently envisaged as the leverage of parameter i and is used to locate those φ_i's which are best able to fit residual $\{\varepsilon\}$. It uniquely combines the measured and predicted FRFs and their differences at N_{f_u} frequency points. One may also say that L_i indicates the level of 'fitness' of parameter i.

5.3 Intrinsic Limitations of Sensitivity Studies

Sensitivity studies allow one to distinguish between more and less sensitive elements. They are therefore a relative measure. It may be argued that more sensitive regions are indeed the elements in error, but this will only hold true if the level of perturbation is relatively small, i.e. if the initial model parameters are close to the correct model. Although this is indeed a frequently-expressed pre-requisite for the validity of many model updating techniques, it is often not a realistic assumption to make. This is particularly true if the FE model representation is very coarse and some characteristic features of the structure are not captured. In this case, the physical cause of the error is not represented in the FE model and the sensitivity study will eventually lead to flawed conclusions.

An illustration of this characteristic is the presence of joints or grounded co-ordinates in a the structure. It is known that in these cases, the rigid FE representation must be replaced by a less-than-rigid model. This is conveniently done by modelling a joint using simple (and linear) spring-mass-damper systems. The initial estimation of these lumped parameters, however, is very difficult and usually the magnitudes of the spring-mass-damper properties can only be guessed.

In these cases, the locations of erroneous elements are known. The magnitude of the design parameter, however, is not known and it can easily be demonstrated that the corresponding sensitivities studies only capture these particular design parameters if the initial estimates are fairly accurate.

Typically, one may encounter sensitivity patterns as shown in figure 5.1. Here, the eigenvalue-sensitivities of four different modes are displayed and they show that the sensitivity of individual modes is only apparent for a narrow range of design parameter settings. If the initial estimate is too low or too high, the magnitude of the sensitivities become negligible and it is unlikely that the actual parameter in error will be identified through an sensitivity-based error localisation procedure.

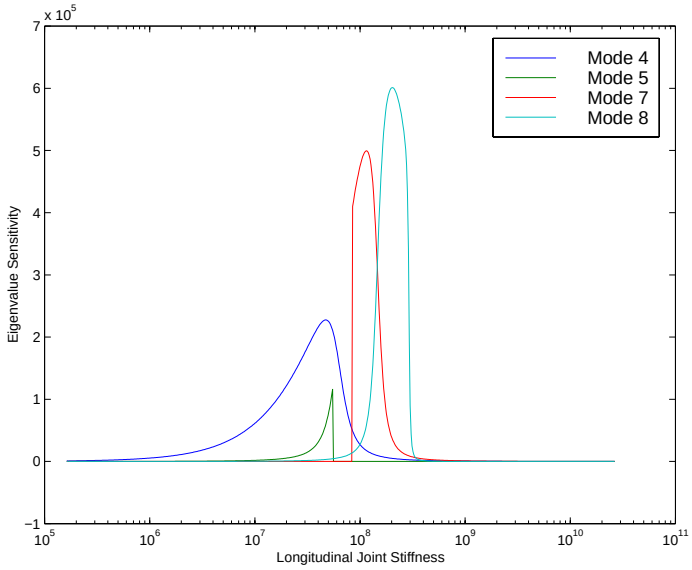

Figure 5.1: Location of sensitive regions of a sample design parameter across the frequency spectrum

It is also interesting to note that the location of sensitive regions changes from one mode to another. That is to say, if changes are introduced to the model based on a given initial estimate, a number of modes will change while others remain unchanged. For example, if mode 8 in figure 5.1 needs to be improved and a sensitivity analysis is conducted, but the initial estimate of the design parameter is such that it only exhibits sensitivity for mode 4, then one may naturally conclude that the design parameter analysed in figure 5.1 is ineffective in changing mode 8. A minor change in magnitude of this design parameter, however, already shifts the parameter in a highly sensitive region, although this information is concealed when analysing sensitivities only.

5.4 Identification of Sensitive Boundary Elements

As has been highlighted in the previous section, the FE modelling of boundary conditions and joints is generally very difficult. Often, approximate lumped spring-mass-damper parameters are used to represent the local stiffness, mass, and damping properties. Assuming the configuration of these approximate models is sufficiently able reflect the measured dynamic properties, the estimation of the initial values of these elements is still a delicate task.

Scenarios of this kind are not unusual and must be addressed if lumped parameter models are to be adjusted using sensitivity-based model updating techniques. However, identifying sensitive regions may turn out to be a problem itself using, for instance, equation (5.3). It was found, that the direct search for sensitive regions can be easily turned into a root-finding problem by employing the second order eigenvalue sensitivity. Using equation (5.3), the second order eigenvalue sensitivity can be shown to be,

$$\frac{\partial^2 \lambda_r}{\partial \varphi_i^2} = \frac{\partial \{\phi\}_r^T}{\partial \varphi_i} \frac{\partial [Z]}{\partial \varphi_i} \{\phi\}_r + \{\phi\}_r^T \frac{\partial^2 [Z]}{\partial \varphi_i^2} \{\phi\}_r + \{\phi\}_r^T \frac{\partial [Z]}{\partial \varphi_i} \frac{\partial \{\phi\}_r}{\partial \varphi_i} \tag{5.10}$$

where, as usual, r denotes the mode number and i the design parameter.

Assuming that the dynamic stiffness elements of $[Z]$ change linearly with the changes introduced to the boundary elements, then

$$\frac{\partial^2 [K]}{\partial \varphi_i^2} = 0 \quad \text{and} \quad \frac{\partial^2 [M]}{\partial \varphi_i^2} = 0 \tag{5.11}$$

and for $[M] = [M]^T$, $[K] = [K]^T$, equation (5.10) simplifies to,

$$\frac{\partial^2 \lambda_r}{\partial \varphi_i^2} = 2 \{\phi\}_r^T \left(\frac{\partial [K]}{\partial \varphi_i} - \lambda_r \frac{\partial [M]}{\partial \varphi_i} \right) \frac{\partial \{\phi\}_r}{\partial \varphi_i} - \frac{\partial \lambda_r}{\partial \varphi_i} \frac{\partial [M]}{\partial \varphi_i} \tag{5.12}$$

where equation (5.12) is a function of the first order eigenvalue-sensitivity, the eigenvector-sensitivity (Appendix A.3) and the partial derivatives of the mass and stiffness matrices, $[M]$ and $[K]$.

With the help of this second-order eigenvalue-sensitivity, sensitive regions of design parameters i may be located in conjunction with the first order sensitivities in an optimisation routine (Mathworks 1997) or independently by searching for the maximum by setting $\partial^2 \lambda_r / \partial \varphi_i^2 = 0$. However, one must be aware that the search for higher sensitivities is expensive for larger systems as a successive number of modal solutions are required.

5.5 Parameter Sub-Set Selection Procedure

The amount of possible error locations in FE models usually exceeds by far the number of equations available to formulate an over-determined updating problem. To date, sensitivity-based error localisation procedures provide the only realistic means to find potential error sources in large models. However, once a number of updating parameters have been identified, one may face the problem that some of the N_φ selected updating parameters are linearly dependent.

Since linear dependent parameters inflict rank deficient sensitivity matrices $[S]$, numerical techniques to select a subset out of N_φ parameters should be employed. As the sensitivity matrix is now of manageable size, subset selection procedures may be contemplated which are based on matrix decomposition techniques, such as the one proposed by Yang and Brown (1997).

The QR decomposition technique allows the factorisation of $[S]$ into an orthogonal base, $[Q]$, and an upper triangular matrix, $[R]$, so that,

$$[S] = [Q]\,[R] \tag{5.13}$$

where the diagonal elements of $[R]$ are usually dominant compared to the off-diagonal terms. Because $[Q]$ is orthogonal, the diagonal elements of $[R]$ disclose which columns (updating parameters) of $[S]$ are most linearly independent with largest elements in magnitude.

As a result, by selecting only a limited amount of design parameters whose corresponding columns in $[S]$ are associated with the largest diagonal elements in $[R]$, the reduced sensitivity matrix is better conditioned. However, it is generally not known how many of the N_φ design parameters may be included before $[S]$ turns ill-conditioned.

In these circumstances, good experience was gained by defining a variable threshold, κ_{mn}, which must not be exceeded by the condition number of $[S]$. That is, if the size of $[S]$ is successively increased by one column (updating parameters), the computed condition number should be below κ_{mn}. The threshold is defined as:

$$\kappa_{mn} = 1 + \kappa_\infty \left(\frac{n}{m}\right)^2 \tag{5.14}$$

where m and n reflect the current dimensions $[S] = [S]_{m\times n}$ and κ_∞ is the maximum permissible condition number of a square matrix of dimension $N_\varphi \times N_\varphi$. The scalar expression κ_∞ is usually in the region of $1 \times 10^7 < \kappa_\infty < 1 \times 10^{10}$.

To illustrate the working principles of the above-mentioned updating parameter selection criterion, let us assume that the initial number of updating frequencies is N_{f_u} and that N_φ is the initial number of identified updating parameters using a sensitivity-based error-localisation procedure. In this case, the corresponding dimensions of the sensitivity matrix are $m = N_{f_u}$ and $n = N_\varphi$. As $[S]_{m\times n}$ must generally be assumed to be poorly conditioned, a successive number of most linearly independent columns is then used to form a reduced sensitivity matrix whose resulting condition number must be below κ_{mn}. Once this threshold is exceeded, the previous number of columns, n, is used to solve for the updating parameters while the remaining updating parameters remain unchanged in that iteration.

It is worth noting that N_φ remains constant throughout the updating computations while N_{f_u} is changing from one iteration to the next. In particular, N_{f_u} usually decreases as

the computation progress and the level of correlation is improved. As the predictions are improved, the confidence in the FE model improves and according to (5.14), κ_{mn} increases also. This generally allows the inclusion of more updating parameters than in the initial iterations.

5.6 Validation of Proposed Error Localisation Method

In line with the numerical example in Chapter 4, a simulated case study was performed on the structure as shown in figure 5.2 (fig. 2.8, p. 35) (tab. 2.1, p. 35). The location of the modelling errors remained unchanged and the Young's modulus of the indicated shell elements was reduced by 50%.

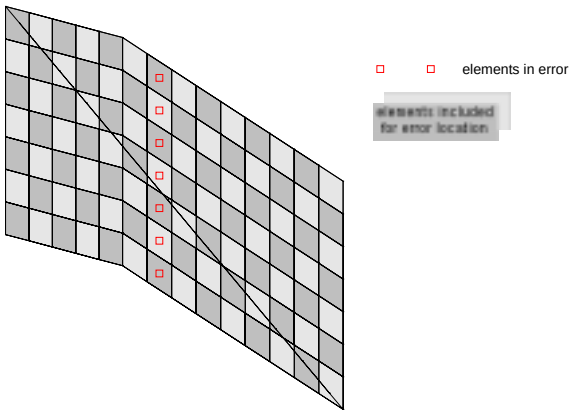

Figure 5.2: Updating parameters and locations of erroneous elements (Case 1)

A full solution was used to simulate the measurements and the updating model was condensed using the Craig-Bampton fixed-interface method. As before, the response and excitation coordinates are as indicated by figure 4.2 (p. 80) and the three measurements included were contaminated by 15% noise.

Based on the above mentioned configuration, it was sought to identify most sensitive shell elements for a number of modes using the eigenvalue sensitivity analysis, equation (5.3), and compare the results obtained with those using equation (5.9), the correlation-based error-localisation procedure. As the sensitivities of the Young's modulus were considered directly, both error localisation procedures should therefore be able to reconstruct the number and location erroneous elements.

Using the error indicator function as defined by equation (5.9), design parameters leading to higher leverages perform better than others. The results of this identification are displayed in figure 5.3 and highlight three regions of finite elements with higher leverages (minimum residuals), one of which indicates the position of the error.

An alternative solution is provided by the eigenvalue sensitivity analysis. Here, all six modes in the frequency range of interest needed to be analysed separately and the sensitivity plots are shown in figure 5.4.

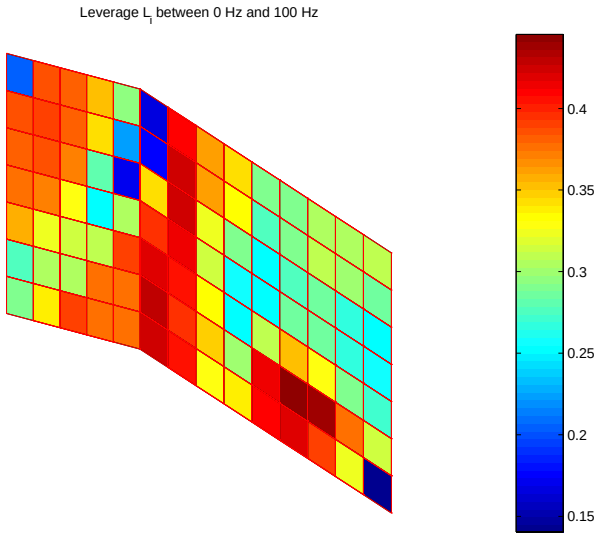

Figure 5.3: Error localisation results for Case 1

In both error localisation tools presented, none of the techniques provides a clear picture of where the erroneous elements are located. The eigenvalue sensitivities are largely inconclusive and fail to identify the perturbed finite elements. Here, an extra difficulty is added by the fact the results must be interpreted in view of six independent plots.

The newly-developed approach, covers the full frequency spectrum with one error localisation analysis and the decision-making process is consequently more straightforward. It can be argued that the results presented in figure 5.2 highlight all erroneous elements and that the majority of the remaining elements exhibit lower leverages. A more pessimistic point of view, however, may stress that there are potentially three regions of elements in error, instead of one.

The simulation has shown that the new error localisation procedure is more conclusive than the traditional eigenvalue sensitivity analysis and, if the correlation-based error identification procedure was used in a repetitive manner, the error locations could possibly be encircled.

Concluding the these findings, the configuration of the case study was altered and, instead of analysing each finite element, the updating parameters included directly pointed to the strip of erroneous finite elements. By dividing the entire FE model into strips of shell elements, the new number of updating parameters was reduced to 14. The location of these strips is shown in figure 5.5.

The identification results based on the P-C method are presented in figure 5.6. This time, the group of erroneous finite elements has been identified and the leverages, L_i, of the erroneous elements are up to 50% higher than those obtained updating parameters.

The results of the same study using the eigensensitivity approach are shown in figure 5.7. It is seen that some modes are generally more sensitive than others and that only the sensitivities of mode number 3 point at the erroneous group of shell elements. The other five modes show also more and less sensitive region, but fail to point at the elements in error.

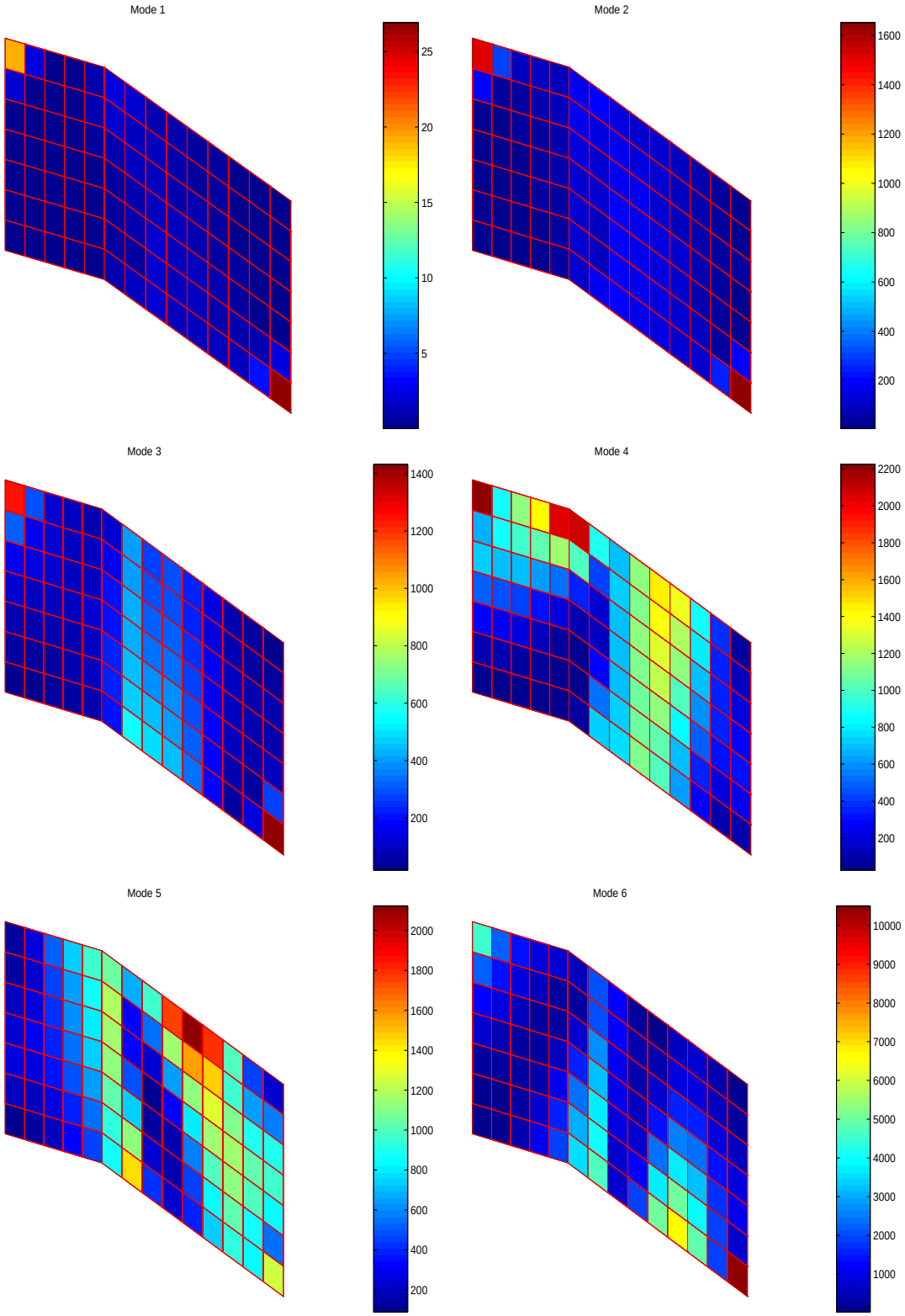

Figure 5.4: Eigenvalue sensitivities of first 6 modes for all elements in structure

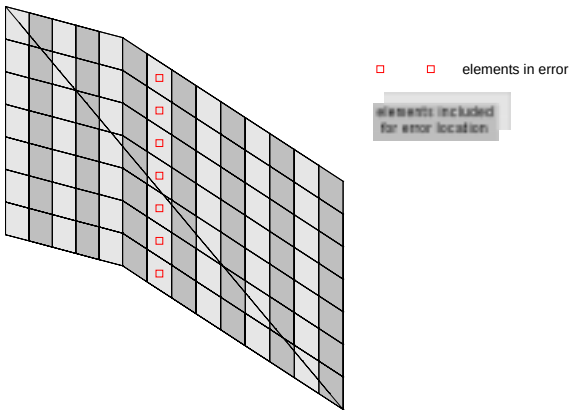

Figure 5.5: Updating parameters and locations of erroneous elements (Case 2)

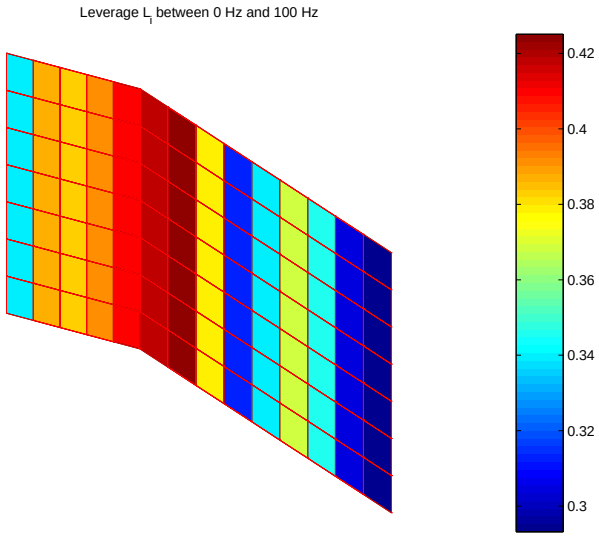

Figure 5.6: Error localisation results for Case 2

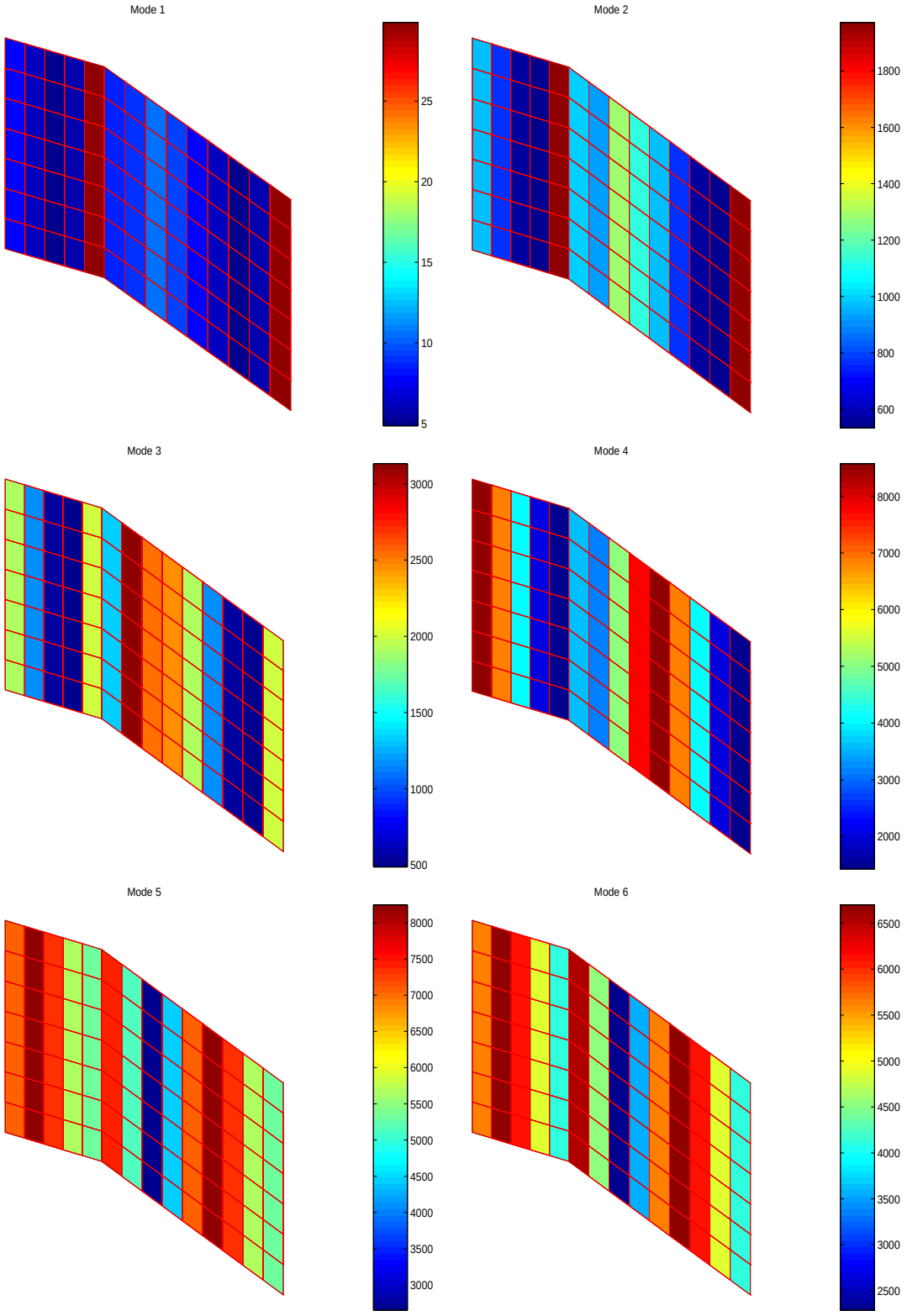

Figure 5.7: Eigenvalue sensitivities of first 6 modes for 14 super-elements

5.7 Concluding Remarks

- Error localisation algorithms are based on the assumption that, in general, changes in design parameters cause detectable changes in the dynamic properties of the system. As the configuration of the FE model is dependent on a large number of design parameters and these are generally non-linearly related to the system's dynamic properties, numerical identification procedures are usually difficult to apply.
- Sensitivity-based error localisation approaches currently seem the only realistic means for application on large FE models. Such methods generally embark on an element-by-element sensitivity study in conjunction with a selected design parameter. However, for these methods to work, the dynamic behaviour must be sensitive to the design parameters of concern.
- The eigenvalue-sensitivities have shown to be widely inconclusive and it was difficult to reconstruct the locations of erroneous elements. Also, these sensitivities are purely analytical expressions and can only be applied on a mode-by-mode basis.
- As a direct consequence of these limitations, a new error localisation procedure has been proposed using two new correlation coefficients and their derivatives. Its advantages are the inclusion of generally complex measurements and its ability to cover the full frequency spectrum of interest in one sweep. This identification approach was found to be more conclusive. However, neither the eigenvalue-sensitivities nor the correlation-based localisation procedure can find the error locations with 100% success.
- It was stressed that, in general, the identified erroneous design parameter are not linearly independent and that the linearity imposes an ill-conditioned sensitivity matrix $[S]$. To cure this problem, it was proposed to employ the QR decomposition along with maximum permissible condition number, κ_∞, to find a numerically optimum sub-set of updating parameters at any one iteration. A reduced $[S]$ is then solved and the corresponding number design parameters updated while the remaining parameters are frozen to unit (i.e. no modification).

Chapter 6

Identification of Damping Properties

6.1 Introduction

Experience has taught us that the motion of any freely vibrating structure is decaying with time and that at some time instant the structure will be at rest. This characteristic forms naturally part of our physical understanding in every-day life and is, indeed, often desirable (e.g. the degenerating tune of a guitar string). From a structural dynamics point of view, the energy content of a system is known to be constant and only a non-conservative mechanism in the vibrating structure can explain such a decline in amplitude. Consequently, as the level of vibration dies away, energy is dissipating and the structure is subject to damping.

Damping forces are 90° out-of-phase with stiffness- and inertia-related forces and of negligible magnitude away from resonances. Close to resonances, stiffness- and inertia-related forces cancel each other out and damping forces are accordingly in-phase with any externally-applied forces. At resonance, damping forces predominantly set the system in equilibrium and are 90° out-of-phase with the response. The physical significance of the inherent phase-lag is reflected by the complexity measured FRFs. In reality, therefore, the measurements are complex across the full spectrum with an increasing complexity around resonances.

Most FE analyses, however, ignore damping as, in general, very little is known about the exact underlying damping mechanisms of the structures under study. The following chapter addresses this lack of theoretical knowledge and introduces, after revisiting the analytical aspects of damped system representations, a new identification algorithm based on the previously introduced P-C model updating method. The algorithm is based on analytically derived sensitivities and may be applied to any number of measured FRFs to extract modal damping coefficients.

6.2 Damping in Structural Dynamics

A detailed description of the geometry and a good understanding of the physical properties often allows us derive a fairly accurate representation of the stiffness and inertia properties

of the system under study. In the context of the work presented, the geometry of the structure is discretised and modelled by finite elements. The physical properties of the elements are determined by the choice of elements and the elemental material properties.

The modelling of damping forces, however, lacks sufficient theoretical understanding and is much less well explored than the stiffness and inertia related forces. Although the distribution of damping may be anticipated and some regions of the FE model may suggest to be more damped than others (e.g. joints), it is usually impossible to predict what the governing rules are, not to mention how to find a good initial quantification of the damping model employed.

A wide variety of possible damping mechanisms have been studied and were derived from the observations made on the tested structure and some underlying theoretical assumptions. Theoretical damping models can be broadly classified into *non-linear* and *linear* models. Non-linear damping forces vary with time (e.g. Coulomb friction) and lead consequently to time dependent coefficients in the equation of motion. Linear damping forces are invariant with time and are represented by constant coefficients proportional to displacement or velocity or both. Such a linear differential equation with constant coefficients is expressed as:

$$[M]\{\ddot{x}(t)\} + [C]\{\dot{x}(t)\} + \mathrm{i}\,[D]\{x(t)\} + [K]\{x(t)\} = f(t) \tag{6.1}$$

Equation (6.1) identifies two constant damping matrices and correspondingly, two damping forces which are in equilibrium with the stiffness- and mass-related forces and an externally applied force vector, $f(t)$, if a forced response analysis is carried out. This standard linear damping model rules that the *viscous* damping matrix, $[C]$, is proportional to velocity and the hysteretic damping matrix, $[D]$, is proportional to displacement.

The viscous damping model is most easily understood together with the well-known dashpot. It frequently finds application in systems with local damping concentrations. These regions typically represent joints or other connecting points between adjacent structures and, of course, dashpot-like structures themselves (e.g. a car suspension). In many practical problems of structural vibration, the linear viscous damping assumption is unlikely to be accurate. When damping arises from internal or material friction, frictional forces are found to be almost independent of velocity (Newland 1975). In this case, therefore, the hysteretic damping model gives a more realistic description of the acting damping forces.

Measured FRFs uniquely describe the dynamic properties of the structure. The measured response is a function of the model's stiffness and mass distribution and its damping properties. Although the mass and stiffness matrices, $[M]$ and $[K]$, can be modelled with a higher confidence, the initial predictability of the damping properties represented by $[C]$ and $[D]$ is very low. Indeed, so little is known about the distribution and magnitude of damping that the FE analysis is often confined to an undamped model representation. This may lead to a poor analytical model, but finds frequently justification if the structure under study is lightly damped.

6.3 Proportional Damping Models

Model updating techniques provide a means to adjust erroneous design parameters but also provide a framework for identifying damping parameters from measurements. However, the complexity of the measurements and that of the predictions of a damped FE model

([C] and [D]) cause a number of numerical problems in conventional updating algorithms. Often, the resulting set of complex equations is partitioned into real and imaginary parts so that the system can be solved for real design parameter changes (eqn. (2.24), p. 28). As a result, the size of the linear system of equations doubles and the of number updating parameters generally increases to accommodate the adjustment of matrices [C] and [D]. Using a response-based updating formulation, Visser (1992) proposed one such an approach and observed that complexity introduces slow convergence properties and numerical instabilities. She concluded further that good initial assumptions about the damping present in the structure and accurate measured response data are required to identify a damping matrix successfully. Similar damping identification techniques were reviewed by Pilkey and Inman (1998) of which some also employ measured modal data. The majority of techniques lead to symmetric, real and positive definite damping matrices [C] and [D], often obtained in an iterative fashion.

Assuming that damping matrices [C] and [D] have been identified in one way or another, the generally-damped system, as expressed by equation (6.1), must then be solved. Typically, the N second-order differential equations are transformed into a first-order problem of $2N$ equations. The resulting state-space representation can take the form,

$$\begin{bmatrix} -([K]+\mathrm{i}\,[D]) & [0] \\ [0] & [M] \end{bmatrix} \begin{Bmatrix} \dot{x}(t) \\ \ddot{x}(t) \end{Bmatrix} + \begin{bmatrix} [0] & ([K]+\mathrm{i}\,[D]) \\ ([K]+\mathrm{i}\,[D]) & [C] \end{bmatrix} \begin{Bmatrix} x(t) \\ \dot{x}(t) \end{Bmatrix} = \begin{Bmatrix} 0 \\ 0 \end{Bmatrix}$$

or using a more compact notation,

$$\left[\tilde{M}\right] \{\dot{w}(t)\} + \left[\tilde{K}\right] \{w(t)\} = \{0\} \tag{6.2}$$

where $\{w(t)\}$ is also known as *state variable*. It should be noted that the first row of equation 6.2 retains the symmetry of the system by equating to identity.

Unlike equation (6.1), equation (6.2) can be formulated as a standard eigenvalue-problem (Appendix A.2). Assuming a trial solution of $\{w(t)\} = \{\mathrm{w}\}\, e^{\lambda t}$, with $\{\mathrm{w}\}$ being a vector of complex and time-independent amplitudes and $\lambda = \alpha + \mathrm{i}\,\beta$, a general complex eigenvalue with its oscillatory frequency β and decay α, the solution to:

$$\left(\left[\tilde{K}\right] + \lambda \left[\tilde{M}\right]\right) \{\mathrm{w}\} = \{0\} \tag{6.3}$$

is obtained in the form of $2N$ eigenvectors and eigenvalues:

$$[\Theta]_{2N\times 2N} \qquad \left[\begin{smallmatrix} \lambda_r & \\ & \ddots \end{smallmatrix}\right]_{2N\times 2N}$$

which are complex and exist in complex conjugate pairs (see also Notation, p. viii).

As can be seen from above, solving generally-damped FE models requires doubling the size of the system and increases the computational effort immensely. Also, an increased number of updating parameters associated with matrices [C] and [D] makes such a general approach increasingly unsuitable for application to larger FE models.

In seeking a new damping identification algorithm, it is shown that the so-called *proportional* damping model is in many respects easier to analyse and that the assumption of proportionality reduces the number of unknowns to a minimum within the framework of the P-C method. General damping cases, as discussed above, are classified as *non-proportional* damping models. Proportional damping models, on the other hand, find their origins of the terminology by assuming that,

$$\begin{aligned} [D] &= \beta_D\,[K] + \gamma_D\,[M] \\ [C] &= \beta_C\,[K] + \gamma_C\,[M] \end{aligned}$$

where β and γ are constants so that matrices $[C]$ and $[D]$ are linear combinations of the mass and stiffness matrices.

If the damping matrices are proportional to the mass and stiffness matrices of the system, then it is not difficult to see that the mode shapes of the undamped system also allow the uncoupling of equation (6.1). That is,

$$\left[m_{\diagdown}\right]\{\ddot{q}(t)\} + \left[c_{\diagdown}\right]\{\dot{q}(t)\} + \mathrm{i}\left[d_{\diagdown}\right]\{q(t)\} + \left[k_{\diagdown}\right]\{q(t)\} = [\Psi]^T f(t) \tag{6.4}$$

using the eigensolution of the undamped system,

$$[\Psi]_{N\times N} \qquad \left[\lambda_{r\diagdown}\right]_{N\times N} \tag{6.5}$$

In particular, it is found that the mode shapes of a proportionally-damped system are identical to those of the undamped system and that the eigenvalues are close also (Ewins 1984). Therefore, the undamped system solution is sufficient to derive the damped modal properties by just making corrections to the natural frequencies.

The proportional damping model has found wide application and is found to be in good agreement for many practical problems. This is especially true for the experimentally determination of modal damping factors where proportional damping model builds the necessary theoretical foundation. However, it should be noted that not all structures are subject to this type of distribution.

6.4 Analytical Identification of Damping

In the framework of model updating calculations, the identification of damping properties has only been performed with limited success. Frequently, damping is conveniently ignored as it places extra constraints on model updating algorithms and often leads to numerical instabilities. This section addresses these problems and proposes an alternative damping identification algorithm based on P-C model updating formulation (chap. 4) using analytically exact sensitivity terms.

6.4.1 Viscously-Damped FRFs and their Sensitivities $\frac{\partial H(\zeta)}{\partial \zeta}$

If a viscous damping model is assumed, and the structural damping matrix $[D] = [0]$, then the viscous damping ratio is defined according to Ewins (1984) as,

$$\zeta_r = \frac{1}{2}\left(\beta\,\omega_r + \frac{\gamma}{\omega_r}\right) \tag{6.6}$$

which is seen to be proportional to the mass and stiffness matrices with the constants $\beta \neq 0$ and $\gamma \neq 0$.

Since a proportional damping approach is assumed, equation (6.1) is decoupled by using the mass-normalised mode shapes $[\Phi]$ of the undamped system solution. The decoupling property of the eigenvectors can be used advantageously and allows the computation of individual receptance elements (Ewins 1984) by,

$$\alpha_{ij}(\omega) = \sum_{r=1}^{N} \frac{{}_r\phi_i\,{}_r\phi_j}{\omega_r^2 - \omega^2 + 2\ \mathrm{i}\ \omega\,\omega_r\,\zeta_r} \tag{6.7}$$

which is the receptance at response coordinate, i, and excitation coordinate, j, and excitation frequency, ω. This modal summation is exact if all N modes of the system are used.

In the framework of the P-C model updating method, it was shown that any design parameter can be considered provided a response sensitivity of the form of $\frac{\partial H}{\partial \varphi_i}$ is available. Based on equation (6.7), such a sensitivity can be derived as,

$$\begin{aligned}\frac{\partial \alpha_{ij}(\omega)}{\partial \zeta_r} &= \frac{\partial}{\partial \zeta_r}\left(\frac{{}_r\phi_i\,{}_r\phi_j}{\omega_r^2-\omega^2+2\,\mathrm{i}\,\omega\,\omega_r\,\zeta_r}\right)\\ &= -\frac{{}_r\phi_i\,{}_r\phi_j}{\left(\omega_r^2-\omega^2+2\,\mathrm{i}\,\omega\,\omega_r\,\zeta_r\right)^2}\frac{\partial\left(\omega_r^2-\omega^2+2\,\mathrm{i}\,\omega\,\omega_r\,\zeta_r\right)}{\partial \zeta_r}\\ &= \frac{{}_r\phi_i\,{}_r\phi_j}{\frac{1}{2\,\omega\,\omega_r}\left(\omega_r\left(\omega_r+2\,\mathrm{i}\,\omega\,\zeta_r\right)-\omega^2\right)^2\mathrm{i}}\end{aligned} \tag{6.8}$$

Equation (6.8) greatly simplifies the computation of the sensitivity and it is seen that no explicit numerical differentiation of $[C]$ is needed. Both analytical expressions of the viscously-damped FRF and its sensitivity with respect to its damping coefficients have been numerically validated. The MATLAB function `visc_frf.m` used can be found in the Appendix B.

6.4.2 Structurally-Damped FRFs and their Sensitivities $\frac{\partial H(\eta)}{\partial \eta}$

Along with viscously-damped FRFs, a structurally-damped system may similarly be treated under the assumption of proportionality. If the viscous damping matrix is ignored, i.e. $[C] = [0]$, and it is assumed that $[D] \neq [0]$ and proportional to the system mass and stiffness matrices, then the so-called structural damping loss factor is defined by Ewins (1984) as,

$$\eta_r = \beta + \frac{\gamma}{\omega_r^2} \tag{6.9}$$

in which case both γ and β are constants generally different from zero.

Since the mode shapes of a proportionally-damped systems are identical to those of undamped systems, the equation of motion of the structurally-damped system is decoupled, as before, and a modal summation may be employed to compute individual FRF elements as,

$$\alpha_{ij}(\omega) = \sum_{r=1}^{N} \frac{{}_r\phi_i\,{}_r\phi_j}{\omega_r^2-\omega^2+\mathrm{i}\,\omega_r^2\,\eta_r} \tag{6.10}$$

where the summation includes all N modes, as for the viscoelastic case. The resemblance to the viscously-damped FRFs is obvious. Yet, the loss factor η is not proportional to the excitation frequency and thereby reflects its proportionality to displacement.

Upon derivation of equation (6.10), the sensitivity of the FRF to changes in the structural

damping parameters are:

$$\begin{aligned}\frac{\partial \alpha_{ij}(\omega)}{\partial \eta_r} &= \frac{\partial}{\partial \eta_r}\left(\frac{{}_r\phi_i\, {}_r\phi_j}{\omega_r^2 - \omega^2 + \mathrm{i}\ \omega_r^2\, \zeta_r}\right) \\ &= -\frac{{}_r\phi_i\, {}_r\phi_j}{\left(\omega_r^2 - \omega^2 + \mathrm{i}\ \omega_r^2\, \eta_r\right)^2}\frac{\partial\left(\omega_r^2 - \omega^2 + \mathrm{i}\ \omega_r^2\, \zeta_r\right)}{\partial \eta_r} \\ &= \frac{{}_r\phi_i\, {}_r\phi_j}{\left(\omega_r\left(1 + \mathrm{i}\ \eta_r\right) - \frac{\omega^2}{\omega_r^2}\right)^2 \mathrm{i}}\end{aligned} \tag{6.11}$$

which is the derivative of the FRF for mode, r, at response coordinate, i, and excitation coordinate, j. The MATLAB function `hyst_frf.m` included in Appendix B allows the computation of the structurally-damped FRFs as well as the calculation of their derivatives with respect to a selected loss factor η_r.

6.4.3 Identification of Damped Responses

One of the characteristic features of the P-C method introduced in Chapter 4 is the inclusion of the full frequency spectrum in the model updating exercise, as opposed to selected frequency points, and the computation of the FRFs using a truncated number modes. This model updating technique accepts generally complex FRFs and sensitivities, and effectively maps these complex quantities into a real set of correlation coefficients and a real set of updating equations (i.e. the sensitivities of the correlation coefficients are also real).

The updating parameters considered in the P-C method, so far, were directly linked to the design parameters of the mass and stiffness matrices. The updating parameters, however, could have also been damping matrices $[C]$ and $[D]$ as long as analytical (complex or real) response sensitivities of the form,

$$\frac{\partial H}{\partial \varphi_i}$$

are known or available. In this case, it has been shown that numerical differentiation of the dynamic stiffness matrix can be avoided if the sensitivities in equations (6.8) (6.11) are employed directly. These analytically well-defined sensitivities can then be utilised directly to compute the sensitivities of the shape- and amplitude-correlation coefficients (eqn. (4.10) p. 74, eqn. (4.11) p. 74), which are themselves analytically exact. Therefore, based on both sets of sensitivities, damping parameters can be updated within the environment of the P-C updating algorithm.

It is not difficult to see that the sensitivities of the damping parameters are linearly independent to each other as they only peak at their corresponding resonance and are of smaller magnitude elsewhere. A localisation of erroneous damping coefficients is therefore immaterial since the number of modes, and therefore the number of updating parameters, is in any case limited to the number of modes in the frequency region of interest. Assuming that a FE model is to assume a structural (and proportional) damping model and the number of modes in the spectrum considered is 10, then there are 10 independent sensitivities for the parameters $\eta_r, r = 1, 2, \cdots 10$ and the updating problem leads to a well-conditioned sensitivity matrix, $[S]$, i.e. none of the columns of $[S]$ are linearly dependent and the resulting system is of rank 10.

Conflicting Definition of Proportionality

Often, a constant modal damping factor, say $\eta_r = 0.01, \quad r = 1, 2, 3, \cdots m$, is employed as an initial estimate or found to be closest to the measurements. Assuming that the damping is proportional to stiffness-related properties only, then equation (6.9) identifies,

$$\eta_r = \beta \quad \text{and therefore} \quad [D] = \beta[K] \quad \text{and} \quad \beta[\Phi]^T[K][\Phi] = \left[\omega_r^2\right] \beta$$

in order to comply with the definition of proportionality in Section 6.3. If, however, the structural loss factor varies from one mode to another, the above relations do not hold true anymore and change to,

$$\eta_r = \beta_r \quad \text{and therefore} \quad [D]_r = \beta_r[K] \quad \text{and} \quad \beta_r \{\phi\}_r^T [K] \{\phi\}_r = \omega_r^2 \beta_r$$

i.e. β is only proportional on a mode-by-mode basis and such a damping model does not comply with the definition of proportionality.

Therefore, the identified damping model of the above mentioned algorithm is, in a strict sense, not proportional. The identified modal damping factors (η_r or ζ_r) are local to mode r and, consequently, a construction of damping matrix $[D]$ based on the identified loss factors is not possible.

6.5 Numerical Validation of Damping Identification Algorithm

In line with the simulated case for the P-C method in Chapter 4, the proposed damping identification algorithm is validated on the same 2-plate, 1-beam structure (fig. 2.8, p. 35) (tab. 2.1, p. 35). To prove the methods ability, only a limited number of *measurements* were simulated from the uncondensed FE model, as shown in figure 6.1, and the analytical model was condensed from 864 DOFs to 126 DOFs. As before, the simulated measurements were contaminated by 15% multiplicative noise and the locations of the excitation and response points are highlighted in figure 6.1.

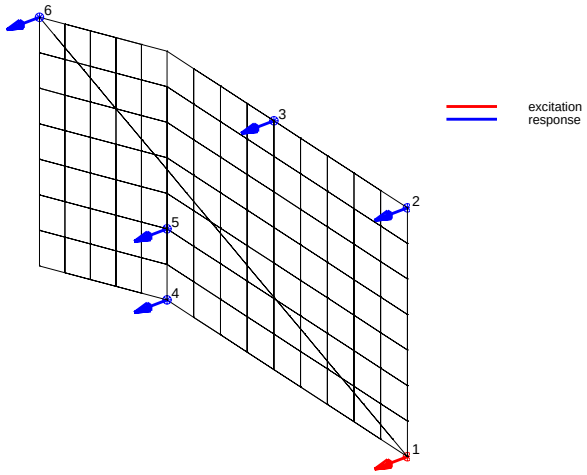

Figure 6.1: FE model and locations of excitation and response co-ordinates

The development of the damping identification procedure has shown that numerical differentiation of dynamic stiffness terms has become obsolete and that the sensitivities derived can be used in the same fashion as those of the spatial parameters. The following case study is therefore invaluable to prove the correctness of the derivatives (6.8) and (6.11) as well as their ability to update damping parameters as part of the P-C method.

A relatively high modal density of the structure in the low frequency region led to chose a frequency region from $0Hz$ to $100Hz$ in which nine elastic modes reside and six rigid-body modes.

6.5.1 Identifying η_r from Structurally-Damped Responses

In a first attempt to identify appropriate damping parameters, both sets of FRFs were generated using the structural damping model defined by equation (6.7) and all available six measurement locations were considered (fig. 6.1). The differences in the structural damping factors were set considerably higher for the first four elastic modes in the analytical predictions and can be seen in table 6.1.

Based on these perturbations, the initial correlation between the *measurements* and the analytical predictions were computed and are shown in figures 6.4 and 6.2.

With the aim to identify the changes in damping, the updating computations were then initiated using the sensitivity defined in equation (6.11) together with the P-C model

η_r	$\eta_1 \rightarrow \eta_6$	η_7	η_8	η_9	η_{10}	$\eta_{11} \rightarrow \eta_\infty$
Correct value	0.007	0.010	0.050	0.090	0.150	0.007
Initial estimate	0.003	0.003	0.003	0.003	0.003	0.003

Table 6.1: Perturbations before updating structural damping factors η_r

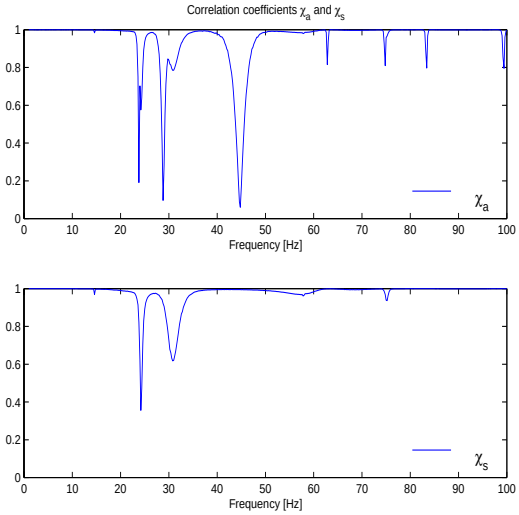

Figure 6.2: Correlation functions $\chi_s(\omega)$ and $\chi_a(\omega)$ before updating η_r of six DOFs

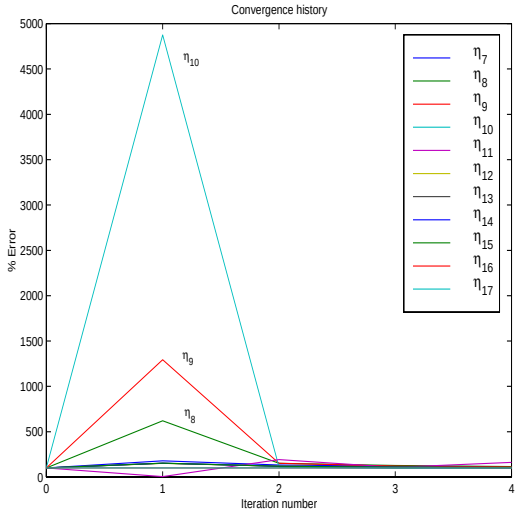

Figure 6.3: Computed changes in η_r during updating calculations using six DOFs

updating approach. The first six structural damping factors, i.e. $\eta_1 \rightarrow \eta_6$, were correctly computed to zero sensitivity since these are associated with the rigid-body modes and the structure is not subject to damping. Excluding these in the following calculations, 11 damping factors remained to be identified. Nine of these modes reside in the frequency range of interest and two extra modes were included to ensure possible damping effects are caught from out-of-band modes. The changes computed are shown in figure 6.3 and suggest that the computations essentially converged after one iteration. After four iterations the calculations were stopped and the identified changes in structural damping parameter are shown in table 6.2 .

η_r	$\eta_1 \rightarrow \eta_6$	η_7	η_8	η_9	η_{10}	η_{11}	$\eta_{12} \rightarrow \eta_{15}$	$\eta_{16} \rightarrow \eta_\infty$
Correct	0.007	0.010	0.050	0.090	0.150	0.007	0.007	0.007
Updated	0.003	0.010	0.045	0.088	0.145	0.004	0.006	0.003

Table 6.2: Identified structural damping factors η_r after updating six DOFs

The identified damping factors are close to the true values and the two out-of-band modes remained unchanged throughout the computations. Based on the updated damping parameters, figure 6.5 shows the updated level of correlation and sample FRF $\alpha_{11}(\omega)$. Here, it is interesting to note that the correlation functions display the noise content of the simulated measurements and that at this level of correlation, the P-C method is unlikely to discriminate any further between measurement noise and structural response.

Based on these encouraging results, the number of *measurements* included was reduced to $\alpha_{11}(\omega)$ only and subsequently, the initial proportional damping model of the 864-DOF

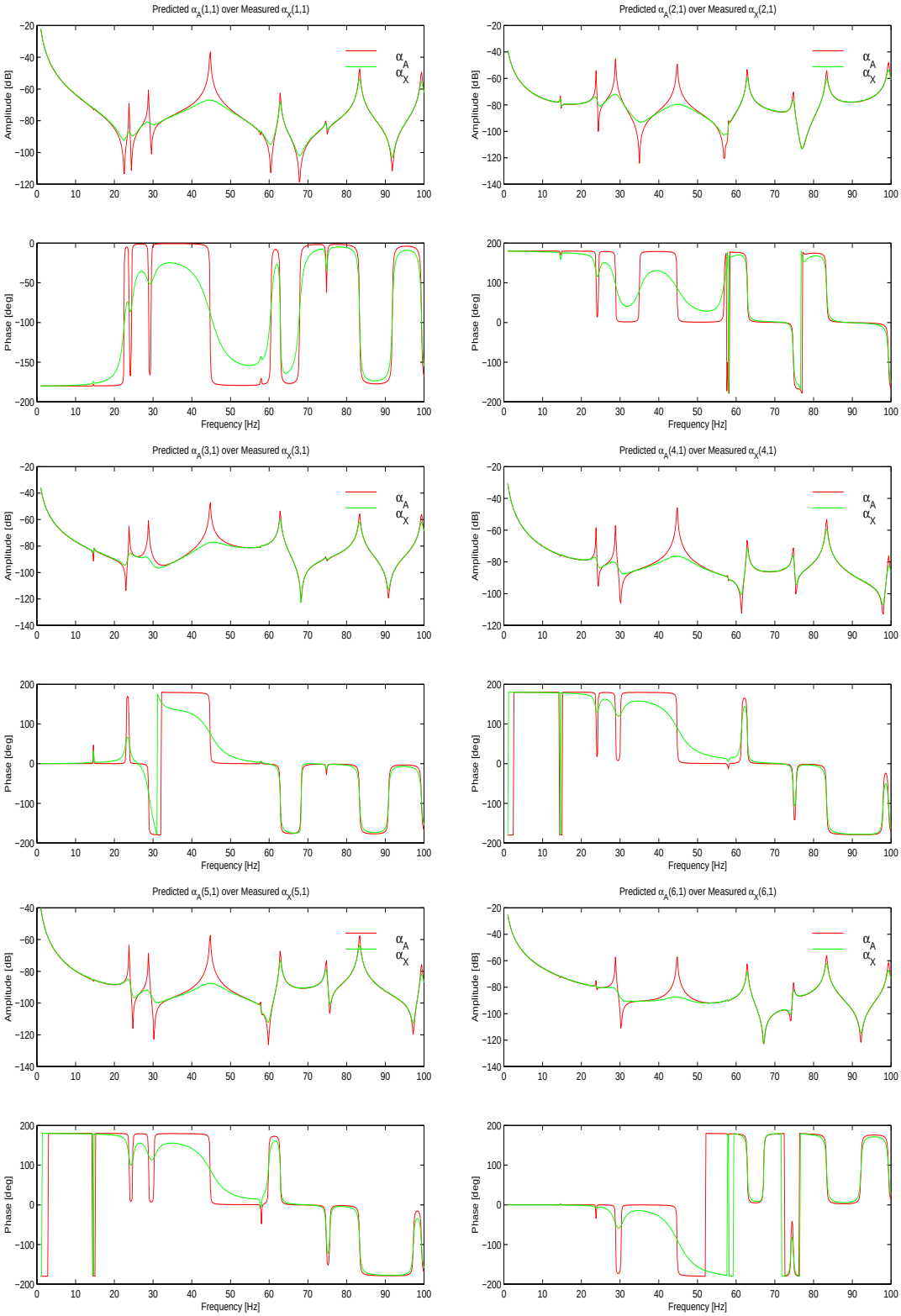

Figure 6.4: FRF overlays of six co-ordinates (fig. 6.1) before updating structural damping factors η_r

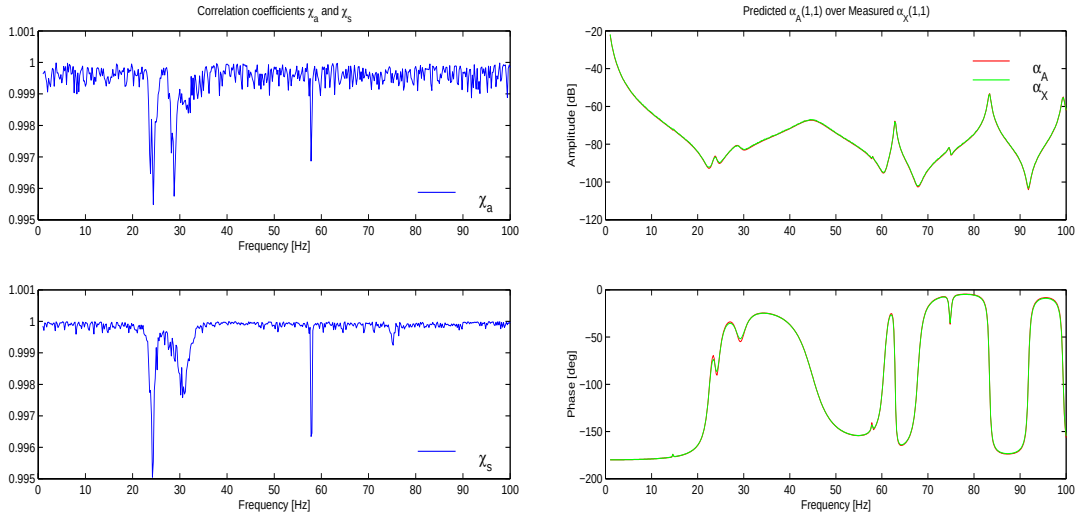

Figure 6.5: Response correlation after updating η_r of six DOFs

FE model was aimed to be adjusted in the light of this simulated measurement.

Figure 6.6 shows the initial correlation, in which case only discrepancies in amplitude are apparent and no error is indicated by $\chi_s(\omega)$ since its immunity to scaling, i.e. each predicted frequency point can be scaled to match its *measured* counterpart.

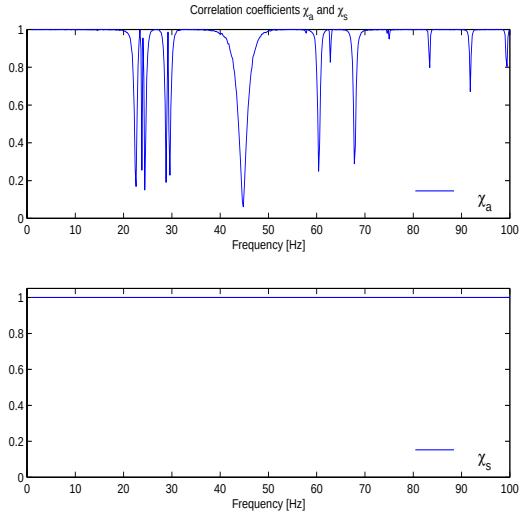

Figure 6.6: Correlation functions $\chi_s(\omega)$ and $\chi_a(\omega)$ before updating η_r of one DOF

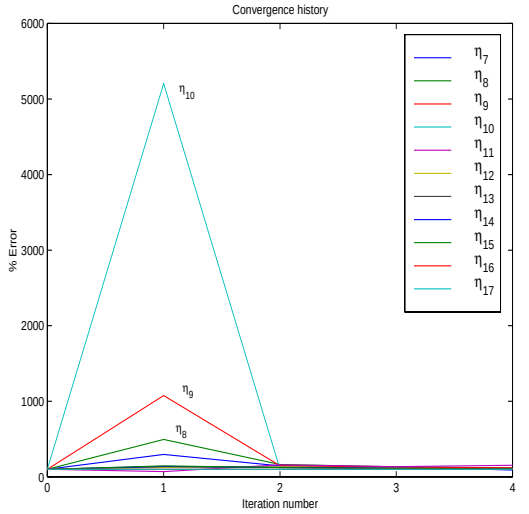

Figure 6.7: Computed changes in η_r during updating calculations using one DOF

The updating calculations were done for mode 7 to 17, as before, and the computations stopped after four iterations as the calculations converged as quickly as in the previous case. Figure 6.7 again shows that the majority of corrections were introduced after the first iteration and that subsequent iterations introduced only minor adjustments.

The structural damping factors computed to the values as indicated in table 6.3 and were found to be very similar to those identified by using 6 *measurements*. The correlation between *measurement* $\alpha_{11}(\omega)$ and the updated FE model is presented in figure 6.8.

η_r	$\eta_1 \rightarrow \eta_6$	η_7	η_8	η_9	η_{10}	η_{11}	$\eta_{12} \rightarrow \eta_{15}$	$\eta_{16} \rightarrow \eta_\infty$
Correct	0.007	0.010	0.050	0.090	0.150	0.007	0.007	0.007
Updated	0.003	0.015	0.039	0.072	0.153	0.007	0.006	0.003

Table 6.3: Identified structural damping factors η_r after updating one DOF

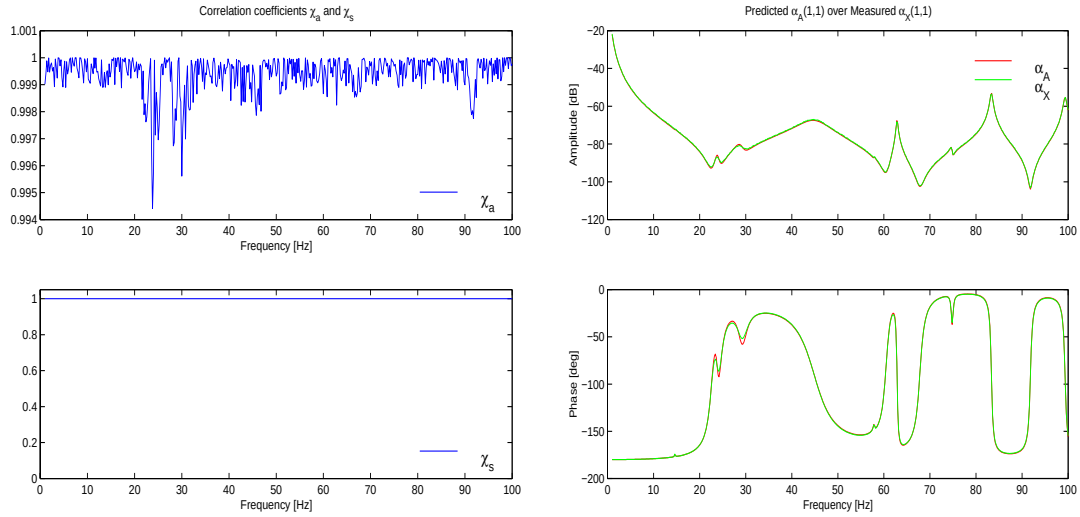

Figure 6.8: Response correlation after updating η_r of 1 DOF

Equivalent to the above presented validation of structurally-damped responses, the viscous damping model and its associated sensitivities defined by equation (6.8) were also validated. Both the convergence properties and the accuracy of the updated FRF(s) were analogous to those presented above. Therefore, instead of presenting an equivalent case study of viscously-damped responses, the next section demonstrates the method's ability to identify viscous damping ratios from structurally-damped measurements.

6.5.2 Identifying ζ_r from Structurally-Damped Responses

In the preceding section, the measurements as well as the analytical predictions of the simulated case studies have both assumed a common damping model and subsequent computations have shown that, in this case, erroneous modal damping factors may be identified correctly. Although the objectives were to validate the ability of the method to converge, in practical cases one does not know what the underlying damping mechanism is. In fact, it is very unlikely that either of both damping models is the correct one in realistic circumstances. Often one prescribes a structural or viscous damping model for the analysis and then tries to fit the response as closely as possible to what has been measured.

Mode r	$1 \rightarrow 6$	7	8	9	10	$11 \rightarrow \infty$
Correct value of η_r	0.007	0.010	0.050	0.090	0.150	0.007
Initial estimate of ζ_r	0.003	0.003	0.003	0.003	0.003	0.003

Table 6.4: Structural loss factors η_r of *measurements* and initial viscous damping ratios ζ_r of analytical responses

Concluding the above-mentioned remarks, the viscous damping properties of the FE model

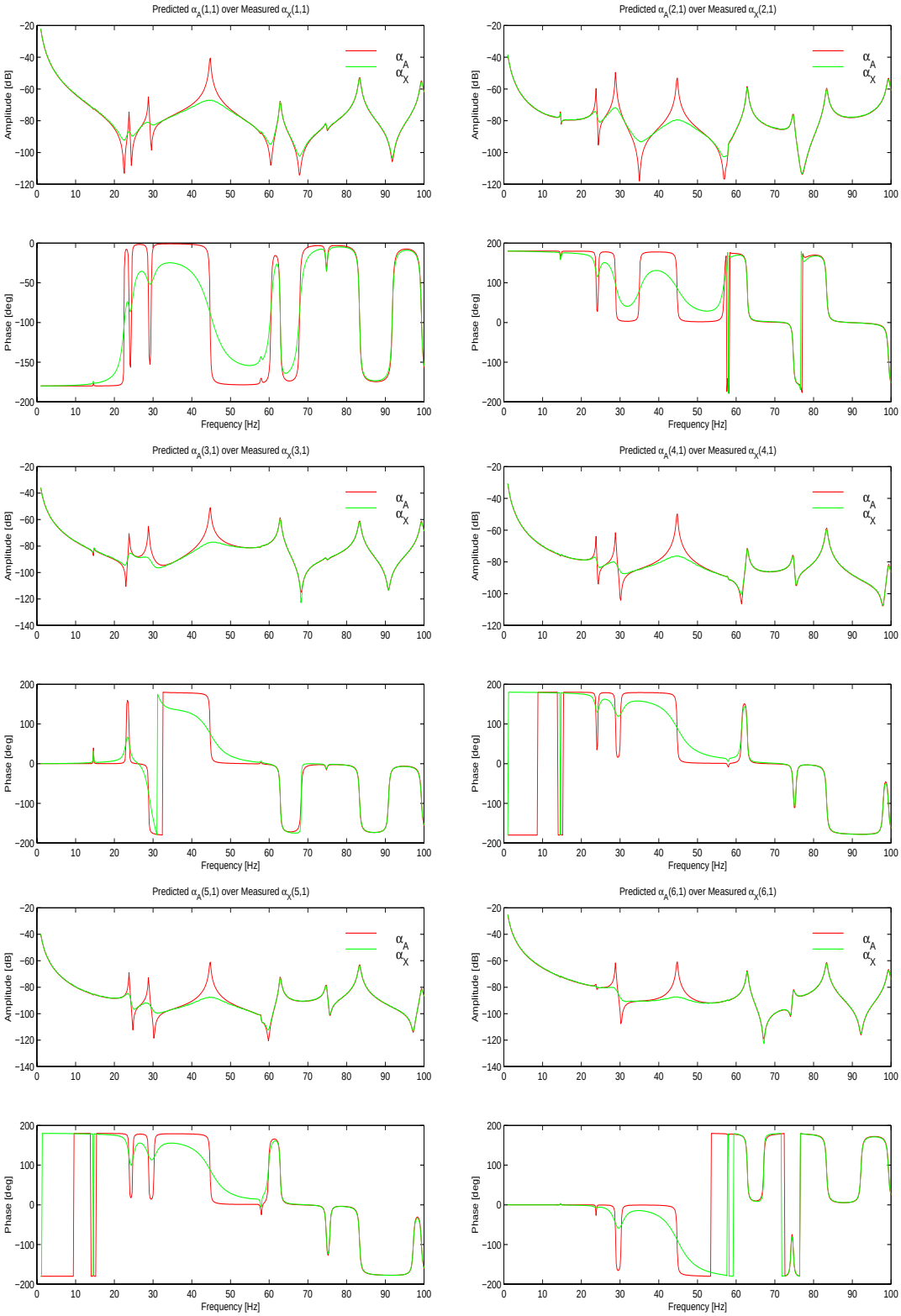

Figure 6.9: FRF overlays of six co-ordinates (fig. 6.1) before updating viscous damping ratios ζ_r on structurally-damped *measurements*

shown in figure 6.1 was updated in the light of structurally-damped simulated measurements. As a result, the updating calculations were performed on two damping models which were incompatible to each other. Using all six *measurement* locations, the initial values of the viscous damping ratios as well as the structural damping factors are listed in table 6.4. The level of correlation of the FRFs before updating is shown in figures 6.9 and 6.10.

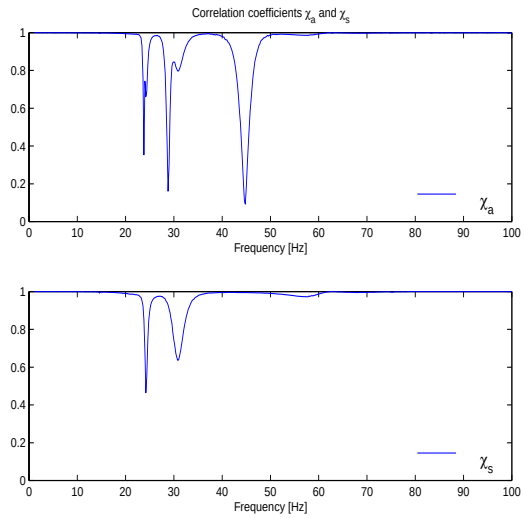

Figure 6.10: Correlation functions $\chi_s(\omega)$ and $\chi_a(\omega)$ before updating ζ_r of six DOFs

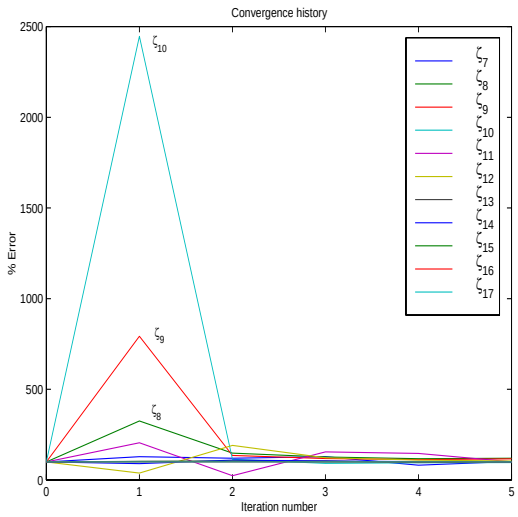

Figure 6.11: Computed changes in ζ_r during updating calculations using six DOFs

As can be seen in figure 6.11, the convergence history resembles the ones observed earlier. After one iteration, major changes have been introduced and the identified changes of viscous damping ratios in the following iterations are comparatively small. Furthermore, the results clearly indicate that only those modes changed whose damping parameters are truly in error while the others remained unchanged. After 5 iterations the computations stopped and indicated the viscous damping ratios as listed in table 6.5.

Mode r	$1 \rightarrow 6$	7	8	9	10	11	$12 \rightarrow 15$	$16 \rightarrow \infty$
Correct η_r	0.007	0.010	0.050	0.090	0.150	0.007	0.007	0.007
Updated ζ_r	0.003	0.005	0.026	0.050	0.071	0.034	0.032	0.003

Table 6.5: Structural loss factors η_r of *measurements* and updated viscous damping ratios ζ_r of analytical responses

Based on the identified viscous damping ratios, a new correlation analysis was performed and the resulting shape- and amplitude-correlation functions $\chi_s(\omega)$ and $\chi_a(\omega)$ are displayed in figure 6.12. The corresponding FRF overlays of all six *measurement* locations are presented in figure 6.13.

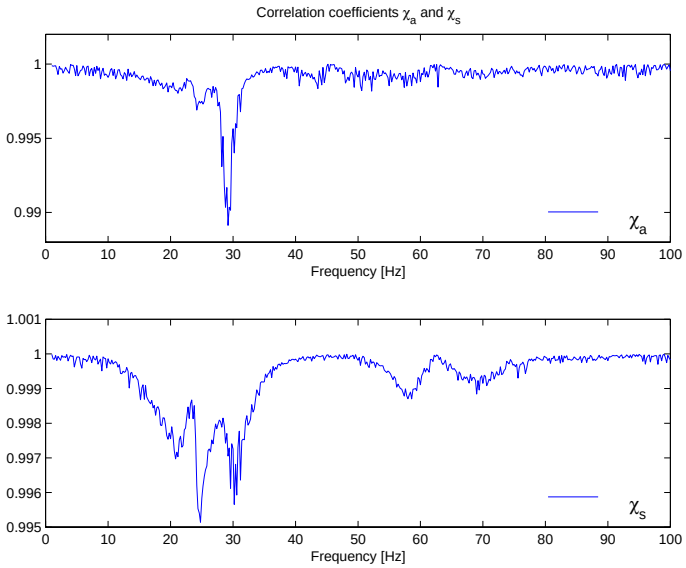

Figure 6.12: Response correlation after updating ζ_r from six DOFs

Both the shape- and amplitude-correlation functions, $\chi_s(\omega)$ and $\chi_a(\omega)$, in figure 6.12 exhibit values higher than 0.99 and are therefore close to a perfect value of unity. After five iterations, the remaining discrepancies are mainly around the first two elastic modes of $\alpha_{11}(\omega)$ (fig. 6.13). Throughout the spectrum the correlation functions $\chi_s(\omega)$ and $\chi_a(\omega)$ again have been improved to a level where the measurements noise becomes visible.

In the above-presented case studies, fast convergence properties were observed throughout the validation of the identification algorithm. Whereas the first simulated case study concentrated on proving the method's ability to locate errors in damping using identical damping models for the predictions and *measurements*, the second test case put emphasis on the capabilities to update an FE model whose damping model is uncorrelated to that used for simulating the *measurements*.

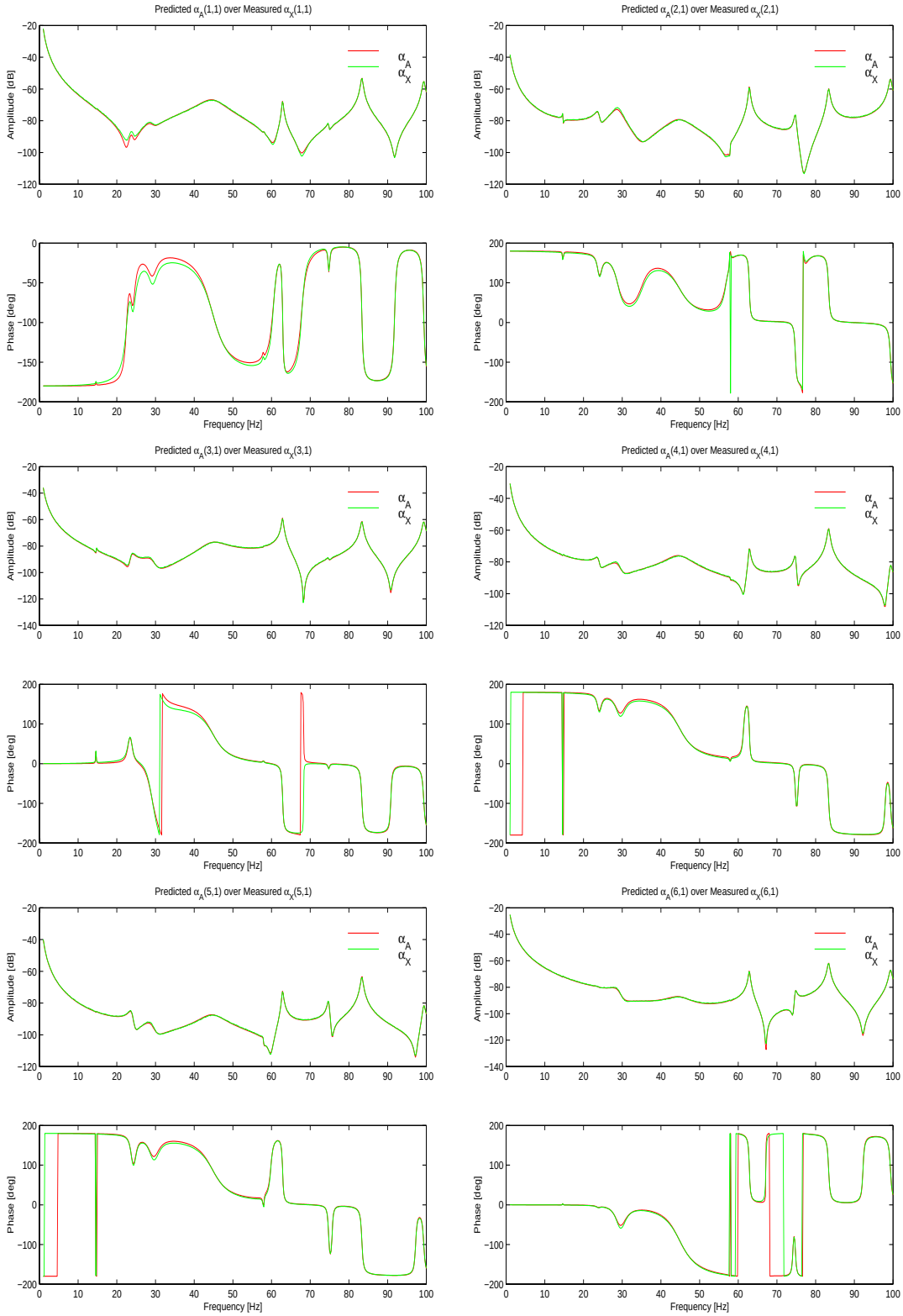

Figure 6.13: FRF overlays of six co-ordinates (fig. 6.1) after updating viscous damping ratios ζ_r on structurally-damped *measurements*

6.6 Concluding Remarks

- A new algorithm to identify viscous and/or structural damping parameters has been introduced. The algorithm is based on analytically-derived first-order sensitivities (eqn. (6.11), (6.8)) in conjunction with the previously-developed P-C model updating formulation (chap. 4). Whereas many other updating algorithms inherently lead to complex linear sets of equations, the proposed identification routine maps the estimation problem into real algebraic equations. Assuming there are no multiple modes, the modal damping parameters and their associated columns in sensitivity matrix $[S]$ are linearly independent and therefore, additional explicit updating parameter selection schemes are redundant. The mutual independency of the updating parameters as well as the minimum number of real algebraic equations is distinctly different to methods identifying damping matrices $[D]$ and $[C]$ directly. The latter have been reported to lead to numerical instabilities and poor convergence properties (Visser 1992).
- An initial proportionally-damped FE model is assumed and it has been shown that the proportionality, in a strict sense, is lost by assigning damping factors local to the modes. The locality of the identified damping model became particularly apparent when the shape correlation coefficient $\chi_s(\omega)$ assumed values different from unity. Since the shape correlation coefficient is invariant to scaling, these less-than-unity values suggest a non-homogeneous distribution of damping in the structure.
- Throughout the case studies, the procedure exhibited rapid convergence and improved the response to a level where the shape- and amplitude-correlation coefficients were dominated by noise. Since the P-C method is updating $\chi_s(\omega)$ and $\chi_a(\omega)$ directly (and not the FRFs), it was unrealistic to expect any further improvement as the P-C cannot anymore discriminated between noise and structural response. Therefore, the less noisy the measurements, the better the damping parameter estimates. Similarly, it was found that with higher frequency resolutions better damping parameter estimates are obtained.

Chapter 7

Applications

7.1 A Clamped Beam-Assembly

7.1.1 Problem Definition and Objectives of Study

The dynamic analysis of simple beams is readily accomplished by using finite elements and the predicted dynamic properties usually agree to a large extent with what has been measured. In fact, standard text books often show that if the number of elements goes to infinity, the solutions converge to those which can be obtained analytically.

The analysis of an assembly of beams is less straightforward as usually very little is known about the dynamic properties of the joints of the assembly. There may be welded or 'rigidly' bolted connections or similar joints in the assembly. These are known to be less-than-rigid connections and inappropriately modelled as a rigid FE assembly. The same argument holds true for the boundary conditions of the tested structure and its corresponding FE model representation. Although the tested specimen may seem firmly clamped, comparisons between the measurements and the analytically computed responses suggest that the clamping conditions are softer in reality than assumed in the model.

The following experimental study is a case where the straight beams can be modelled fairly accurately but the dynamics of the joints are largely unknown.

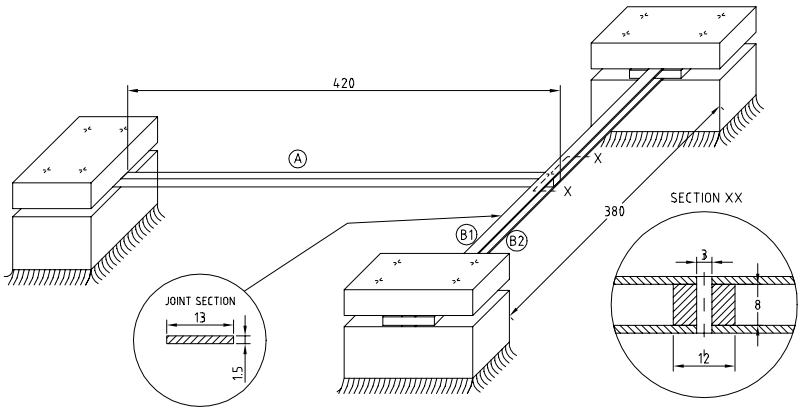

Figure 7.1: Geometry of clamped 3-beam assembly

Very accurate FE element predictions were required to validate a theoretical model in nonlinear structural dynamics (Ferreira 1998). The structure of concern is shown in figure 7.1 and is an assembly of three slender beams of which one is sandwiched between and perpendicular to the other two beams. The trailing ends of the assembly are grounded and static measurements have shown the structure's inbuilt nonlinear (cubic) stiffness properties when loaded vertically at the bolted joint (section xx, fig. 7.1). For smaller input forces, however, the ratio of force to displacement was observed to be almost linear and it was these force levels which were then used to perform dynamic response measurements. The measurements were subsequently employed to update a corresponding FE model to validate the developments of nonlinear response predictions when the structure is excited with higher force levels.

From an updating point of view, the size of the FE model, N, and the number of measurements, n, resulted in a distinctly smaller incompleteness ratio i_r (eqn. (2.7), p. 23) than those often reported for other response-based updating formulations. Altogether there were three measurements and the FE model had 648 DOFs in unclamped conditions (i.e. $i_r = 3/648$). The objectives of this study, and the FE and measurement data available, gave a good opportunity to validate the ability of the P-C model updating technique developed in Chapter 4. Although a limited number of global design parameters might have been updated using an inverse eigensensitivity formulation, the number of unknowns (i.e. boundary conditions) far exceeded the number of measured modes in the frequency range of interest. Also, the P-C method has proven to be able to update FE models from a minimum number of measurements and to be robust against measurements contaminated by noise.

7.1.2 The FE Model of the 3-Beam Assembly

According to the specifications given by figure 7.1, the assembly consisted of three separate slender beams, a joint section and the clamping conditions at the trailing ends of the assembly. Timoshenko beams were used throughout the study and thus accounted for the effects of shear on the vibration of the beams (Gasch and Knothe 1989). The material properties are listed in table 7.1. A relatively large number of beam elements were used to ensure that the modes in the frequency region of interest had converged (tab. 7.2).

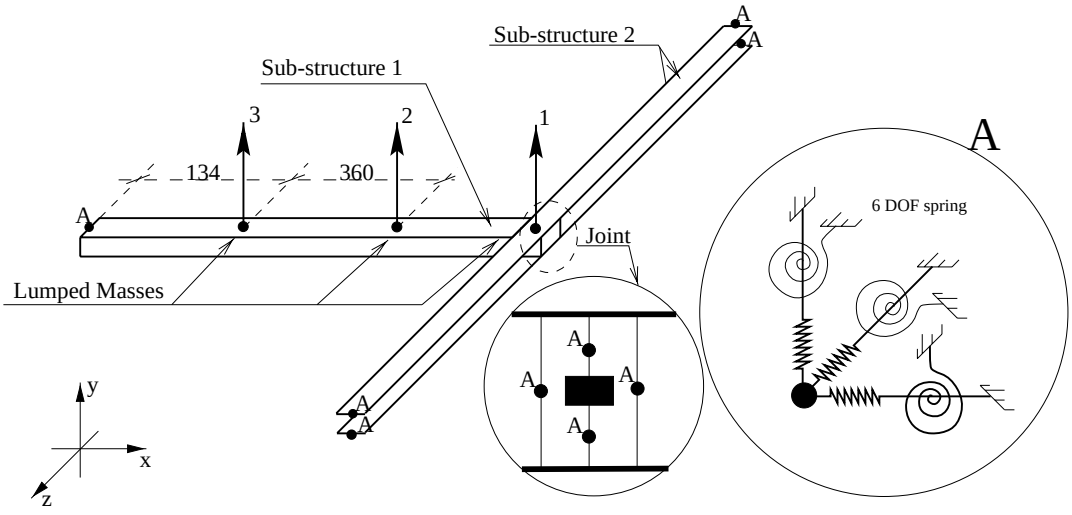

Figure 7.2: Measurement and locations of lumped springs in 3-beam assembly

Figure 7.2 details the locations of the measurement points and the lumped parameter models for the joint and the clamped boundary conditions. Each node, A, denotes a six DOFs lumped spring and the lumped masses at the measurement locations assumed a mass in six directions, too.

Young's Modulus E	Poissoin's Ratio ν	Mass Density ρ
210 e9 N/m^2	0.3	7900 kg/m^3

Table 7.1: Material properties of 3-beam assembly

Number of...	Beams	Lumped masses	Lumped springs
Sub-structure 1	21	3	8 of which 4 are grounded
Sub-structure 2	88	1	0

Table 7.2: Type and number of finite elements used in 3-beam assembly

The FE model was partitioned into two sub-structures and the Craig-Bampton CMS method, presented in Chapter 3, was used to condense the 648 DOFs FE model to a reduced representation consisting of 21 active (hybrid) DOFs. Since the frequency range of interest was defined from $0Hz$ to $225Hz$, all modes of each sub-structure within $0Hz$ and $450Hz$ were computed resulting in 12 modal coordinates of the condensed model. Therefore, nine out of the 21 DOFs represented the coordinates at the joint (JDOFs) and the three measurement locations. The condensed FE model, as seen in figure 7.3, was then used to make any further response predictions using a constant structural damping factor of $\eta_r = 0.01$.

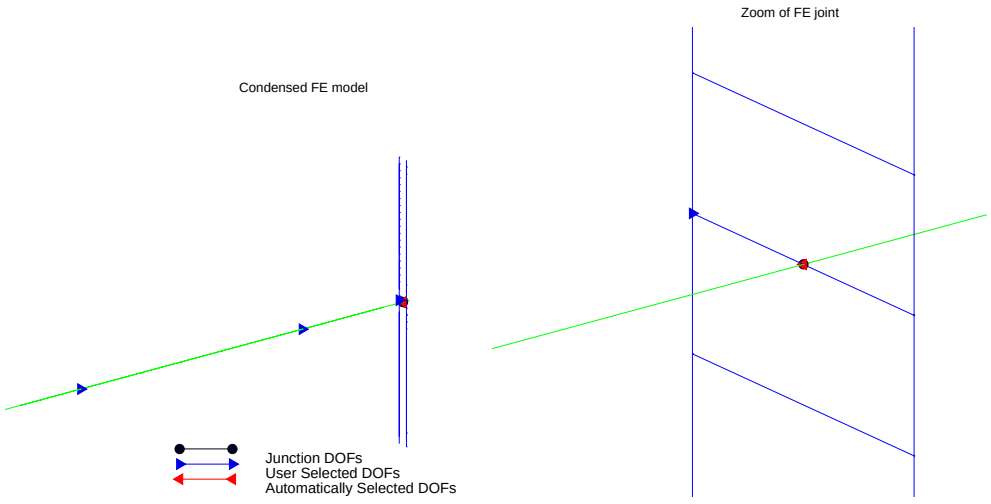

Figure 7.3: Condensed FE model of 3-beam assembly

Section 5.4 highlights the difficulties associated with estimating initial lumped parameter models and proposes to shift the initial estimates of such models into sensitive regions. As the initial response predictions revealed (fig. 7.4) that there are two dominant modes in the frequency region of interest, the sensitivities of these were used to adjust the lumped parameter models of the clamping conditions. The identified stiffness values are listed in tables 7.3 to 7.4.

The joint stiffnesses of the four lumped springs were derived by considering each stiffness to be equivalent to that obtained from a bolt of $d = 4mm$ diameter, $l = 4mm$ in length (see detail in figure 7.1). The corresponding stiffness values are shown in table 7.5 and the three lumped masses attached to the structure are given in tables 7.6 to 7.8.

7.1.3 Updating Computations

Based on the initial stiffness and mass estimates of the lumped parameter models used, the FE model predictions were then correlated with those actually measured. Taking all three measured DOFs, as introduced in figure 7.2, the initial correlation between the prediction and the measurements is seen in figure 7.4.

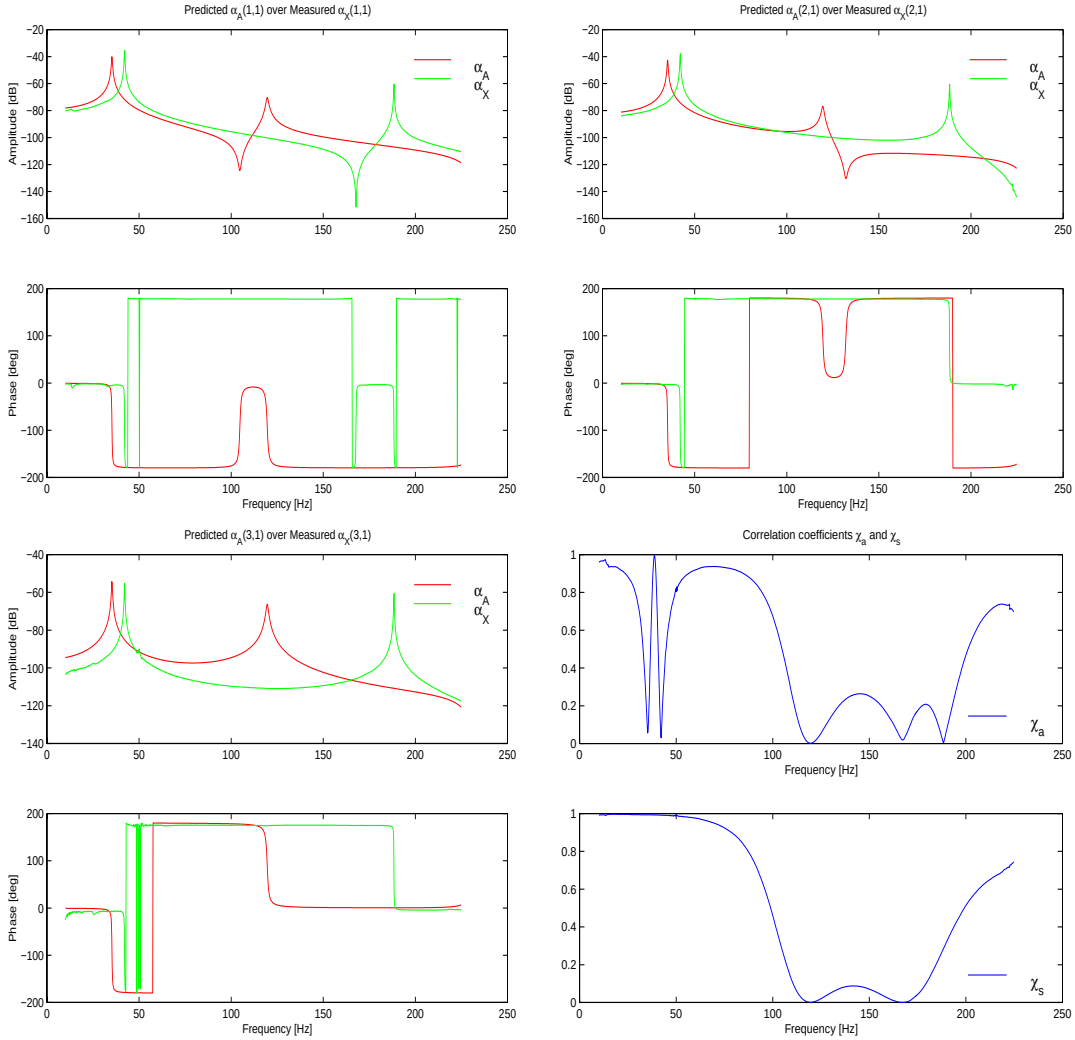

Figure 7.4: Initial FRFs and correlation function of 3-beam assembly

The FRF overlays, as well as the correlation functions, $\chi_s(\omega)$ and $\chi_a(\omega)$, indicate a poor level of correlation. Whereas the first predicted mode is closer to the measured resonance, the second mode is largely displaced. Although the boundary conditions have been replaced by a softer lumped spring model, the poor correlation partially reflects the difficulty to find good initial estimates of lumped parameter models. It is also interesting to

note that the shape-correlation function $\chi_s(\omega)$ ignores the discrepancies in the first mode whereas $\chi_a(\omega)$ captures any presence of response differences.

Without trying to improve the initial level of correlation, the FE model was then submitted for model updating calculations using the P-C method. All three measurements were used and, assuming that the beam elements were sufficiently accurate, 30 lumped stiffness and mass variables at the joints were defined as updating parameters whose details can be seen in tables 7.3–7.8. Using the sub-set selection procedure presented in Section 5.5, the maximum permissible condition number was set to $\kappa_\infty = 5e7$ and the updating computations were performed over the full frequency range.

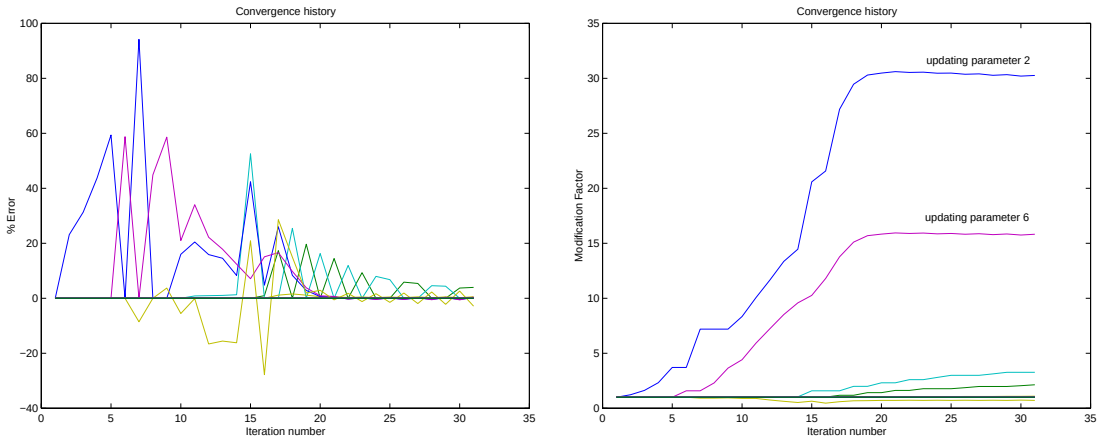

Figure 7.5: Convergence history of spatial parameters of 3-beam assembly

The convergence history of the updating computations is shown in figure 7.5 and suggests that after 30 iterations, considerable changes were introduced to the lumped stiffness parameters in direction y and θ_z of sub-structure 1 (fig. 7.2, tab. 7.3). During the updating calculations, one to seven design parameters were updated at any one iteration while the remaining parameters were temporarily frozen at unity (i.e. no change). The sub-set selection procedure employed also meant that, in general, an increasing number of design changes were introduced as the level of correlation between the prediction and the measurements improved. This is because of a decreasing number of updating frequencies N_{f_u} and a simultaneous increase of the threshold condition number κ_{mn}.

The bulk of the design parameter changes had been introduced after 20 iterations and subsequent updating computations concentrated on frequency points around both resonances. After 30 iterations, the computations were aborted and tables 7.3 to 7.8 display the updated design parameters. These tables show that no parameters were updated other than those which affect the response in the direction of the measurements. Tables 7.3 to 7.8 also indicate that neither joint-stiffness changes nor changes of the lumped masses at measurement location 1 and 2 have been introduced. These parameters have been automatically excluded at each iteration and their initial values have been shown to be sufficiently accurate to improve the overall level of correlation.

The updated FRFs and their measured counterparts are seen in figure 7.6. Both correlation coefficients $\chi_s(\omega)$ and $\chi_a(\omega)$ indicate a high level of correlation and it can be concluded that the accuracy of the predictions has been improved to a large extent and the design parameter changes are physically justifiable.

So far, a proportional structural damping loss factor of $\eta_r = 0.01$ has been assumed for the

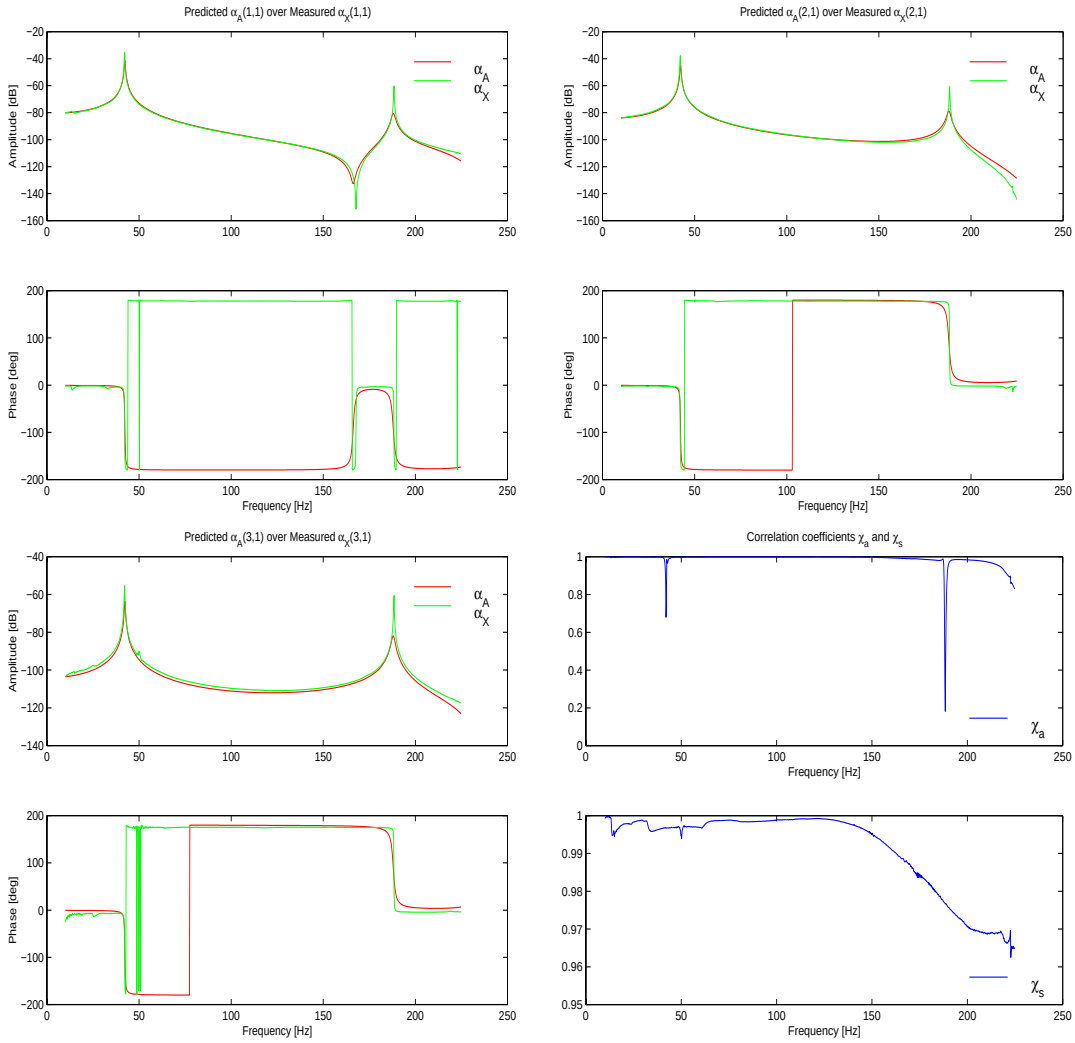

Figure 7.6: Responses after updating spatial parameters of 3-beam assembly

initial FE predictions. Although the overall level of correlation is already very high and the initial damping model seems sufficiently accurate (fig. 7.6), the damping values were nevertheless updated using the procedures as proposed in Chapter 6. The corresponding convergence history is seen in figure 7.7.

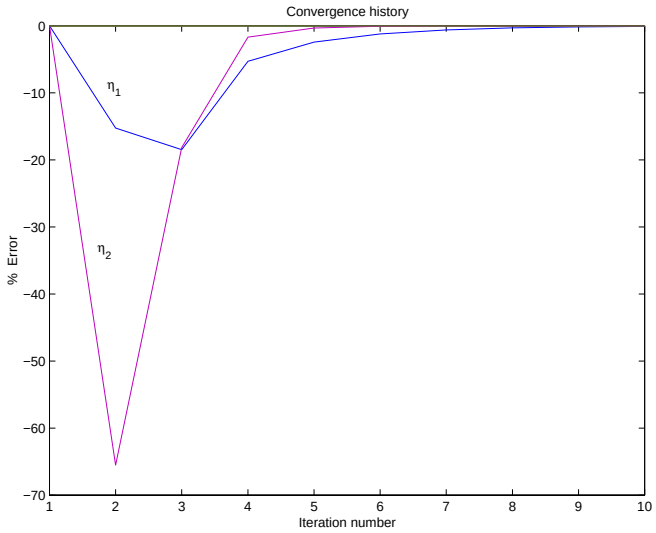

Figure 7.7: Convergence history of damping parameters of 3-beam assembly

Figure 7.7 shows that the damping parameters converge as quickly as previously observed in Chapter 6. The two structural damping loss factors obtained after 10 iterations were $\eta_1 = 0.0068$ and $\eta_2 = 0.0028$. The updated responses and correlation functions $\chi_s(\omega)$ and $\chi_a(\omega)$ are shown in figure 7.8. This displays only minor improvements which are most obvious in the phases of the responses.

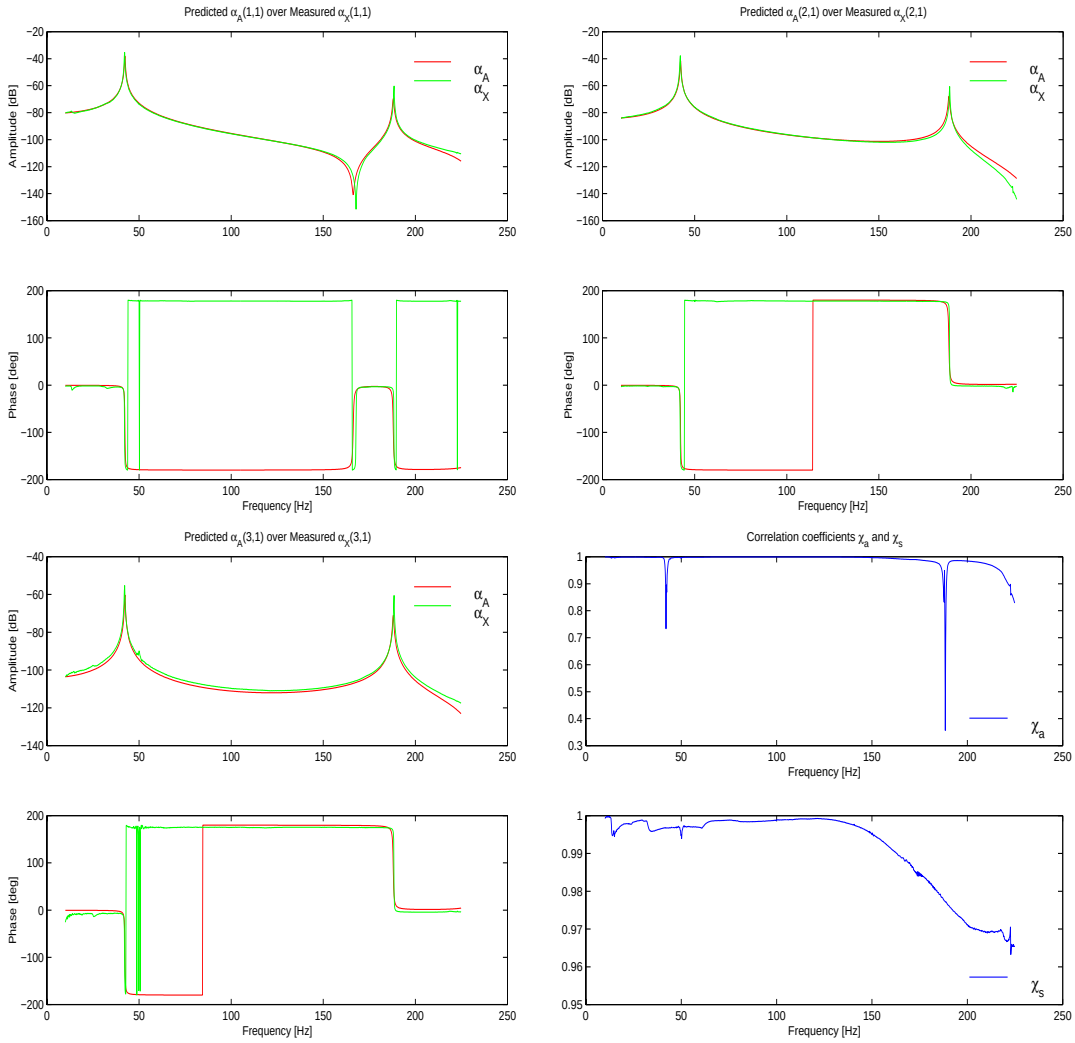

Figure 7.8: Responses after updating damping parameters of 3-beam assembly

Clamped boundary conditions of sub-structure 1 using 1 lumped spring						
parameter	φ_1	φ_2	φ_3	φ_4	φ_5	φ_6
direction	x	y	z	θ_x	θ_y	θ_z
unit	$[N/m]$			$[Nm/rad]$		
initial	1.000e5			1.000e1	1.000e1	1.000e3
updated	1.000e5	3.020e6	1.000e5	1.000e1	1.000e1	1.575e4
% error	0	2926	0	0	0	1482

Table 7.3: Updating parameters φ_1 to φ_6 of 3-beam assembly

Clamped boundary conditions of sub-structure 2 using 4 lumped springs						
parameter	φ_7	φ_8	φ_9	φ_{10}	φ_{11}	φ_{12}
direction	x	y	z	θ_x	θ_y	θ_z
unit	$[N/m]$			$[Nm/rad]$		
initial	1.000e6			1.000e3	1.000e2	1.000e1
updated	1.000e6	2.052e6	1.000e6	3.267e3	1.000e2	1.086e1
% error	0	113.3	0	226.7	0	9.203

Table 7.4: Updating parameters φ_7 to φ_{12} of 3-beam assembly

Joint between sub-structures 1 and 2 using 4 lumped springs						
parameter	φ_{13}	φ_{14}	φ_{15}	φ_{16}	φ_{17}	φ_{18}
direction	x	y	z	θ_x	θ_y	θ_z
unit	$[N/m]$			$[Nm/rad]$		
initial	3.400e8	5.500e8	3.400e8	5.500e3	1.100e2	5.500e2
updated	3.400e8	5.500e8	3.400e8	5.500e3	1.100e2	5.500e2
% error	0	0	0	0	0	0

Table 7.5: Updating parameters φ_{13} to φ_{18} of 3-beam assembly

Lumped Mass						
Measurement location 1						
parameter	φ_{19}			φ_{20}	φ_{21}	φ_{22}
direction	x	y	z	θ_x	θ_y	θ_z
unit	$[kg]$			$[Nm/rad]$		
initial	3.000e-2			1.000e-8	1.000e-8	1.000e-8
updated	2.207e-2			1.000e-8	1.000e-8	1.359e-8
% error	-28.52			0	0	35.92

Table 7.6: Updating parameters φ_{19} to φ_{22} of 3-beam assembly

Lumped Mass						
Measurement location 2						
parameter	φ_{23}			φ_{24}	φ_{25}	φ_{26}
direction	x	y	z	θ_x	θ_y	θ_z
unit	$[kg]$			$[Nm/rad]$		
initial	1.000e-3			1.000e-8	1.000e-8	1.000e-8
updated	1.000e-3			1.000e-8	1.000e-8	1.000e-8
% error	0			0	0	0

Table 7.7: Updating parameters φ_{23} to φ_{26} of 3-beam assembly

Lumped Mass						
Measurement location 3						
parameter	φ_{27}			φ_{28}	φ_{29}	φ_{30}
direction	x	y	z	θ_x	θ_y	θ_z
unit	$[kg]$			$[Nm/rad]$		
initial	1.000e-3			1.000e-8	1.000e-8	1.000e-8
updated	1.000e-3			1.000e-8	1.000e-8	1.000e-8
% error	0			0	0	0

Table 7.8: Updating parameters φ_{27} to φ_{30} of 3-beam assembly

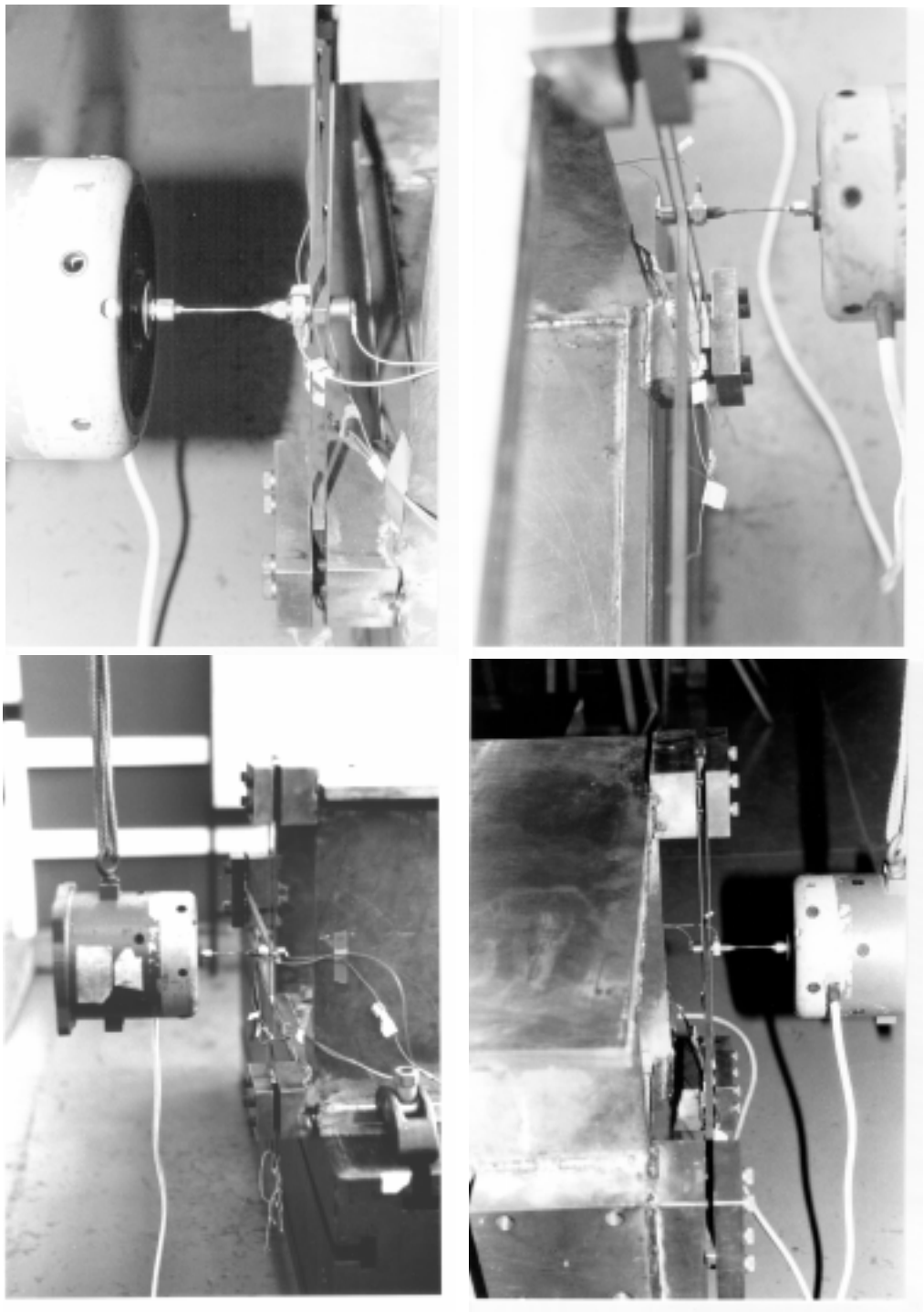

Figure 7.9: Experimental set-up of 3-beam assembly

7.2 An Assembly of Plates and Beams

7.2.1 Problem Definition and Objectives of Study

In contrast to the preceding clamped beam-assembly, this second experimental case study is concerned with a larger FE model and a frequency range in which a higher number of modes reside. The structure is made of aluminium alloy and consists of three plates and two beams assembled using steel screws. This S1203 structure (fig. 7.10) has been serving as a standard benchmark for many years at Imperial College, Dynamics Section, and is typically used to validate new developments in the area of model updating.

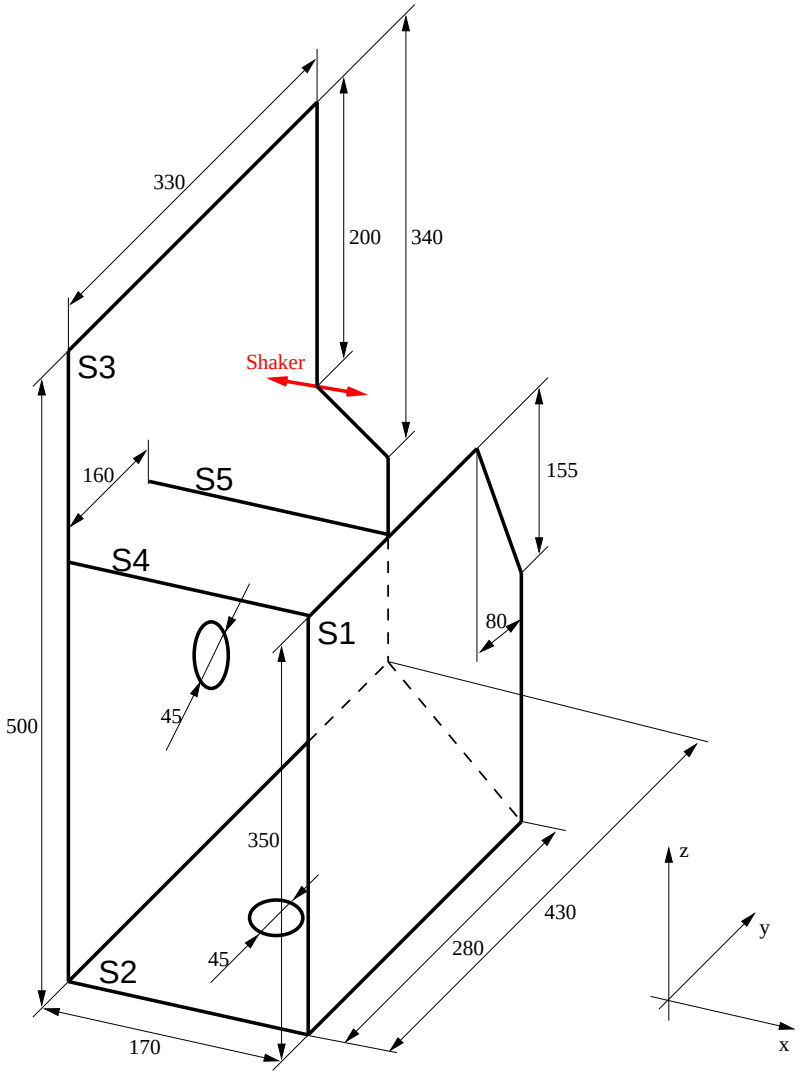

Figure 7.10: Geometry of Imperial College benchmark structure: S1203

Measurements have shown that the structure exhibits a combination of strong and weak modes as well as a balanced combination of well-separated and close modal behaviour within the measured frequency range of $0Hz$ to $800Hz$. The test data also suggest that some modes are more heavily damped than others and that damping, in general, cannot be ignored to find matching analytical predictions.

There are therefore several good reasons for attempting a model updating exercise on this

particular structure as it is subject to several identifiable levels of difficulties frequently encountered in practice, including the limited amount of measurements available.

7.2.2 The FE Model of the S1203 Structure

In line with the nomenclature introduced with Chapter 3, the beams and plates naturally lead to the partition of the structure into sub-structures 1 to 5 (i.e. S1–S5), as shown in figure 7.10, and all further FE analysis was performed using a constraint interface method (Craig-Bampton) to condense the full model.

To ensure convergence of the modes between $0Hz$ and $800Hz$, each sub-structure had to be discretised using a relatively high number of finite elements. Timoshenko beams were used throughout the analysis and the plates (S1–S3) were modelled using 4-noded shell elements. The number of finite elements used and their associated basic material properties are shown in tables 7.9 and 7.10.

Number of...	Beams	Shells	Lumped springs
Sub-structure S1	0	140	0
Sub-structure S2	0	183	25
Sub-structure S3	0	197	0
Sub-structure S4	30	0	2
Sub-structure S5	30	0	2

Table 7.9: Numbers of finite elements used in S1–S5 of S1203

Young's Modulus E	Poissoin's Ratio ν	Mass Density ρ
71 e9 N/m^2	0.36	2660 kg/m^3

Table 7.10: Basic material properties of aluminium (S1203)

Since the joints may present a potential source of error (screws), the junction DOFs between all sub-structures were replaced by lumped spring elements. These need to assume a physical length different from zero and a gap of $1.5mm$ was introduced between the interfacing sub-structures (fig. 7.10: width $170mm$ becomes $173mm$). The number of lumped springs used was thus equal to the number of junction nodes (tab. 7.9) and the initial stiffnesses were equal to those obtained from a steel bolt of diameter $d = 5mm$ with a length of $l = 1.5mm$.

The structure was excited at the location as indicated in figure 7.10 and the responses were measured at 63 DOFs in the x-direction. A number of extra DOFs had to be included in the condensed FE representation to retain the measurement locations. The full FE model of 4044 DOFs was therefore reduced to 245 DOFs as a sum of 174 junction DOFs, 51 extra measurement DOFs and 20 modal DOFs. The full and condensed FE models are shown in figure 7.11. The extra selected number of measurement DOFs are indicated as "User Selected DOFs" in figure 7.11 and the remaining 12 response locations are equally distributed on the interfaces S1-S2 and S2-S3.

Based on the above configuration of the structure and the initial estimates of the lumped springs, the FE model was subsequently condensed to be valid within $0Hz$ and $1000Hz$.

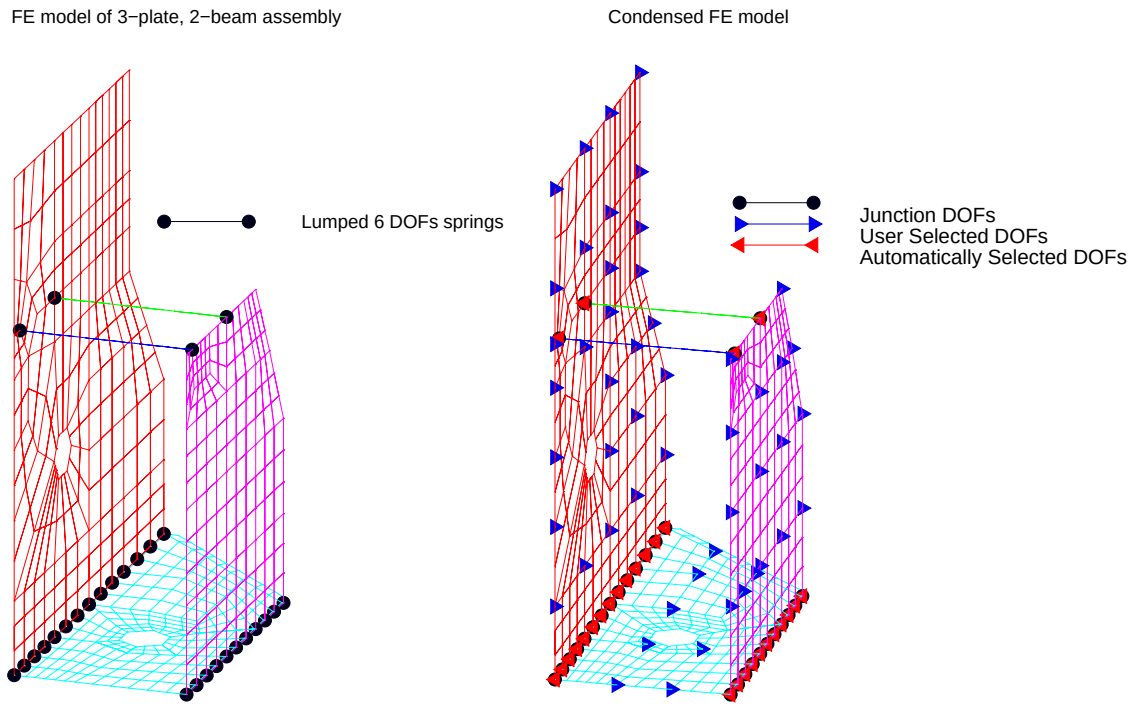

Figure 7.11: Full and condensed FE model of S1203

7.2.3 Initial Correlation and Error Localisation

Using the sub-structured FE model, a first correlation analysis was performed between the 63 measurements and their corresponding predictions computed from the 245 DOFs FE model. An initial proportional structural damping factor of $\eta_r = 0.005$ was used throughout the analysis and the resulting shape- and amplitude-correlation functions (chap. 4) are shown in figure 7.12.

The correlation functions in figure 7.12 reveal that the response predictions in the lower frequency regions are closer to the measurements and that the level of correlation between the measurements and the predictions decreases with increasing frequency. The relatively high level of correlation exhibited by $\chi_s(\omega)$ in the frequency region from $300Hz$ to $500Hz$ is interesting. It indicates that the deformation the structure experienced at the measured DOFs is very close to what has been measured. Only the much more stringent amplitude-correlation function $\chi_a(\omega)$ discloses that considerable discrepancies exist in amplitude in the same frequency region.

Although both correlation functions provide a unique picture of the initial level of correlation, three response overlays are shown in figure 7.13, representing examples of best, worst and typical levels of correlation encountered among the 63 measured DOFs. At the end of the section, another 6 FRF overlays are presented in figure 7.25. This time, the locations of the DOFs (fig. 7.24) was selected arbitrarily.

The problem of identifying erroneous finite elements was discussed in Chapter 5 and an error location procedure was proposed that employs the sensitivities of the P-C model updating method directly. It was shown in that chapter that the proposed procedure generally gives better identification results than those obtained from a classical eigenvalue-sensitivity study. The usability of the leverage defined by equation (5.9) (p. 91) was

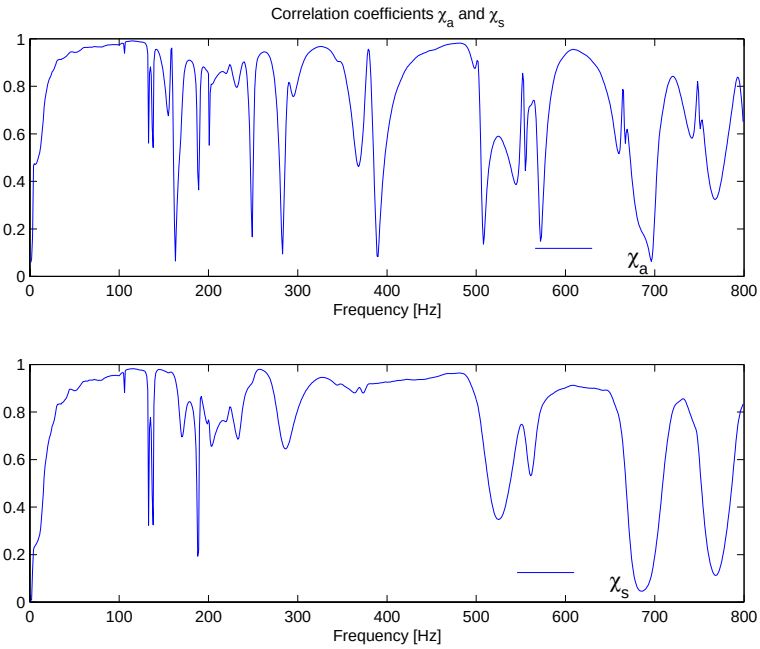

Figure 7.12: Initial correlation functions of S1203 case

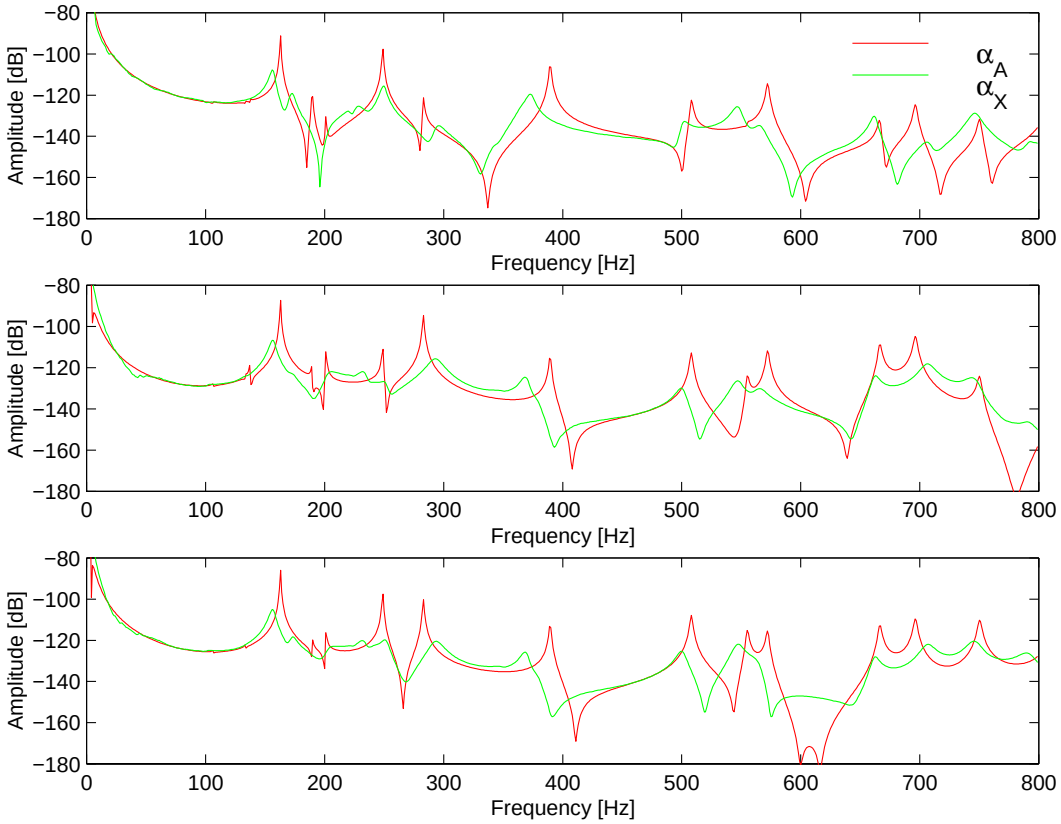

Figure 7.13: Sample FRF overlays before updating S1203

therefore also tested in this experimental case study to locate erroneous regions in the FE model for this structure.

The Young's modulus of each finite element was considered as the design parameter and the sensitivity calculations were performed across the full frequency spectrum. Figure 7.14 shows the results when the error location procedure was applied to the plates, S1 to S3, and figure 7.15 displays the leverages obtained for the intermediate beams, S4 and S5. Similarly, the leverages of the lumped springs attached to S2, S4 and S5 were analysed in all 6 DOFs and are shown in figure 7.16.

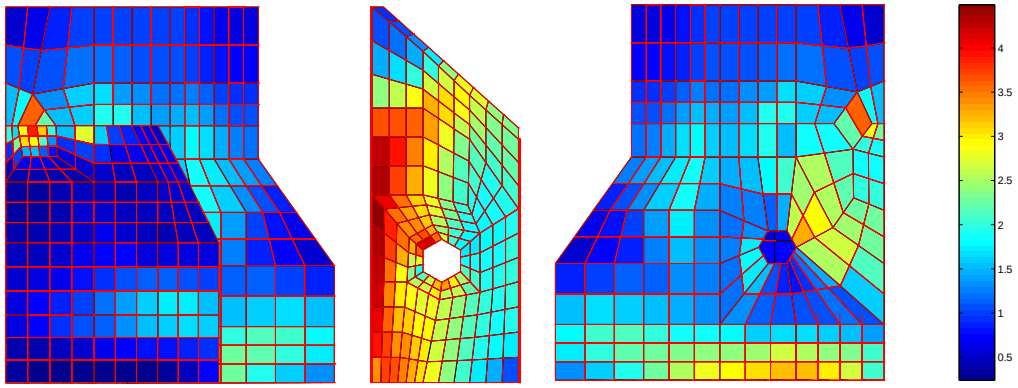

Figure 7.14: Leverages of shell elements in S1–S3 of S1203

The majority of shell elements assume low leverage values, L_i, except the interfacing shell elements between S2 and S3, where the values are highest and in the region of $L_i = 4.0$. The same cannot be said about the interfacing shell elements between S2 and S1 where the elements indicate values around $L_i = 2.0$. However, it is interesting to note that all shell elements at locations close to junction DOFs exhibit leverages which are higher-than-average. This includes the shell elements connected to S4 and S5.

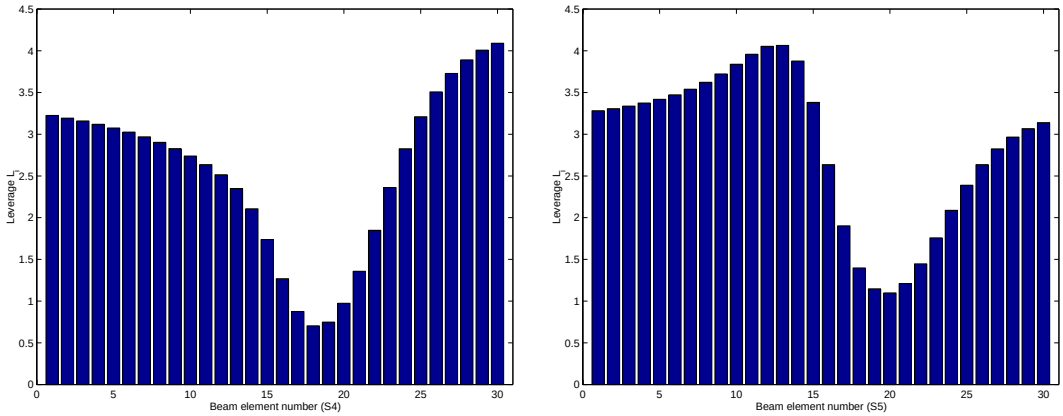

Figure 7.15: Leverages of beam elements in S4 and S5 of S1203

Similar conclusions can be drawn from figure 7.15. Each beam element number corresponds geometrically to the location of the finite element in the sub-structure and both bar charts display high leverages at the ends of S4 and S5. Thus, elements close to the interfaces also assumed high values.

Finally, the leverages computed for the lumped springs in figure 7.16, which present the

interfacing elements themselves, exhibit average values ($L_i \approx 2.0$), the only exception being the spring stiffness in the θ_y-direction which affects the bending stiffness of the structure around the y-axis (fig. 7.10).

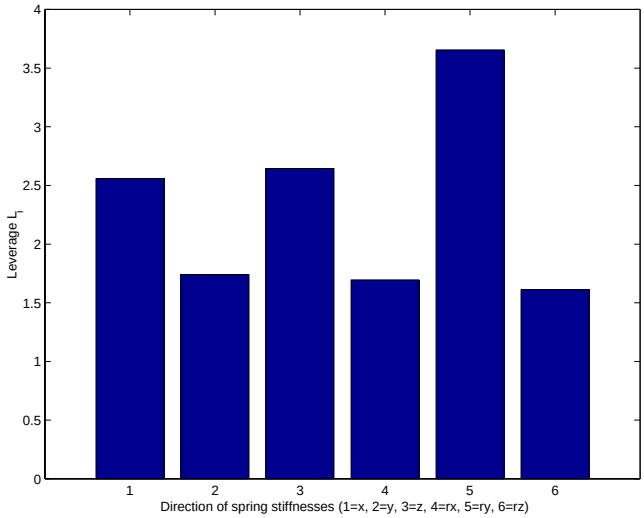

Figure 7.16: Leverages of lumped springs of S1203

In line with the objectives of this error location procedure, a number of elements have been identified which are better able to minimise existing discrepancies in response than others. However, from an engineering point of view, the locations and distributions of these elements are unlikely to be representative of the true error sources. FE modelling of simple flat plates can be performed quite accurately and each of the elements shown in figure 7.14 is subject to about the same degree of modelling uncertainty. Geometrically-induced local stiffness errors were therefore difficult to justify. However, to allow for possible global stiffness errors, the Young's modulus (E) of each separate sub-structure, i.e. S1–S5, was nevertheless included in the updating calculations.

From the modelling point of view, the lumped springs are the least accurate of the finite elements since the initial stiffnesses could only be estimated. This uncertainty is reflected by the tendency of finding higher leverages with elements close to the interfaces of the sub-structures. Therefore, all 6 DOFs of the lumped springs in S2, S4 and S5 were included as updating parameters.

The initial magnitudes of the resulting 23 updating parameters, φ_i, and their reference numbers, i, can be seen in tables 7.11 to 7.14.

7.2.4 Updating Spatial Parameters

Using all 23 updating parameters, the P-C model updating calculations were initiated. It was found that by setting the maximum permissible condition number to $\kappa_\infty = 1e9$ (eqn. (5.14), p. 94), immediate convergence was reached using the sub-set selection procedure as outlined in Chapter 5. The convergence history is shown in figure 7.17.

In a consecutive step, κ_∞ was increased to $\kappa_\infty = 1e10$ and the updating computations were continued using the identified model of the first 20 iterations. The convergence history of these computations is shown in figure 7.18. The change in κ_∞ allowed for a higher

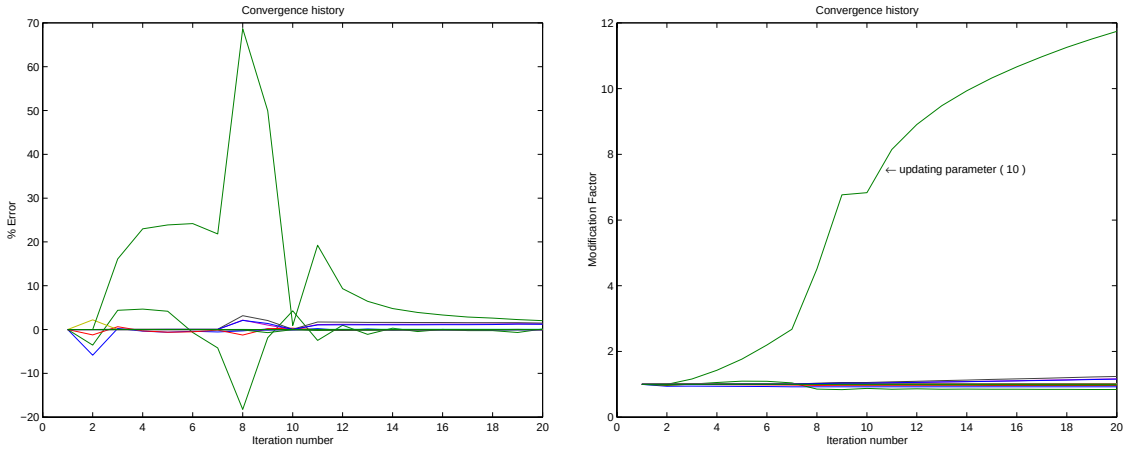

Figure 7.17: Convergence history of spatial parameters of S1203 ($\kappa_\infty = 1e9$)

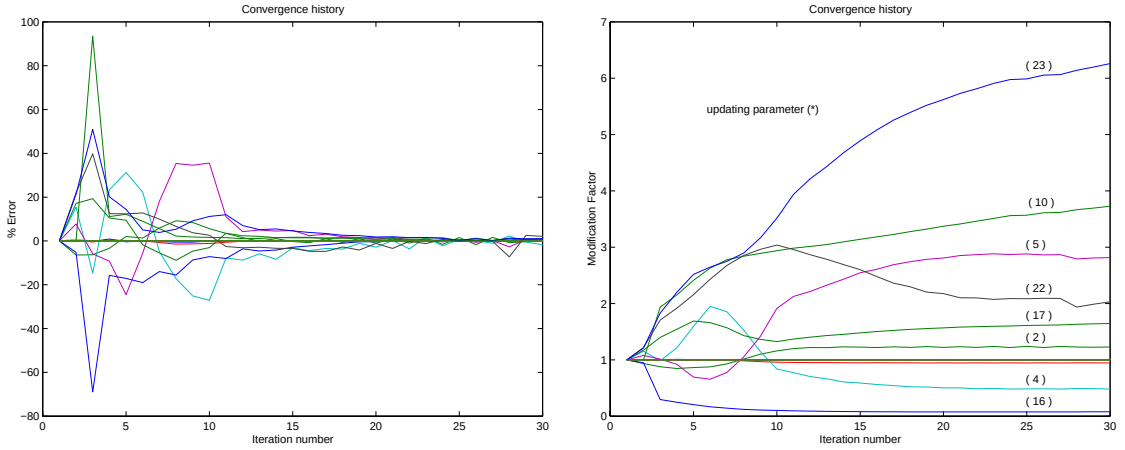

Figure 7.18: Convergence history of spatial parameters of S1203 ($\kappa_\infty = 1e10$)

number of updating parameters to change at each iteration (chap. 5) and, after major discrepancies had been eliminated, to adjust updating parameters other than the most erroneous ones.

The updating parameter numbers, i, in figures 7.17 and 7.18 correspond to the nomenclature adopted in tables 7.11 to 7.14 and reveal that during the first 20 iterations predominant changes were introduced to φ_{10}, the rotational stiffness θ_y of the 25 lumped springs attached to S2. The changes introduced to the remaining 22 updating parameters were comparatively small but increased after iteration number eight.

As none of the updating parameters had converged after 20 iterations, the subsequent change of threshold in the sub-set selection procedure allowed for further improvements of the response predictions (fig. 7.18). This is particularly true for the updating parameters associated with sub-structures S4 and S5. Here, major alterations were introduced to the lumped springs in the θ_y- and θ_z-directions and the Young's modulus, but also the updating parameter φ_{10} continued to rise.

After an overall number of 50 iterations, the updating computations were stopped. The identified parameter changes are shown in tables 7.11 to 7.14 and the improved response predictions are shown in figures 7.20 and 7.19 using a structural damping loss factor of $\eta_r = 0.005$, as before.

The amplitude correlation function $\chi_a(\omega)$, shown in figure 7.20, exhibits distinct areas of low correlation at resonant frequencies. These discrepancies in response are the result of differences in amplitude, as seen in figure 7.19, and can be minimised by adjusting the damping properties of the FE model.

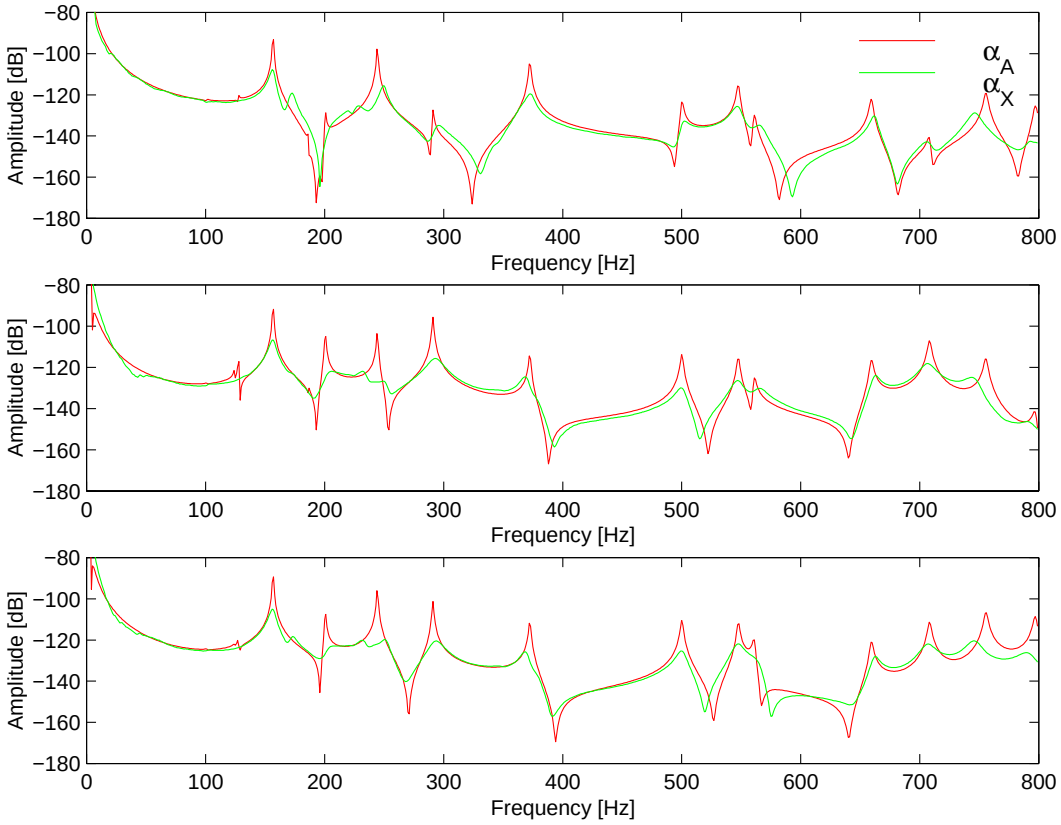

Figure 7.19: Sample FRF overlays after updating spatial parameters of S1203

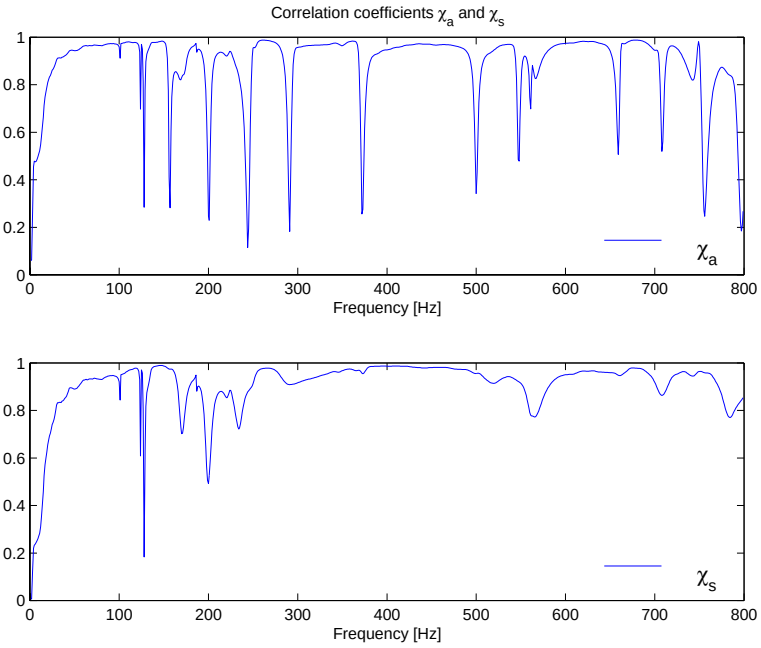

Figure 7.20: Correlation functions after updating spatial parameters of S1203

7.2.5 Updating Damping Parameters

The initially assumed constant structural damping of $\eta_r = 0.005$ was accordingly updated using the damping identification algorithm as proposed in Chapter 6. Here, all the modes in the frequency range of interest are adjusted on a mode-by-mode basis and the convergence history of the first 11 major modes is shown in figure 7.21.

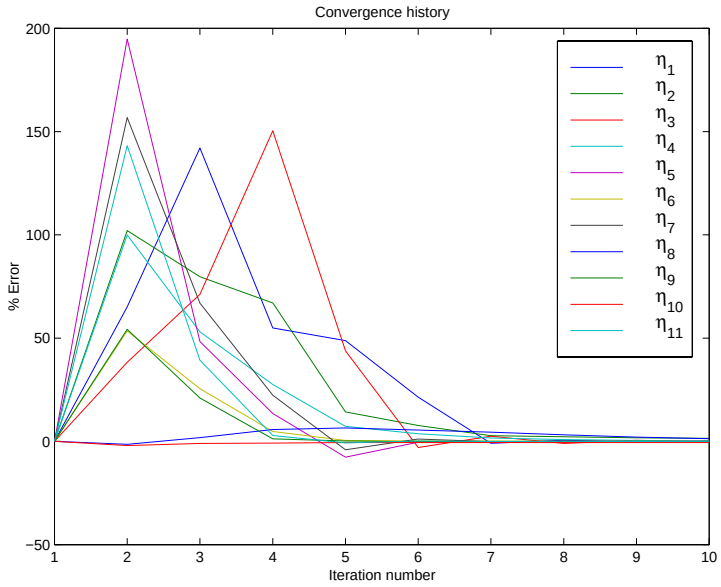

Figure 7.21: Convergence history of damping parameters of S1203

The identified loss factor of these 11 modes are listed in table 7.15 and the improved

response predictions are shown in figures 7.23 and 7.22.

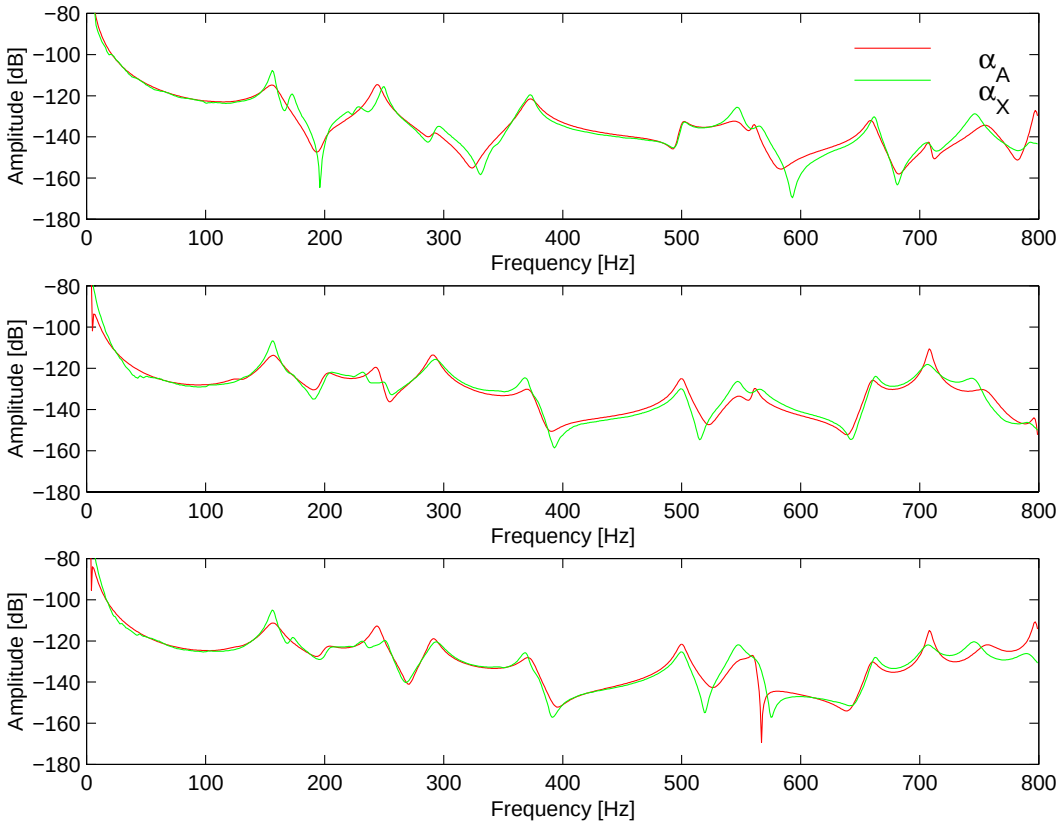

Figure 7.22: Sample FRF overlays after updating damping parameters of S1203

After updating 23 design parameters and damping properties of the FE model, both correlation functions shown in figure 7.23 indicated a good level of correlation for the vast majority of frequency points with values higher than 0.9. The response predictions of all 63 measured DOFs have therefore been improved considerably.

Most of the computed design changes are physically justifiable. This is specifically true for the stiffnesses of the lumped springs in S2 and the Young's modulus of S1 to S3. However, the changes introduced to sub-structures S4 and S5 are physically less meaningful. The Young's modulus of both sub-structures was subject to major changes, while the stiffnesses changes of the lumped springs were less dramatic than those observed in sub-structure S2. In fact, the stiffness of the intermediate beam S5 was increased in every respect while the stiffness of sub-structure S4 decreased by a large amount.

The computed stiffness properties of the intermediate beams (S4, S5) suggest that the distribution of stiffness is not critical. Unlike S2 where a higher stiffness concentration was computed for the lumped springs, sub-structures S4 and S5 also allowed changes in the Young's modulus. However, the computed decrease in stiffness of sub-structure S4 was unexpected and may be attributed to a softer bolted connection than that of S5.

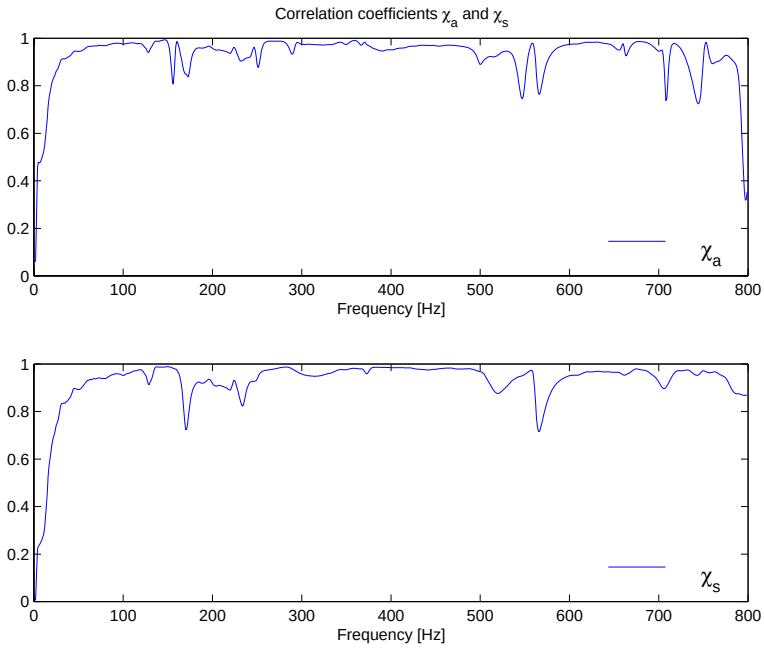

Figure 7.23: Correlation functions after updating damping parameters of S1203

Young's Modulus of Sub-structures S1–S5					
parameter	φ_1	φ_2	φ_3	φ_4	φ_5
sub-structure	S1	S2	S3	S4	S5
unit	$[N/m^2]$				
initial	7.100e10	7.100e10	7.100e10	7.100e10	7.100e10
updated	6.554e10	7.356e10	6.693e10	3.300e10	24.31e10
% error	-7.690	3.610	-5.720	-53.59	242.3

Table 7.11: Initial and updated Young's Modulus of S1–S5 of S1203

Lumped Springs in Sub-structure S2						
parameter	φ_6	φ_7	φ_8	φ_9	φ_{10}	φ_{11}
direction	x	y	z	θ_x	θ_y	θ_z
unit	$[kg]$			$[Nm/rad]$		
initial	2.800e9	1.000e9	1.000e9	3.300e3	4.300e3	4.300e3
updated	2.885e9	1.000e9	0.994e9	3.295e3	188.2e3	4.300e3
% error	3.050	0	-0.570	-0.140	4276	0

Table 7.12: Initial and updated lumped springs in S2 of S1203

Lumped Springs in Sub-structure S4						
parameter	φ_{12}	φ_{13}	φ_{14}	φ_{15}	φ_{16}	φ_{17}
direction	x	y	z	θ_x	θ_y	θ_z
unit	$[kg]$			$[Nm/rad]$		
initial	2.800e9	1.000e9	1.000e9	3.300e3	4.300e3	4.300e3
updated	2.798e9	1.000e9	1.000e9	3.300e3	0.334e3	6.953e3
% error	-0.050	0	0	0	-92.23	61.69

Table 7.13: Initial and updated lumped springs in S4 in S1203

Lumped Springs in Sub-structure S5						
parameter	φ_{19}	φ_{19}	φ_{20}	φ_{21}	φ_{22}	φ_{23}
direction	x	y	z	θ_x	θ_y	θ_z
unit	$[kg]$			$[Nm/rad]$		
initial	2.800e9	1.000e9	1.000e9	3.300e3	4.300e3	4.300e3
updated	2.800e9	1.000e9	1.000e9	1.000e3	10.82e3	31.19e3
% error	0	0	0	0	151.6	625.4

Table 7.14: Initial and updated lumped springs in S5 of S1203

mode r	1	2	3	4	5	6	7	8	9	10	11
η_r [%]	7.8	5.9	6.1	3.1	3.2	1.4	3.5	0.9	1.3	0.6	2.4
ω_r [Hz]	156	200	243	291	371	498	546	561	658	710	754

Table 7.15: Identified structural damping factors of S1203

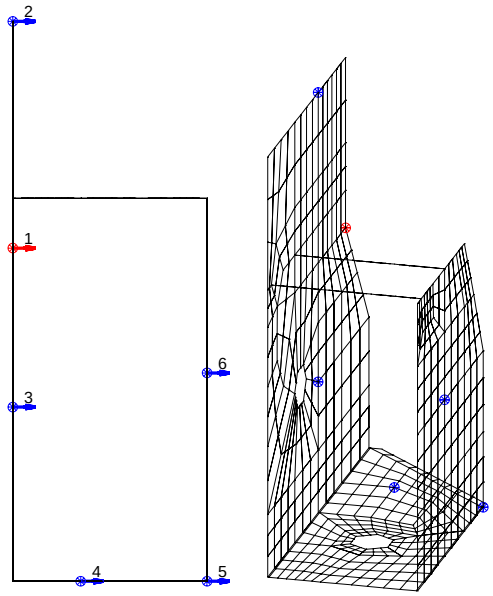

Figure 7.24: Location of six arbitrarily selected measured DOFs in S1203

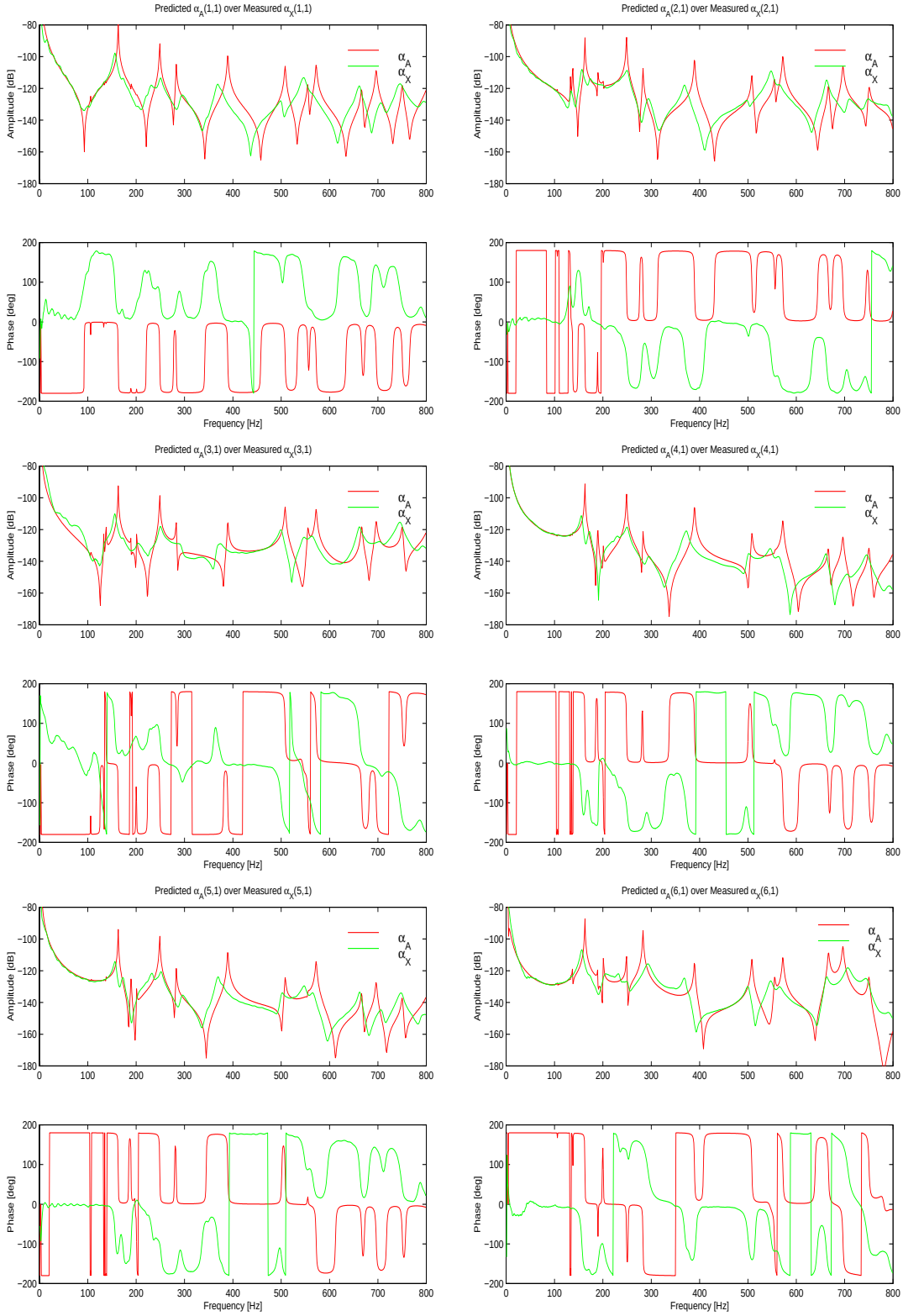

Figure 7.25: Initial FRF overlays of S1203 (fig. 7.24)

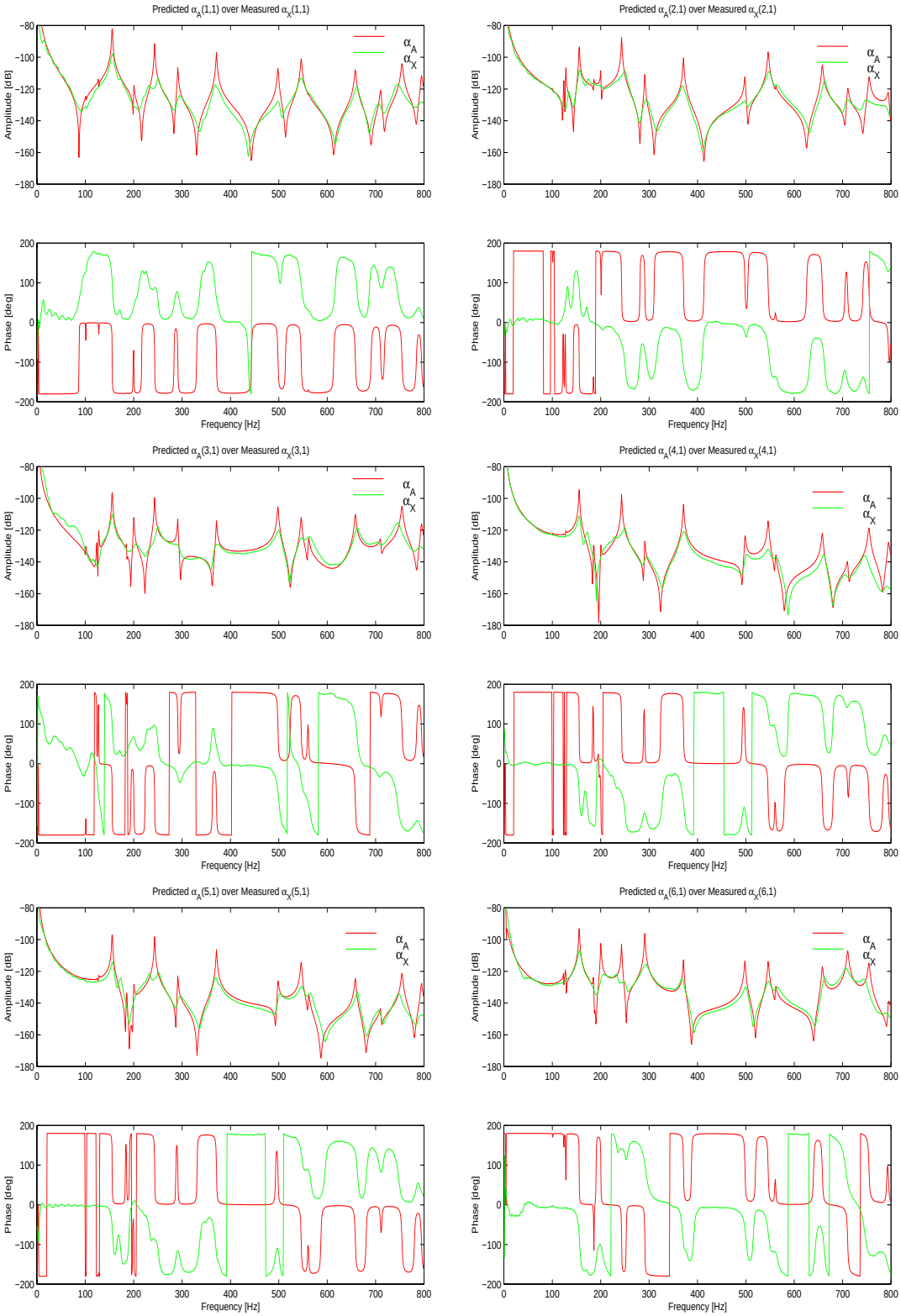

Figure 7.26: FRF overlays of S1203 after updating spatial parameters (fig. 7.24)

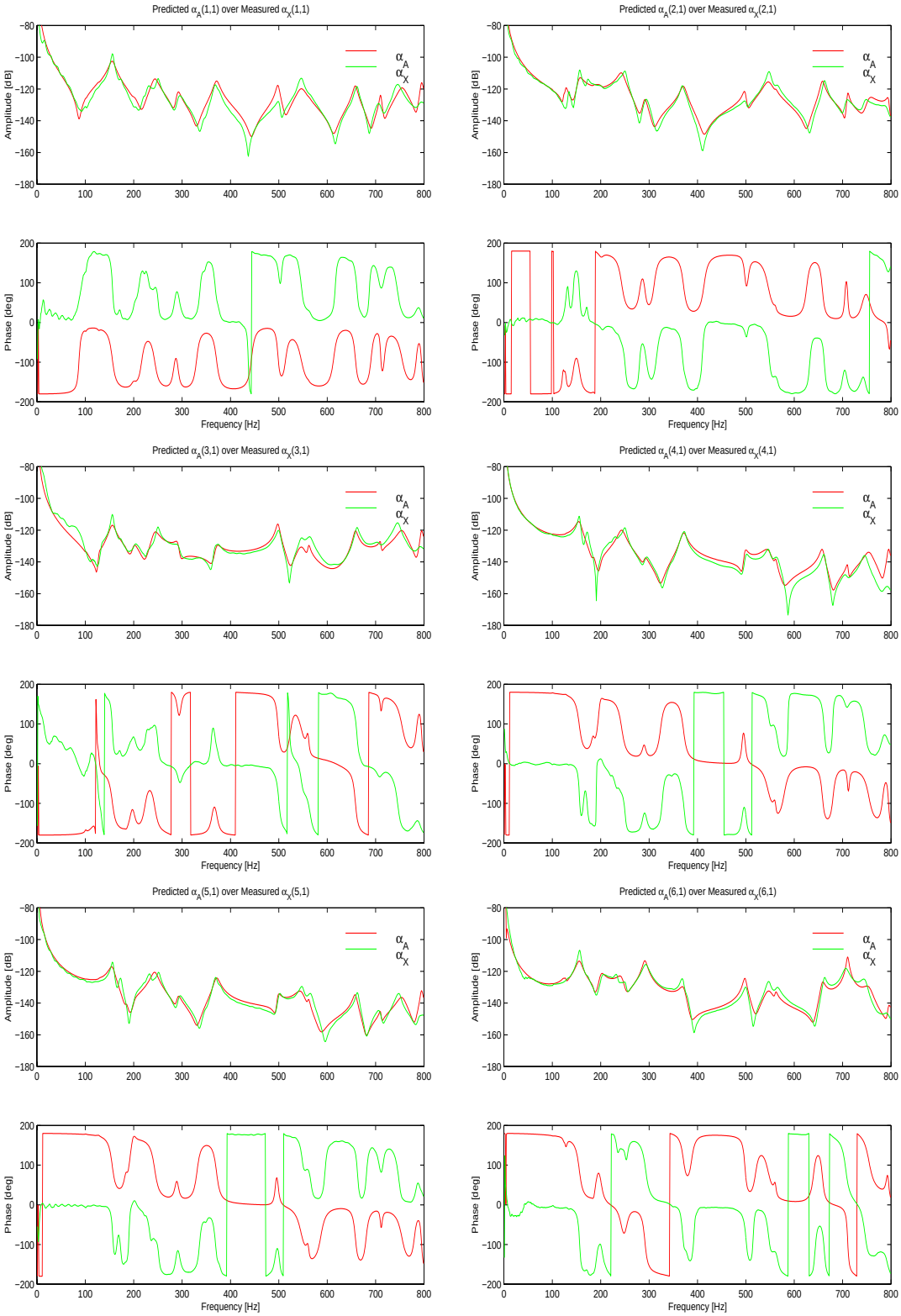

Figure 7.27: FRF overlays of S1203 after updating damping parameters (fig. 7.24)

7.3 An Automotive Muffler

The research presented in this thesis was part of an EU-BRITE project (URANUS 1994) and one of the industrial applications was the automotive muffler shown in figure 7.28. The industrial partners took a keen interest in applying response-based model updating techniques to validate their FE models over frequency ranges wider than those usually accessible for modal-based updating formulations.

In the course of the project, two main problem areas were identified as critical to satisfy the project objectives. Firstly, it was difficult to establish a sufficient level of correlation between the measurements and the initial FE predictions (between $0Hz$ and $2000Hz$) and, most of all, the *state-of-the-art* FRF model updating techniques (in 1995) were incapable of dealing with large FE models. In fact, it was found that not so much the size of the FE model limited the application of FRF-based model updating formulations (as this limit is computer-hardware depend), but rather the limited number of measurements provided in relation the number of DOFs in the FE model was a major problem. For a more detailed discussion on this aspect, see Section 2.3.

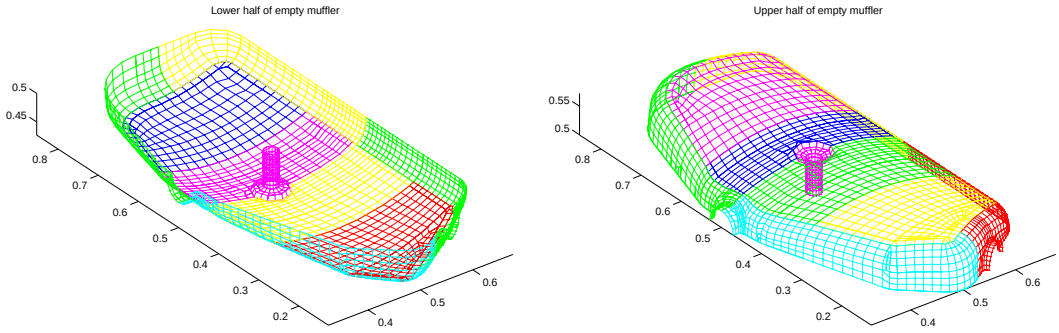

Figure 7.28: Sub-structured FE model of automotive muffler

This particular case study was used to verify that the P-C model updating formulation, introduced in Chapter 4, is applicable for any number of available measurements and that it is able to cope with small values incompleteness ratio i_r (eqn. (2.7), p. 23). Furthermore, it also provided a good case to show that large FE model can be reduced considerably using CMS methods (chap. 3).

The empty muffler has 26 352 DOFs and was partitioned into 18 sub-structures (fig. 7.28). The frequency range of validity of the condensed model was set at $0Hz$ to $2000Hz$ and a modal analysis was performed between $0Hz$ and $4000Hz$ for each sub-structure. The majority of sub-structures converged to about 10 modes within this frequency range, except the intermediate tube, which was much stiffer and only converged to 3 modes. After analysing and assembling the components using the Craig-Bampton CMS method, the new number of (hybrid) coordinates was 3544.

Subsequently, the reduced FE model was submitted for a new eigensolution in MATLAB. However, the computations failed as the condensed global mass and stiffness matrices, $[M]$ and $[K]$, had lost their sparsity and the memory load required exceeded that available on the local computer (IBM RS 6000, 256 Mb memory). This limitation is due to the sparse matrix representation within MATLAB and is unlikely to occur in any other software programmed in C or FORTRAN. It is worth noting that the previous case study included

the analysis of a sparse system with 4044 DOFs. Although MATLAB provides a good analysis environment for research purposes, the problem size that can be analysed is clearly limited.

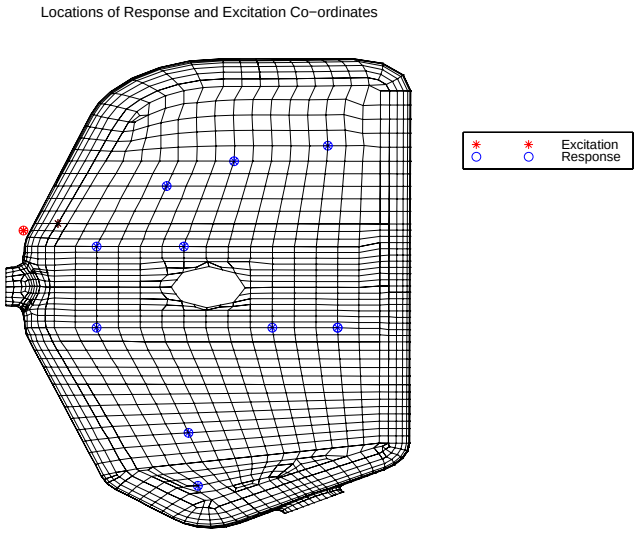

Figure 7.29: Excitation and response locations of simulated measurements

As a result of these limitations, the simulated case study was reduced to 8 sub-structures only, representing the upper half of the full muffler. Here, the same frequency range of validity and CMS method were applied to the FE model, including an extra 10 arbitrarily selected measurements DOFs. The location of these excitation and response DOFs is shown in figure 7.29. Including the measurement DOFs, the full model size of 13 176 was subsequently condensed to 636 DOFs.

All shell elements in the initial FE model assumed a element thickness of $t = 1.42mm$. To simulate measured data (subsequently referred to as *measurements*), the FE model was perturbed and two strips of shells were assigned a thickness of $t = 2mm$. The locations of the perturbed elements are shown in figure 7.30 and correspond to two strengthening folds which are not considered in the FE model. The *measurements* and the predictions were subject to $\eta_i = 0.01$ structural damping and the *measurements* were contaminated with 15% multiplicative noise. A representative FRF overlay is shown in figure 7.31.

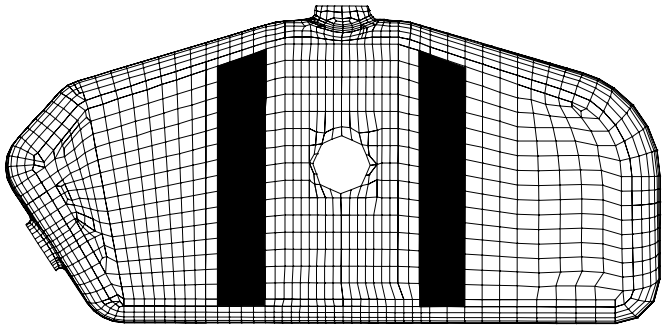

Figure 7.30: Location of perturbed shell elements (black-marked)

The lower and upper halves of the muffler are interconnected by a lap joint whose presence is reflected by a string of beam elements in the upper shell at corresponding locations.

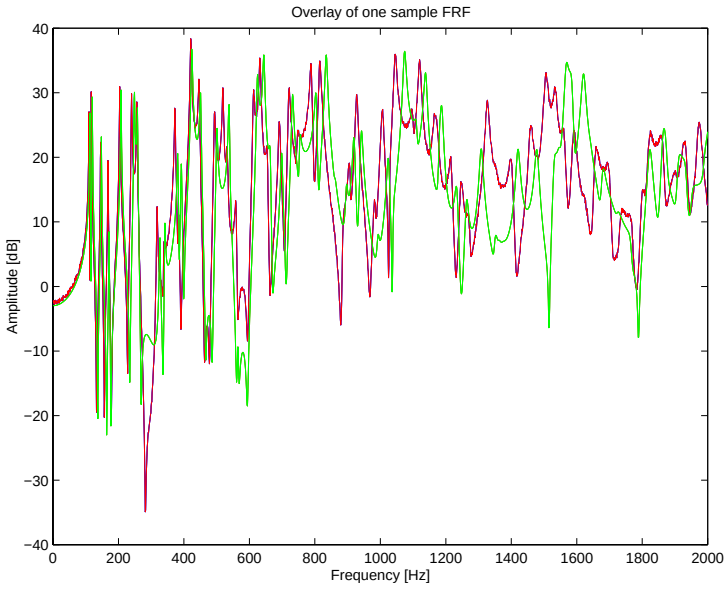

Figure 7.31: Sample FRF overlay before updating

The Young's modulus of this group of beam elements and the thickness, t, of the two strips of shell elements (fig. 7.30) were included as updating parameters. As the sensitivities of these three updating parameters can be shown to be linearly independent, the updating computations were performed without the sub-set selection procedure proposed in Chapter 5 and with a target updating frequency range from $0Hz$ to $400Hz$. Figure 7.32 presents the results of the updating computations and denotes both strips of shell elements as updating parameters φ_1 and φ_2, whereas the beams are associated with φ_3.

Figure 7.32 presents the graphical output one obtains after each iteration in OPTIMA (Grafe 1997c) and shows correctly that no alterations needed to be introduced to the lap joint of this structure (i.e. φ_3). The P-C model updating formulation only changed φ_1 and φ_2, namely the shell element thicknesses. Both parameters converged after 6 iterations to $\varphi_1 = 1.52mm$ and $\varphi_2 = 1.39mm$, which are closer to the correct thickness of $t = 1.42mm$ than before. The sample FRF overlay of the updated FE model is shown in figure 7.33.

Concluding this case study, a set of ten noise contaminated measurements were generated and three updating parameters of an FE model of 13 176 DOFs were updated. All three updating parameters were linearly independent and ensured immediate convergence. The incompleteness ratio for this application was $\mathrm{i}_r = 10/13176$ and thereby closer to those possibly encountered in industry. This particular case study has confirmed that the P-C model updating can update large FE models (small, i_r) using appropriate updating parameters. The quality of results does not degenerate with incomplete measurements.

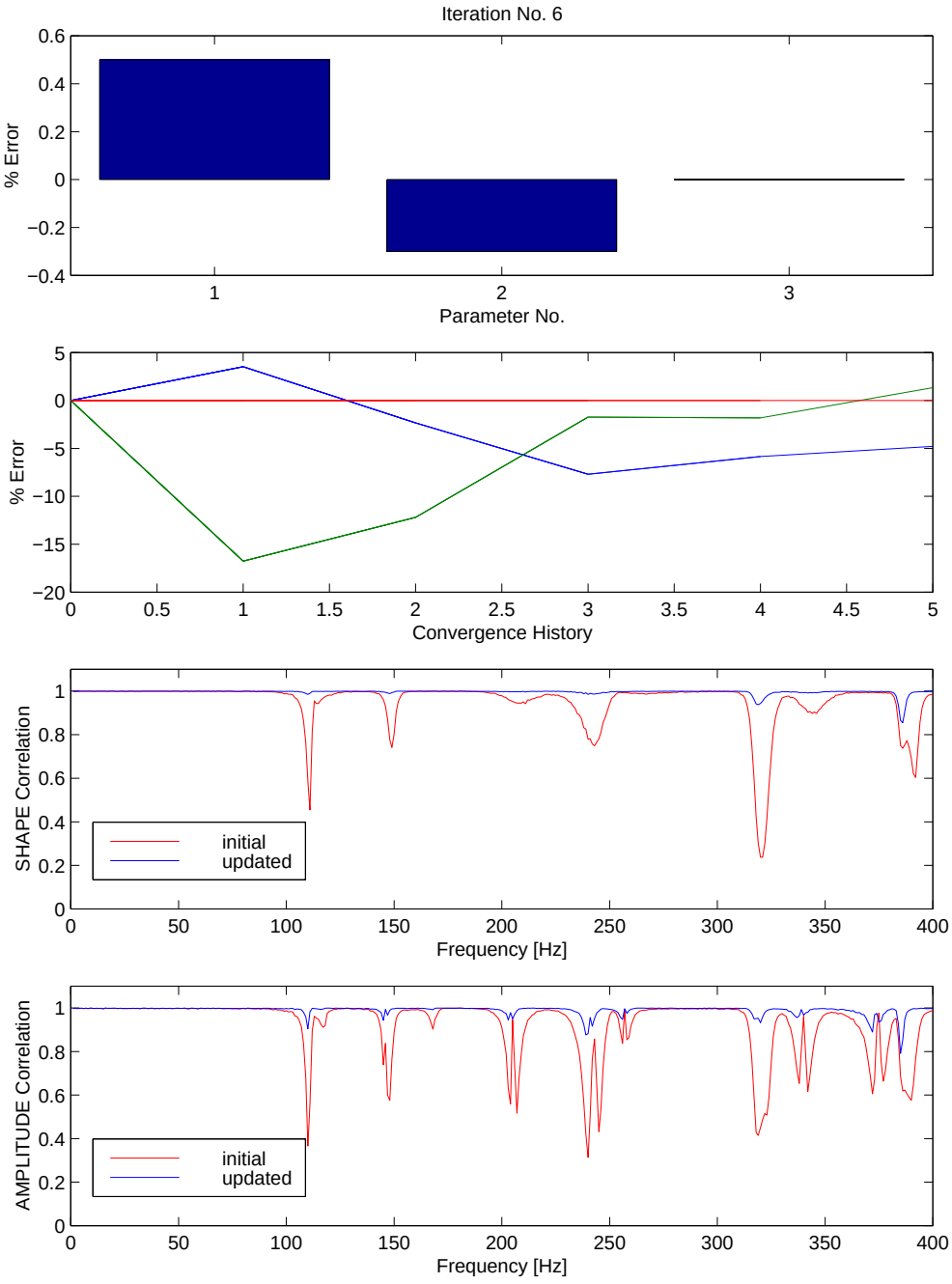

Figure 7.32: Updating results of automotive muffler

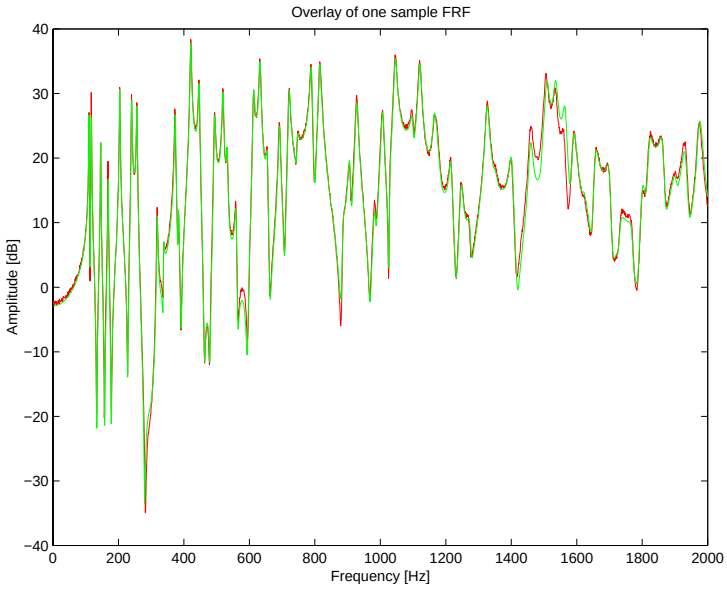

Figure 7.33: Sample FRF overlay after updating

7.4 Concluding Remarks

Three case studies have been presented in this chapter to validate the theories developed in Chapters 3 to 6. Common to all applications was a smaller incompleteness ratio usually seen in other FRF model updating publications. The incompleteness ratios decreased in value for each case and were about 1/60, 1/210 and 1/1320 respectively. The two experimental case studies and the simulated case study were successfully completed. The following conclusions can be drawn:

- The P-C model updating technique produces non-unique parameter adjustments, as do most other updating formulations. Depending on the initial value of maximum permissible condition number, considerable design changes may be introduced at each iteration (here, errors in excess of 100% were identified). The changes in updating parameters decrease steadily as the computations continue and the correlation improves. For instance, the errors decreased almost exponentially in the clamped-beam case-study (fig. 7.5). A large number of iterations seemed inevitable but enabled the updating formulation to introduce major parameter changes (e.g. $\approx$ 4000% error in tab. 7.12). Once the computations had converged, the response predictions improved to a level where each analytical resonant frequency matched by an experimental counterpart (fig. 7.26).

- A relatively large number of updating parameters was considered in each experimental case study and the sub-set selection procedure employed was able to condition the sensitivity matrix and to depict appropriate parameters. In general, the number of selected updating parameters increased as the computations progressed and the correlation improved. The maximum permissible condition number, κ_∞, must be set manually and should be increased if the initial level of parameter changes are of negligible magnitude.

- The error location procedure did not indicate physically meaningful error sources in the S1203 structure. However, combining the results obtained with engineering insight, a set of updating parameters was identified which was subsequently able to diminish the errors in response. Yet, more work must be devoted to error localisation techniques.

- Proportionally-damped FE models were used for all the case studies and after updating $[K]$ and $[M]$, the initial damping estimates were adjusted on a mode-by-mode basis. As before, the damping identification procedure converged quickly and did not lead to ill-conditioned sensitivity matrices. From a practical point of view, the way the analytical responses changed was interesting to observe. In cases where the measured and predicted resonances did not match, the algorithm adjusted the analytical response at resonance to the measured amplitude at the corresponding frequency point. This may have distorted the overall picture of the FRF (over-damped modes) but achieved a definite improvement of $\chi_s(\omega)$ and $\chi_a(\omega)$ (fig. 7.27).

- From a computational viewpoint, the fixed interface method proposed by Craig Jr. and Bampton (1968) was found to be reliable and very efficient. In general, the cost of computing response sensitivities ($\partial[H]/\partial\varphi_i$) dominates the updating computations. Although a truncated modal solution of a reduced FE model was used to compute these sensitivities, the computing time for the S1203 structure was about 24 hours on an IBM RS 6000 (model 300) workstation (256 Mb). It is the author's belief that the OPTIMA code (Grafe 1997c) can be speeded up by about a factor of 10 using

the C or FORTRAN programming language. This would also resolve the memory loading problem encountered in the automotive muffler case. However, this is a commercial exploitation issue and not related to basic algorithm development, so it was not pursued further within this thesis.

Chapter 8

Conclusions and Suggestions for Further Work

Model updating can be defined as the systematic adjustment of FE models in the light of experimental data. The state-of-the-art in model updating technology has long been based on modal-based model updating procedures as these are, in general, numerically more robust and better suited to cope with larger applications.

Response-based model updating techniques have been in existence for 20 years and are, by definition, far more attractive than the modal-based formulations. They make direct use of the measured responses and therefore relate to the true damped response. It is not necessary to perform an experimental modal analysis.

At the outset of this project in 1995, issues such as numerical instability of the updating equations and problems associated with incomplete measurements had not been resolved. The computing time required by FRF updating algorithms generally exceeded that of modal-based updating formulations when applied to large FE models.

The interest in applying FRF model updating techniques to large FE models was the essential motivation of this research and the main conclusions drawn will be listed in the following.

8.1 Conclusions

FRF model updating in 1995: FRF model updating formulations were critically reviewed and it was observed that the demands put on the test data were difficult, if not impossible, to meet. Methods often required large system matrix inversions to formulate the updating equations and the computations involved were not economical as often many more responses were computed than actually needed. The phenomenon of non-unique parameter estimation was analysed and an analytically-derived mechanism has shown that whole families of parameter changes satisfy the updating equations if band-limited measurements are employed or the set of updating equations is ill-defined. A numerically-simulated updating case has shown that these phenomenon also arise when the measurements are incomplete, noise-contaminated or when the number and location of updating frequencies change. The incompleteness of measurements, measured by the incompleteness ratio $\mathrm{i}_r = N/n$, predominantly limited the applicability of response-based

updating formulation to large FE model. Missing response measurements can be shown to violate the integrity of response-based updating formulations.

Error modelling: Model updating methods rely on appropriate representations of likely error sources in the FE model. The implication of using simple elemental modification factors (the p-values) was reviewed and was found that such a simplistic approach inherently fails to introduce model changes in a physically representative manner. A physically representative error model was therefore proposed in this work. It obtains its associated derivatives from contemplating the dynamic stiffness matrix directly and introduces the computed design parameter changes into the FE model by re-evaluating the corresponding finite elements (rather than scaling element matrices).

FE model reduction: Constraint- and fixed-interface CMS methods have been introduced and validated to allow for more economical updating computations and to address the incompleteness aspect in FRF model updating. The three CMS methods presented introduced a considerable level of reduction while retaining a good level of accuracy of the predicted dynamic properties of the full system. A fixed-interface method was favoured in most of the case studies presented in this thesis as the transformation matrices involved were generally faster to compute. CMS methods produce frequency-independent transformation matrices and therefore allowed the condensation of the FE model (component) at many frequency points without the need to reduce the system at each frequency point separately.

FRF correlation: At the outset of this project, it was customary to employ visual means to inspect the closeness between the response measurements and their analytical counterparts. Little use was made of numerical correlation measures and if so, these were mostly based on comparing identified modal properties. In this thesis, two new correlation functions have been introduced which allow the correlation of any number of measurements and their corresponding predictions in a consistent manner. The shape- and amplitude-correlation coefficients, $\chi_s(\omega)$ and $\chi_a(\omega)$, can measure the closeness between two corresponding sets of FRFs at any measured frequency point and return a value between zero and unity.

Correlation-based updating: The updating formulation developed in this thesis, the P-C method, distinguishes itself from many other FRF model updating techniques by updating $\chi_s(\omega)$ and $\chi_a(\omega)$ rather than the analytical responses directly. Like the correlation functions, the formulation is defined for any number of measurements (and any combination of response and excitation DOFs) and the integrity of the updating equations involved is not violated for incompleteness ratios smaller than unity ($\mathrm{i}_r = n/N$). It uniquely maps generally complex responses into a real set of liner equations and always produces a well-balanced "response" residual, $\{\varepsilon\}$, with element entries between zero and unity. Unlike many other FRF updating algorithms, the P-C method is therefore numerically better balanced and has demonstrated its ability to modify design parameter by orders of magnitudes.

Updating frequencies: The basic requirement to select specific updating frequencies has been circumvented in the P-C model updating formulation. In general, all measured

frequency points are considered excluding those which are associated with a high level of correlation. This very consistent approach of solving updating problems, i.e. there is no interference by the analyst, allows for comparative studies of the method's performance using different structures. Neither the consistency of the formulation nor the redundancy of selecting updating frequency points can be found with other FRF model updating formulations.

Noise robustness: Throughout the thesis, the simulated measurements were contaminated with up to 15% noise. The P-C model updating formulation has shown to be robust against these disturbances and allowed for response improvements up to a level where the correlation coefficients, $\chi_s(\omega)$ and $\chi_a(\omega)$, could not discriminate anymore between noise and response signal. This robustness to noise derives from the fact that the P-C method updates these correlation measures rather than a noise-free analytical response using noise-contaminated measurements.

Weighting matrices: The estimation of weighting matrices for a weighted least-square solution is a difficult subject and often external statistical means are employed to estimate these. The extended weighted least-square solution, proposed for the P-C method, uses weighting matrices whose diagonal entries are $\chi_s(\omega)$ and $\chi_a(\omega)$ themselves, a feature, which also makes the updating formulation very consistent.

Error localisation: The localisation of erroneous regions in the FE models is a difficult subject and sensitivity-based methods present the only realistic means to perform such a task in larger applications. Unlike purely analytical expressions like the eigenvalue-sensitivities, the error-localisation procedure proposed in this thesis combines the information provided by the measurements and the predictions across the full measured frequency spectrum. Although the results of this new method were more conclusive than those obtained by using the eigenvalue-sensitivities, localising erroneous regions in the FE models remains a difficult and largely unresolved problem. More research must be devoted to this subject.

Sub-set selection: The number and kind of updating parameters identified from an error-localisation procedure can impose ill-conditioned sensitivity matrices if the corresponding sensitivities (columns in $[S]$) are linearly dependent. This research has introduced a sub-set selection procedure using the QR matrix decomposition technique to search for linearly independent updating parameters. The eventual number of parameters is variable and depends on a user-selected constant and the dimensions of $[S]$. As the response predictions improve, the number of included updating parameters generally increases and the last iterations usually introduce changes to updating parameters other than the most erroneous ones.

Identification of damped responses: The theoretical analysis of damping is not well understood and, often, response predictions are derived from an undamped FE model. A damping identification algorithm was proposed using analytically well-defined sensitivities. It identified viscous as well as structural damping parameters on a mode-by-mode basis and lead to well-conditioned sensitivity matrices. Case studies have shown the method's rapid convergence properties.

Computational aspects: The cost of running the P-C model updating algorithm is determined by the size of the (condensed) FE model. The overwhelming majority of CPU time is spent on computing the response sensitivities. In the case studies presented, the computational effort was reduced by employing a truncated modal solution of an already-condensed FE model. However, the need to perform an independent modal analysis of each component can be used advantageously to implement the algorithm into a multi-processor computing environment. In addition, the model updating computations can be performed equally well on several processors at the same time. There are N_f independent response computations, N_φ sensitivity calculations and at least N_φ design changes to be introduced after each iteration. Thus, the architecture of the model updating algorithm is suited for parallelisation. In particular, applications of industrial size would benefit from a reduction in computer time.

Parameter studies Response sensitivities of the kind of $\partial\chi_s(\omega)/\partial\varphi$ and $\partial\chi_a(\omega)/\partial\varphi$ return real values for generally complex responses. As real quantities are easier to interpret than complex quantities, these sensitivities can be conveniently used in parameter studies. Parameters can then be identified which are more sensitive than others in certain frequency regions.

FRF reciprocity It is good practice to perform a reciprocity test of some of the measured FRFs and, so far, the quality of these has been assessed by visual means. By using the shape- and amplitude-correlation coefficients, such assessments can be done systematically.

8.2 Summary of Contributions

1. It was analytically shown that the limited frequency range of measurements introduces non-unique parameter estimation results. The same phenomenon was shown to occur with incomplete measurements, noise and varying updating frequencies.
2. Two consistent FRF correlation functions have been introduced. Both uniquely describe the level of closeness between any number of measurements and their analytical counterparts with a value between zero and unity across the full measured frequency spectrum.
3. A correlation-based model updating algorithm has been proposed and successfully applied to large FE models using few measurements. Its formulation is independent of the number of measurements used and therefore the problems associated with incomplete measurements have been resolved. The residual of this sensitivity-based formulation is numerically well balanced and leads to smooth convergence properties. Further improvements to the state-of-the-art of FRF model updating in 1995 are that, in this new method
   - no specific updating frequencies need to be selected,
   - the formulation is much more resistant to measurement noise,
   - defined weighting matrices allow for consistent and stable least-square solutions.
4. Analytically-derived sensitivities of damped responses have been successfully applied to identify a viscous or structural damping coefficients on a mode-by-mode basis. This iterative procedure is not subject to any numerical approximation and has exhibited rapid convergence properties.
5. Substructuring methods have been introduced and validated for use in FRF model updating. Especially the fixed-interface method has proven to be numerically reliable and very economical.
6. A variant of an established parameter sub-set selection procedure was proposed. The number of included updating parameters varies from one iteration to the next as a result of the current level of correlation.
7. The localisation of erroneous finite elements was addressed by employing correlation measures and analytically defined sensitivities of these. It was shown to produce more conclusive results than those obtained by using eigenvalue-sensitivities.
8. A physically-representative error model that is fully compatible with the definition of the FE model has been proposed. Model parameter changes are integrated by re-evaluating the finite elements of concern.

8.3 Suggestions for Further Work

Error localisation: The localisation of erroneous finite elements is the key to success in model updating and more work should be devoted to the development of such techniques. To date, there is no reliable and generally applicable method available and the problem of localising erroneous regions in the FE model is largely unresolved. The effect of various measurement set-ups on the quality of identified errors should be investigated further. For this purpose, it is suggested to make use of the leverages, introduced in Chapter 5, and the P-C method in a combined manner. As the sensitivities $\partial\chi_s(\omega)/\partial\varphi$ and $\partial\chi_a(\omega)/\partial\varphi$ change with changing numbers and locations of measurements, questions could be answered such as:

- What measurement configuration leads to better identification results ? and,
- What distribution patterns are followed by the response/excitation points of that measurement set-up ?
- Are finite elements remote from the measurement locations less sensitive than those close to response/excitation points ? and, if so,
- How can the information about the distribution of element sensitivities with the associated measurement set-up be quantified and used to improve current error localisation methods ?

A systematic investigation into this subject is probably still best performed using simulated case-studies.

Uniqueness aspect: Non-unique parameter estimations seem inevitable in model updating and initial attempts have been made to explain this phenomenon in this thesis. The identified mathematics behind non-unique design parameter changes should be further investigated. But also the influence of the number of measurements on the uniqueness of computed design parameter changes should be further explored.

Algorithm implementation: Most algorithms proposed in this thesis have been developed under MATLAB (Mathworks 1997) and experience shows that the use of dedicated programming languages can speed up the solution by about a factor of 10. Furthermore, FRF model updating algorithms are suited for parallelisation as there are many computational elements which can be performed completely independently from each other. It is therefore recommended to perform any further research using a programming language like FORTRAN (or C) and/or a parallelised code. The P-C method is currently implemented by Dynamic Design Solutions (FEMtools 1995), a partner in the BRITE project who provides commercially available software.

8.4 Closure

The objectives of this research were to analyse critically existing FRF model updating techniques and to develop further this technology for large applications. The inherent incompleteness of measurements was resolved by developing a correlation-based model updating algorithm. At the same time, problems associated with frequency point selection and measurement noise have also bee addressed. However, the selection of appropriate

updating parameters based on error-localisation procedures remains a major problem. Unless this critical issue is resolved and better techniques become available, model updating technology can only be applied with limited success.

Bibliography

Allemang, R. and D. Brown (1982). A correlation coefficient for modal vector analysis. In *1st International Modal Analysis Conference, Orlando, USA*.

Arruda, J. R. F. and M. A. V. Duarte (1990). Parameter estimation and model updating of rotor-bearing systems by the direct curve fit of frequency response functions. In *3rd International Conference on Rotordynamics, Lyon, France*.

Atalla, M. J. and D. J. Inman (1996). Model updating using neural networks. In *Second International Conference: Structural Dynamic Modelling: Test, Analysis and Correlation,Cumbria, UK; organised by DTA, NAFEMS, SECED*.

Balmes, E. (1993a). *Experimental/Analytical Preditcive Models Of Damped structural models*. Ph. D. thesis, Massachusetts Institute of Technology, Department of Aeronautics and Astronautics, Massachusetts, USA.

Balmes, E. (1993b). A finite element updating procedure using frequency response functions. applications to the MIT/SERC interferometer testbed. In *11th International Modal Analysis Conference, San Diego, USA*.

Baruch, M. (1978). Optimisation procedure to correct stiffness and flexibility matrices using vibrtaion tests. *AIAA Journal 16*(11), 1208–1210.

Bathe, K. J. (1982). *Finite Element Procedures in Engineering Analysis*. Prentice - Hall.

Ben-Haim, Y. (1992). Adaptive diagnosis of faults in elastic structures by static displacement measurements: The method of selective sensitivity. *Mechanical Systems and Signal Processing 6*(1), 85–96.

Ben-Haim, Y. and U. Prells (1993). Selective sensitivity in the frequency domain–I. Theory. *Mechanical Systems and Signal Processing 7*(5), 461–475.

Berman, A. and E. J. Nagy (1983). Improvement of a large analytical model using test data. *AIAA Journal 21*(8), 1168–1173.

Bishop, R. E. D. and D. C. Johnson (1960). *The Mechanics of Vibration*. Cmbridge University Press.

Brahmi, K., N. Bouhaddi and R. Fillod (1995a). Reduction of junction degrees of freedom in certain methods of dynamic substructure synthesis. In *13th International Modal Analysis Conference, Nashville, USA*.

Brahmi, K., N. Bouhaddi and R. Fillod (1995b). Reduction of the junction degrees of freedom before assembly in dynamic substructuring. In *1995 Design Engineering Technical Conferences, ASME, Boston, USA*.

Bucher, I. and S. Braun (1993). The structural modification inverse problem: An exact solution. *Mechanical Systems and Signal Processing 7*(3), 217–238.

Caesar, B. (1987). Updating system matrices using modal test data. In *5th International Modal Analysis Conference, London, England*.

Chatterje, S. and A. S. Hadi (1988). *Sensitivity Analysis in Linear Regression*. John Wiley and Sons.

Chen, J. C. and J. A. Garba (1980). Analytical model improvement using modal tests. *AIAA Journal 18*(6), 684–690.

Chen, T. Y. (1986). *Finite Element Model Refinement Using Modal Analysis Data*. Ph. D. thesis, University of Texas at Arlington, Texas, USA.

Cottin, N. (1983). *Parameterschätzung mit Hilfe des Bayesischen Ansatzes bei linearen elastomechanischen Systemen*. Ph. D. thesis, Universität Hannover, Hannover, Germany.

Cottin, N., H. P. Felgenhauer and H. G. Natke (1984). On the parameter identification of elastomechanical systems using inout and output residuals. *Ingenieure Archiv 54*(5), 378–387.

Craig Jr., R. R. (1987). A review of time domain and frequency domain component mode synthesis methods. *The International Journal of Analytical and Experimental Modal Analysis 2*(2), 59–72.

Craig Jr., R. R. and M. C. C. Bampton (1968). Coupling of substructures for dynamic analysis. *AIAA Journal 6*(7), 1313–1319.

D'Ambrogio, W., A. Fregolent and P. Salvini (1993). Updateability conditions of non-conservative FE models with noise on incomplete input - output data. In *International Conference Structural Dynamic Modelling Test, Analysis and Correlation, Milton Keynes, UK; organised by DTA, NAFEMS with the support of DTI*.

Dascotte, E. (1990). Practical applications of finite element tuning using experimental modal data. In *8th International Modal Analysis Conference, Kissimme, USA*.

Dascotte, E. and P. Vanhonacker (1989). Development of an automatic updating program. In *7th International Modal Analysis Conference, Las Vegas, USA*.

Doebling, S. W., C. R. Farrar and M. B. Prime (1998). A summary review of vibration-based damage identification methods. *The Shock and Vibration Digest 30*(2), 91–105.

Ewins, D. J. (1980). Measurement and application of mechanical mobility data. Solartron Instrumentation Group, Farnborough, Hampshire, England.

Ewins, D. J. (1984). *Modal Testing*. Research Studies Press.

Ewins, D. J. and M. Imregun (1986). State-of-the-art assessment of structural dynamic response analysis methods. *Shock and Vibration Bulletin 56*(1), 91–105.

Ewins, D. J. and M. Imregun (1988). On the reliability of computational dynamic response prediction capabilities (DYNAS). *Society of Enviromental Engineering Journal 56*(1), 91–105.

FEMtools (1995). *FEMtools. Integrating Test and Analysis, Version 1.0*. Dynamic Design Solutions, Leuven, Belgium: FEMtools.

Fenner, R. T. (1986). *Engineering Elasticity*. Ellis Horwood.

Fenner, R. T. (1996). *Finite Element Methods for Engineers*. Imperial College Press.

Ferreira, J. V. (1998). *Dynamic Response Analysis of Structures with Nonlinear Components*. Ph. D. thesis, Imperial College of Science, Technology & Medicine, Department of Mechanical Engineering, London, UK.

Foster, C. D. and J. E. Mottershead (1990). A method for improved finite element models by using experimental data: Application and implication for vibration monitoring. *International Journal of Mechanical Science 32*(3), 191–202.

Fox, R. L. and M. P. Kapoor (1968). Rate of change of eigenvectors and eigenvalues. *AIAA Journal 12*(6), 2426–2429.

Friswell, M. I. and J. Mottershead (1995). *Finite Element Model Updating in Structural Dynamics*, Volume 38 of *Solid Mechanics and its Application*. Kluwer Academic Publishers, Dordrecht / Boston / London.

Friswell, M. I., J. E. Mottershead and H. Ahmadian (1997). Combining subset selection and parameter constraints in model updating. In *1997 Design Engineering Technical Conferences, ASME, Sacramento, USA*.

Friswell, M. I., J. E. T. Penny and D. A. L. Wilson (1994). Using vibration data and statistical measures to locate damage in structures. *Modal Analysis: The International Journal of Analytical and Experimental Madal Analasis 9*(4), 239–254.

Fritzen, C. P. (1986). Identification of mass, damping and stiffness matrices of mechanical systems. *ASME Journal of Vibration, Acoustics, Stress and Reliability in Design 108*(4), 9–16.

Fritzen, C. P. (1992). Localization and correction of errors in finite element models based on experimental data. In *17th International Seminar on Modal Analysis, Katholieke Universiteit Leuven, Belgium*.

Gasch, R. and K. Knothe (1987). *Structurdynamik, Band 1: Diskrete Systeme*. Springer Verlag.

Gasch, R. and K. Knothe (1989). *Structurdynamik, Band 2: Kontinua und Ihre Diskretesierung*. Springer Verlag.

Golub, G. H. and C. F. van Loan (1996). *Matrix Computations* (3rd ed.). The Johns Hopkins University Press.

Grafe, H. (1995, May). Review of frequency response function updating methods. Technical report no. 1.01, BRITE-URANUS BRE2-CT94-0946.

Grafe, H. (1997a, March). FRF updating of rail system (phase a). Technical report no. 5.04a, BRITE-URANUS BRE2-CT94-0946.

Grafe, H. (1997b, January). An improved FRF updating method. Technical report no. 1.03b, BRITE-URANUS BRE2-CT94-0946.

Grafe, H. (1997c, January). Optima users' guide. Supplementary guide for MATLAB based software developed in BRITE-URANUS BRE2-CT94-094.

Grafe, H. (1997d, June). Updating of an automotive muffler (phase a). Technical report no. 4.03a, BRITE-URANUS BRE2-CT94-0946.

Grafe, H., M. Imregun and D. Ewins (1997). A refined p-value formulation for finite element model updating. In *15th International Modal Analysis Conference Japan, Tokyo, Japan*.

Guyan, R. J. (1965). Reduction of stiffness and mass matrices. *AIAA Journal 3*(2), 380.

Gysin, H. (1990). Expansion: The achilles heel of FE model updating. In *15th International Seminar on Modal Analysis, Katholieke Universiteit Leuven, Belgium*.

Hemez, F. M. (1997a). Finite element updating of sub-structured models. In *15th International Modal Analysis Conference, Orlando, USA*.

Hemez, F. M. (1997b). Structural damage detection with very large dimensional finite element models. In *15th International Modal Analysis Conference, Orlando, USA*.

Heylen, W. and P. Avitabile (1998). Correlation considerations - part 5 (degree of freedom correlation techniques). In *16th International Modal Analysis Conference, Santa Barbara, USA*.

Heylen, W. and S. Lammens (1996, March). FRAC: a consistent way of comparing frequency response functions. In *Identification in Engineering Systems, Proceedings of the Conference held at Swansea*.

Hintz, R. M. (1975). Analytical methods in component mode synthesis. *AIAA Journal 13*(8), 1007–1016.

Hughes, T. J. R. (1987). *The Finite Element Method*. Prentice - Hall.

Hurty, W. C. (1965). Dynamic analysis of structural systems using component modes. *AIAA Journal 3*(1), 678–685.

Ibrahim, S. R., W. D'Ambrogio, P. Salvini and S. Sestieri (1992). Direct updating of nonconservative finite element models using measured input - output. In *10th International Modal Analysis Conference, San Diego, USA*.

Imregun, M. (1992, September). Correlation and updating of finite element models using vibration test data. *Noise and Vibration Worldwide 23*(9), 16–24.

Imregun, M. (1994). A review of case studies in model updating. In *19th International Seminar on Modal Analysis, Katholieke Universiteit Leuven, Belgium*.

Imregun, M. and D. J. Ewins (1994). Mesh density effects on finite element model updating. In *12th International Modal Analysis Conference, Honolulu, Hawaii*.

Imregun, M., K. Y. Sanliturk and D. J. Ewins (1995). Finite element model updating using frequency response function data-II. case study on a medium size finite element model. *Mechanical Systems and Signal Processing 9*(2), 203–213.

Imregun, M. and W. J. Visser (1991, January). A review of model updating techniques. *The shock and Vibration Digest 23*(1), 9–20.

Imregun, M., W. J. Visser and D. J. Ewins (1995). Finite element model updating using frequency response function data-I. theory and initial investigation. *Mechanical Systems and Signal Processing 9*(2), 187–202.

Jung, H. (1991, February). Model updating using sensitivity analysis. Internal Report, Imperial College, Dynamics Section Reprot No. 91002.

Kammer, D. C. (1992). Effects of noise on sensor placement for on-orbit modal identification of large space structures. *Journal of Dynamical Systems, Measurement and Control - Transactions of the ASME 114*(3), 436–443.

Lammens, S. (1995). *Frequency Response Based Validation of Dynamic Structural Finite Element Models*. Ph. D. thesis, Katholike Universiteit, Department Werktuikkunde, Leuven, Belgium.

Larsson, P. O. and P. Sas (1992). Model updating based on forced vibration testing using numerically stable formulations. In *10th International Modal Analysis Conference, San Diego, USA*.

Lenoir, D., S. Cogan, G. Lellement and J. N. Briscout (1998). Model updating by modal synthesis of experimental forced responses. In *16th International Modal Analysis Conference, Santa Barbara, USA*.

Levin, R. I. and N. A. J. Lieven (1998). Dynamic finite element model updating using simulated annealing and genetic algorithms. *Mechanical Systems and Signal Processing 12*(1), 91–120.

Lieven, N. A. and D. J. Ewins (1988). Spatial correlation of mode shapes, the coordinate modal assurance criterion (COMAC). In *6th International Modal Analysis Conference, Kissimmee, USA*.

Lin, R. M. and D. J. Ewins (1990). Model updating using FRF data. In *15th International Seminar on Modal Analysis, Katholieke Universiteit Leuven, Belgium*.

Link, M. (1986). Identification of physical system matrices using incomplete vibration test data. In *4th International Modal Analysis Conference, Los Ageles, USA*.

Link, M. (1990). Identification and correction of errors in analytical models using test data - theoretical and practical bounds. In *8th International Modal Analysis Conference, Kissimme, USA*.

Link, M. (1998). Updating analytical models by using local and global parameters and relaxed optimisation requirements. *Mechanical Systems and Signal Processing 12*(1), 7–22.

Link, M. and J. Mardorf (1996). The role of finite element idealisation and test data errors in model updating. In *Second International Conference: Structural Dynamic Modelling: Test, Analysis and Correlation,Cumbria, UK; organised by DTA, NAFEMS, SECED*.

Lombard, J. P., N. Bouhaddi and R. Fillod (1997). A variant of the McNeal component mode synthesis method based on a congruent transformation. In *15th International*

Modal Analysis Conference, Orlando, USA.

MacNeal, R. H. (1971). A hybrid method of component mode synthesis. *Computer and Structures 1*, 581–601.

Magnus, K. and K. Popp (1997). *Schwingungen* (5th ed.). Teubner Verlag, Stuttgart.

Maguire, J. R. (1996). A correlation benchmark for dynamic analysis. In *Second International Conference: Structural Dynamic Modelling: Test, Analysis and Correlation,Cumbria, UK; organised by DTA, NAFEMS, SECED*.

Mai, N. M. M., J. M. M. Silva and R. P. C. Sampaio (1997). Localization of damage using curvature of the frequency response functions. In *15th International Modal Analysis Conference, Orlando, USA*.

MATFEM (1997, Aug). *MATFEM USERs GUIDE, first draft* (1 ed.). Prof. Dr.-Ing. M. Link, Moenchebergstrasse 7, Universitaet Gesamthochschule Kassel, Germany: MATFEM.

Mathworks (1997). *MATLAB, The Language of Technical Computing, Version 5*. Mathworks Inc., MA, USA: Mathworks.

Motterhead, J. E. and M. I. Friswell (1998). Editorial. *Mechanical Systems and Signal Processing 12*(1), 1–6.

Mottershead, J. E. (1990). Theory for the estimation of structural vibration parameters from incomplete data. *AIAA Journal 28*(3), 559–561.

Mottershead, J. E. (1996). On discretization error estimates for finite element model updating. *The International Journal of Analytical and Experimental Modal Analysis 11*(3), 155–164.

Mottershead, J. E. and C. D. Foster (1991). On the treatment of ill-conditioning in spatial parameter estimation from measured vibration data. *Mechanical Systems and Signal Processing 5*(2), 139–154.

Mottershead, J. E. and M. I. Friswell (1993). Model updating in structural dynamics: A survey. *Journal of Sound and Vibration 167*, 347–375.

Mottershead, J. E., E. L. Goh and W. Shao (1995). On the treatment of discretisation errors in finite element model updating. *Mechanical Systems and Signal Processing 9*(1), 101–112.

Natke, H. G. (1977). Die Korrektur des Rechenmodells eines elastomechanischen Systems mittels gemessener erzwungener Schwingungen. *Ingenieur-Archiv 46*, 169–184.

Natke, H. G. (1983). *Einfuehrung in Theorie und Praxis der Zeitreihen- und Modalanalyse* (3rd ed.). Vieweg Verlag, Wiesbaden.

Natke, H. G. (1988). Updating computational models in the frequency domain based on measured data: a survey. *Probabilistic Engineering Mechanics 3*(1), 28–35.

Natke, H. G., G. Lallement, N. Cottin and U. Prells (1995). Properties of various residuals within updating of mathematical models. *Inverse Problems in Engineering 1*, 329–348.

Nefske, D. J. and S. H. Sung (1996). Correlation of a coarse-mesh finite element model using structural system identification and a frequency response criterion. In *14th International Modal Analysis Conference, Dearborn, USA*.

Newland, D. E. (1975). *An Introduction to Random Vibrations, Spectral and Wavelet Analysis* (3rd ed.). Longman, Scientific and Technical.

Newland, D. E. (1989). *Mechanical Vibration Analysis and Computation*. Longman, Scientific and Technical.

O'Callahan, J. (1998). Correlation considerations - part 4 (modal vector correlation techniques). In *16th International Modal Analysis Conference, Santa Barbara, USA*.

O'Callahan, J., P. Avitabile and R. Riemer (1989). System equivalent reduction expansion process. In *7th International Modal Analysis Conference, Las Vegas, USA*.

Pascual, R., J. C. Golinval and M. Razeto (1997). A frequency domain correlation technique for model correlation and updating. In *15th International Modal Analysis Conference, Orlando, USA*.

Pilkey, D. F. and D. J. Inman (1998). A survey of damping matrix identification. In *16th International Modal Analysis Conference, Santa Barbara, USA*.

Press, W. H., S. A. Teukolsky, W. T. Vetterling and B. P. Flannery (1992). *Numerical Recipes in Fortran, The Art of Scientific Computing* (2nd ed.). Cambridge University Press.

Randall, R. B. (1987, September). *Frequency Analysis*. Brüel & Kjær, Denmark.

Roy, N. A., L. P. Bugeat, S. Cogan and C. Berthod (1997). An innovative structural analysis platform for large industrial finite element models. In *15th International Modal Analysis Conference, Orlando, USA*.

Rubin, S. (1975). Improved component-mode representation for structural dynamic analysis. *AIAA Journal 13*(8), 995–1006.

Saad, Y. (1996). *Iterative Methods for Sparse Linear Systems*. PWS Publishing Company.

Seshu, P. (1997). Review: Substructuring and component mode synthesis. *The Shock and Vibration Digest 4*(3), 199–210.

Sestieri, A. and W. D'Ambrogio (1989). WHY BE MODAL: How to avoid the use of modes in the modification of vibrating systems. *The International Journal of Analytical and Experimental Modal Analysis 4*(1), 25–30.

Sidhu, J. and D. J. Ewins (1984). Correlation of finite element and modal testing studies of a practical structure. In *2nd International Modal Analysis Conference, Orlando, USA*.

Szabó, I. (1956). *Einführung in die Technische Mechanik*. Springer Verlag, Berlin, Heidelberg, New York, Tokyo.

Targoff, W. P. (1976). Othogonality check and correction of measured modes. *AIAA Journal 14*(2), 164–167.

Thomson, W. T. (1950). *Mechanical Vibration*. Allen & Unwin.

URANUS (1994, May). Development of techniques integrating test and analysis for an improved dynamic design. Project Proposal, BRITE-EURAM BRE2-CT94-0946.

Visser, W. J. (1992). *Updating Structural Dynamics Models Using Frequency Response Data*. Ph. D. thesis, Imperial College of Science, Technology & Medicine, Department of Mechanical Engineering, London, UK.

Visser, W. J. and M. Imregun (1991). A technique to update finite element models using frequency response data. In *9th International Modal Analysis Conference, Florence, Italy*.

Yang, M. M. and D. L. Brown (1997). SVD/QR based model error indicator function. In *15th International Modal Analysis Conference, Orlando, USA*.

Zhang, Q., G. Lallement, R. Fillod and J. Piranda (1987). A complete procedure for the adjustment of a mathematical model from the identified complex modes. In *5th International Modal Analysis Conference, London, England*.

Ziaei Rad, S. (1997). *Methods for Updating Numerical Models in Structural Dynamics*. Ph. D. thesis, Imperial College of Science, Technology & Medicine, Department of Mechanical Engineering, London, UK.

Ziaei-Rad, S. and M. Imregun (1996). On the accuracy required of experimental data for finite element model updating. *Journal of Sound and Vibration 196*(3), 323–336.

Zienkiewicz, O. C. (1967). *The Finite Element Method*. McGraw Hill.

Appendix A

Mathematical Derivations and Proofs

A.1 Attachment Modes for Singular Stiffness Matrices

When component k is unrestrained and a free-interface CMS method is to be employed, the definition of the attachment modes in equation (3.15) (p. 53) becomes obsolete since the stiffness matrix is singular. As was demonstrated by Hintz (1975), the original static response is then replaced by the response of a uniformly accelerating system in the direction of the rigid-body DOFs. The resulting modes are then also defined as *inertia-relief modes*.

Consistent with the definition of attachment modes in equation (3.15) (p. 53), the inertia-relief modes can be derived from the full equation of motion,

$$[M]\,[\ddot{x}] + [K]\,[x] = [F] \tag{A.1}$$

where $[F]$ is the force matrix with unit entries at the junction DOFs, as defined before. To extract the forces the component experiences during rigid-body motion, the rigid-body displacement $[x_r] = [\Phi_r]\,[q_r]$ is induced as:

$$[\Phi_r]^T\,[M]\,[\Phi_r]\,[\ddot{q}_r] + [\Phi_r]^T\,[K]\,[\Phi_r]\,[q_r] = [\Phi_r]^T\,[F] \tag{A.2}$$

and because $[K]\,\{x_r\} = 0$, the corresponding acceleration is obtained:

$$[\ddot{x_r}] = [\Phi_r]\left([\Phi_r]^T\,[M]\,[\Phi_r]\right)^{-1}[\Phi_r]^T\,[F] \tag{A.3}$$

which is further simplified to,

$$[\ddot{x_r}] = [\Phi_r]\,[\Phi_r]^T\,[F] \tag{A.4}$$

since $[\Phi_r]$ denotes the mass-normalised rigid-body modes. Thus, the imposed forces due to uniform acceleration in the rigid-body DOFs can be expressed as,

$$\begin{aligned}[F_r] &= [M]\,[\ddot{x_r}] \\ [F_r] &= [M]\,[\Phi_r]\,[\Phi_r]^T\,[F]\end{aligned} \tag{A.5}$$

The unrestrained structure is externally excited with $[F]$, as can be seen in equation (A.1), and it implicitly experiences inertia forces due to the presence of r rigid-body DOFs. To have access to the elastic forces acting upon the structure only, one can write:

$$[F_e] = [F] - [F_r] \tag{A.6}$$

which has been shown to be,

$$[F_e] = \left([I] - [M]\,[\Phi_r]\,[\Phi_r]^T \right) [F] \tag{A.7}$$

$$[F_e] = [P]\,[F] \tag{A.8}$$

where $[P]$ designates the inertia-relief loading matrix (Hintz 1975) and is simply an identity matrix when there are no rigid-body modes. The elastic forces derived are conveniently envisaged as the forces at the junction DOFs equilibrated from the inertia-forces induced by rigid-body acceleration.

In approaching the more general definition of *attachment modes*, it is useful to define the flexibility matrix of the unrestrained system as:

$$[G] = \begin{bmatrix} [\tilde{K}]^{-1}_{(N-r)\times(N-r)} & [0]_{(N-r)\times(r)} \\ [0]_{(r)\times(N-r)} & [0]_{(r)\times(r)} \end{bmatrix}_{N\times N} \tag{A.9}$$

where the singular stiffness system matrix $[K]$ has been constrained at r DOFs to remove rigid-body motion and $[\tilde{K}]^{-1}$ is its corresponding flexibility matrix. The flexibility matrix $[G]$ is therefore expanded with zeros at r DOFs to all N DOFs of the FE model. Hence, the singularity of $[K]$ and $[G]$ is the same and both matrices are of rank $(N - r)$.

Upon applying the elastic forces onto the static flexibility matrix $[G]$ the corresponding deflection of the constraint component is:

$$\left[\hat{\Phi}\right] = \left[G\right]\left[F_e\right] \tag{A.10}$$

Since it is of interest to find elastic attachment modes $[\Phi^a]$ and elastic modes are orthogonal to all r rigid-body modes, i.e.:

$$[\Phi_r]^T\,[M]\,[\Phi^a] = [0] \tag{A.11}$$

and the contribution of the constraint component of r rigid-body modes can be removed from $\left[\hat{\Phi}\right]$ by:

$$\left[\Phi^a\right] = \left[\hat{\Phi}\right] - \left[\Phi_r\right]\,[q_r] \tag{A.12}$$

then the attachment modes are found by pre-multiplying equation (A.12) with $\left[\Phi_r\right]^T\,[M]$ and solving for the generalised coordinates $[q_r]$ of the rigid-body modes from:

$$\left[\Phi_r\right]^T\,[M]\,\left[\Phi^a\right] = \left[\Phi_r\right]^T\,[M]\,\left[\hat{\Phi}\right] - \left[\Phi_r\right]^T\,[M]\,\left[\Phi_r\right]\,[q_r] \tag{A.13}$$

which resolves simply to:

$$[q_r] = \left(\left[\Phi_r\right]^T\,[M]\,\left[\Phi_r\right]\right)^{-1}\left[\Phi_r\right]^T\,[M]\,\left[\hat{\Phi}\right] \tag{A.14}$$

Substituting equation (A.14) into equation (A.12) leads therefore to:

$$\left[\Phi^a\right] = \left([I] - \left[\Phi_r\right]\left(\left[\Phi_r\right]^T\,[M]\,\left[\Phi_r\right]\right)^{-1}\left[\Phi_r\right]^T\,[M]\right)\left[\hat{\Phi}\right] \tag{A.15}$$

$$\left[\Phi^a\right] = \left([I] - \left[\Phi_r\right]\left[\Phi_r\right]^T\,[M]\right)\left[\hat{\Phi}\right] \tag{A.16}$$

which are the flexible attachment modes as a linear combination of the columns of the constraint deflections.

Close inspection of equations (A.8) and (A.12), however, reveals that equation (A.16) is also:

$$\left[\Phi^a\right] = \left[P\right]^T \left[\hat{\Phi}\right] \tag{A.17}$$

$$\left[\Phi^a\right] = \left[P\right]^T \left[G\right] \left[F_e\right] \tag{A.18}$$

$$\left[\Phi^a\right] = \left[P\right]^T \left[G\right] \left[P\right] \left[F_j\right] \tag{A.19}$$

or

$$\left[\Phi^a\right] = \left[G^e\right] \left[F_j\right] \tag{A.20}$$

which may be summarised in the same fashion as in equation (3.18) (p. 53) for the attachment modes of a constrained component as follows,

$$\begin{bmatrix} \begin{bmatrix} \Phi_j^a \end{bmatrix} \\ \begin{bmatrix} \Phi_i^a \end{bmatrix} \end{bmatrix} = \begin{bmatrix} \begin{bmatrix} G_{jj}^e \end{bmatrix} & \begin{bmatrix} G_{ji}^e \end{bmatrix} \\ \begin{bmatrix} G_{ij}^e \end{bmatrix} & \begin{bmatrix} G_{ii}^e \end{bmatrix} \end{bmatrix} \begin{bmatrix} \begin{bmatrix} I \end{bmatrix} \\ \begin{bmatrix} 0 \end{bmatrix} \end{bmatrix} \tag{A.21}$$

$$\left[\Phi^a\right] = \begin{bmatrix} \begin{bmatrix} G_{jj}^e \end{bmatrix} \\ \begin{bmatrix} G_{ij}^e \end{bmatrix} \end{bmatrix} \tag{A.22}$$

where $[G^e]$ will be referred to as the elastic flexibility matrix. Therefore, in order to gain access to the flexibility matrix $[G]$, artificial boundary conditions have been imposed on the stiffness matrix $[K]$ and these have, in effect, been eliminated with the transformation (or projection) matrix $[P]$ leading to $[G^e]$.

In both cases where the component has rigid-body DOFs and is rigidly constrained, the attachment modes are columns of the flexibility matrix of the component. In fact, the flexibility terms for the constrained case is obtained directly from the inverse of the stiffness matrix. For the unconstrained case, the flexibility terms have been derived under inertia loading effects leading to the elastic flexibility matrix $[G^e]$, which serves as the inverse of the singular stiffness matrix. It should be noted that $[G^e]$ is still singular.

The treatment of generally damped systems in conjunction with free-interface CMS methods lead to the inclusion of present damping forces and is presented in references (Rubin 1975). The treatment of non-proportionally damped systems, however, will not be discussed here.

Numerical Illustration of Attachment Modes

Throughout the literature review of CMS methods, it has been found beneficial to accompany the formulated concepts of elastic forces, rigid-body forces etc. and flexibility terms involved by small numerical examples. These were helpful to crystallise the meaning of each term but the numerical illustrations were also a safeguard to ensure that the end results remained unchanged for whatever coordinates were fixed to obtain a statically determined stiffness matrix.

In figure (A.1), a simple lumped spring-mass system is shown and it is assumed that a free interface method is used to analyse this component. To the left of the component,

an adjacent sub-structure is indicated and coordinate x_1 assumes the role of the junction DOF. Since none of the coordinates in this example is grounded, the system is statically indeterminate.

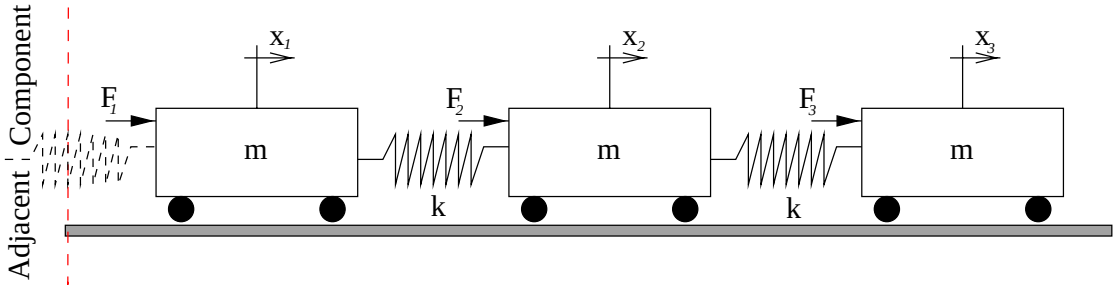

Figure A.1: A simple 3 DOFs lumped mass-spring system with DOF x_1 attached to adjacent component ($x_1 \Longrightarrow$ JDOF)

To gain access to the attachment modes, simple inversion of the stiffness matrix is not possible and the system must be analysed by applying inertia-forces induced by rigid-body motion, as has been shown in the previous section. It is these steps that will be the matter of attention in the following.

The equation of motion of the component in figure (A.1) for a free-interface method comprises,

$$[F]^T = \begin{Bmatrix} 1 & 0 & 0 \end{Bmatrix} \quad [M] = \begin{bmatrix} m & 0 & 0 \\ 0 & m & 0 \\ 0 & 0 & m \end{bmatrix} \quad [K] = \begin{bmatrix} k & -k & 0 \\ -k & 2k & -k \\ 0 & -k & k \end{bmatrix}$$

and a harmonic solution gives for $m = 1kg$ and $k = 1000\frac{N}{m}$,

$$\left[\lambda\right] = \begin{bmatrix} 0 & 0 & 0 \\ 0 & 31.6 & 0 \\ 0 & 0 & 54.8 \end{bmatrix} rad/s \quad [\Phi] = \begin{bmatrix} +0.577 & -0.707 & -0.408 \\ +0.577 & \pm 0.000 & +0.817 \\ +0.577 & +0.707 & -0.408 \end{bmatrix}$$

and the intermediate forces result in,

$$\begin{aligned} [\ddot{x_r}]^T &= \begin{Bmatrix} 0.333 & 0.333 & 0.333 \end{Bmatrix} \\ [F_r]^T &= \begin{Bmatrix} 0.333 & 0.333 & 0.333 \end{Bmatrix} \\ [F_e]^T &= \begin{Bmatrix} 0.667 & -0.333 & -0.333 \end{Bmatrix} \end{aligned}$$

By constraining coordinate x_1,

$$[G] = \begin{bmatrix} 0 & 0 & 0 \\ 0 & 1.00 & 1.00 \\ 0 & 1.00 & 2.00 \end{bmatrix} \quad [\hat{\Phi}]^T = \begin{Bmatrix} 0.00 & -0.667 & -1.00 \end{Bmatrix} \quad [\Phi^a] = \begin{Bmatrix} 0.556 & -0.111 & -0.444 \end{Bmatrix}$$

constraining coordinate x_2 gives,

$$[G] = \begin{bmatrix} 1.00 & 0 & 0.00 \\ 0 & 0 & 0 \\ 0.00 & 0 & 1.00 \end{bmatrix} \quad [\hat{\Phi}]^T = \begin{Bmatrix} 0.667 & 0.00 & -0.333 \end{Bmatrix} \quad [\Phi^a] = \begin{Bmatrix} 0.556 & -0.111 & -0.444 \end{Bmatrix}$$

and finally, by construing coordinate x_3, the attachment modes are,

$$[G] = \begin{bmatrix} 2.00 & 1.00 & 0 \\ 1.00 & 1.00 & 0 \\ 0 & 0 & 0 \end{bmatrix} \quad [\hat{\Phi}]^T = \begin{Bmatrix} 1.00 & 0.333 & 0.00 \end{Bmatrix} \quad [\Phi^a] = \begin{Bmatrix} 0.556 & -0.111 & -0.444 \end{Bmatrix}$$

The sizes of the force matrices are seen to be of one column only as just one coordinate is presenting a junction DOF (note $[F] \rightarrow \{F\}$). This is generally not the case. The harmonic solution of the unconstrained components rightly computes to one rigid-body mode and two elastic modes. Since the derivation of the free interface method has not indicated which coordinates must be grounded to allow an inversion of the system stiffness matrix, all three coordinates have been fixed at any one time. This has led to three different flexibility matrices expanded to the full system size by inserting zero rows and columns. It is interesting to note the changes it introduced to the constraint deflection modes $[\hat{\Phi}]$ but that it still correctly exhibits a zero displacement entry at the constraint coordinate. By filtering these, however, the elastic modes, i.e. the attachment modes, are the same for each case. This proves numerically the ability of the filtering mechanism of $[P]$ and also indicates, with non-zero entries at all coordinate, that the rigid-body constraints have successfully been removed.

A.2 Transformation Matrix for Force Coupling

Section 3.5.4 reports on a free-interface CMS method using a force coupling procedure. Such an approach is advantageous for some practical applications as the junction DOFs are made redundant and only a small number of physical coordinates are retained in the condensed FE model. It was stressed, however, that the assembly of the transformation matrix must be handled with care. The number of retained DOFs, i.e. the MDOFs, and number of boundaries N_b (as defined by figure 3.1, p. 48) must be known in advance and determine the format of the transformation matrix.

To give a simulated example of the procedure, the component force vector (eqn. (3.47), p. 59) needs to be divided into N_b sub-vectors:

$$\left\{F_j^k\right\}^T = \left\{ \left\{{}_1F_j^k\right\}^T \left\{{}_2F_j^k\right\}^T \left\{{}_3F_j^k\right\}^T \cdots \left\{{}_{N_b}F_j^k\right\}^T \right\}$$

Now, let us assume that there are $N_s = 5$ sub-structures and that we want to compute the transformation matrix for sub-structure $k = 1$. After an identification procedure, two sections of junction DOFs are found at which the number of interacting components is the same. Boundary $l = 1$ joints sub-structures $k = 1$ and $k = 2$, and boundary $l = 2$ couples sub-structures $k = 1$, $k = 2$ and $k = 3$. Sub-structures $k = 4$ and $k = 5$ are not interacting with either of the boundaries.

Therefore, the first sub-matrix of the overall transformation at boundary $l = 1$ is found:

$$\left\{{}_1F_j^1\right\} = \left[T_{jj}^1\right]^{-1} \left[\left[\kappa \left[T_{jj}^1\right]^{-1} \left[T_{jm}^1\right] - \left[T_{jm}^1\right] \right] \left[\kappa \left[T_{jj}^2\right]^{-1} \left[T_{jm}^2\right] \right] \left[0\right] \left[0\right] \left[0\right] \right] \left\{ \begin{Bmatrix} \{x_m^1\} \\ \{x_m^2\} \\ \{x_m^3\} \\ \{x_m^4\} \\ \{x_m^5\} \end{Bmatrix} \right\}$$

where

$$\kappa = \left[\sum_i \left[T_{jj}^i\right]^{-1} \right]^{-1} \qquad i = 1, 2$$

The second sub-matrix identifies the forces at boundary $l = 2$ as:

$$\left\{{}_2F_j^1\right\} = \left[T_{jj}^2\right]^{-1} \left[\left[\kappa \left[T_{jj}^1\right]^{-1} \left[T_{jm}^1\right] - \left[T_{jm}^1\right] \right] \left[\kappa \left[T_{jj}^2\right]^{-1} \left[T_{jm}^2\right] \right] \left[\kappa \left[T_{jj}^3\right]^{-1} \left[T_{jm}^3\right] \right] \left[0\right] \left[0\right] \right] \left\{ \begin{Bmatrix} \{x_m^1\} \\ \{x_m^2\} \\ \{x_m^3\} \\ \{x_m^4\} \\ \{x_m^5\} \end{Bmatrix} \right\}$$

where

$$\kappa = \left[\sum_i \left[T_{jj}^i\right]^{-1} \right]^{-1} \qquad i = 1, 2, 3$$

As a result, therefore, the complete force vector defined at junction DOFs is found from:

$$\left\{F_j^1\right\} = \left\{ \begin{Bmatrix} \{{}_1F_j^1\} \\ \{{}_2F_j^1\} \end{Bmatrix} \right\}$$

which is equivalent to junction force vector shown in equation (3.47) (p. 59) for $k = 1$.

A.3 Definition of Left and Right Eigenvectors

Left and right eigenvectors can both be derived from the standard form of *Eigensystems* (Press et al. 1992) or *Eigenvalue Problems* (Golub and van Loan 1996) which is stated as:

$$\big[A\big]\big\{\psi\big\}_r = \lambda_r\big\{\psi\big\}_r \tag{A.23}$$

where $[A]$ is of dimension $N \times N$ and represents the eigensystem.

Rearranging equation (A.23) to,

$$\Big[\big[A\big] - \lambda_r\Big[\diagdown I \diagdown\Big]\Big]\big\{\psi\big\}_r = \big\{0\big\} \tag{A.24}$$

then the eigenvalues of system $[A]$ are the roots of the N degree polynomial obtained from the determinant:

$$\det\Big|\big[A\big] - \lambda_r\Big[\diagdown I \diagdown\Big]\Big| = 0 \tag{A.25}$$

There are N, not necessarily *distinct*, eigenvalues. Eigensystems with multiple roots are referred to as *degenerate*. The right eigenvectors are defined as the non-zero vectors $\{\psi\}_r$ that satisfy together with the eigenvalues:

$$\big[A\big]\big\{\psi\big\}_r = \lambda_r\big\{\psi\big\}_r \qquad \textbf{Right Eigenvectors} \tag{A.26}$$

and the left eigenvectors are the non-zero vectors $\{\psi\}_r$ that satisfy together with the eigenvalues:

$$\big\{\psi\big\}_r^T\big[A\big] = \lambda_r\big\{\psi\big\}_r^T \qquad \textbf{Left Eigenvectors} \tag{A.27}$$

Taking the transpose of equation (A.27), one can see that the left eigenvector, r, is the transpose of the right eigenvector of the transpose of $[A]$ (Press et al. 1992). That is to say, the right and left eigenvectors, denoted $\{\psi^R\}_r$ and $\{\psi^L\}_r$ might as well be defined as:

$$\big[A\big]\big\{\psi^R\big\}_r = \lambda_r\big\{\psi^R\big\}_r \quad \text{and} \quad \big[A\big]^T\big\{\psi^L\big\}_r = \lambda_r\big\{\psi^L\big\}_r \tag{A.28}$$

Since the determinant of a matrix equals the determinant of its transpose, the definitions of the right and left eigenvectors shows that the **left and right eigenvalues** are **identical**. Also, the definition of the right eigenvector (A.26) and the formal definition of the standard eigenvalue problem in equation (A.23) coincide and therefore, "eigenvector" means "right eigenvector", unless otherwise stated.

By combining both equations in (A.28) to a matrix identity, it can be shown (Press et al. 1992) that the operation,

$$\big[\Psi^L\big]^T\big[\Psi^R\big] = \Big[\diagdown\big[\Psi^L\big]^T\big[\Psi^R\big]\diagdown\Big] \tag{A.29}$$

leads to a diagonal matrix. Hence, each left eigenvector is *orthogonal* to all right eigenvectors except its corresponding one. If corresponding eigenvectors are normalised in such a way that their dot product is unity, then:

$$\big[\Phi^L\big]^T\big[\Phi^R\big] = \Big[\diagdown I \diagdown\Big] \tag{A.30}$$

Hence, the inverse of the right eigenvector matrix $[\Phi^R]$ is the transpose of the left eigenvector matrix $[\Phi^L]$, and vice versa. The same relationship holds even for most degenerate systems.

Concluding the inverse relationship of left and right eigenvectors, it is apparent from (A.28) that if system matrix $[A]$ is symmetric, i.e. $[A] = [A]^T$ or $[A] = [A]^H$, $[\Phi^L]$ and $[\Phi^R]$ are identical. Therefore, the transpose of the eigenvector matrix is its inverse and the eigenvectors are orthogonal among themselves.

Left and Right Eigenvectors in Structural Dynamics

The computational analysis of structural dynamics problems usually involves the discretisation of the domain and expressing the so-called structural eigenproblem (Friswell and Mottershead 1995) using the mass and stiffness matrices $[M]$ and $[K]$ such that:

$$\big[K\big]\,\{\psi\}_r = \lambda_r \big[M\big]\,\{\psi\}_r \tag{A.31}$$

where the eigenvalue $\lambda_r = \omega_r^2$ and equation (A.31) represents a generalised eigenvalue problem (Press et al. 1992). As it is only intended to demonstrate the relevance of the left and right eigenvectors in relation to structural dynamic problems, no damping has been included for the sake of simplicity. Equation (A.31) may be solved for the system's eigenvalues and eigenvectors by transforming it to a standard eigenvalue problem, as defined by (A.23), so that:

$$\Big[\big[M\big]^{-1}\big[K\big]\Big]\,\{\psi\}_r = \lambda_r\,\{\psi\}_r \tag{A.32}$$

It should be noted that from a computational point of view, the structural eigenproblem may equivalently be solved by employing the Cholesky decomposition:

$$[M] = [L][L]^T \quad \big([L]^{-1}[K][L]^{-T}\big)\,\big\{\bar{\psi}\big\}_r = \lambda_r\,\big\{\bar{\psi}\big\}_r \quad \big\{\bar{\psi}\big\}_r = [L]^T\,\{\psi\}_r \tag{A.33}$$

where $[L]$ is a lower triangular matrix and the eigensolution is obtained from a symmetric standard eigenvalue problem although the resulting eigenvectors $[\bar{\psi}]$ are not the system's eigenvectors. These are only obtained by a transformation of the form $[L]^{-T}\,\big\{\bar{\psi}\big\}_r$.

In general, the stiffness matrix $\big[K\big]$ and mass matrix $\big[M\big]$ are symmetric. The system matrix $[A] = \big[M\big]^{-1}\big[K\big]$, however, is generally not. Because matrix $[A]$ is not symmetric,

$$\big[\Phi^R\big]^T \neq \big[\Phi^L\big] \tag{A.34}$$

in structural dynamics problems. However, the well known orthogonality conditions of mass-normalised eigenvectors can be stated as (Ewins 1984),

$$\big[\Phi^R\big]^T\big[M\big]\big[\Phi^R\big] = \Big[\diagdown I \diagdown\Big] \quad \text{and} \quad \big[\Phi^R\big]^T\big[K\big]\big[\Phi^R\big] = \Big[\diagdown \lambda_r \diagdown\Big] \tag{A.35}$$

from which it can easily be deduced that,

$$\big[\Phi^L\big]^T = \big[\Phi^R\big]^T\big[M\big] \tag{A.36}$$

$$= \Big[\diagdown \lambda_r \diagdown\Big]^{-1}\big[\Phi^R\big]^T\big[K\big] \tag{A.37}$$

Therefore, the left eigenvectors do not need to be specifically computed from equation (A.27). They are simply obtained by pre-multiplying the computed (right) eigenvectors with the mass matrix.

A.4 Eigenvector Derivatives

The identification of appropriate updating parameters is crucial to the success of any model updating technique employed. In chapter 5 numerical selection procedures are discussed and it is argued that sensitivity-based error location procedures are to date the only realistic means to identify erroneous finite elements in large FE models. Sensitivity-based error location procedures and model updating algorithms in general, however, are unable to find and adjust such elements if they are insensitive.

Although many finite element properties are fairly well known, the modelling of boundary conditions using lumped spring-mass-damper representations is often associated with a high level of uncertainty. To identify reasonably sensitive boundary elements, the second-order derivative of the eigenvalues may be used to find these.

The first order derivative of the eigenvalues was derived in Section 5.2.1 and it was shown in Section 5.4 that the second order derivative of the eigenvalues requires the first order eigenvector derivatives.

A complete derivation of these was presented by Fox and Kapoor (1968) and will be outlined below.

For an undamped equation of motion, one obtains,

$$\left([K]-\lambda_r[M]\right)\frac{\partial\{\phi\}_r}{\partial\varphi_i}+\left(\frac{\partial[K]}{\partial\varphi_i}-\lambda_r\frac{\partial[M]}{\partial\varphi_i}-\frac{\partial\lambda_r}{\partial\varphi_i}[M]\right)\{\phi\}_r=\{0\} \tag{A.38}$$

which includes the eigenvector and eigenvalue sensitivities of mode r with respect to a selected design parameter, φ_i. Unlike the eigenvalue sensitivity in section 5.2.1, equation (A.38) cannot be directly solved for the eigenvector sensitivity as $([K]-\lambda_r[M])$ is singular. Fox and Kapoor (1968) proposed therefore to assume that,

$$\frac{\partial\{\phi\}_r}{\partial\varphi_i}=\sum_{j=1}^{N}\kappa_{rj}^{i}\{\phi\}_r \tag{A.39}$$

i.e. the eigenvector derivative is a linear combination of the eigenvectors itself. Although this assumption is reasonable, the number of available modes is often limited and N is usually smaller, namely m, and therefore, the number of included modes m directly affects the accuracy of the eigenvector sensitivities.

The coefficients κ were shown to be:

$$\kappa_{rj}^{i}=\frac{\{\phi\}_j^T\left(\frac{\partial[K]}{\partial\varphi_i}-\lambda_r\frac{\partial[M]}{\partial\varphi_i}\right)\{\phi\}_r}{\lambda_r-\lambda_j}\quad\text{for}\quad r\neq j \tag{A.40}$$

and

$$\kappa_{rj}^{i}=-\frac{1}{2}\{\phi\}_j^T\frac{\partial[M]}{\partial\varphi_i}\{\phi\}_r\quad\text{for}\quad r=j \tag{A.41}$$

where it is seen that a distinction is made between mode j and mode r and that the computational effort of the eigenvector sensitivities exceeds that required for the eigenvalue sensitivities.

Appendix B

MATLAB m-files

B.1 Shape-Correlation Coefficient χ_s and $\frac{\partial \chi_s}{\partial \varphi}$

```
function [f,df]=chi_s(Fa,Fx,dFa,swtch)
%
%     [f,df]=chi_s(Fa,Fx,dFa,swtch)
%
%     Shape Correlation Coefficient   [chi_s]
%                  and/or
%             its derivative          [d(chi_s)/dp]
%
% NOTE: 0 < chi_s < 1
%
% IN:
% Fa,Fx     => LINEAR FRF predictions and measurements
% dFa       => LINEAR FRF sensitivities of predictions
%              (may be set empty if swtch(2)==1)
% Fa,Fx,dFa => all the same size
%              ([rows=frequencies; columns=coordinates])
% swtch(1)  => ==1, LINEAR correlation coefficient and sensitivitiy (f,df)
%              ==0, LOGARITHMIC correlation coefficient and sensitivitiy (f,df)
% swtch(2)  => ==1, to compute f  only
% swtch(2)  => ==2, to compute df only
% swtch(2)  => ==3, to compute f and df
%
% OUT:
% f         => Correlation Coefficient [chi_s]
% df        => Sensitivity [d(chi_s)/d(p)]
f=[];
df=[];
% CHECK Input Arguments
%
if     nargin<3
  return
elseif nargin==3
  swtch=[1 3];        % Defaults to LINEAR sensitivities
                      % and computing f and df
  if size(Fx,2)~=size(Fa,2) & size(Fx,2)~=size(dFa,2)
    error('Input Arguments are not of same size !')
  end
elseif nargin==4
  if length(swtch)<=2
    if swtch(2)==3 | swtch(2)==2
       if size(Fx,2)~=size(Fa,2) | size(Fx,2)~=size(dFa,2)
          error('Input Arguments are not of same size !')
       end
    elseif swtch(2)==1
       if size(Fx,2)~=size(Fa,2)
          error('Input Arguments are not of same size !')
       end
       dFa=[]; % not needed
    else
       error('Unknown entry in swtch')
    end
  else
    error('Control flag swtch requires 2 elements')
  end
```

```
end
[m,n]= size(Fa);
if swtch(2)==1 | swtch(2)==3
    f    = zeros(m,1);
end
if swtch(2)==2 | swtch(2)==3
    df   = zeros(m,1);
end

% SET  Logarithmic
%
if ~swtch(1)         % LOGARITHMIC responses and
                     % response sensitivities
  if swtch(2)==2 | swtch(2)==3
    dFa=20/log(10) * ((real(Fa).*real(dFa) + imag(Fa).*imag(dFa))./...
                             (real(Fa).^2 + imag(Fa).^2)) ;
  end
  Fa = dB(Fa); Fx = dB(Fx);
end

% COMPUTE sensitivities (df) and correlation function (f)
%
if (isreal(Fa) & isreal(Fx))
   for nf=1:m
     a  = Fa(nf,:).'; x  = Fx(nf,:).';
     xa = x'*a;       xx = x'*x;       aa= a'*a;
     if swtch(2)==1 | swtch(2)==3            % correlation coefficient from
      f(nf) = (xa)^2/(xx*aa);                % REAL responses
     end
     if swtch(2)==2 | swtch(2)==3            % sensitivities from
      da= dFa(nf,:).';                       % REAL responses
      xda= x'*da;      ada= a'*da;
      df(nf)= 2*(xa*xda/(xx*aa)-xa^2*ada/(xx*aa^2));
     end
   end
else
   for nf=1:m
     a = Fa(nf,:).'; x = Fx(nf,:).';
     aa= a'*a;       xx= x'*x;       xa= x'*a;
     if swtch(2)==1 | swtch(2)==3            % correlation coefficient from
      f(nf) = abs(xa)^2/(xx*aa);             % COMPLEX responses
     end
     if swtch(2)==2 | swtch(2)==3            % sensitivities from
      da= dFa(nf,:).';                       % COMPLEX responses
      df(nf)=2/(xx*aa)*( real(xa)*( real(x')*real(da)-imag(x')*imag(da) )...
                        +imag(xa)*( real(x')*imag(da)+imag(x')*real(da) )...
                  +abs(xa)^2/(aa)*( imag(a')*imag(da)-real(a')*real(da) ) );
     end
   end
end
% Swap output arguments
%
if nargout==1 & swtch(2)==2
  tmp=df; df=f; f=tmp;
end
return
```

B.2 Amplitude-Correlation Coefficient χ_a and $\frac{\partial \chi_a}{\partial \varphi}$

```
function [f,df]=chi_a(Fa,Fx,dFa,swtch)
%
%   [f,df]=chi_a(Fa,Fx,dFa,swtch)
%
%   Amplitude Correlation Coefficient [chi_a]
%                and/or
%            its derivative           [d(chi_a)/dp]
%
% NOTE: 0 < chi_a < 1
%
% IN:
% Fa,Fx     => LINEAR FRF predictions and measurements
% dFa       => LINEAR FRF sensitivities of predictions
%              (may be set empty if swtch(2)==1)
% Fa,Fx,dFa => all the same size
%              ([rows=frequencies; columns=coordinates])
% swtch(1)  => ==1, LINEAR correlation coefficient and sensitivitiy (f,df)
%              ==0, LOGARITHMIC correlation coefficient and sensitivitiy (f,df)
% swtch(2)  => ==1, to compute f  only
% swtch(2)  => ==2, to compute df only
% swtch(2)  => ==3, to compute f and df
%
% OUT:
% f         => Correlation Coefficient [chi_a]
% df        => Sensitivity [d(chi_a)/d(p)]
f=[];
df=[];
% CHECK Input Arguments
%
if     nargin<3
  return
elseif nargin==3
  swtch=[1 3];        % Defaults to LINEAR sensitivities
                      % and computing f and df
  if size(Fx,2)~=size(Fa,2) & size(Fx,2)~=size(dFa,2)
    error('Input Arguments are not of same size !')
  end
elseif nargin==4
  if length(swtch)<=2
    if swtch(2)==3 | swtch(2)==2
       if size(Fx,2)~=size(Fa,2) | size(Fx,2)~=size(dFa,2)
          error('Input Arguments are not of same size !')
       end
    elseif swtch(2)==1
       if size(Fx,2)~=size(Fa,2)
          error('Input Arguments are not of same size !')
       end
       dFa=[]; % not needed
    else
       error('Unknown entry in swtch')
    end
  else
    error('Control flag swtch requires 2 elements')
  end
end
[m,n]= size(Fa);
if swtch(2)==1 | swtch(2)==3
    f    = zeros(m,1);
end
if swtch(2)==2 | swtch(2)==3
    df   = zeros(m,1);
end

% SET  Logarithmic
%
if ~swtch(1)         % LOGARITHMIC responses and
                     % response sensitivities
  if swtch(2)==2 | swtch(2)==3
    dFa=20/log(10) * ((real(Fa).*real(dFa) + imag(Fa).*imag(dFa))./...
                                (real(Fa).^2 + imag(Fa).^2)) ;
  end
  Fa = dB(Fa); Fx = dB(Fx);
end

% COMPUTE sensitivities (df) and correlation function (f)
%
if (isreal(Fa) & isreal(Fx))
```

```
   for nf=1:m
     a  = Fa(nf,:).'; x  = Fx(nf,:).';
     xa = x'*a;       xx = x'*x;       aa= a'*a;
     if swtch(2)==1 | swtch(2)==3            % correlation coefficient from
      f(nf) = 2*abs(xa)/(xx+aa);             % REAL responses
     end
     if swtch(2)==2 | swtch(2)==3            % sensitivities from
      da= dFa(nf,:).';                       % REAL responses
      xda= x'*da;      ada= a'*da;
      df(nf)= 2*abs(xa)*( xda/((xx+aa)*xa) - 2*ada/(xx+aa)^2 );
     end
   end
else
   for nf=1:m
     a = Fa(nf,:).'; x = Fx(nf,:).';
     aa= a'*a;       xx= x'*x;       xa= x'*a;
     if swtch(2)==1 | swtch(2)==3            % correlation coefficient from
      f(nf) = 2*abs(xa)/(xx+aa);             % COMPLEX responses
     end
     if swtch(2)==2 | swtch(2)==3            % sensitivities from
      da= dFa(nf,:).';                       % COMPLEX responses
      df(nf)=2/( abs(xa)*(xx+aa) )*(...
                          real(xa)*( real(x')*real(da)-imag(x')*imag(da) )...
                         +imag(xa)*( real(x')*imag(da)+imag(x')*real(da) )...
              +2*abs(xa)^2/(xx+aa)*( imag(a')*imag(da)-real(a')*real(da) ) );
     end
   end
end

% Swap output arguments
%
if nargout==1 & swtch(2)==2
  tmp=df; df=f; f=tmp;
end
return
```

B.3 Structurally Damped Response $H(\eta)$ and $\frac{\partial H(\eta)}{\partial \eta}$

```
function [freq,frf,Dfrf]=hyst_frf(D,Y,er,eta,lf,df,uf,r)
%
%
%   [freq,frf,Dfrf] = hyst_frf(D,Y,er,eta,lf,df,uf,r)
%
%   Structurally damped frequency response function and its derivative
%   w.r.t. modal damping factor 'eta(r)'. The derivative is optional
%   and is computed if 3rd output argument is given and mode number 'r'
%   be found in input argument list.
%
%   NOTE: both 'frf' and 'Dfrf' are COMPLEX !
%
%
%
% D     -  [m*1] vector of eigenfrequencies in [Hz]
% Y     -  [N*m] matrix of m mode shapes (mass-normalised)
%                defined at N co-ordinates
% eta   -  [m*1] vector of structural damping factors
% er    -  [n*2] matrix of excitation and response coordinates
%                (must be just 1 row if length(r)>1)
% r     -  [a*1] vector of mode numbers of which derivative is sought
%                (must be just 1 element is size(er,1)>1)
%
% lf    -  lowest frequency point, i.e. f1
% df    -  frequency increment, i.e. f2-f1....
% uf    -  highest frequency point, i.e. fNf
%
% freq  -  excitation frequencies, freq=f(lf,df,uf)
% frf   -  frequency response function, alpha(ii,jj)
% Dfrf  -  *if size(er,1)==1 sensitivities of frf wrt to each modal damping
%                           eta(r), thus its size == [Nf,Nm]
%          *if length(r)==1  sensitivities of frfs wrt to modal damping
%                           factor eta(r), thus its size == [Nf,n]
%
%
%
% Check dimensions of modal data
%
if length(eta)~=size(Y,2) | length(eta)~=length(D)
  error('Inconsistent dimensions of modal data.... !')
end
if max(r)>length(eta)
  error('Specified mode number(s) ''r'' exceed available modes.... !')
end
if size(er,1)>1 & length(r)>1
  error('size of ''er'' and ''r'' are incompatible....!')
end
% Get constants
%
m    = length(D);     n    = size(er,1);
% Set preliminary variables
%
D    = D(:);          freq = [lf:df:uf]';
Nf   = length(freq);
frf  = zeros(Nf,n);   Dfrf = zeros(Nf,n);
eta = eta(:);
wr   = (2*pi*D);      wr2  = (wr).^2;
w    = (2*pi*freq);   w2   = (w).^2;
%  Compute FRF (frf)
%
for kk=1:n
ii=er(kk,2); jj=er(kk,1);
  for nf=1:Nf
  frf(nf,kk) = Y(ii,:)*((Y(jj,:)')./(wr2 + i*wr2.*eta - w2(nf)));
  end
end
% Compute Sensitivity (Dfrf)
%
if nargout==3 & ~isempty(r)
 if length(r)==1
   for kk=1:n
   ii=er(kk,2); jj=er(kk,1);
      Dfrf(:,kk) =  (Y(ii,r)*Y(jj,r))./( (((wr(r)*(1+i*eta(r))...
```

```
                                                              - w.^2/wr(r))).^2)*i ) ;
  end
 elseif size(er,1)==1
  Dfrf = zeros(Nf,length(r));
  ii=er(1,2); jj=er(1,1);
  for kk=1:length(r)
     Dfrf(:,kk) =  (Y(ii,r(kk))*Y(jj,r(kk))./( (((wr(r(kk))*(1+i*eta(r(kk)))...
                                                             w.^2/wr(r(kk)))).^2)*i ) ;
  end
 end
end
```

B.4 Viscously Damped Response $H(\zeta)$ and $\frac{\partial H(\zeta)}{\partial \zeta}$

```
function [freq,frf,Dfrf]=visc_frf(D,Y,er,zeta,lf,df,uf,r)
%
%
%   [freq,frf,Dfrf] = visc_frf(D,Y,er,zeta,lf,df,uf,r)
%
%   Viscously damped frequency response function and its derivative
%   w.r.t. modal damping factor 'zeta(r)'. The derivative is optional
%   and is computed if 3rd output argument is given and mode number 'r'
%   be found in input argument list.
%
%   NOTE: both 'frf' and 'Dfrf' are COMPLEX !
%
%
%
% D     -  [m*1] vector of eigenfrequencies in [Hz]
% Y     -  [N*m] matrix of m mode shapes (mass-normalised)
%                defined at N co-ordinates
% zeta  -  [m*1] vector of viscous damping factors
% er    -  [n*2] matrix of excitation and response coordinates
%                (must be just 1 row if length(r)>1)
% r     -  [a*1] vector of mode numbers of which derivative is sought
%                (must be just 1 element is size(er,1)>1)
%
% lf    -  lowest frequency point, i.e. f1
% df    -  frequency increment, i.e. f2-f1....
% uf    -  highest frequency point, i.e. fNf
%
% freq  -  excitation frequencies, freq=f(lf,df,uf)
% frf   -  frequency response function, alpha(ii,jj)
% Dfrf  -  *if size(er,1)==1 sensitivities of frf wrt to each modal damping
%                           zeta(r), thus its size == [Nf,Nm]
%          *if length(r)==1  sensitivities of frfs wrt to modal damping
%                           factor zeta(r), thus its size == [Nf,n]
%
%
%
% Check dimensions of modal data
%
if length(zeta)~=size(Y,2) | length(zeta)~=length(D)
  error('Inconsistent dimensions of modal data.... !')
end
if max(r)>length(zeta)
  error('Specified mode number(s) ''r'' exceed available modes.... !')
end
if size(er,1)>1 & length(r)>1
  error('size of ''er'' and ''r'' are incompatible....!')
end
% Get constants
%
m    = length(D);     n    = size(er,1);
% Set preliminary variables
%
D    = D(:);          freq = [lf:df:uf]';
Nf   = length(freq);
frf  = zeros(Nf,n);   Dfrf = zeros(Nf,n);
zeta = zeta(:);
wr   = (2*pi*D);      wr2  = (wr).^2;
w    = (2*pi*freq);   w2   = (w).^2;
%  Compute FRF (frf)
%
for kk=1:n
ii=er(kk,2); jj=er(kk,1);
  for nf=1:Nf
  frf(nf,kk) = Y(ii,:)*((Y(jj,:)')./(wr2 + i*2*w(nf)*wr.*zeta - w2(nf)));
  end
end
% Compute Sensitivity (Dfrf)
%
if nargout==3 & ~isempty(r)
 if length(r)==1
   for kk=1:n
   ii=er(kk,2); jj=er(kk,1);
      Dfrf(:,kk) =  (Y(ii,r)*Y(jj,r))./( (((wr(r)*(wr(r)+2*i*zeta(r)*w)...
```

```
                                                - w.^2)).^2)./(2*wr(r)*w)*i ) ;
  end
 elseif size(er,1)==1
   Dfrf = zeros(Nf,length(r));
   ii=er(1,2); jj=er(1,1);
   for kk=1:length(r)
      Dfrf(:,kk) =  (Y(ii,r(kk))*Y(jj,r(kk))./( (((wr(r(kk))*(wr(r(kk))...
                      +2*i*zeta(r(kk))*w) - w.^2)).^2)./(2*wr(r(kk))*w)*i ) ;
   end
 end
end
```

Appendix C

OPTIMA

C.1 Input Specification File

```
%%%%%%%%%%%%%%%%%%%%%%%%%%%%%%%%%%%%%%%%%%%%%%%%%%%%%%%%%%%%%%%%%%%%%%%%%%%%%%%%%%%%
%                  R E A D   file_fe_def    F I L E
%%%%%%%%%%%%%%%%%%%%%%%%%%%%%%%%%%%%%%%%%%%%%%%%%%%%%%%%%%%%%%%%%%%%%%%%%%%%%%%%%%%%
% Variables to read:
%                                                                        FE ANALYSIS
%,,,,,,,,,,,,,,,,,,,,,,,,,,,,,,,,,,,,,,,,,,,,,,,,,,,,,,,,,,,,,,,,,,,,,,,,,,,,,,,,,,,
%            n_strct   array of integers, giving number of substructures
%            n_jobs    matrix[5*length(n_strct)] where the i-th column
%                      corresponds to the i-th substructure in n_strct
%                      and all elements are either 1 or 0 to control
%                      actions taken in this function.
%  fe_prepro.m:
%            1st row:  generate new mesh (.msh-file) if =1,
%                      otherwise leave old .binmshSi file unaltered
%            2nd row:  create new material property tables (.mat-file) if =1,
%                      otherwise leave old .binmatSi file unaltered
%            3rd row:  create new boundary condition (.bcd-file) file if =1,
%                      otherwise leave old .binbcdSi file unaltered
%            4th row:  change new control file for computation (.ctr-file) if =1,
%                      otherwise leave old .binctrSi file unaltered
%  fe_genkmc.m:
%            5th row:  generate new elements (.mtx-file) if =1,
%                      otherwise leave old .binmtxSi file unaltered
%
%                      NOTE: if any entry indicates 0 but no output file (.binxxxSi)
%                            has been created in previous computations, the control
%                            flag is overruled and the computations done
%
%                                                                        FE COUPLING
%,,,,,,,,,,,,,,,,,,,,,,,,,,,,,,,,,,,,,,,,,,,,,,,,,,,,,,,,,,,,,,,,,,,,,,,,,,,,,,,,,,,
%  fe_couple.m:
%            n_dofs    array of integers, same length as n_strct, specifying
%                      the number of dofs which must be retained. These dofs
%                      are typically potential measurement co-ordinates.
%                      If an entry is set to inf, no condensation of that
%                      sub-structure is applied. If an entry is set to zero,
%                      then all retained dofs are identified internally.
%
%            r_dofs    2 column matrix which number of rows must
%                      be equal sum(n_dofs). The first column
%                      contains the node number, whereas the
%                      second column the direction of the
%                      co-ordinates to retain.
%
%                      NOTE: if all entries of n_dofs==inf, then
%                            all sub-structures are simply coupled without
%                            condensation. In other cases, condensation
%                            is used and for sub-structures at which
%                            n_dofs(i)==inf, no corresponding rows in r_dofs
%                            are read.
%                            Therefore r_dofs must have
%                               sum(n_dofs(find(~isinf(n_dofs))))
%                                                                 rows.
```

```
%                         As a result, if all elements in n_dofs are
%                         either 'inf' or '0', then r_dofs=[];
%
%            method    Condensation method applied for elements n_dofs(i)~='inf':
%                      if == 1  1st level Craig Bampton
%                      if == 2  1st level Mac Neal
%                      if == 3  2nd level Craig Bampton (precedes method==1)
%                      if == 4  2nd level Mac Neal      (precedes method==2)
%                      if == 5  Mac Neal based on force assembly
%
%            mxHz      maximum frequency point in [Hz]. This bound effectively
%                      determines the number of modes computed for each sub-structure
%                      and thus also influences the number and location of automatically
%                      selected dofs. As a rule of thumb, 'mxHz' should be set to the
%                      maximum frequency point of interest. Then the condensation
%                      is generally valid within +-1%
%
%            plot_ids  4 plotting flags for coupled structure:
%                      plot_ids(1)==1 if whole assembly to plot
%                      plot_ids(2)==1 if identified junction nodes to plot
%                      plot_ids(3)==1 if nodes of r_dofs to plot
%                      plot_ids(4)==1 if nodes of automatically selected dofs to plot
%
%                                                                              FE UPDATING
%,,,,,,,,,,,,,,,,,,,,,,,,,,,,,,,,,,,,,,,,,,,,,,,,,,,,,,,,,,,,,,,,,,,,,,,,,,,,,,,,,,,,,,,,,
%            paratab   design parameters to be updated:
%
%                       Sub_id  pid  No's.Elm        Elm.No's
%                       [ 7    1     4        13 14 15 16  0  0  0  0  0
%                         3    19    3        8  9  90 0   0  0  0  0  0
%                         :    4     :           :        :        :
%                         12   2     inf         ('all elements')
%                         1    1     9        1  2  3  4   5  6  7  8  9];
%
%                    where [Sub_id] points at the sub-structure number, [No's.Elm]
%                    gives the number of elements in that sub-structure, [Elm.No's]
%                    details what element numbers and [pid] is a pointer to specify
%                    the design parameter to be updated:
%
%                |pid|    |---------- DESCRIPTION -----------|     |- Defined for -|
%                 1)   Young's Modulus   E                  --->    beam and shell elements
%                 2)   Mass Density   rho                  --->    beam and shell elements
%                 3)   Poisson's Ratio   nu                 --->    shell elements
%                 4)   Shell thickness   t                 --->    shell elements
%                 5)   Shear Modulus   G                   --->    beam elements
%                 6)   Cross sectional area   Ayz          --->    beam elements
%                 7)   Shear area   Axz                    --->    beam elements
%                 8)   Shear area   Axy                    --->    beam elements
%                 9)   Second moment of area   Iz          --->    beam elements
%                 10)  Second moment of area   Iy          --->    beam elements
%                 11)  Second moment of area   Ix          --->    beam elements
%                 12)  Beam offset in local direction   Y --->    beam elements
%                 13)  Beam offset in local direction   Z --->    beam elements
%                 14)  Lumped masses                       --->    all co-ordinates
%                 15)  Lumped springs (grounded)           --->    all co-ordinates
%
%
%
%               NOTE: if pid==14 or pid==15,  then |No's.Elm| translates to |No's.DOFs|
%                                         and  |Elm.No's| should be replaced by the |DOF|
%                                         number of the sub-structure, i.e. a number
%                                         between 1:6*Nodes. Also, the specified masses
%                                         and springs must exist (i.e. ~=0). If not,
%                                         the computation stops.
%
%               NOTE: updating stiffnesses
%                        of 2 noded springs,  use pid=6,...,11 to update ...
%                                         Ayz -> stiffness in local x-direction, ie. 1
%                                         Axz -> stiffness in local y-direction, ie. 2
%                                         Axy -> stiffness in local z-direction, ie. 3
%                                         Ix  -> stiffness in local xx-direction, ie. 4
%                                         Iy  -> stiffness in local zz-direction, ie. 6
%                                         Iz  -> stiffness in local yy-direction, ie. 5
%                                             also,
%                                             a 2 noded spring has no mass. Hence, pid==2
%                                             is not applicable here.
%
%               NOTE: if pid==7 or pid==8,    the beams must be TIMOSHENKO beams
```

```
%                                       or 2 NODED SPRINGS since otherwise Axz=Axy=0
%
%               NOTE: if pid==12 or pid==13,  and the current offset==0, an initial and
%                                       arbitrary offset of 1mm will be imposed.
%                                       It is also recommended that the Y and Z offset
%                                       should be the same for node A and B ( to
%                                       have a common initial design value).
%
%
%            Jmin      integer indicating kind of objective function to use,
%                       Jmin=1 ->  min[(FRF_x)-(FRF_a)],
%                                  using predictor-corrector method
%                       Jmin=2 ->  min[log(FRF_x)-log(FRF_a)],
%                                  using predictor-corrector method
%                       Jmin=3 ->  min[(FRF_x)-(FRF_a)],
%                                  using RFM (Lin/Ewins,1990)
%                       Jmin=4 ->
%                         :          :    others to follow
%
%            Mthd      minimisation method to be used
%                       Mthd=1 ->  weighted least square
%                       Mthd=2 ->  simple pseudo inverse (SVD)
%                       Mthd=3 ->    ......      others to follow
%
%            Nplt      Number of FRF overlays to plot after each iteration.
%                      If Nplt~=0, the first Nplt measurements will be overlaid
%                      with the corresponding FE predictions as the computation
%                      advance within the updating computation.
%
%            num_iter  maximum number of iterations of the updating computations
%
%
```